CRACKING BEHAVIOUR OF GFRP-REINFORCED CONCRETE PANELS UNDER UNIAXIAL AND BIAXIAL TENSION

TAMER BERRY A. SABRAH


CENTRE FOR NFLD. STUDIES
MEMORIAL UNIVERSITY
OF NEWFOUNDLAND

CRACKING BEHAVIOUR OF GFRP-REINFORCED CONCRETE PANELS UNDER UNIAXIAL AND BIAXIAL TENSION

by

Tamer Berry A. Sabrah, B.Sc., M.Sc.

A thesis submitted to the
School of Graduate Studies
in partial fulfillment of the requirements for the degree of
Doctor of Philosophy

FACULTY OF ENGINEERING AND APPLIED SCIENCE

MEMORIAL UNIVERSITY OF NEWFOUNDLAND

June 2009

St. John's Newfoundland Canada

وَٱللَّهُ أَخۡرَجَكُم مِّنۢ بُطُونِ أُمَّهَٰتِكُمۡ لَا تَعۡلَمُونَ شَيۡـٔٗا وَجَعَلَ لَكُمُ ٱلسَّمۡعَ وَٱلۡأَبۡصَٰرَ وَٱلۡأَفۡـِٔدَةَ لَعَلَّكُمۡ تَشۡكُرُونَ

"And Allah brought you forth from the wombs of your mothers knowing nothing; and gave you hearing, sights, and hearts: that you might give thanks"
(Quran 16:78)

All the praises and thanks be to Allah

To my Mother

Abstract

Fibre reinforced polymer (FRP) reinforcing bars for concrete have become the subject of research as an alternative to steel reinforcement which is susceptible to corrosion. This thesis encompasses an experimental investigation and theoretical modelling of the cracking behaviour of concrete panels reinforced with glass fibre reinforced polymer (GFRP) bars under uniaxial and biaxial direct tensile loading conditions.

In the experimental phase of this investigation, a special setup is designed to test reinforced concrete panels under uniaxial and biaxial tension. The setup accommodates concrete panels that are reinforced with GFRP and/or steel reinforcing bars. The setup is used to carry out an experimental test program on twelve reinforced concrete panels under uniaxial and biaxial tension. The test parameters are the concrete strength, concrete cover to bar diameter ratio, bar spacing, reinforcement ratio, and bar type (GFRP or steel). The crack patterns, crack widths, and spacings are investigated. The tensile stress-strain relationships, and thus the tension stiffening behaviour, are examined. The tension stiffening behaviour is the concrete contribution in resisting part of the tensile stresses applied.

The experimental results reveal that the crack development under biaxial tension affects the magnitude of the stress in the GFRP-reinforced concrete panels resulting in a decrease in the cracking loads and stresses. GFRP-reinforced concrete panels under uniaxial tension experience an increase in the tension stiffening contribution compared to steel-reinforced concrete at the same level of stress. However, this contribution is not significant under biaxial tension. GFRP-reinforced concrete panels under biaxial tension experience much less tension stiffening contribution than those under uniaxial tension due to different cracking mechanisms for both cases. In general, there

is an increase in the tension stiffening contribution of GFRP-RC panels due to the decrease in the reinforcement ratio. The area of the effective tension zone of GFRP-reinforced concrete is found to be almost half the size of those that develop around steel reinforcing bars. The use of an effective tension zone for GFRP-reinforced concrete equal to seven times the bar diameter is recommended rather than using 15 times the bar diameter which is commonly used for steel reinforcing bars. The use of high strength concrete causes a reduction in the total number of visible cracks, and thus enhancing the structural behaviour of GFRP-reinforced concrete panels.

An analytical cracking model is developed to predict the crack spacing and width of GFRP-reinforced concrete. The model accounts for the bond stress transfer mechanism and surface characteristics of the reinforcing bar. The model is validated through comparisons with test results and other existing experimental data. The proposed model is very suitable to predict the cracking variables of GFRP-reinforced concrete. Furthermore, a tension stiffening constitutive model is proposed for non-linear finite element analysis of GFRP-reinforced concrete. The proposed model accounts for the biaxial tension strength envelope. The model assumes a bi-linear relation in the post-cracking range to reflect the tensile behaviour of the tested GFRP-reinforced concrete panels. This model is incorporated into an incremental elastic plastic concrete model that is used to perform a non-linear finite element analysis of GFRP-reinforced concrete panels. The analysis results show reasonable accuracy in predicting the behaviour of GFRP-reinforced concrete.

Acknowledgments

My time at Memorial University of Newfoundland (MUN) provided me with the great pleasure of meeting unique and interesting colleagues, faculty, students, and staff, as well as forming close friendships with a great number of wonderful people. I owe these individuals a great deal of thanks.

Specifically, I would like to express my deepest gratitude to my supervisors, Dr. H. Marzouk and Dr. A. Hussein, for the trust, enthusiastic support, encouragement and freedom that I was given and benefited from throughout my doctoral program. I was truly inspired by Dr. Marzouk's dedication towards research, and his fruitful discussions and comments, which kept me motivated during this research investigation. I am deeply indebted to Dr. Hussein for his constructive discussions and excellent guidance towards this research. Further appreciation is due to my supervisors for their patience with the preparation of this manuscript.

The experimental work presented in this thesis would not be possible without the help of the Technical Services department at MUN; especially, Messers R. Meaney, B. Bidgood, S. Foster, and C. Carter. The time I spent with my colleagues M. Hossin and E. Eltom in assembling the test setup was full of remarkable moments of challenge and enjoyment. I will be always thankful for such moments. Special thanks to Concrete Products, Newfoundland, for donating the concrete of the test setup. Sincere appreciation is given to the Olympic Construction Company, Newfoundland, for casting the concrete of the reaction frame. I am thankful to Mr. D. Bursey for his assistance in the preparation of the hydraulic system. I am grateful to the technical staff of the engineering laboratories for their valuable services in helping me with my experiments; especially, Messers M. Curtis, S. Organ, and T. Pike. I am also thankful to my fellow students Y. Ebrahim, E. Rizk, N. Dawood, and S. Alam for their help during the experimental program.

Special gratitude is extended to Drs. A. Swamidas, S. Adluri, L. Lye, and C. Daley for their kind encouragement during my study period at MUN. I am also thankful to the Faculty of Engineering - Associate Dean of Graduate Studies and his office staff for their keen administrative assistance with my doctoral study program.

This thesis was completed at MUN as part of a project that is funded by the Natural Sciences and Engineering Research Council of Canada (NSERC) and Canada Foundation for Innovation (CFI). Funding in the form of a graduate fellowship and graduate supplement from the School of Graduate Studies and Faculty of Engineering at MUN is gratefully acknowledged.

Special thanks must go to my wife, Doaa Elkhawas, for her understanding, encouragement, and assistance for many years of my life. The long time I spent working in this thesis kept me away from my children, Ahmed and Lina. So, I owe both of them a thank you and an apology.

At last, but not least, sincere appreciation is given to my family, especially my father, Dr. Berry Sabrah, for his valuable support and encouragement.

Tamer B. Sabrah
June 2009

Contents

List of Tables

List of Figures

Acronyms

ACI	:	American Concrete Institute
AFRP	:	Aramid fibre reinforced polymers
ASTM	:	American Society for Testing and Materials
CFRP	:	Carbon fibre reinforced polymers
C.O.V.	:	Coefficient of variation
CSA	:	Canadian Standards Association
EW	:	East-West
FRP	:	Fibre reinforced polymer
FEA	:	Finite element analysis
GFRP	:	Glass fibre reinforced polymers
ISIS	:	Intelligent Sensing for Innovative Structures (ISIS)
JSCE	:	Japanese Society for Civil Engineering
LPDT		Linear potentiometer displacement transducer
MUN	:	Memorial University of Newfoundland
NS	:	North-South
Rebar	:	Reinforcing bar

Notations

Notation		*Description*
A_b	:	Cross-sectional area of reinforcing bar
A_c	:	Net cross-sectional area of concrete
A_{eff}	:	Effective cross-sectional area of concrete
A_f	:	Cross-sectional area of GFRP reinforcement
A_g	:	Gross cross-sectional area of concrete
A_s	:	Cross-sectional area of steel reinforcement
b_s	:	Reinforcing bar spacing
c_c	:	Clear concrete cover
c_c / d_b	:	Concrete cover to bar diameter ratio
d_b	:	Reinforcing bar diameter
D_{eff}	:	Diameter (or height) of effective tension zone
E_c	:	Elastic modulus of concrete
E_s	:	Elastic modulus of steel
E_f	:	Elastic modulus of GFRP
E_b	:	Elastic modulus of reinforcing bar
f_1, f_2, f_3	:	Principal normal stresses
$f_c^{'}$	:	Uniaxial compressive strength of concrete
f_{cr}	:	Cracking strength of concrete (concrete stress corresponds to N_{cr})
f_{ct}	:	Concrete tensile stress
f_f	:	Stress in FRP rebar
f_r	:	Concrete modulus of rupture
f_{sp}	:	Splitting tensile strength of concrete
f_{scr}	:	Steel rebar stress at crack
$f_t^{'}$	:	Uniaxial tensile strength of concrete (from direct tension test)
f_y	:	Yield strength of steel reinforcing bar
G_f	:	Fracture energy
I_{cr}	:	Cross-section cracked moment of inertia
I_e	:	Cross-section effective moment of inertia
I_g	:	Cross-section gross moment of inertia
kN	:	Kilo Newton
k_b	:	Bond coefficient
K_p	:	Bond factor

Notation		*Description*
L_{sp}	:	Specimen length
l_g	:	Gauge length
l_t	:	Transfer length
m	:	Meter
mm	:	Millimetre
MPa	:	Mega Pascal
M_a	:	Applied bending moment
M_{cr}	:	Cracking bending moment
n	:	Curve fitting factor
n_b	:	Reinforcing bar modular ratio
n_{bars}	:	Number of bars
n_{cr}	:	Number of cracks
n_f	:	GFRP modular ratio (E_f / E_c)
n_s	:	Steel modular ratio (E_s / E_c)
N	:	Newton
N	:	Tensile force
N_{cr}	:	Initial cracking tensile force
N_{stab}	:	Tensile force at stabilized cracking stage
N_{ult}	:	Ultimate tensile force
p_b	:	Circumferential perimeter of reinforcing bar(s)
S_R	:	Transverse bar spacing
S_{rm}	:	Average crack spacing
S_{rmax}	:	Maximum crack spacing
S_{rmin}	:	Minimum crack spacing
w/c	:	Water cement ratio
w_{cr}	:	Crack width
W_{sp}	:	Specimen width
w_m	:	Mean crack width
w_{max}		Maximum crack width
α_o	:	Material constant
α_1	:	Material constant in proposed constitutive model
α_2	:	Material constant in proposed constitutive model
α_3	:	Material constant in proposed constitutive model
$\Delta\varepsilon_{m,cr}$	:	Difference between member strain and bare bar response at cracking load
ε_{b1}	:	Rebar strain at uncracked section (state 1)
ε_{b2}	:	Rebar strain at cracked section (state 2)

Notation		*Description*
ε_{cr}	:	Average tensile strain that corresponds to f_{cr} of RC member
ε_m	:	Average tensile strain of RC member
$\varepsilon_{m,stab}$	:	Average tensile strain of RC member at stabilized cracking stage
ε_s	:	Steel strain
λ	:	Arbitrary parameter that relates S_{rm} to S_{rmax}
με	:	Microstrain
ρ_b	:	Balanced reinforcement ratio
ρ_{eff}	:	Effective reinforcement ratio
ρ_f	:	GFRP reinforcement ratio
ρ_s	:	Steel reinforcement ratio
τ_b	:	Bond stress
τ_{bu}	:	Ultimate (maximum) bond stress
ψ	:	Dimensionless factor in proposed cracking model

Chapter 1

INTRODUCTION

1.1 General

During the past few years, there has been a growing interest in meeting the worldwide increasing demand for energy. The building of new infrastructure projects is being planned for the next three decades including marine structures, offshore platforms, and nuclear power plants. However, most of these reinforced concrete (RC) structures will be likely existing in aggressive environmental conditions. Unless such structures are properly designed and maintained over their lifetime, they will be more vulnerable to corrosion of steel reinforcement and concrete deterioration. The RC cracking behaviour is an important design concern due to its direct relation to corrosion of steel reinforcement and the effect on the structural performance. The control of cracking in RC structures usually leads to high reinforcement ratios, which could increase the costs of the project construction and maintenance.

For many years, the corrosion problems of steel-reinforcement have led to a growing interest in design strategies that would eliminate the structure's susceptibility against corrosive environments. Considerable attention has been given to using high-strength concrete (HSC) for improving the concrete durability against deterioration as opposed to using normal-strength concrete (NSC). Steel protection has been the subject of

considerable research effort, resulting in the development of several techniques, such as steel bar galvanization, cathodic protection, employment of stainless steel reinforcement, and/or epoxy coating. In fact, each protection technique has its own pros and cons. The main disadvantages of these methods are the experienced variations in the protection efficiency, which are due to different structure loading conditions, quality of construction, and degree of exposure to environmental conditions surrounding the structure. With the uncertainty in achieving efficient long term steel-protection, fibre reinforced polymer (FRP) composite bars have become the focus of research as an alternative to steel reinforcement specially where there is a high probability of steel corrosion. FRP bars are deemed to be one of the promising technological advances in material applications in structural engineering. Since the 1980s, the uses of FRP bars have been growing in many highway bridges in Europe, Japan, and North America. More recently, FRP bars have been used on a selective basis for construction of some seawalls, industrial roof decks, base pads for electrical and reactor equipment, and concrete floor slabs in aggressive chemical environments (ACI 440R 1996).

Glass-FRP (GFRP) reinforcement has been the commonly used composite bar type for many civil engineering applications because of an economical balance of cost and strength properties. GFRP has more resistance to corrosion and higher tensile resistance compared to steel (Newhook et al. 2002). The current continuous research and development is leading to GFRP bar types that have better physical and mechanical characteristics (Uomoto 2004; Witt and Jütte 2008).

Further wider applications of GFRP bars in RC structures require more understanding of behaviour of GFRP-RC under different loading conditions. Establishing a rationale for cracking analysis and defining some key aspects for nonlinear analysis are essential for a wider utilization of the GFRP reinforcement in different types of structures. Although in practice, RC structures are subjected to a wide range of complex states of stresses, most of the past research focused on flexural members of beams and one way slabs. Cracks are usually induced in concrete members either due to direct tension or due to bending. Concrete members and structural elements that transmit loads primarily by direct tension rather than bending include bins and silos, tanks and containments, shells, ties of arches, roof and bridge trusses, and braced frames and towers (ACI 224.2 1992). GFRP composite is a relatively new material compared to steel, and thus the analysis and design should be based on rational and well founded design recommendations. Testing a full scale or even prototype models of structures is relatively complicated. Hence, the structure is usually simulated as a combination of different assemblages of concrete panels (panel-type structures). Each panel has a different combination of stresses as those that exist in the full scale structure.

For accurate analysis of concrete structures, it is often important to include the post-cracking resistance of concrete. Concrete subjected to uniaxial tension exhibits post-cracking softening behaviour. The existence of reinforcement stiffens and engages the concrete between cracks through local bond stress transfer which is also associated with local bond-slip. Thus, the concrete between cracks is in fact, resisting part of the tensile stresses applied. This phenomenon is known as "tension stiffening". By ignoring the

effects of tension stiffening, it may results in an overestimation of deflection and/or crack width. Tension stiffening plays a major role in enhancing the calculations required for serviceability requirements of RC structures. In addition, the accurate prediction of cracking is essential for a crack controlled design. Both tension stiffening and the associated propagation of cracks are complicated phenomena that play a significant role in the nonlinear analysis of concrete structure.

Very few experiments have been carried out to study the cracking behaviour and tension stiffening of GFRP-RC under tension. Available information on the cracking behaviour and tensile response of GFRP-RC is scarce and conflicting. The GFRP bar modulus of elasticity and surface characteristics of GFRP bars affect the cracking and tension stiffening. Cracking and tension stiffening are also influenced by several parameters such as states of stress, reinforcement ratio, bar spacing, concrete cover, and bond stresses. Therefore, the results of an extensive experimental program to investigate the behaviour under uniaxial and biaxial tensile loading could be useful in developing design recommendations and analysis tools.

1.2 Research Scope

The current study is carried out to examine the behaviour of GFRP-RC when subjected to uniaxial and biaxial tension. The scope of the current program is as follows:

1. To investigate the cracking behaviour of GFRP-RC panels under uniaxial and biaxial tension.

2. To examine and evaluate the test data such as the displacements and strains developed in the specimen under different loading conditions.

3. To examine and analyze the changes in cracking mechanism, and changes occurring in the crack patterns, widths and spacings.

4. To compare the behaviour of GFRP-RC panels with those reinforced with traditional steel reinforcement.

5. To compare the behaviour of GFRP-RC panels made of HSC with those made of NSC.

6. To study and evaluate the stress-strain relationships recorded for the GFRP-RC panels under different loading conditions.

The experimental results can then be used to establish an approach to predict the cracking characteristics of GFRP-RC under tensile stresses. Moreover, the experimental results can be used to propose and calibrate a suitable constitutive model to idealize the tensile stress-strain relationships of GFRP-RC panels under uniaxial and biaxial tension. This constitutive model is suitable to be used in numerical analysis of GFRP-RC structures.

1.3 Research Objectives

The main objective of this research is to investigate the in-plane behaviour of GFRP-RC panels under direct tension loads. The test results will enrich the literature on the

behaviour of GFRP-RC; and thus help in extending the utilization of this new material in different structural applications. The research objectives of this investigation can be summarized as follows:

1. Review the available methods used in testing steel-RC panels under direct tension, and thus identify suitable methods that can be used to test GFRP-RC panels.

2. Design an appropriate test setup for panel testing under uniaxial and biaxial direct tension that can accommodate GFRP bars and produces reliable test data.

3. Collect and analyze the strength data and load-deformation behaviour of GFRP-RC panels under direct tension. To examine and evaluate the test data, record the deformation characteristics, and observe the failure modes.

4. Identify the main differences in structural behaviour between GFRP- and traditional steel-RC panels. This could be established by testing matching specimens and comparing the test results.

5. Examine the cracking characteristics that include crack spacings and crack widths, for the different structural configurations and loading conditions applied to the test specimens.

6. Evaluate the effect of HSC on the cracking and tensile behaviour of GFRP-RC panels.

7. Propose a methodology that could be used to accurately predict the cracking behaviour of GFRP-RC panels.

8. Examine the tension-stiffening effects of GFRP-RC, and adopt a theoretical constitutive model suitable for non-linear analysis.

1.4 Thesis Outline

The thesis work is presented in nine chapters including the introduction.

Chapter 2 is divided into two parts. The first part introduces a background to the general characteristics of concrete cracking, concrete tensile behaviour under tension, and a literature review of previous experimental and analytical research conducted mainly on steel-RC. The second part is a background review of GFRP reinforcement and its main characteristics, followed by a review of recent studies on cracking and tensile behaviour of GFRP-RC.

Chapter 3 describes the design and construction stages of a new test setup for the current research program. The first part of the chapter introduces a brief review of previous relevant test setups in the literature. The second part addresses the conceptual design, and provides a detailed description of the test setup and its preparation stages.

Chapter 4 describes the experimental investigation. Details of the test program, test parameters, specimen details, measurements and instrumentation used are presented.

Chapter 5 presents the experimental results that focus on the cracking behaviour of the tested GFRP-RC panels. The effects of different test parameters on the cracking behaviour of panels are discussed.

Chapter 6 is divided into two main parts. The first part focuses on the analysis of the tensile stress-strain relationships of GFRP-RC under uniaxial and biaxial tension. The second part deals with developing an appropriate constitutive law for the tensile stress-strain relationship of GFRP-RC.

Chapter 7 discusses an analytical approach that is used to develop a constitutive relation to predict the crack spacings of GFRP-RC panels under direct uniaxial and biaxial tension. The verification of the proposed model is also presented.

Chapter 8 deals with the calibration and implementation of a tension stiffening model of GFRP-RC in a general purpose finite element program.

Finally, a summary of the current investigation and the conclusions reached are given in Chapter 9.

Chapter 2

LITERATURE REVIEW

2.1 Introduction

This chapter summarizes the literature pertaining to the background and different aspects of the present research work. The first part of this chapter presents the general characteristics of concrete cracking. The concrete tensile behaviour under direct tension is presented and discussed. Different previous constitutive models for predicting concrete tensile behaviour are summarized. Also, the results of previous research programs that were conducted to predict crack widths and spacings are presented. A review of different codes and cracking models is given. The majority of these research studies reviewed in this part were conducted on steel-RC.

The second part of this chapter provides a brief background on GFRP reinforcement. The mechanical characteristics of GFRP reinforcement bars are presented. The current state of the art about the serviceability and crack control of GFRP-RC is summarized. Relevant recent research work on cracking and tensile behaviour of GFRP-RC is discussed.

2.2 Cracking of Concrete

Concrete is a non-homogenous material characterized by weakness in tension and good performance under normal compression. Thus, cracks are generally expected to occur in RC structures with or without prestressing when the tensile stress exceeds the tensile strength of

concrete. When a crack controlled design is conducted, small acceptable crack widths and a number of cracks can be achieved. However, excessive and wide cracks are undesirable. The significance of cracks depends on the type of structure as well as the nature of the cracking. For instance, cracks that are acceptable for buildings may not be acceptable in liquid retaining structures (for example, water tanks). Cracks may solely affect appearance; indicate significant structure disintegration, distress or a lack of durability.

2.2.1 Plain concrete under tension

Concrete subjected to uniaxial tension exhibits post-cracking softening behaviour similar to the response under uniaxial compression (Gopalaratnam and Shah 1985). Cracked plain concrete shows strain softening associated with the localization of a single crack and a corresponding sharp tensile stress release (Hillerborg et al. 1976; Bazant and Oh 1983). As cracks start to develop, the energy stored in the material eventually gets converted into fracture energy. Hillerborg et al. (1976) first introduced the area under the stress-deformation curve and defined it as the 'fracture energy', G_f (Figure 2-1 (a)). The definition of G_f identifies the energy needed to create a crack of unit length and unit width. This energy advances the opening of existing cracks and causes concrete to soften at relatively high rates. The rate of crack propagation is mainly dependent on the concrete material properties. For instance, HSC exhibits a post-cracking resistance under direct tension. However, it was found that HSC appears to be more brittle and stiffer than NSC. Marzouk and Chen (1995) reported that for an NSC of $f_c^{'}$ = 35 MPa, G_f is ~ 110 N/m, while for HSC of $f_c^{'}$ = 75 MPa, G_f is ~160 N/m. After the peak load, the stress-deformation curve of HSC descends more sharply than that of NSC (Phillips and Binsheng 1993; Giaccio et al. 1993; Marzouk and Chen 1995).

Several researchers studied plain concrete under biaxial stresses. Kupfer et al. (1969) showed that the ultimate strength of NSC under biaxial tension loads results in a strength almost equal to the uniaxial tensile strength. This means that the strength under tension is found to be independent of the stress-loading ratio (f_1 / f_2), where f_1 and f_2 are the principal stresses. Hussein and Marzouk (2000) investigated HSC under different biaxial loading combinations. It was observed that the crack patterns and failure mode under biaxial stresses for the HSC are similar to those of NSC. The investigators concluded that there is no fundamental difference in the formation of crack patterns and failure modes due to the increase in the concrete compressive strength under different biaxial loading combinations.

2.2.2 Reinforced concrete under tension

The existence of reinforcement stiffens and engages the concrete between the cracks through local bond stress transfer associated with local bond-slip. This improves the softening behaviour by introducing the tension stiffening effect, which causes the average concrete stress in tension to gradually reduce to zero as the cracks progress extensively. Hence, tension stiffening and local bond slip are an interconnected phenomenon, which is very difficult to isolate. Tension stiffening stress-strain characteristics are different from those of tension softening of plain concrete due to the presence of reinforcement and the effect of bond (Figure 2-1 (b)).

The tension stiffening behaviour is well established for steel-RC. Nonetheless, it is worthwhile to introduce some of the basics of the tension stiffening behaviour. These concepts are described in detail in other references (Ghali and Favre 1994; Collins and Mitchell 1991).

Consider a RC member that is subjected to an axial tension N (Figure 2-2). The RC member can be a stand alone member under N or a tension zone in a flexural member. The RC member will not crack until the stress in concrete exceeds its tensile strength. Hence, in this stage, the member is free from cracks and the reinforcement and concrete undergo compatible strains. This uncracked condition is referred as 'state 1'. When the tensile strength in concrete is exceeded, cracks develop. At the crack location, the tensile stress is assumed to be resisted completely by the reinforcement. The section at the crack location is fully cracked and this condition is referred to as 'state 2'. The sudden increase in stress in the reinforcing bar produces strain that is incompatible with the strain in the adjacent concrete and results in widening of the crack.

In a section situated between two cracks, the bond between the concrete and reinforcing bars restrains the elongation of the bars and thus part of the tensile force in the reinforcement is transmitted to the concrete situated between the cracks. The stress and strain in the section will be in an intermediate condition between states 1 and 2. This means that the strain in the reinforcing bar varies from a maximum value at the cracks to a minimum value midway between the cracks. The rigidity varies between consecutive cracks in a similar way. The contribution of the concrete between cracks to the rigidity of the members is referred as 'tension stiffening'. By ignoring the effect of tension stiffening, it results in an overestimation of deflection and crack width.

As shown in Figure 2-3, the value of $\Delta\varepsilon_b$ represents the difference between the mean bar strain and the strain of the bar at a fully cracked section. This difference has a maximum value,

$\Delta\varepsilon_{cr}$ at the start of cracking, when $N = N_{cr}$. Mathematically, a cracking dimensionless coefficient ζ is introduced to represent the extent of cracking in the member, where $\zeta = 0$ for an uncracked section ($N < N_{cr}$), $0 < \zeta < 1$ for a fully cracked section. The value of ζ is given by:

$$\zeta = 1 - \left(\frac{N_{cr}}{N}\right)^2 \tag{2.1}$$

The mean strain in the reinforcing bar is:

$$\varepsilon_{bm} = (1-\zeta)\varepsilon_{b1} + \zeta\varepsilon_{b2} \tag{2.2}$$

where ε_{b2} is the bar strain at the cracked section. The second term of Eq. (2.2) $(\zeta\varepsilon_{b2})$ represents the supplementary of strain in the reinforcing bar compared with the strain in concrete.

Several researchers realized the importance of the tension stiffening effects on the response of concrete structures. Goto (1971) described the mechanism of crack formation while testing RC specimens under tension. The formation of cracks starts with the development of the primary cracks at the cracking strain. Next, internal cracks form along the deformed bar due to bond transfer to the surrounding concrete in between the primary cracks. A secondary transverse network of cracks may grow from the splitting crack due to insufficient concrete cover. As shown in Figure 2-4, with increasing distance away from the crack, the concrete stress is less than the cracking strength f_{cr}. The concrete stress will increase until at some distance, l_t, the stress distribution remains unaffected by the crack. The length l_t is often

referred as the 'transfer length'. This l_t is defined as the distance at which there is a significant change in the bar strain distribution. This means that the crack influence on the stresses in the concrete is within a distance $\pm l_t$ of the crack location. Hence, the next crack to develop should form outside the l_t. The new crack can form anywhere else and so the spacing between the cracks cannot be less than l_t. Successive further cracks can form until there remains no part of the member where the stress has not been reduced by cracking. When this occurs, the resulting pattern is the so called 'stabilized crack pattern'.

The average crack width w_m of a crack is:

$$w_m = S_{rm}\zeta\varepsilon_{b2} = S_{rm}\varepsilon_m \tag{2.3}$$

where S_{rm} is the average crack spacing; and ε_m is the average tensile strain of the member, which is often referred to as member strain (Beeby 1972; Somayaji and Shah 1981).

The S_{rm} depends on the bond properties, amount of cover to the reinforcement, and shape of distribution of tensile stress over the section. The next section covers a review of several proposed equations to predict crack width and spacing based on the results of different experimental investigations in the literature.

2.3 Cracking Research on Steel-Reinforced Concrete

Most of the early work was conducted on plain bars and is no longer relevant with the current use of deformed bars. However, it forms the basis for most of the assumptions that are currently used.

The earlier work by Watstein and Parsons (1943) concluded that the major factor affecting the crack width and spacing for steel RC is the bar diameter to reinforcement ratio, (d_b / ρ_s), upon which the researchers proposed Eq. (2.4) that is only applicable for axially RC members.

$$w_m = C_1 \frac{d_b}{\rho}\left[f_s - C_2\left(\frac{1}{\rho_s} + n_s\right)\right] \tag{2.4}$$

where w_m is the mean crack width; C_1 and C_2 are coefficients that depend upon the distribution and magnitude of bond strength and tensile strength of concrete; f_s is the stress in the reinforcement, and n_s is the modular ratio.

Clark (1956) assumed that the crack width is proportional to $(d_b / \rho_s)(h - d)$ for flexural members instead of (d_b / ρ_s) proposed by Watstein and Parsons (1943) for direct tension, where h is beam height; and d is the effective depth of longitudinal reinforcement.

Chi and Kirestian (1958) investigated the effect of concrete compressive strength on the cracking behaviour. It was concluded that for a concrete compressive strength range of 14 – 41 MPa (2000 – 6000 psi), crack widths are practically independent of the concrete strength. The most important aspect of their research is that they introduced the concept of an "effective area", A_{eff} resisting the cracking, which is the area of concrete surrounding the reinforcing bar. The concept of the A_{eff} is described in the next paragraph.

The transfer of force between concrete and steel occurs at the interface between them through bond. The stress that develops in the concrete at a section is non-uniformly distributed over the net cross sectional area A_c. The stress values of concrete at different locations are dependent on the distance to the reinforcing bar. Maximum

stress values occur in the region adjacent to the steel, and decrease off farther away from the bar. This A_{eff} is less than the total area of concrete in tension. Chi and Kirestian (1958) assumed that the A_{eff} in tension is nearly $(16\ d_b)^2$. Later, several codes, such as the CEB-FIP (1990) and NBR (1992), adopted this fact and described a zone of effective concrete which may carry tensile force. As shown in Figure 2-5, the effective zone of tension surrounding each longitudinal reinforcing bar is commonly taken as a maximum of $(15\ d_b)^2$. The tensile stress carried in this effective concrete area is assumed to be uniformly distributed. When the net concrete area of the section is less than the A_{eff}, then A_{eff} is taken as equal to the net area, or $A_{eff} = A_c$. Overlapping effective zones of tension, which may result from adjacent longitudinal bars, are shared between the two adjacent bars.

With the evolution of high strength deformed bars in the late 1950s, more research was conducted by Watstein and Mathey (1959) and Hognestad (1962). By testing steel-RC beams, Hognestad (1962) concluded that: (1) both maximum and average crack widths are proportional to steel stress, (2) deformed bars are much better in controlling cracks than plain bars, (3) crack width is less dependent on bar diameter for deformed bars, (4) crack width is independent of concrete compressive strength, (5) concrete cover strongly affects the crack widths, and (6) the best control of cracks is obtained by appropriate distribution of reinforcing bars over effective area in tension.

Broms (1965) tested 37 tension members and 10 flexural members reinforced with a single high strength steel bar. It was found that the average crack spacing S_{rm} is closer to twice the cover thickness. Broms assumed that the elongation of concrete between cracks is small in

comparison to that of reinforcement and can be ignored. Broms assumed the following equations for S_{rm} and w_m:

$$S_{rm} = 2t \tag{2.5}$$

$$w_m = S_{rm}\varepsilon_s \tag{2.6}$$

where t is the distance form the center of reinforcing bar to the nearest concrete surface.

Gergely and Lutz (1968) performed a statistical analysis of different crack width equations. This study was performed due to the large scatter in the predictions of the equations available at that time. It was concluded that steel stress is the most important factor that influences the crack width. Equation (2.7) proposed by the researchers was later adopted by the ACI 318 committee to calculate w_{max} as follows:

$$w_{max} = 2.2\beta\varepsilon_{scr}\sqrt[3]{t_b A_{eff}} \tag{2.7}$$

where t_b is the bottom cover measured from the center of the lowest bar; A_{eff} is the effective concrete area around a single bar; ε_{scr} is the strain in the reinforcing bar at the crack location; and β is the factor accounting for strain gradient.

Desayi and Kulkarni (1976) proposed a crack spacing model (Eq. 2.8) based on equilibrium and compatibility relations for steel-RC. The importance of this model is that it accounts for the effect of transverse bars on the crack spacing, by introducing two terms in the denominator; namely, term A = $\pi d_{b1} k_b \tau_{bu}/b_{s1}$ and term B = $d_{b2} f_{bb}/b_{s2}$.

$$S_{rm\ 1}=\frac{k_t f_t' A_{ct1}}{\left(\pi d_{b1} k_b \tau_{bu}/b_{s1}\right)+\left(d_{b2} f_{bb}/b_{s2}\right)} \tag{2.8}$$

where d_{b1} and d_{b2} are the bar diameters in longitudinal and transverse directions, respectively; b_{s1} and b_{s2} are the rebar spacings in longitudinal and transverse directions, respectively; τ_{bu} is the maximum bond stress; k_t is the tensile stress factor which depends on the distribution of tensile stress on the concrete area A_{ct1}. The k_t is assumed equal to unity for a uniform tensile stress distribution. The k_b is a constant that depends on the surface characteristics of the bar. Desayi and Kulkarni (1976) defined f_{bb} as the bearing stress exerted by a transverse bar on the concrete as the magnitude of this stress may also depend on the distance of the bar from the existing crack. However, it was found that it is difficult to estimate such an amount of stress, thus for the sake of simplicity, it was assumed that on average, this bearing stress on all bars in crack spacing length is half of the tensile strength of concrete.

Leonhardt (1977) found that stress in steel increases suddenly after the cracking of concrete due to its tensile strength being exceeded by the stress due to the applied loads. If the sudden increase of steel stress is large, it may result in bond-slip and thus the resulting cracks can be due to a combination of bond-slip and internal cracking. Leonhardt assumed the following equations to find a value for S_{rm} and w_m:

$$S_{rm}=\frac{1}{2}l_o+l_t \tag{2.9}$$

where l_o is the length of "almost no bond stress", and is given by the following equation:

$$l_o = \frac{f_{s2,cr}}{6500} d_b \tag{2.10}$$

where $f_{s2,cr}$ (psi) is the stress in steel at the cracked section immediately after cracking.

The l_t represents active bond stress length, where it can be calculated from the following expression:

$$l_t = K_1 + 0.1\frac{d_b}{\rho_s} \tag{2.11}$$

where K_1 is a factor that depends on the minimum concrete cover and the spacing between the longitudinal reinforcement. The w_m is given by:

$$w_m = l_o \varepsilon_{s2} + l_t \varepsilon_m \tag{2.12}$$

where ε_{s2} is the steel strain at the cracked section; and ε_m is the average strain measured over the cracks defined as follows:

$$\varepsilon_m = \varepsilon_s \left[1 - \left(\frac{f_{s2,cr}}{f_{s2}} \right)^2 \right] \tag{2.13}$$

where $f_{s2,cr}$ is the stress in steel at the crack; and $f_{s2} = N/A_s$ (where N and A_s are the axial tension force and steel area, respectively).

Beeby (1972, 1979) proposed the following expressions for S_{rm} and w_m:

$$S_{rm} = \left[1.33 \cdot c_c + 0.88\frac{d_b}{\rho_s} \right] \tag{2.14}$$

$$w_m = S_{rm}\varepsilon_m = S_{rm}\left(\varepsilon_{s2} - \frac{Kf_t' f_{s2,cr}}{E_s \rho_s f_{s2}}\right) \tag{2.15}$$

where ε_m is the average gross strain; and K is a constant depending upon the type of bar.

Rizkalla and Hwang (1984) tested several steel-RC specimens under tension and compared their results with equations proposed by Leonhardt (1977) and Beeby (1979). It was concluded that Eqs. (2.13) and (2.15) may underestimate the average gross strain after cracking of concrete. Rizkalla et al. (1983) also studied the effect of transverse bars on the cracking behaviour of the tension specimens. It was found that the transverse bars act as crack initiators, and thus influence the crack spacing. The researchers modified the Leonhardt (1977) equations to reflect their experimental data and also to consider the effect of transverse bar spacing as follows:

$$S_{rm} = \left[(d_b - 7.2) + 1.33 \cdot c_c + 0.08\frac{d_b}{\rho_s}\right] \tag{2.16}$$

To account for the effect of transverse bar spacing, S_R; Eq. (2.16) is multiplied by a factor β, where $\beta = 0.96/R^{0.02}$, so that:

$$R = \frac{S_R}{S_{rm}} \tag{2.17}$$

Based on several tests on steel-RC members subjected to tension, Haqqi (1983) introduced a crack spacing model (Eq. 2.18) analogous to the Leonhardt (1977) model. However, it is in terms of the square of c_c / d_b as follows:

$$S_{rm}=0.06\cdot\left(\frac{c_c}{d_b}\right)^2+0.11\frac{d_b}{\rho_s} \tag{2.18}$$

Several building codes have adopted the concept of combining bond-slip and internal cracking failure as presented by Leonhardt (1977) and its derivatives. Some modifications have been incorporated to reflect more experimental data. For instance, the NBR (1992) building code assumed the following form to calculate the S_{rm}:

$$S_{rm}=2\cdot\left(c_c+\frac{s_b}{10}\right)^2+k_1k_2\frac{d_b}{\rho_{eff}} \tag{2.19}$$

where c_c is the clear concrete cover; s_b is the longitudinal bar spacing (not greater than 15 d_b); k_1 is the bar surface characteristic coefficient as mentioned; k_2 is a coefficient that takes into account the strain distribution over the cross section: $k_2=0.125\left(\frac{\varepsilon_1+\varepsilon_{II}}{\varepsilon_1}\right)$. The effective reinforcement ratio ρ_{eff} is the ratio of the steel reinforcement area A_s to the A_{eff}. The A_{eff} is calculated according to Figure 2-6, and described as the part of the tensile zone that is assumed to contribute effectively to resist tensile forces transferred from the reinforcement to the concrete by bond.

The EC2 (2004) adopted the following equation to calculate S_{rm}:

$$S_{rm}=2c_c+k_1k_2\frac{d_bA_{eff}}{4A_s} \tag{2.20}$$

where d_b is the bar diameter; c_c is the clear concrete cover; k_1 is a coefficient that depends on the bond quality: equal to 0.8 for high bond bars and 1.6 for plain bars. For cracking due to restraint (shrinkage), k_1 is multiplied by 0.8, and k_2 is a coefficient that depends on the shape of the strain diagram. Thus, k_2 is equal to 0.5 in case of flexural members, i.e. bending moment without axial force, while it is equal to 1.0 in case of axial tension. In the cases of eccentric tension: $k_2=(\varepsilon_1+\varepsilon_2)/2\varepsilon_1 \quad (\varepsilon_1 > \varepsilon_2)$, and A_s is the steel area. The A_{eff} is calculated based on an effective concrete tension zone of 15 d_b around each steel bar.

Frosch (1999) recognized that thick concrete covers and corrosion protection techniques are currently being used in RC structures. Frosch proposed the following model to determine the w_{max} for uncoated and coated reinforcements:

$$w_{max}=2\frac{f_s}{E_s}\beta\sqrt{d_c^2+\left(\frac{s_b}{2}\right)^2} \tag{2.21}$$

where β is a factor to account for strain gradient; f_s is the reinforcement stress at service loads; d_c is the distance from the extreme fibre in tension to the center of the reinforcing bar that is closest to the surface; and s_b is the bar spacing. Frosch proposed the following equation to calculate the permissible s_b:

$$s_b = 12\alpha_s\left(2 - \frac{d_c}{3\alpha_s}\right) \qquad (2.22)$$

where α_s is a reinforcement factor = $(36/f_s)\gamma_c$. Here, γ_c reinforcement coating factor: 1.0 for uncoated reinforcement; 0.5 for epoxy-coated reinforcement.

Instead of placing a limit on the maximum crack width w_{max}, the ACI 318 (2005) building code adopted a major change by limiting the spacing of reinforcement for crack control. Hence, the code limits the reinforcement spacing to be:

$$s_b = \frac{540}{f_s} - 2.5c_c \qquad \text{(Imperial)} \qquad (2.23)$$

where f_s (ksi) is the calculated stress in reinforcement at service load; and c_c (in.) is the clear concrete cover from the nearest surface in tension to the tension reinforcement.

2.4 Tension Stiffening of Steel-Reinforced Concrete

There are many models that have been proposed to define the tension stiffening behaviour for steel-RC found in the literature. Due to the large volume of work, a complete list is not possible. Only the key research work is summarized in the following paragraphs.

Branson (1977) proposed an approach to incorporate the tension stiffening effect in flexural members through introducing the definition of effective moment of inertia I_e that gradually decreases to the fully cracked moment of inertia I_{cr}. This approach was subsequently adopted by both the ACI 318 (2005) and CSA A23.3 (2004) for deflection calculations.

$$I_e = \left(\frac{M_{cr}}{M_a}\right)^3 I_g + \left[1 - \left(\frac{M_{cr}}{M_a}\right)^3\right] I_{cr} \leq I_g \tag{2.24}$$

where M_{cr} is the cracking moment; M_a is the applied moment; and I_g is the gross moment of inertia.

A more general approach known as the 'load sharing approach' is explained by Collins and Mitchell (1991), in which the tensile force is carried by both the reinforcement and concrete. This is based on an effective stress strain relation for concrete in tension. In this case, by plotting the average tensile stresses carried by concrete, the concrete stress gradually decreases in the post cracking range, which represents the gradual reduction in stiffness as cracking progresses. Figure 2-7 shows an ascending branch for the pre-cracking, and a descending branch for the post-cracking failure. The descending branch represents the degradation in the concrete stress that can be carried by concrete as the cracks progress. This approach was initially proposed by Scanlon and Murray (1974) who suggested a step wise reduction in the effective stress strain relation for concrete in tension after cracking. Similar models were proposed by Lin and Scordelis (1975) and Damjanic and Owen (1984).

Based on extensive tests conducted on steel-RC panels under in-plane stresses, Vecchio and Collins (1986) and Collins and Mitchell (1991) proposed the following model to estimate the average tensile stress f_{ct}.

$$f_{ct} = \frac{\beta_1 \beta_2 f_{cr}}{1 + \sqrt{500 \varepsilon_{ct}}} \tag{2.25}$$

where β_1 is a factor that accounts for bond characteristics; β_2 is a factor accounting for sustained or repeated loading; and ε_{ct} is strain in concrete caused by stress.

Abrishami and Mitchell (1996) found that the tension stiffening effect decreases as the bar diameter is increased. Larger bar sizes result in more splitting cracks that appear, showing a reduction in tension stiffening. It was found that splitting cracks are significant when the cover-bar diameter (c_c/d_b) ratio is less than 2.50. Thus, the researchers proposed a modification to Eq. (2.25) to be as follows:

$$f_{ct} = \frac{\beta_1 \beta_2 \beta_3 f_{cr}}{1+\sqrt{500\varepsilon_{ct}}} \tag{2.26}$$

where β_3 is a splitting crack factor.

Link et al. (1989) derived a biaxial tension-stiffening model shown in Eq. (2.27) that accounts for multiple generally oriented reinforcing layers and cracks. The model was based on assuming an equivalent reinforcing ratio normal to the crack, which maintains strain compatibility with the actual layers. However, the bond slip was not accounted in the proposed model which is as follows:

$$f_{ct} = f_t' \left(\frac{f_{seq}^{cr}}{f_{seq}} \right) \tag{2.27}$$

where f_{seq}^{cr} and f_{seq} are, respectively, the equivalent layer stresses at cracking and the current equivalent layer stresses, assuming no bond contribution.

Stevens et al. (1991) extended the work of Vecchio and Collins (1986) and proposed a constitutive model for finite element analysis of two-dimensional RC structures. In the proposed model, the average tensile stress in the concrete reduces exponentially from f_{cr} at cracking to a limiting value of αf_{cr} at large tensile strains. The parameter α is a function of the reinforcing ratio and distribution. The equation proposed to model the uniaxial concrete tensile response after cracking is as follows:

$$f_{ct} = f_{cr}\left[(1-\alpha)e^{-\lambda_t(\varepsilon_t-\varepsilon_{cr})}+\alpha\right] \tag{2.28}$$

where λ_t is the parameter that controls the rate at which the response decays to the limiting value. The proposed model was extended to biaxial behaviour by modifying the value of α to account for the orientation of the principle tensile strain direction relative to the various contributing groups of reinforcement.

Marzouk and Chen (1993) studied the behaviour of HSC steel-RC slabs, from which, the researchers proposed Eq. (2.29) to define the tension stiffening of HSC slabs. The relationship was based on an idealization of tension softening behaviour measured from direct tension tests of HSC specimens. The relation was further calibrated to account for the tension stiffening behaviour. The calibration was done by modifying two incorporated parameters; namely, α and β, according to the reinforcement ratio.

$$f_{ct} = \frac{f_t'(\varepsilon_t/\varepsilon_{to})}{\alpha((\varepsilon_t/\varepsilon_{to})-1)^{\beta}+(\varepsilon_t/\varepsilon_{to})} \tag{2.29}$$

where ε_t is the concrete tensile strain; and ε_{to} is the concrete tensile strain at f_t'.

The influence of using HSC concrete on tension stiffening was further studied by other researchers. Lorrain et al. (1998) conducted an experimental program to describe the effects of HSC (f_c' up to 100 MPa) on the cracking and tension stiffening behaviour of steel-RC ties. The researchers concluded that tension stiffening effect is greatly improved at the crack formation phase and tends to decrease during the stabilized phase, due to bond damage between the steel and HSC. However, the crack spacing is not significantly influenced due to higher concrete strength; but it is more influenced by the change in the reinforcement ratio.

Fields and Bischoff (2004) also studied the effect of using HSC on the tension stiffening and cracking of steel-RC members subject to uniaxial tension. It was found that HSC specimens exhibit larger crack spacing than NSC. In addition, the HSC specimens exhibit larger amounts of tension stiffening than the companion NSC specimens. After a significant deformation in the post-cracking range, the tensile response of the HSC specimens approached that of the NSC specimens. It was concluded that as the bar diameter increases, the beneficial influence of HSC on tension stiffening is reduced.

Mitchell et al. (1996) studied the effect of epoxy coated reinforcement on tension stiffening and cracking of RC. The experiments were conducted using uniaxial steel-RC tension members made of NSC ($f_c' = 30 \sim 35$ MPa) and HSC ($f_c' = 66 \sim 90$ MPa). The researchers concluded that specimens reinforced with epoxy coated bars show larger crack widths than specimens reinforced with uncoated bars. There was no

significant difference in the tension stiffening between the epoxy coated reinforced specimens and the uncoated ones. The researchers also found that specimens made with NSC and HSC show the same degree of tension stiffening. HSC resulted in smaller crack widths compared to those developed in NSC specimens.

Cho et al. (2004a, 2004b) conducted an experimental investigation on steel-RC panels subjected to biaxial tension. The researchers used the behaviour and theory of RC members subjected to uniaxial tension, to derive a stress-strain relationship of concrete in biaxial tension. The researchers defined the tension stiffening behaviour of the tested panels under uniaxial and biaxial tension by adopting the model proposed by Okamura et al. (1985) (Eq. 2.30). Earlier, this model was found applicable to steel-RC panels subject to in-plane stresses, including shear (Belarbi and Hsu 1994; Hsu and Zhang 1996). Cho et al. (2004b) proposed a modification in this model to reflect lower tensile stresses experienced under biaxial tensile loads.

$$f_{ct} = f_{cr}\left(\frac{\varepsilon_{cr}}{\varepsilon_c}\right)^c \tag{2.30}$$

where ε_c is the strain in concrete caused by stress; ε_{cr} is the cracking strain; and c is a stiffening parameter that represents the inclination in the stress-strain descending branch and depends on the surface characteristics of the bar (equal 0.40 for steel deformed bars).

2.5 Background on FRP Composites

FRP composites is defined as a polymer (plastic) matrix, that is reinforced (combined) with a fibre or other reinforcing material with a sufficient aspect ratio (length to thickness) to provide a discernable reinforcing function in one or more directions (ACMA 2008). The fibres

provide strength and stiffness to the composite and generally carry most of the applied loads. The matrix acts to bond and protect the fibres and provides transfer of stress from the fibre through shear stresses. The most common fibre types are glass (GFRP), carbon (CFRP), and aramid (AFRP). The matrix types are typically epoxies, polyesters, vinylesters, or phenolics.

Glass has been the predominant fibre for many civil engineering applications because of an economical balance of cost and specific strength properties. Glass fibres are commercially available in E-glass, which is the most widely used form of composite reinforcement. E-glass fibres have high electrical insulating properties, low susceptibility to moisture, and high mechanical properties. Glass is generally a good impact-resistant fibre, but denser than carbon or aramid (ACI 440R 2007).

FRP bars are commonly manufactured by pultrusion, which is a technique for manufacturing continuous lengths of FRP bars that are of constant or nearly constant profile. The pultrusion process can be used to make FRP products with different profiles, such as rods, beams, channels, plates, etc. FRP bars are produced in various cross-sectional shapes, such as round, square, rectangular, or as a reinforcing grid (Figure 2-8). The resin surrounding the fibres generally provides fairly smooth surface characteristics. Thus, to improve the bond to concrete characteristics, the surface of the bars is usually sand coated, ribbed, helically wrapped, or braided.

2.5.1 FRP reinforcement material characteristics

FRP composites are different from traditional construction materials, such as steel or aluminum. The FRP bars are anisotropic, with the longitudinal axis being the strong axis.

Unlike steel, FRP composites may vary significantly from one product to another. Factors, such as volume and type of fibre and resin, fibre orientation, dimensional effects, and quality control, play a major role in establishing product characteristics. The mechanical properties of FRP composites, like all structural materials, are affected by factors, such as moisture, ultraviolet rays, loading history and duration, and fire and temperature (ACI 440 1996; ISIS 2001).

Tensile strength - FRP bars and tendons do not exhibit any plastic behaviour (yielding) up to their ultimate tensile strength. Figure 2-9 shows typical stress-strain relationships for different types of FRP reinforcement where such a relation is linear up to failure.

Tensile elastic modulus - The tensile elastic modulus of GFRP bars is approximately 25% that of steel. GFRP bars usually have tensile elastic modulus in the range of 40 to 55 GPa. However, CFRP tendons, which usually employ stiffer fibres, have higher modulus than that of GFRP bars by approximately three times (ISIS 2001).

The tensile strength and modulus of elasticity (stiffness) are found to be dependent on different factors, such as the fibre ratio, fibre type, bar diameter, and manufacturing conditions (Wu 1990; ACI 440.1 2001). In general, glass fibre polymers achieve the lowest strength, while carbon and aramid fibre polymers achieve higher strength (ISIS 2001). The bar diameter affects the tensile properties; as smaller bars are more efficient. This is attributed to what is known as shear lag, where fibres near the outer surface are stressed more than those near the center of the bar (Faza 1991; ACI 440.1 2003).

Compressive strength - FRP bars are weaker in compression than in tension. This is the result of difficulties in accurately testing unidirectional composites in compression. The difficulties are due to gripping and aligning procedures, and the stability effects of fibres. Compressive strength in the range of 317 to 470 MPa has been reported for GFRP bars having a tensile strength in the range of 552 to 896 MPa (Wu 1990).

Compressive elastic modulus - The compressive elastic modulus varies with FRP bar size, type, quality control in manufacturing, and length-to-diameter ratio of the specimens. In general, the compressive modulus of elasticity is approximately 70 to 80% of the tensile modulus of elasticity (Bedard 1992; Challal and Benmokrane 1993).

Shear strength - In general, shear strength of composites is very low. This shortcoming can be overcome in most cases by orienting the FRP bars such that they will resist the axial loads through axial tension (ACI 440 1996; ISIS 2001).

2.5.2 Concrete-GFRP bond characteristics

The tension force is transferred to the reinforcement through the bond between the reinforcement and the surrounding concrete. Bond stresses exist whenever the force in the tensile reinforcement changes. Bond between FRP reinforcement and concrete is developed through a mechanism nearly similar to that of steel reinforcement and depends on FRP bar type, elastic modulus, and surface deformation (ACI 440.1 2006). The main differences in the mechanics of stress transfer between GFRP and steel arise due to the fact that steel is completely homogenous, but GFRP bar has a fibre reinforced plastic core. This core is enveloped by resin rich outer layers that could be embedded sand particles or glass fibres

wound spirally in order to create undulations on the surface of the bar, which results in the following main differences as observed in several studies (Uppuluri et al. 1996; Cosenza et al. 1997; Kanakubo et al. 1993; Makitani et al. 1993; Faza and GangaRao 1993; Malvar 1995; Tighiouart et al. 1998):

- Steel reinforcement does not experience significant chemical adhesion to concrete, but commercially available GFRP reinforcing bars generally have good adhesion due to sand particles. The bond of GFRP bar to concrete depends mainly on adhesion and friction, while the load transfer through mechanical bearing depends on the surface deformations of the GFRP bar. However, for steel, it depends mainly on the mechanical bearing for transferring bond.

- The resin-dependent strength may be lower than the concrete compressive strength, resulting in a different bond interaction from the steel reinforcement with failure damage of ribs instead of cracking of concrete. Therefore, the failure stresses and strains in the longitudinal and transverse directions are very influential on bond behaviour.

Some researchers showed that the bond strength increases with increasing the concrete compressive strength (Rossetti et al. 1995). This increase depends on the surface characteristics of bars. The GFRP smooth bars are inadequate for use in RC structures as low values of bond strength appear in the bond-slip curves. This is attributed to the activation of a friction mechanism with substantial damage of bar surface, without cracks in the surrounding concrete (Cosenza et al. 1997; Nanni et al. 1995). Cosenza et al. (1997) explained that for the case of smooth FRP bars, the bond was found to be dependent on fibre and resin properties, whereas it

is not affected by concrete strength. However, for the case of deformed FRP bars, the bond strength was observed to be dependent on the concrete compressive strength. This is only the case when a bar possesses adequate characteristics to provide enough lateral confinement through bearing ribs and the mechanical interlock mechanism.

Benmokrane et al. (1996a) conducted pullout and beam tests on GFRP-RC. The investigators found that the bond strength of GFRP is nearly equal to 60% to 90% that of traditional steel bars. It was concluded that the distribution of tensile and bond stresses along the embedment portion of GFRP reinforcing bars is nonlinear and similar to that of steel reinforcing bars. The bond stresses were found to be exponentially distributed along the embedment length before de-bonding. Tighiouart et al. (1998) also reported that GFRP bars show lower bond strength values by about 30% compared to the steel rebars. Malvar (1994, 1995) found that the GFRP bond strength increases with increasing the confining pressure around the bar, which is usually linked to the concrete c_c/d_b.

It was also found that the bond strength of GFRP decreases with increasing the bar diameter (Benmokrane et al. 1996a; Tighiouart et al. 1998; Achillides and Pilakoutas 2004). This characteristic is attributed to: (1) the embedment length effect, as large bar diameters require longer embedment lengths to develop the same normal bond stress; (2) Poisson's ratio effect, as it can lead to slight reductions in the bar diameter as a result of longitudinal stress. The reduction in bond strength increases with bar size, which could lead to reduced frictional/mechanical-locking stresses; (3) shear-lag effect, which occurs in larger diameters between fibres in core and the fibres in the outer diameter of the bar; and (4) top bar effect, as

larger diameters of the bar result in higher quantities of bleeding water trapped beneath the top bars, creating greater voids that reduce the contact interface between the bar and concrete.

2.6 Cracking Research on GFRP Reinforced Concrete

Most of the research related to cracking is based on testing flexural members. The early experimental research conducted by Nawy and Neuworth (1971) showed that GFRP-RC simply supported beams developed three to five times more cracks than in the corresponding reference steel-RC beams. It was suggested that due to good bond at the interaction surface between GFRP bars and concrete, a larger number of well-distributed cracks is formed. Later, Nawy and Neuworth (1977) found that beams with lower percentages of GFRP reinforcement develop very few cracks whereas specimens with greater amounts of reinforcement develop larger numbers of considerably narrower cracks. The researchers proposed a modification to the ACI 318 (1971) equation, which was based on the Gergely and Lutz (1968) equation, when applied to FRP-RC as follows:

$$w = 0.002 f_f \sqrt[3]{d_c A_e} \tag{2.31}$$

where f_f is the FRP reinforcing bar stress; d_c is the concrete cover measured from the center of tension reinforcement; and A_e is the effective tension area of concrete surrounding the flexural tension reinforcement.

Based on tests of FRP-RC beams, Daniali (1990) showed that the amount of FRP reinforcement required to meet the serviceability requirements must be at least three times more than that for steel. Confirming this conclusion, Faza and Gangarao (1992) found that the existing ACI 318 equation of crack width is invalid, since the modulus of elasticity of FRP is

approximately four times smaller than that for steel. The researchers proposed the following expression to estimate the w_{max}:

$$w_{max} = \left(\frac{f_f}{E_f}\right)\left(\frac{2 f_t' A_e}{\tau_{bu} \pi d_b}\right) \tag{2.32}$$

where f_f is the maximum stress in the FRP reinforcement at service level load; A_e is the effective tension area surrounding the principal reinforcement divided by the numbers of bars; E_f is the elasticity modulus of FRP bars; f_t' is the tensile strength of concrete; τ_{bu} is the maximum bond stress; and d_b is the bar diameter.

Benmokrane et al. (1995) investigated the effect of the beam span-to-depth ratio and surface deformation of GFRP bars on the flexural behaviour of concrete beams. The results were compared to steel-RC beams. The tests results showed that cracking in the flexural span was mostly vertical, but at higher loads, shear stress induced inclined cracks. Cracks formed in the GFRP-RC specimens were wider than those formed in the steel-RC specimens.

Mahmood (2002) tested six concrete prisms reinforced with GFRP-bars (C-bar type) of the same dimensions as those tested by Jaccoud (1987) as shown in Figure 2-10. The specimens had a total length of 2500 mm with a tension zone length that was equal to 1000 mm for the measurements. Tests were conducted under axial imposed strain conditions. It was concluded that there was no substantial difference in the width of the first crack for both steel and GFRP in the range of the strains that are commonly encountered in practice (i.e. up to ~ 1000 με). It was also found that the w_{max} decreased with an increase in the reinforcement ratio. The experimental results showed that the first cracks initiated at the same imposed strain for both

steel and GFRP. Finally, the researcher concluded that the crack spacing did not vary with the change of reinforcing material.

Recently, Ospina and Bakis (2006) recognized the changes in the ACI 318 (2005) code, where a crack spacing parameter was introduced for the first time. The researchers proposed an alternative model for flexural crack control of FRP-RC members. The following expression was proposed to determine the maximum bar spacing s of FRP bars in FRP-RC beams and one-way slabs:

$$s = 0.8\frac{E_f}{f_f k_b} - 2.5c_c \leq \frac{E_f}{f_f k_b} \tag{2.33}$$

where f_f and E_f are the reinforcing bar stress and bar modulus of elasticity, respectively; c_c is the concrete cover; and k_b = 1.4 for limiting crack widths of 0.7 and 0.91 mm.

FRP bars are corrosion resistant; therefore, most of the current design guidelines for FRP-RC allow wider cracks. Crack width limitations are introduced only when there are aesthetic reasons, concerns about personal safety, shear effects, and where leakage is a concern. The limits of w_{max} vary, based on different conditions, such as: the exposure type (i.e. internal or external), aggressiveness of the environment, type of structure (whether the intended use of the structure may be affected by cracking), visibility of concrete surfaces, and anticipated life of the structure (ISIS 2001).

The JSCE (1997) considers only aesthetics in setting a maximum allowable crack width of 0.5 mm (0.020 in.). CSA S806 (2002) implicitly allows crack widths of 0.5 mm (0.020 in) for

exterior exposure and 0.7 mm (0.028 in) for interior exposure when FRP reinforcement is used. ACI 440.1 (2006) follows the limits of the CSA S806 (2002).

ISIS (2001) recommends that the width of cracks allowed for FRP-reinforced members to be 1.7 or 1.5 times the value allowed for steel-reinforced members. ISIS (2001) assumes that the ratio between crack widths of FRP and steel-reinforced beams is 5/3. The width of cracks is assumed to be proportional to the strain in the reinforcement. Thus, the allowable strain and stress in the FRP reinforcement at service is:

$$\varepsilon_{frps} = \frac{5}{3}\varepsilon_s = 2000 \times 10^{-6} \tag{2.34}$$

where ε_{frps} is the FRP strain; and ε_s is the allowable steel strain at service load. The maximum strain in FRP, 2000×10^{-6}, is the limiting factor for crack width. When applicable, this strain may be increased up to 3000×10^{-6}.

Some research studies are carried out to identify the applicability of the Gergely and Lutz (1968) equation for FRP-RC (Gao et al. 1998; Masmoudi et al. 1996). ISIS (2001) adopted the Gergely-Lutz (1968) equation (Eq. 2.35) to evaluate the crack width for certain applications. Some modifications were incorporated in the original equation to take into account the bond characteristics of FRP. However, these modifications have been developed for a specific type of FRP reinforcement, and therefore, their use is limited.

$$w = 11\frac{E_s}{E_{frp}} k_b f_{frp} \frac{h_2}{h_1} \sqrt[3]{d_c A_e} \times 10^{-6} \qquad \text{(SI)} \tag{2.35}$$

where E_s is the modulus of elasticity of steel; f_f is the stress in FRP reinforcement at the location of a crack; h_1 is the distance from the centroid of the reinforcement to the neutral axis;

h_2 is the distance from the extreme tension face to the neutral axis; d_c is the concrete cover measured from the center of tension reinforcement; and A_e is the effective tension area of concrete surrounding the flexural tension reinforcement and having the same centroid as that reinforcement, divided by the number of bars. For FRP bars with inferior bond quality, $k_b >$ 1.0, and for FRP bars with superior bond quality, $k_b < 1.0$. Gao et al. (1998) proposed three values for this factor, including 0.71, 1.00, and 1.83, for three different types of GFRP bars.

The ACI 440.1 (2006) adopted the ACI 318 (2005) provisions to control cracking through the maximum reinforcement spacing. This is based on the Frosch (1999) model that modified the empirical equation by Gergely and Lutz (1968). The maximum probable crack width for FRP-reinforced members is calculated using the following expression:

$$w_{max} = 2\frac{f_f}{E_f}\beta k_b\sqrt{d_c^2 + \left(\frac{s_b}{2}\right)^2} \tag{2.36}$$

where f_f is the FRP reinforcement stress; E_f is the reinforcement modulus of elasticity; β is the ratio of distance between the neutral axis and tension face to distance between the neutral axis and centroid of reinforcement; d_c is the thickness of cover from the tension face to center of closest bar; and s_b is the bar spacing. The k_b term is a coefficient that accounts for the degree of bond between the FRP bars and surrounding concrete.

For FRP bars having bond behaviour that is similar to uncoated steel bars, $k_b = 1.0$. For FRP bars having bond behaviour that is inferior to steel, $k_b > 1.0$, For FRP bars having bond behaviour that is superior to steel, $k_b < 1.0$. The ACI 440.1 (2006) recognizes that further research is required to obtain more data for commercially available FRP smooth bars or when

there is unknown information about the FRP bars, so it assumes a conservative value for k_b = 1.4.

2.7 Tension Stiffening of FRP Reinforced Concrete

Serviceability of FRP-RC flexural members is described in terms of deflection and cracking. FRP-RC members have a relatively small stiffness after cracking. Consequently, permissible deflections under service loads can control the design (ACI 440.1 2006). In general, designing FRP reinforced cross sections after concrete crushing failure satisfies serviceability criteria for deflection and crack width (Nanni 1993; GangaRao and Vijay 1997; Theriault and Benmokrane 1998). Deflections should be within acceptable limits imposed by the use of the structure.

The prediction of deflection and crack width for RC flexural members requires proper evaluation of tension stiffening. Thus, tension stiffening behaviour of FRP-RC has been the focus of several research studies carried out mostly on flexural members such as one way slabs and beams.

ACI 440.1 (2006) adopts the ACI 318 (2005) methods to control the deflection of one-way flexural members. This is done by mandating a minimum thickness of the member. Based on work by Ospina et al. (2001), ACI 440.1 (2006) recommends generic values for maximum span ratio limitations corresponding to the limiting curvature associated with the target deflection span-ratio (Eq. 2.37).

$$\frac{l}{h}=\frac{48\eta}{5K_1}\left(\frac{1-k}{\varepsilon_f}\right)\left(\frac{\Delta}{l}\right)_{max} \tag{2.37}$$

where $\eta = d/h$; $k=\sqrt{2\rho_f n_f+\left(\rho_f n_f\right)^2}-\rho_f n_f$; $(\Delta / l)_{max}$ is the limiting service deflection-span ratio; l is span length; h is minimum thickness; and K_1 is a parameter that accounts for boundary conditions.

The above expression is valid for any type of reinforcement. The suggested equation assumes no tensile contribution from concrete between cracks which is referred to as tension stiffening. To consider the effects of tension stiffening, the values resulting from Eq. (2.37) are modified by the ratio of effective and fully cracked moments of inertia computed at service load level. The I_e is calculated based on Branson's equation (1977) developed for steel-RC beams (Eq. 2.24). Branson's equation reflects two different phenomena: variation of EI stiffness along the member and the effect of concrete tension stiffening.

Yost et al. (2003) tested 48 beams reinforced with GFRP bars. Their test results showed that upon cracking, the I_e decayed very quickly from I_g to a level very close to I_{cr}. This means that the transition from gross to cracked section does not occur in the gradual manner as predicted by the current I_e formula (Eq. 2.24). This reduced tension stiffening may be attributed to the lower modulus of elasticity and different bond stress level for the GFRP reinforcement compared with those of steel.

Research done by Toutanji and Saafi (2000) demonstrated that the degree of tension stiffening of GFRP-RC beams is affected by the amount and stiffness of the flexural reinforcement and relative reinforcement ratio (ρ_f/ρ_b); where ρ_b is the balanced reinforcement

ratio. Yost et al. (2003) concluded that because beam stiffness decreases so abruptly upon cracking, the basic nonlinear form of Branson's equation is inherently a poor model for GFRP-RC beams. Gao et al. (1998) also concluded that to account for the reduced tension stiffening in FRP-RC members, a modified expression for the I_e is required. Hence, it was found that Branson's equation in its original form overestimates the I_e of FRP-RC beams, especially lightly reinforced beams, implying a lesser degree of tension stiffening than in comparable steel-RC beams (Nawy and Neuwerth 1977; Benmokrane et al. 1996b; Engel et al. 1999; Toutanji and Saafi 2000). Therefore, ACI 440.1 (2006) adopted a modified expression for Branson's equation, which is given by Eq. (2.38).

$$I_e = \left(\frac{M_{cr}}{M_a}\right)^3 \beta_d I_g + \left[1 - \left(\frac{M_{cr}}{M_a}\right)^3\right] I_{cr} \leq I_g \tag{2.38}$$

where β_d is a reduction coefficient related to the reduced tension stiffening exhibited by FRP-RC members, calculated as:

$$\beta_d = \frac{1}{5}\left(\frac{\rho_f}{\rho_b}\right) \leq 1.0 \tag{2.39}$$

Razaqpur et al. (2000) proposed a method for determining deflections of FRP-RC beams by assuming that the moment curvature relation of FRP sections is linear in the pre-cracked and post-cracked stages and that the tension stiffening effect can be ignored. Bischoff (2005) suggested other methods to calculate the I_e that are not based on Branson's equation.

Few studies have been conducted to investigate the cracking behaviour and tension stiffening of FRP-RC under direct tension. Most of the studies found in the literature examine

the tension-stiffening of FRP-RC using simple uniaxial tension members. Aiello et al. (2002) conducted a preliminary investigation to evaluate the tension stiffening of CFRP-RC under uniaxial tension, from which it was concluded that there is a significant tension stiffening contribution, which is very influential and effective in reducing the strain of CFRP reinforcing bars. It was also concluded that the c_c/d_b influences the tension stiffening. For optimal design, it was recommended to use c_c/d_b value of 3.

Bischoff and Piaxio (2004) tested eight axial tension members reinforced either with a steel or GFRP-bar (C-bar type). All specimens were 1100 mm in length with a typical cross-section of 100 × 100 mm. Three bar diameters were tested; namely, 12.7, 15.9, and 19.0 mm. In contrary to the other discussed research on GFRP-RC beams, the researchers concluded that for any given value of the member strain, the GFRP-RC exhibits greater tension stiffening than the steel-RC (Figure 2-11). The researchers attributed that to the lower GFRP modulus of elasticity. Thus, the bare GFRP response has less inclined slope and more strains can be reached. Therefore, the difference between the member response and GFRP bare bar response, which represents the tension stiffening, is higher than the steel-reinforced member. The researchers also showed that cracks in GFRP-RC develop at much higher strain values than those in steel-RC, resulting in a crack pattern that is not as likely to reach its stabilized stage under service loads. Hence, despite the observed increase in tension stiffening and similarity in the final stabilized crack spacing (for the tests reported in this paper), concrete reinforced with GFRP will have larger crack widths because of both an increase in crack spacing while the cracks are still developing and lower stiffness of the bar. Bischoff and Paixao (2004) proposed a constitutive model for tension stiffening (Eq. 2.40) as follows:

$$f_{ct} = f_{cr} \exp\left[-1100(\varepsilon_m - \varepsilon_{cr})\left(\frac{E_b}{200}\right)\right] \quad (2.40)$$

The model indicates that the effect of modulus of elasticity of the reinforcing bar has a major influence on the tension stiffening response of a GFRP-RC element.

Sooriyaarachchi et al. (2005) conducted an experimental investigation on GFRP-RC uniaxial tension members. Several test parameters were examined, which included the influence of concrete strengths (50 MPa and 90 MPa), reinforcement ratios (0.56% - 1.27%), and bar diameters (13 mm and 19 mm). The GFRP bars used were specially manufactured with internal strain gauges to measure the strain patterns occurring between cracks during direct tension tests. The test results showed that there is an appreciable amount of tension stiffening contribution that exists in GFRP-RC members. This tension stiffening increases with decreasing the reinforcement ratio and increasing the concrete strength. However, the researchers did not observe significant changes in tension stiffening due to changing the bar diameter at a constant reinforcement ratio. It was also concluded that the bond stress distribution suggests that a degree of bond damage takes place initially near the cracks and then progresses along the bar with increasing load. The research also showed the CEB-FIP (1990) model (Eq. 2.41) grossly overestimates the tension stiffening effect, particularly at a low reinforcement ratio. The research also showed that even with the implemented modifications of the ACI 440.1 (2006) to account for the bond, the ACI equation overestimates the tension stiffening effect. Sooriyaarachchi et al. (2007) proposed a modification in the CEB-FIP (1990) model for estimating the tension stiffening by changing the bond degradation factor

k in Eq. (2.41) to account for the difference in the bond behaviour of the GFRP reinforcement as follows:

$$\varepsilon_m = \varepsilon_f \left[1 - k \left(\frac{f_{scr}}{f_f} \right)^2 \right] \tag{2.41}$$

where f_{scr} = rebar stress at crack = $\frac{N_{cr}}{A_f} = f_t' \left(\frac{1}{\rho_f} - 1 + n_f \right)$

Al-Sunna et al. (2006) conducted an experimental investigation on GFRP-RC beams to study their tension-stiffening behaviour. The researchers tested a total of six beams reinforced with GFRP bars. To correlate the beam tests to tension member tests, the beams had a reinforcement ratio of about 0.4% which corresponds to a ratio of about 1.25% for an RC tie in the tension zone. It seems that this was calculated based on an A_{eff} equal to $(15d_b)^2$ that is the used for steel RC. The researchers compared their findings with test results reported by Sooriyaarachchi et al. (2005) who conducted their research on RC members subject to uniaxial tension. It was concluded that in the pre-cracking and crack formation phases, the stress versus average strain relationship for a GFRP-RC tension tie should not be different from that of a steel RC-tie. However, in a flexural member, a tension tie develops progressively under cracking, until it becomes a fully defined tie at the end of the crack formation phase. Hence, the first part of the stress-average strain relationship does not have any resemblance to a tension tie; it is a curve that shows reduction of stiffness as additional cracks form. However, the end of the curve clearly identifies the beginning of the stabilized cracking phase. Therefore, it was concluded that, contrary to the case of steel reinforcement, the amount of GFRP

reinforcement seems to have a negligible effect on tension stiffening in the stabilized cracking phase. The researchers concluded that for a practical range of reinforcement ratios, the stabilized phase can be reasonably estimated by an average modulus of elasticity, which is about 10% higher than the modulus of the bare bar. The researchers observed that tension stiffening is much lower for GFRP than steel bars. This was attributed to the relatively high level of bar strains involved for GFRP.

Nayal and Rasheed (2006) conducted a study to develop effective tension stiffening model parameters for nonlinear analysis of concrete beams reinforced with steel and GFRP bars. The researchers suggested an incremental iterative numerical analysis procedure to study the nonlinear behaviour of beams, in which a tension-stiffening model has a sudden drop at first cracking, followed by a bilinear descending branch. The researchers agreed with the conclusion of Bischoff and Paixao (2004) that GFRP-RC exhibits greater tension stiffening than steel-RC prisms at any level of axial strain. The most significant effect is that GFRP reinforcement, with its lower axial stiffness, offers substantially longer lasting tension stiffening effects due to the lower bond stresses transferred to concrete, leading concrete in between cracks to provide larger stiffening prior to the progressive initiation of secondary cracks. Accordingly, it was concluded that the contribution of tension stiffening to the global response increases for the lower reinforcement stiffness of similar reinforcement ratios. This conclusion defies the notion derived from the term 'stiffening' that a higher ratio of the reinforcement or reinforcement stiffness means higher tension stiffening effects.

2.8 Summary and Conclusions

This chapter presents a general background relevant to this research. GFRP-reinforcement is deemed to be a promising advanced material that could completely substitute steel reinforcement vulnerable to corrosion. Cracking and tension stiffening are two important phenomena that play a major role in the non-linear analysis of RC and establishment of serviceability requirements that include basically, crack width and deflections. The review of the available literature reveals some issues that can be summarized as follows:

1. The main point of agreement between researchers is that the tension stiffening model for FRP bars is likely to be very different from that of steel bars. It also appears that the main factors that influence the tension stiffening behaviour are the reinforcement ratio and bar modulus of elasticity. Most research concludes that GFRP-RC has less tension stiffening contribution, and thus the deflection calculations may be inaccurate using the currently available equations.

2. However, there are also some research which contradicts the above conclusions and shows that GFRP-RC in fact, has a significant tension stiffening contribution (Bischoff and Paixao 2004; Nayal and Rasheed 2006). Kaklauskas et al. (2007) concluded that further research is needed to develop a universal tension stiffening relationship applicable to different reinforcing materials.

3. Most of the available design provisions of FRP-RC focus on the limitations of crack width. To the best of the author's knowledge, there is no available equation that exclusively predicts the crack spacing for FRP-RC. The numerous possible combinations

of resin matrix, fibre and surface treatments have a direct impact on the crack spacing and profile of bond stress between cracks. A generalized approach may need to be established, which relates the cracking to each FRP bar type. The few available studies may not be enough to ascertain the cracking behaviour and tension stiffening mechanism of GFRP-RC that are affected by different parameters.

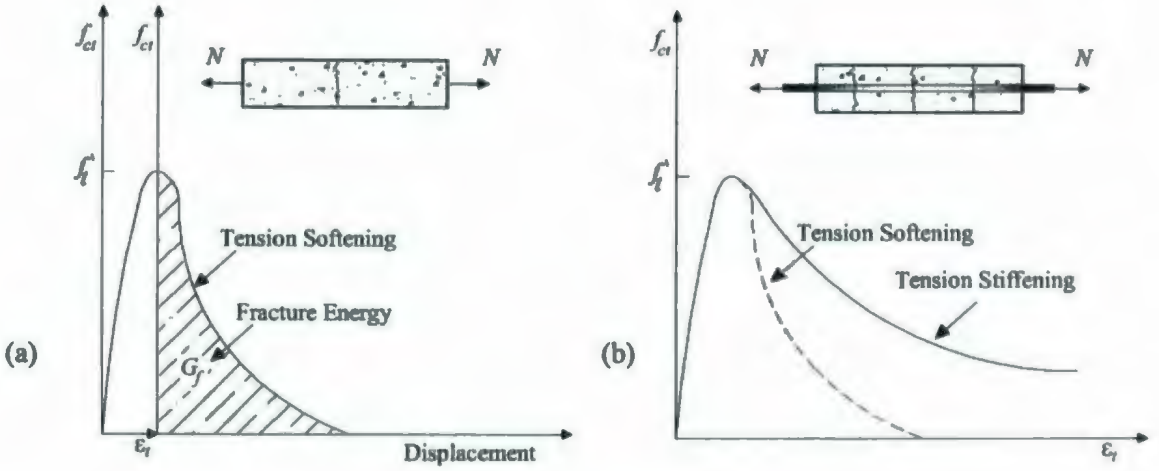

Figure 2-1: (a) Tension softening and (b) tension stiffening response

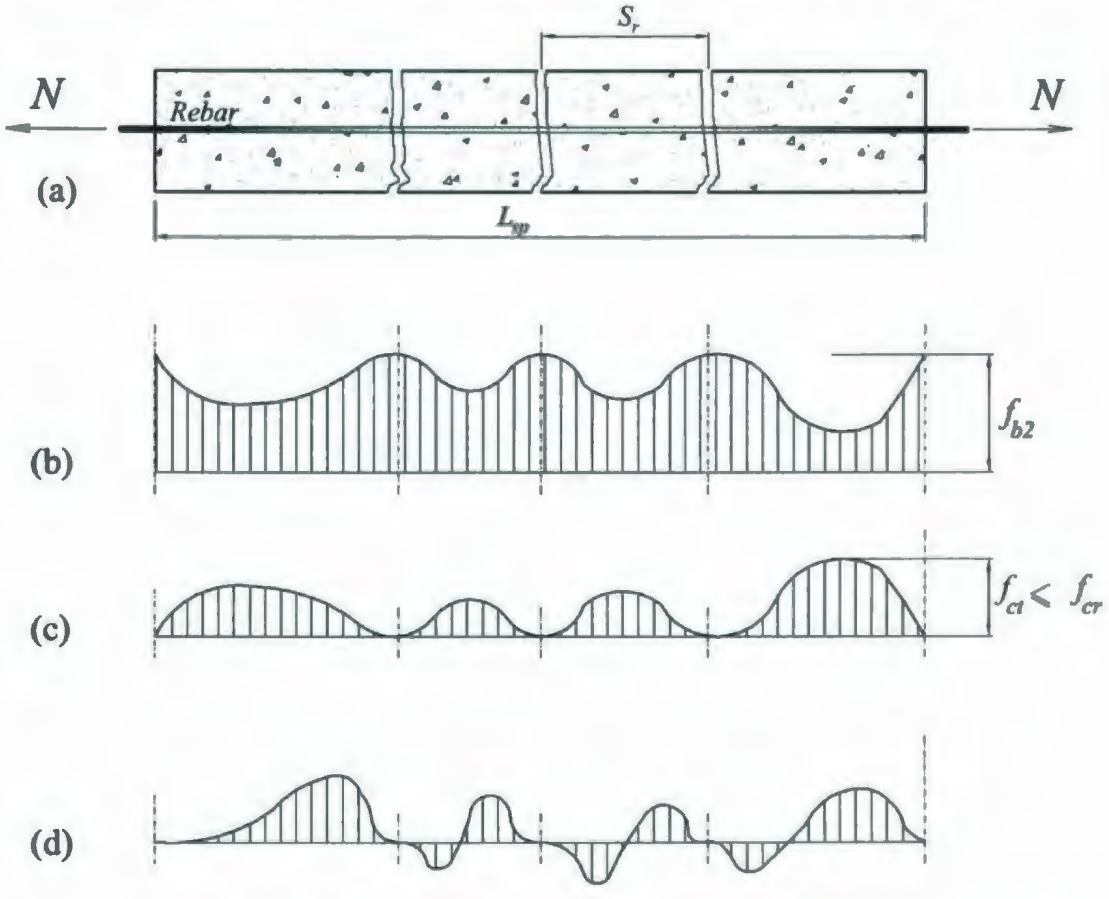

Figure 2-2: Stress in a RC member cracked due to axial forces
(a) cracking of a tie, (b) stress in reinforcement, (c) stress in concrete, and (d) bond stress

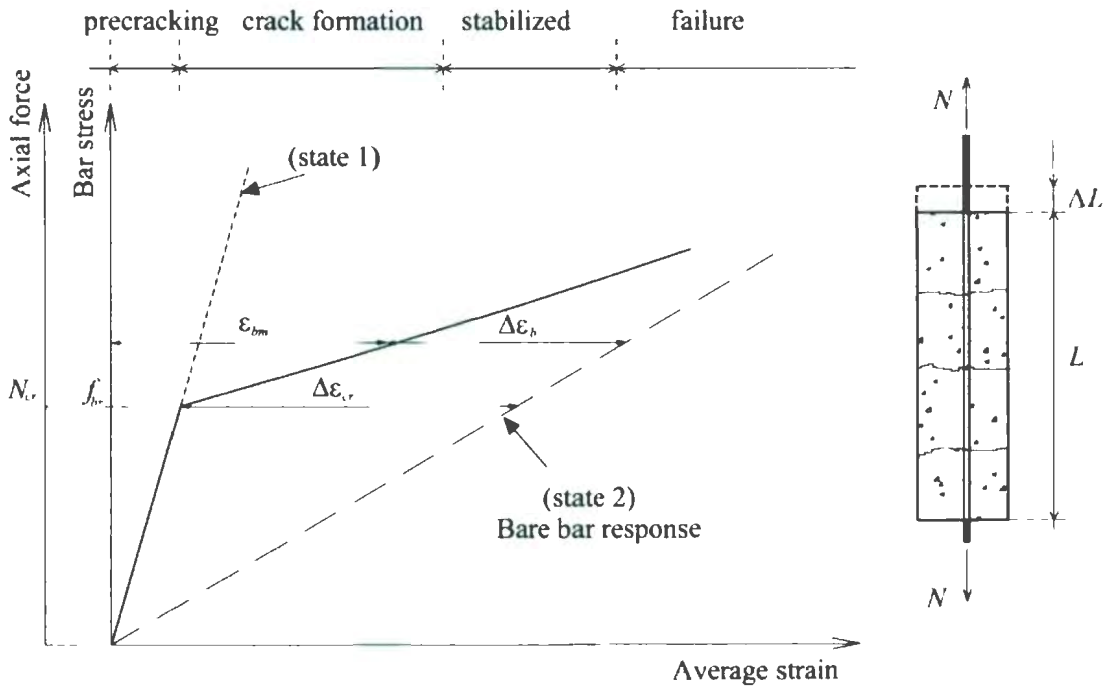

Figure 2-3: Axial force versus average strain in a member subjected to axial tension

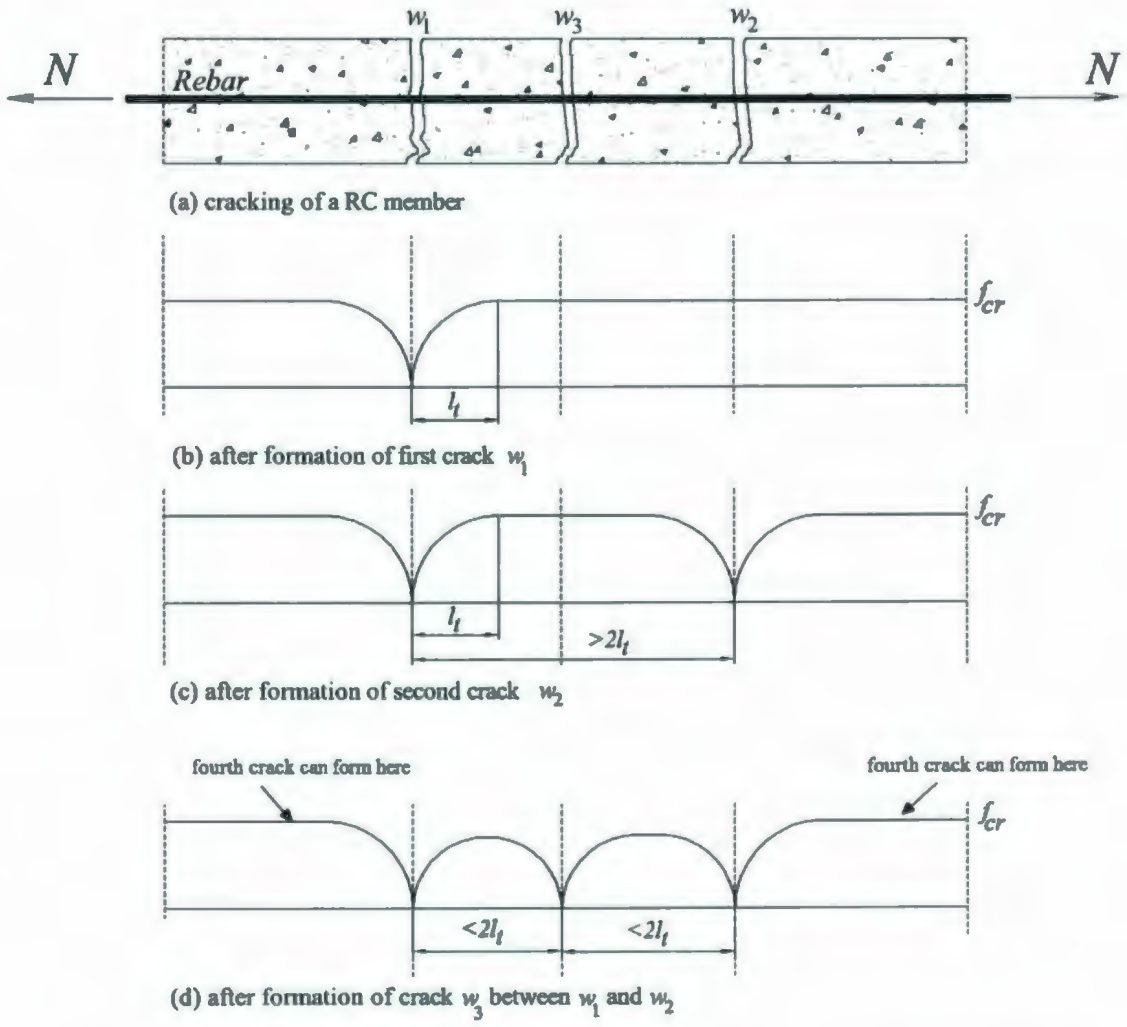

Figure 2-4: Distribution of concrete stress along a member under uniaxial tension

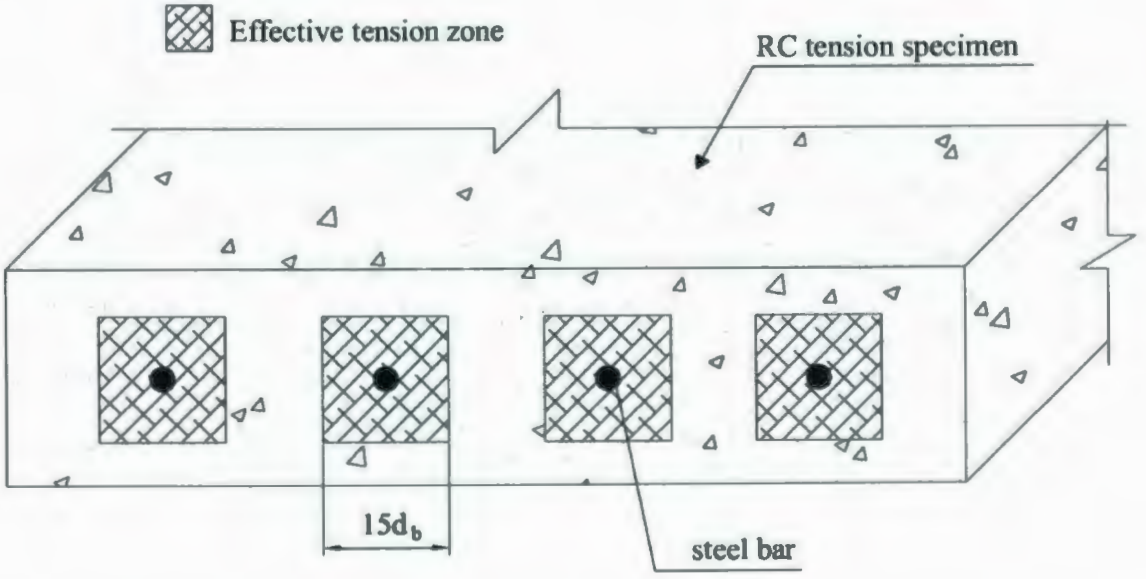

Figure 2-5: Effective zones for steel RC in tension

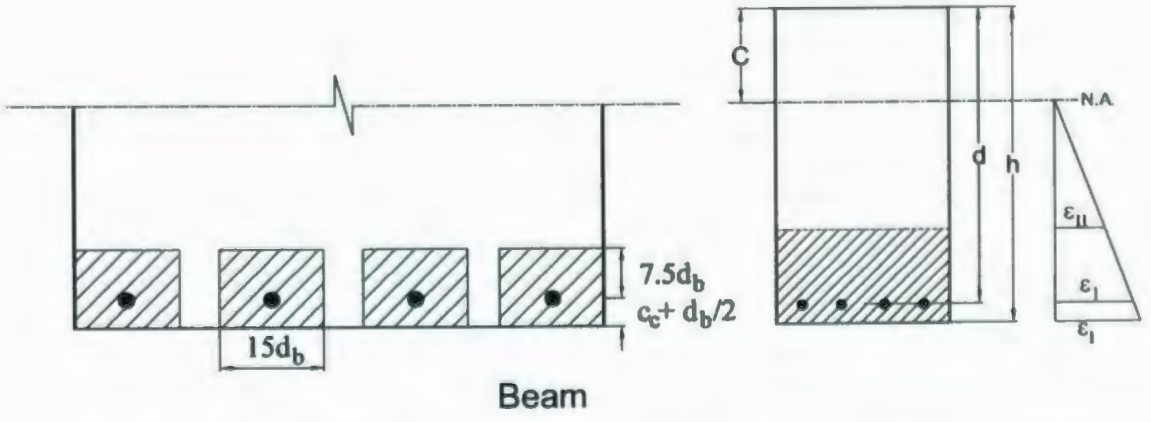

Figure 2-6: The NBR (1992) guidelines for determination of effective concrete area

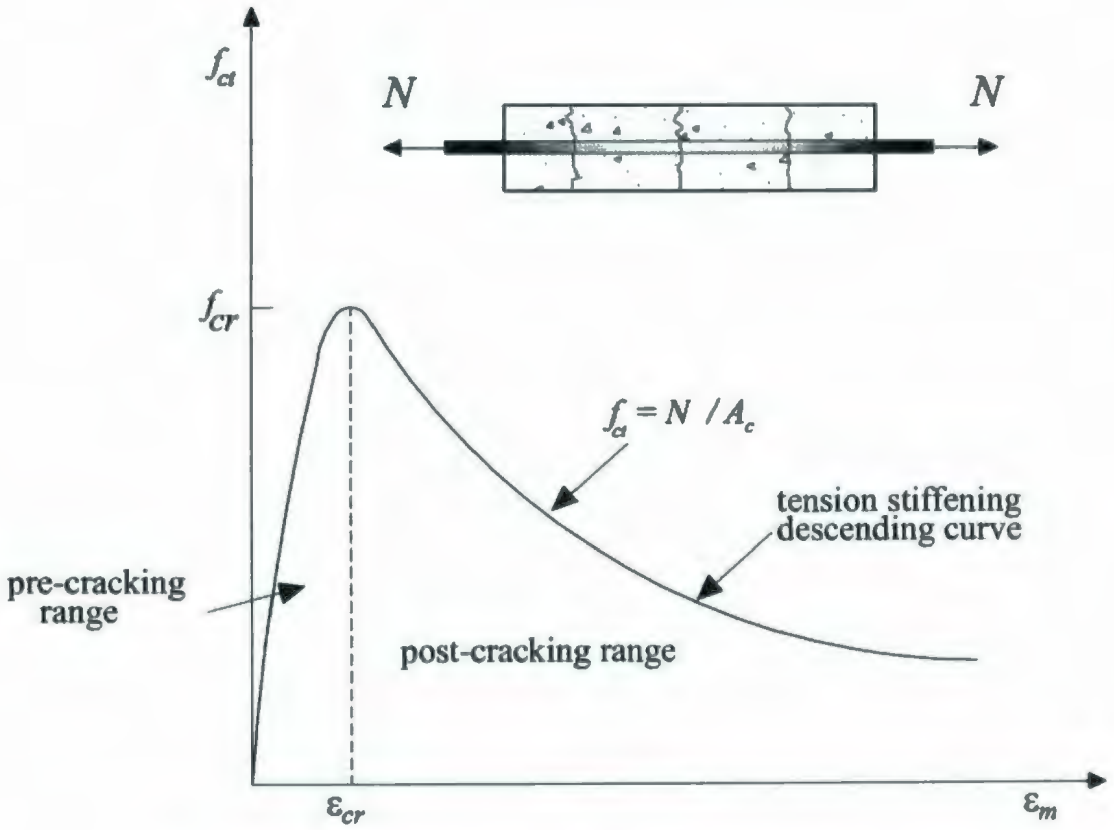

Figure 2-7: Change in average tensile stress carried by concrete

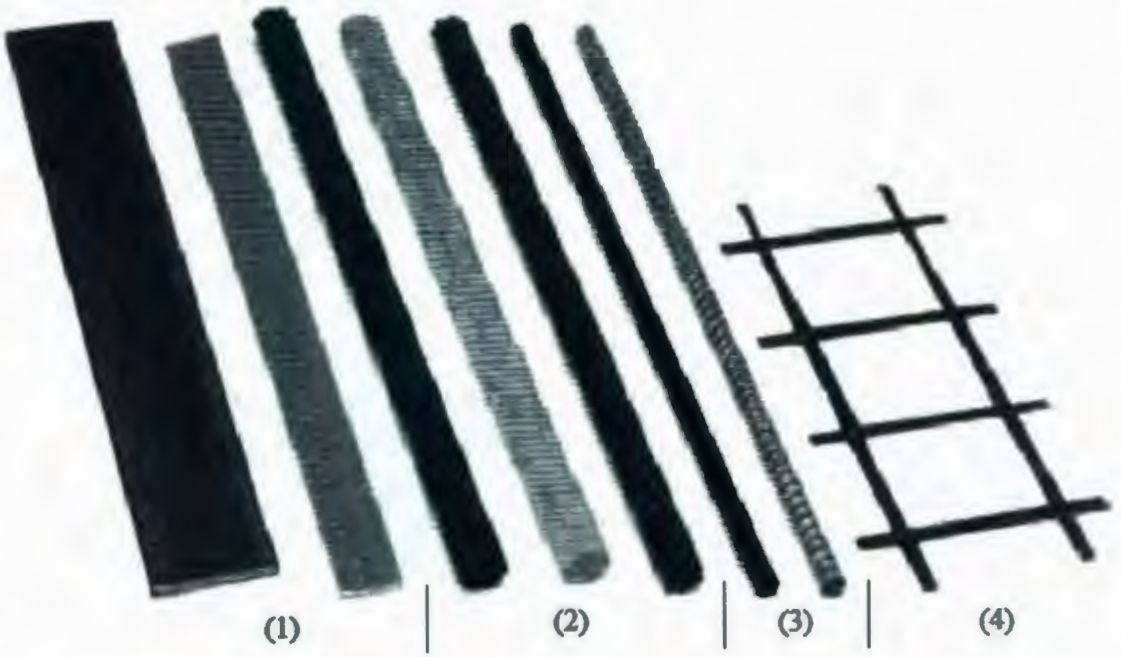

(1) Flat bars
(2) GFRP & CFRP tendons
(3) GFRP & CFRP bars
(4) Glass reinforcing gird

Figure 2-8: Samples of different products of FRP reinforcement

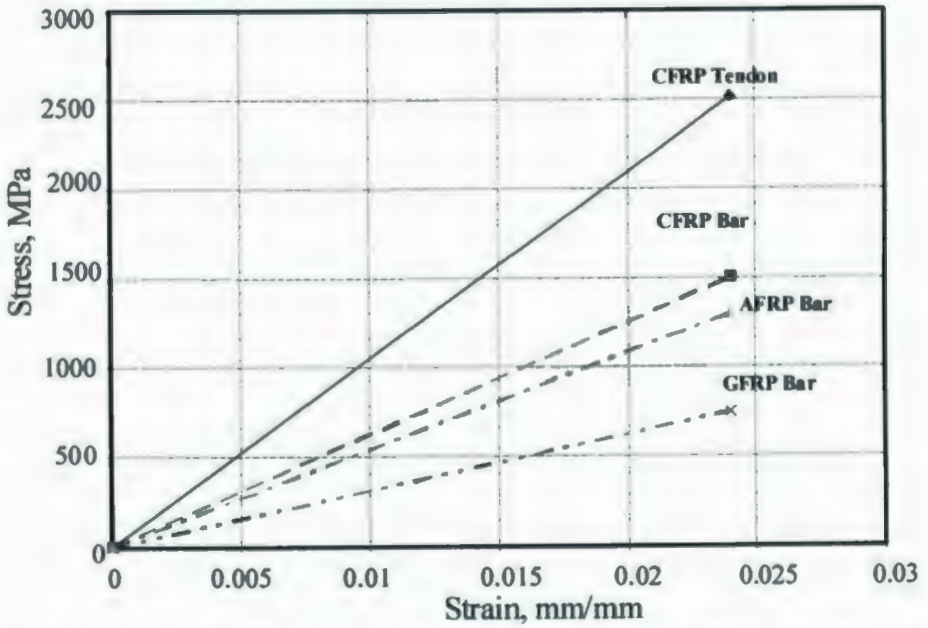

Figure 2-9: Typical stress-strain relationships of different FRP bars

Figure 2-10: Cross section of GFRP-RC specimens tested by Mahmood (2002)

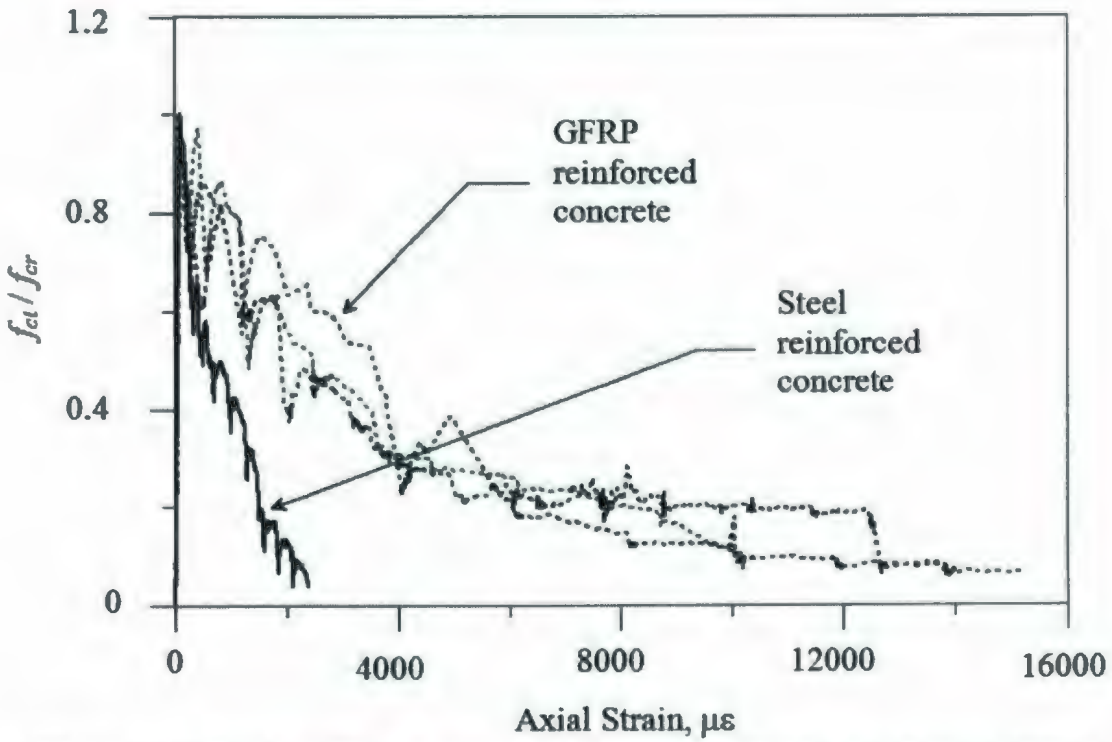

Figure 2-11: Tension stiffening responses measured by Bischoff and Paixao (2004)

Chapter 3

DESIGN AND CONSTRUCTION OF THE TEST SETUP

3.1 Introduction

This chapter describes the design and construction stages of a test setup that is required to carry out the experimental investigation at MUN. The main function of this setup is to test the RC panels under uniaxial and biaxial direct tension. The test setup is also designed to accommodate panels with different sizes and configurations.

The first part of this chapter is a brief review of previous test setups that were used to examine the behaviour of steel-RC panels under in-plane stresses. The second part of the chapter addresses the design concept and provides a detailed description of the test setup and its preparation stages. Finally, a description of the experimental equipment, instrumentation, and data acquisition system is provided.

3.2 Literature on Previous Test Setups

RC specimens that have the shape of panels or shell elements allows for the influence of multiple bar layers to be investigated. The technique of testing RC panels is practically simple, yet reasonably accurate, and it could eliminate many complicated difficulties associated with testing full-scale or prototype models of the RC structures.

Few research programs have been conducted to test RC panels subject to in-plane stresses. Since the 1970s, there has been a growing interest in the nuclear power industry. Thus, research projects were carried out on concrete panels that were used to simulate portions of the walls of nuclear reactors. The experimental data collected are significantly helpful in establishing the design requirements for such important facilities. At the University of Alberta, MacGregor et al. (1980) tested several reinforced and prestressed wall segments (800 × 800 × 260 mm) that were quarter sized models of parts of the walls of secondary nuclear containment vessels. The segments were loaded by uniaxial or biaxial tensile loads. In this project, a special loading apparatus was utilized. The loading apparatus was made of steel sections as shown in Figure 3-1. The loading apparatus had a 6227 kN (1400 kips) capacity MTS testing machine. The MTS loading head applied a "circumferential" load on the specimen. A specially designed load frame and four 890 kN (200 kips) hydraulic rams were used to apply a "longitudinal" load to the specimen. The test specimen was turned 90 degrees so that the circumferential load (horizontal in the prototype) was applied vertically in the laboratory. The design was recommended so that the large capacity of the MTS machine could apply the larger of the two loads. The vertical test loads were controlled by the MTS electro-hydraulic loading controllers. The horizontal loads were applied by tension rams that were controlled by a manually operated console which used air to apply pressure to the hydraulic fluid.

Cho et al. (2004a; 2004b) used another technique to test steel RC panels under uniaxial and biaxial direct tension. Their research project simulated an actual response of the cracking behaviour and tensile response of a steel-RC structure of nuclear containment structure walls. As shown in Figure 3-2, the test setup is made of a steel reaction frame with three hydraulic

jacks that were mounted on each side of the frame. The steel bars were passed through slots in the frame and then into a hole in the hydraulic jacks. Four steel couplers were utilized to accommodate an increased number of reinforcing bars that were subjected to tension. The setup was used to test specimens with a side that is up to 1500 mm and thickness of 600 mm.

Earlier, Oesterle and Russell (1980) used a large apparatus to test steel-RC panels under biaxial tension and shear stress loading cases to simulate parts of nuclear containment structures. Their apparatus consisted of a prestressed concrete reaction frame, biaxial and shear hydraulic loading systems, and instrumentation. The prestressed concrete reaction frame was about 6 × 6 m in plan and 1.5 m in height. This test setup is relatively similar to that of Cho et al. (2004a), in terms of placing the specimen horizontally, and also passing the loading rods through slots in the reaction frame to be coupled to the orthogonal steel in the specimens.

There have been other research projects related to steel-RC panels with special focus on shear behaviour and field theories, such as the "Panel Element Tester" developed at the University of Toronto (Vecchio and Collins 1982) and the "Universal Panel Tester" developed at the University of Houston (Hsu et al. 1995).

As seen from the literature, previous research primarily investigated the behaviour of steel-RC panels under in-plane stresses. To the best of the author's knowledge, there is no research work in the literature that deals with FRP-RC panels under direct tension; especially biaxial tension.

3.3 Main Challenges of Testing FRP Bars under Tension

Testing FRP bars under tension has been relatively challenging, due to the different mechanical characteristics of the commonly produced FRP bars compared to conventional steel bars. The conventional gripping systems of the universal testing machines usually cause crushing of the FRP bars inside the grips, leading to premature failure. The relatively low friction nature of the FRP bar surface could lead to slippage, causing errors in the load-displacement relations recorded during testing. There are several suggested techniques that adopt almost the same principle, which is protecting the FRP bar between the grips and transferring forces to the bars. This is a typical concept in several research, such as tests conducted by Pleinmann (1991), Porter and Branes (1991), Faza and GangaRao (1993), and the testing techniques that are recommended in ASTM D3916 (2002) and ACI 440.3 (2004). FRP bars were protected by injecting epoxy or grouting around the bar ends, and thus pulling from these ends, allowing a relatively smooth transfer of tension to the rest of the bar without experiencing premature crushing of the bar inside the machine gripping heads.

All of the previous techniques could not be directly used in the current investigation, where the objective was to test concrete panels orthogonally that were reinforced with multiple layers of FRP bars.

3.4 MUN Test Setup

The main purpose of the test setup that was designed and built at MUN is to simulate direct tension loads at the boundaries of the GFRP-RC panels. The tension loads are applied either in the uniaxial or biaxial in-plane directions. The preliminary assessment to fabricate a complete

test setup made of steel showed that large steel section sizes are required in order to minimize the deformations under high loading. This would have required relatively high initial costs of manufacturing, due to the high prices of steel and labour costs. Therefore, it was decided that a combination of concrete and steel cross-sections will be used to manufacture the setup as described in the following subsections. The design has relatively high cross-section stiffness, and reduces the total costs of the test setup.

The construction of the setup was completed over different stages as explained in the following sections. During the preliminary design stages of this research project, the main challenge is testing GFRP-RC panels in direct tension without the common gripping problems that these types of bars tend to experience, as mentioned in the previous section. In addition, the test panels are reinforced with several bars in more than one layer which increases the complexity of testing. As mentioned in the previous review of similar setups, the researchers used load actuators, prestressed hydraulic center-hole (hollow) jacks, or steel couplers that are suitable for tensioning of the steel bars. This is a standard procedure in all of the test setups that deal with steel. Testing GFRP bars is relatively more difficult than testing steel bars due to the gripping problems of GFRP. Neither the hollow jacks nor the couplers could be used. GFRP bars have relatively weak strength in the transverse direction, and some bar types have inferior bond strength. The GFRP weakness in the transverse direction can result in bar crushing if over gripped to stop any slippage that could develop while using these types of jacks. Also, GFRP bar types with inferior bond strength will require a longer development length to prevent slippage. These issues are more challenging for testing the panels under two different cases of loading; i.e. uniaxial and biaxial. Moreover, the setup is designed to accommodate

different specimen sizes, bar diameters, bar types, and various bar spacing and loading conditions. This allows flexibility in using this setup for any future research.

The design concept of the setup is to effectively and securely transfer the tension loads to the GFRP bars and consequently, to the panels. This should be achieved without experiencing; or at least minimize, any additional transverse stresses that can cause premature failure. In addition, there should not be any potential slippage during the application of the tension loads to the GFRP bars.

After investigating several design alternatives and carrying out some test trials, the final design of the test setup is shown schematically in Figure 3-3. A sectional elevation of the setup is shown in Figure 3-4. The test setup consists of five main components: (1) a RC fixed reaction frame; (2) four moving walls on the four sides of the frame; (3) a hydraulic loading system; (4) a gripping system behind each moving wall; and (5) instrumentation and data acquisition system. A detailed description of each component is given in the following sections.

3.4.1 RC fixed reaction frame

The RC fixed reaction frame is designed to sustain the reactions of the hydraulic jacks that push back on the moving walls, and therefore, transfer the loads to the specimen through the GFRP bars. The GFRP bars are connected to the gripping block behind the moving walls.

The frame is square in plan with side dimensions of 2200 mm and a height of 750 mm. The frame has a RC base that was cast monolithically with the frame walls to form an L-shape

as shown in the elevation of the test setup (Figure 3-4). The frame is fixed to the floor slab of the structural laboratory which is a one-meter thick RC slab. The laboratory structural floor was originally constructed with grid-holes spaced at 600 mm in orthogonal directions. The frame is fixed using eight steel anchor bolts passing through the holes. Each anchor bolt is about 60 mm in diameter, and threaded at its two ends for placing washers and nuts to fix the frame to the floor.

The frame is reinforced using a combination of deformed steel bars and plates. The deformed steel bars conform to Canadian CSA Standard Grade 400 while the steel plates conform to CSA G40.20/G40.21 (2004). Eight steel plates (580 × 380 × 20 mm) are welded to the four sides of the frame to the steel reinforcement cage. The purpose of the steel plates is to provide a surface for the hydraulic jack reaction in order to uniformly sustain the high local stresses that are expected to develop in the corner regions of the frame.

After placing the reinforcement in the fabricated formwork, a ready-mix concrete is delivered to cast the frame (Figure 3-5). The maximum aggregate size used in the concrete is limited to 10 mm to accommodate the placing in a relatively heavily reinforced member. Moreover, special care is paid towards the casting and compaction of the concrete using electrical vibrators. Special attention is given during the casting and finishing of the concrete surface of the frame. After casting, the RC frame is covered by polyethylene sheets and wet burlap. In order to minimize any shrinkage effects, water-spray curing is applied regularly twice a day, for more than 15 days. The formwork is then removed from around the frame that is kept in ambient laboratory temperatures. The average compressive strength of the cylinders of the used concrete is 42 MPa after 28 days.

Eight steel hooks are placed in the frame to facilitate its handling in the laboratory area. The weight of the frame is about 6.0 tons, which is the appropriate handling weight using the existing overhead cranes in the structural laboratory. The cranes can handle a maximum loading capacity of 10 tons.

3.4.2 Moving walls

The purpose of the moving walls is to transfer the loads from the jacks to the gripping blocks and therefore, pulling the GFRP bars in each direction. These walls are free-to-slide over the floor under the loads of the hydraulic jacks while their reactions act back on the fixed reaction frame.

Four identical moving walls surround the fixed frame and are placed at a suitable distance from the fixed frame. The moving walls are designed and constructed of composite sections of RC and steel plates. Two steel plates (1620 × 645 mm, and 16-mm in thickness) are used at the front and back side of each wall. The steel plates are connected to the steel boxes, forming seven slots in each wall, and enabling the reinforcing bars to pass through the wall to the gripping concrete block.

The steel sections of the walls are fabricated and the steel reinforcement bars are appropriately placed inside each wall as shown in Figure 3-6 (a). A ready concrete mix is used to cast the concrete in the wall forms that are made of the steel plates and enclosing the steel reinforcement bars to form the total section of the moving wall. The four walls are made identical in their dimensions. The total dimensions of a typical moving wall are 1620 × 660

mm, and 300 mm in thickness. The total weight of each wall is about 1.0 ton, and each wall has two steel hooks on top to facilitate handling during usage with the overhead cranes.

A steel base plate is installed around the fixed frame. Four steel plates of 16 mm thick. were used. After casting, the moving walls are positioned over the base steel plates. As shown in Figure 3-6 (b), at the bottom of each moving wall, a hard plastic sheet is mechanically attached to the concrete surface by using counter-sink screws to eliminate friction and facilitate its sliding.

3.4.3 Hydraulic system

Figure 3-7 shows a schematic diagram of the hydraulic system used to control the applied loads and its different components. Eight double-acting cylinder jacks are used to apply loads in the four main directions of the fixed reaction frame; two jacks are placed on each side of the setup. These are double-acting jacks with a total maximum capacity of 4000 kN in pushing and 1920 kN for pulling per the direction. Each jack has a maximum stroke of 300 mm. All of the jacks have tilt saddles to accommodate any potential eccentricity.

The eight jacks are connected together with a closed pipe (hydraulic hose) system and an electric hydraulic pump. The hydraulic pressure is distributed by using four manifolds and valves located at designated points across the system. The main purpose is to uniformly distribute the hydraulic pressure in the biaxial directions in order to avoid any potential eccentricity. The hydraulic pump has an oil reservoir with a capacity of 40 litres and an ability to apply pressure up to 70 MPa over the system, with an oil flow that is equal to 2 litres/min. The jacking forces are designed to apply the load in the two directions with the required

loading ratio. The load pressures are measured through two pressure gauges of the dial type, with one connected in each direction. Two pressure transducers are connected to the system to directly measure the hydraulic pressure and directly transfer electrical signals to the data acquisition system for recording the load level in each direction.

Two jacks are installed on each side of the frame and aligned between the fixed frame and moving walls. Steel floor beams are used to position the hydraulic jacks at the required position level.

3.4.4 Gripping system

Unlike steel, the relative weakness of GFRP bars in its cross-section transverse direction, and the lack of adequate deformed ribs, can cause slippage under high loads. A special design for the gripping system is required.

Different gripping systems were proposed and two test trials were conducted. Adopting the ACI 440.3 (2004) testing method, the ends of each bar were inserted in a plastic pipe, and an expanding cementitious grout was injected around it, see Figure 3-8(a). Unfortunately, such a gripping technique was not strong enough, and failed at a very early loading stage. The construction of this system is very tedious and time consuming. Also, this system did not seem to provide uniform loading per each bar. One failed pipe was enough to cause the premature failure of the whole gripping system.

The lessons learned from the initial trial were important in developing another more simple and creative gripping system. For this new system, the GFRP bars are attached by ties to a

cage of steel or GFRP bars placed horizontally and vertically around the GFRP bars as shown in Figure 3-8 (b). Concrete is then cast around this cage to form a RC anchor block used for gripping GFRP bars (see Figure 3-8 (c)). Similar to the moving walls, the concrete gripping blocks are cast over hard plastic sheets to eliminate friction and facilitate sliding over the steel plates that are mounted over the floor area surrounding the test setup.

This gripping system is successful and strong enough to carry as much load as required. Compared to the initial trial technique, the RC concrete block gripping system is simple and time-saving. Moreover, the mechanism of transferring the loads to the GFRP bars is uniform with minimum local stresses and no slippage is experienced.

3.4.5 Instrumentations and data acquisition system

The instrumentation and data acquisition system is designed to measure applied forces and deformations of the specimen during testing. Forces are applied to test panels through reinforcing bars. The forces are applied through four hydraulic jacks per direction and measured by monitoring the oil pressure in the hydraulic pipe lines using: (1) electrical pressure transducers; and (2) pressure dial gauges. All of the eight jacks and pressure transducers are calibrated, and the forces are directly calculated based on the effective area of the jack piston.

The deformations and cracking properties are monitored by linear potentiometer displacement transducers (LPDT). A minimum of five LPDTs is typically attached to the concrete surface of the test specimen. The electrical strain gauges are 8 mm long with a nominal resistance of 120 Ω and gauge factor of 2.08 ± 0.5%. The gauges are used to measure

the strains in selected locations of the GFRP reinforcement. In some test specimens, concrete gauges are also utilized to measure any slippage that could develop between the concrete and GFRP reinforcement.

For processing and acquiring the data, an automatic data acquisition (DAQ) system is used. The DAQ system consists of several channels connected to a personal computer. Data processing software (National Instruments 2003) is used to collect the data from the different transducers.

3.5 Assembly of the Test Setup

General views of the test setup after the completion of all of its construction and installation stages are shown in Figures 3-9 and 3-10 for typical specimens under uniaxial and biaxial loading, respectively.

As aforementioned, the primary objective of the design of this test setup is to test GFRP-RC panels under direct tension. However, this setup can accommodate other testing conditions. It is capable of testing specimens with different sizes, up to 1350 × 1350 × 500 mm. The specimens can be located at different heights from the floor, allowing more flexibility in testing. Both the fixed frame and moving walls of the test setup are provided with seven aligned slots in each direction at 150 mm spacing. Consequently, different alternative bar spacings can be tested (150 mm, 300 mm, and 450 mm). The test setup system has the ability to test specimens reinforced with different bar diameters up to 35 mm. In addition, the setup can accommodate one or two layers of reinforcing bars within the specimen. Furthermore, it has the capability of testing different types of reinforcement, including traditional steel and all

types of fibre composite bars. In general, the setup can be used to investigate different research studies that deal with bond behaviour, cracking behaviour, and constitutive modelling of RC panels.

The test setup is designed to resist loads up to 4000 kN per direction. However, it is recommended that the maximum load is within 80% of the capacity of the hydraulic jacks (Enerpac 2003).

Meanwhile, the setup is mainly designed to test concrete panels under uniaxial and biaxial tension. By adding special fittings, it can also be used to simulate shear loads at the specimen boundaries.

3.6 Summary

For the purpose of this research investigation, a test setup is designed and constructed at MUN to apply either uniaxial or biaxial direct tension tests on RC panels. The test setup required nearly 18 months in several stages for design and construction which includes five main components; namely, a RC reaction frame, four moving walls, hydraulic system, gripping system, and measuring instrumentations. The unique aspect of this test setup is its ability to accommodate both the FRP and steel reinforcing bars. The proposed design provides a simple solution to the common gripping problems of FRP bars. For future research investigations, the test setup is designed to accommodate different specimen sizes, bar diameters, various bar spacings and loading conditions. The design of the setup combines the high stiffness of RC cross-sections and the adaptability of steel plates attached to the setup to attach any additional fittings that may be required during the experimental program.

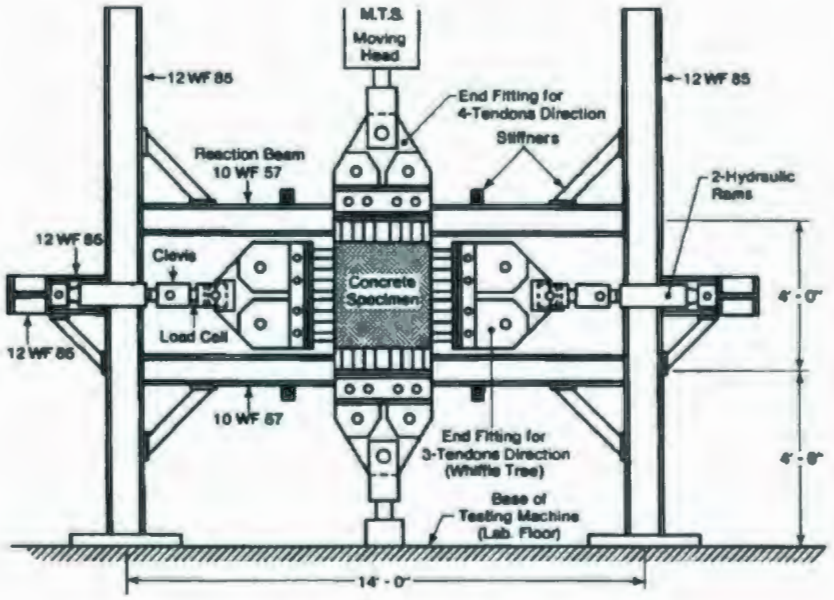

Figure 3-1: Loading frame used by MacGregor et al. (1980)

Figure 3-2: Test setup used by Cho et al. (2004a)

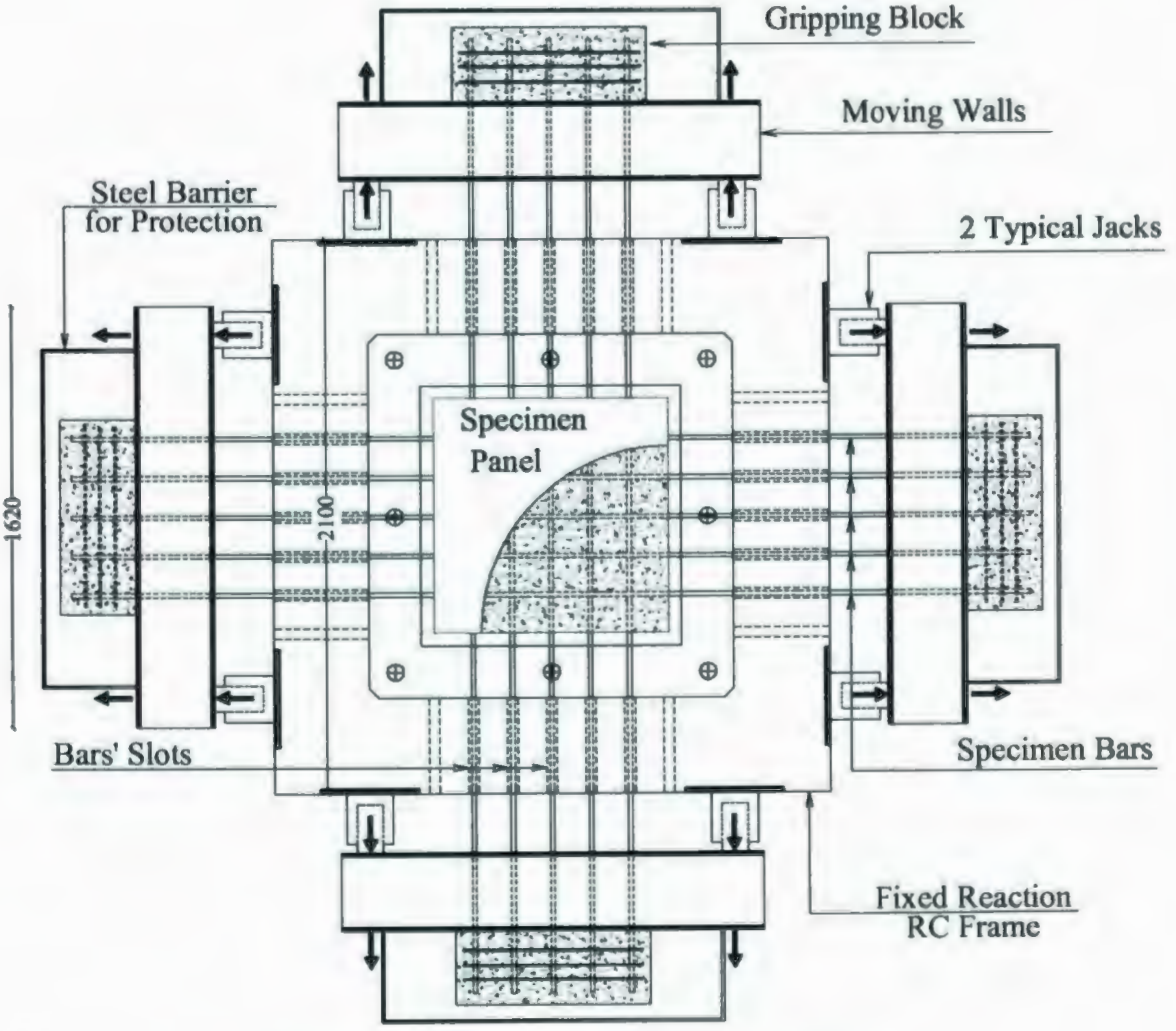

Figure 3-3: Schematic plan for MUN test setup
(Dimensions are in mm)

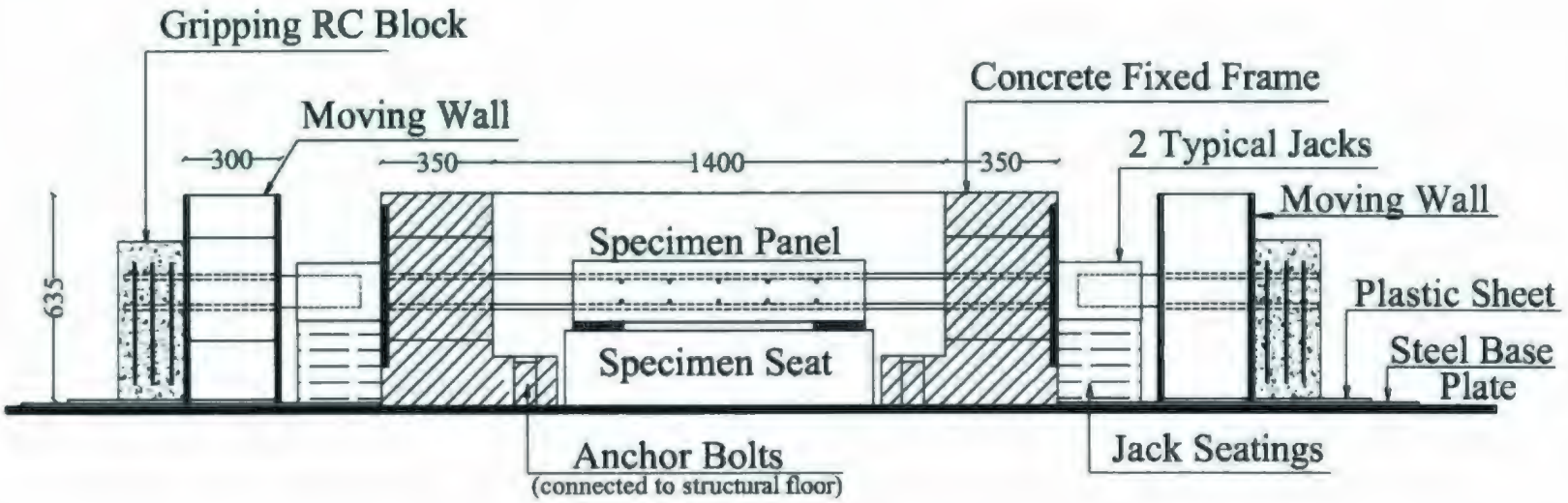

Figure 3-4: Schematic sectional elevation for MUN test setup
(Dimensions are in mm)

(a) Form work & steel cage

(b) Typical steel cage in one side of formwork

(c) Finishing concrete surface

(d) After concrete casting

(e) During curing period

(f) After removing form work

Figure 3-5: Construction stages of RC fixed reaction frame

(a) The moving walls just prior to the concrete pour

(b) A typical moving wall (upside down) after attaching a plastic sheet to minimize friction

Figure 3-6: Construction stages of Steel-Composite RC moving walls

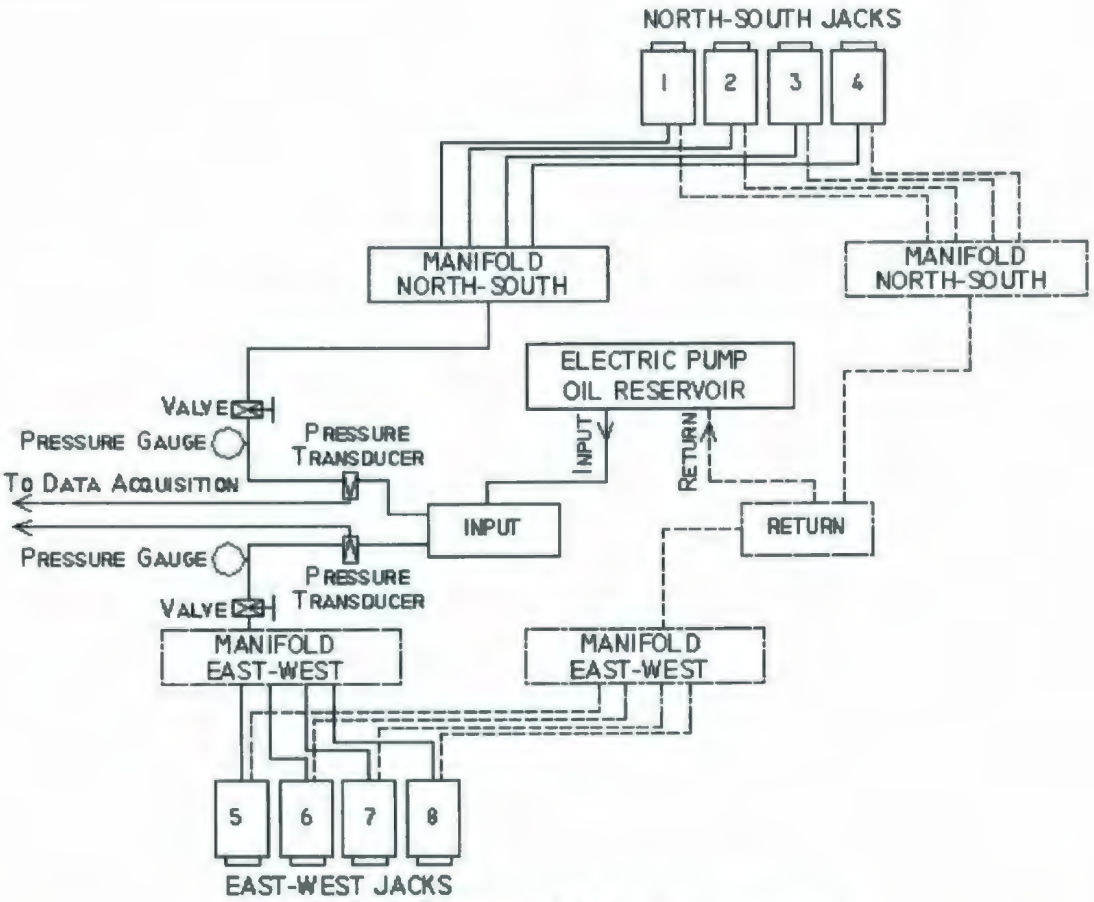

(a) Schematic diagram of the hydraulic system

(b) Electrical hydraulic pump

(c) Typical jacks after installation

Figure 3-7: Hydraulic system of the test setup

(a) Unsuccessful gripping trial done by grouting around GFRP bars

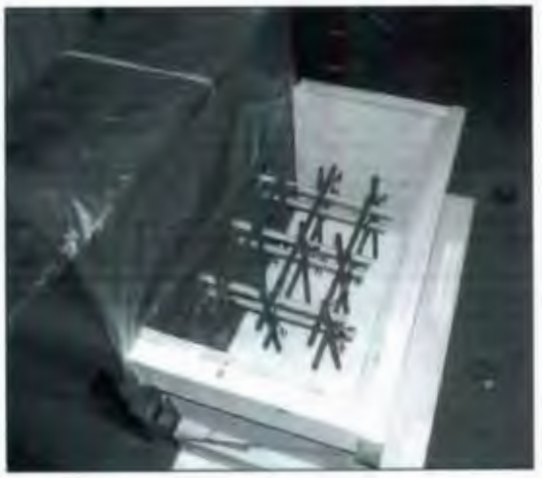

(b) Typical form and reinforcing cage for gripping blocks

(c) Typical reinforcing concrete gripping block

Figure 3-8: Development of testing gripping system of GFRP bars

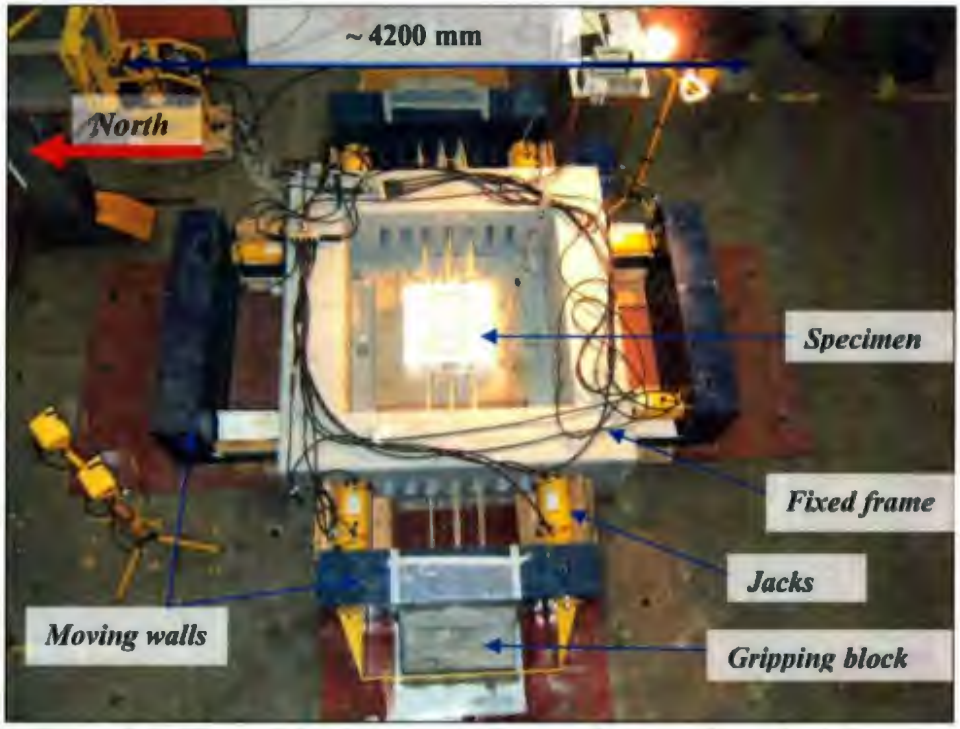

Figure 3-9: View of the test setup with a specimen under uniaxial tension

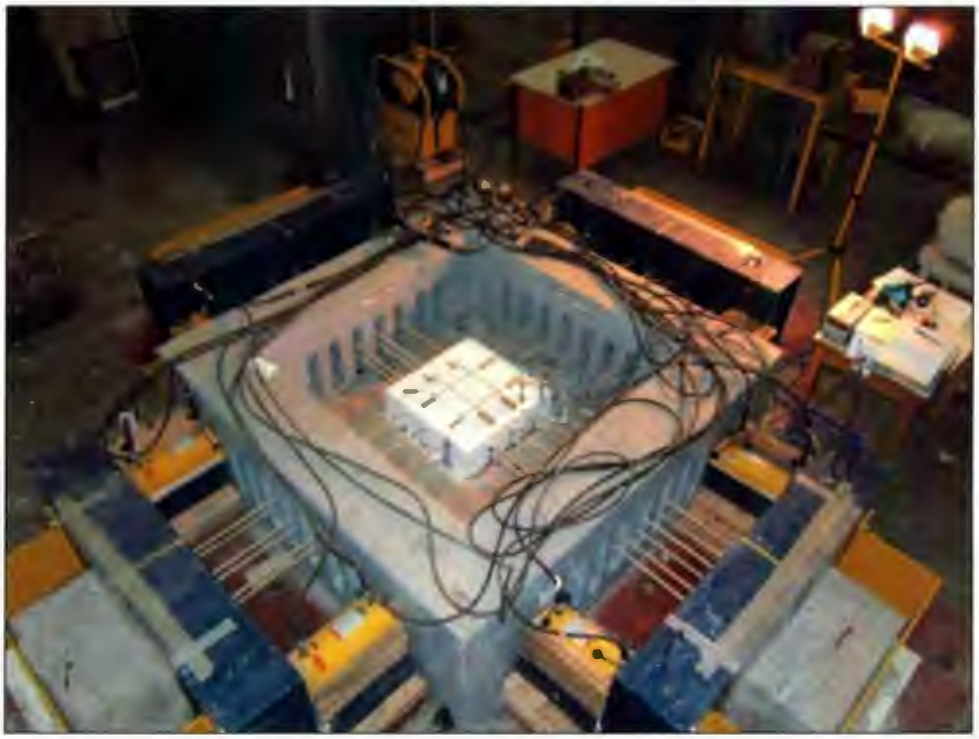

Figure 3-10: View of the test setup with a specimen under biaxial tension

Chapter 4

THE EXPERIMENTAL INVESTIGATION

4.1 Introduction

This chapter provides a detailed description of the experimental program. The test parameters and details of the test specimens are provided. The preparation of the formwork, mixing concrete, testing procedures, and measurements is described. Detailed descriptions of the material properties used in this investigation are given. These materials are the concrete, GFRP and steel reinforcing bars.

4.2 Test Parameters

The loading type, concrete strength, bar type and diameter, concrete cover to bar diameter ratio, bar spacing, and reinforcement ratio are considered as the main parameters, which are described as follows:

Loading type — includes two direction tension load cases applied in the uniaxial and biaxial directions. For the biaxial tension loading case, the tension load is maintained equal in the longitudinal and transverse directions, i.e. the loading ratio is 1:1.

Concrete strength, f_c' — includes two levels of target compressive strength; namely, 40 MPa for NSC, and 75 MPa for HSC. This range of concrete strengths is selected to reflect a

practical range between the strength bounds of the NSC (20 MPa to 45 MPa) and the commonly used concrete strength values for HSC (70 - 80 MPa).

Reinforcing bar diameter, d_b — includes two GFRP bar sizes; namely, 13 and 16 mm. A common steel bar diameter of size 15M (16 mm) is also selected for comparison.

Concrete cover to bar diameter ratio, c_c / d_b — includes two ratios of 1.5 and 2.5. ACI-440.1 (2001) recommends that the concrete cover for FRP reinforcement should not be less than d_b. Later, ACI 440.1 (2006) puts a limit on c_c / d_b should not be larger than 3.5 so that the development length equations can be used for splitting and pullout failure modes. ISIS (2001) design guidelines correlate the concrete cover selection to the bar diameter, coefficient of thermal expansion, and type of environmental exposure of the FRP-flexural concrete members. A maximum concrete cover that equals to 2.5 d_b or 50 mm is recommended for flexural members. Thus, the selected c_c /d_b ratios lie within the range of these design recommendations.

Bar spacing, b_s — includes two different bar spacings; namely, 150 mm and 300 mm. The b_s is maintained equal in the orthogonal directions.

Reinforcement ratio, ρ — includes two different values for the reinforcement ratio; namely, 0.7% and 1.0%. In order to conduct a complete examination of the cracking behaviour, several preliminary calculations are conducted to establish these ratios, and thus ensure that the selected reinforcement ratios will probably result in the rupture of GFRP bars beyond the stage of cracking stabilization. Consequently, it is practical to change the

reinforcement ratio by either changing the bar diameter or bar spacing. This means that the cross-sections of the specimens are not changed.

4.3 Test Specimens

A total of twelve specimens were tested under monotonic loading during the experimental program. The tested specimens are RC panels that are typically square in plan with a side length of 600 mm and thickness of 190 mm. As shown in Figure 4-1, the reinforcing bars are placed orthogonally in two layers on the top and bottom.

The dimensions of the panel were selected to address the following requirements: (1) accommodate the development length required for the type of GFRP bars used in the experiments; (2) ensure that the utilized gripping system would maintain enough and stable gripping throughout the experimental program; (3) accommodate the loading capacity of the hydraulic jacks available in the laboratory facility; and (4) attain certain reinforcement ratios using the bar diameters employed.

A summary of the tested panels is presented in Table 4-1. The tests are subdivided into five series:

- Series I consists of three GFRP-RC panels made of NSC that have a reinforcement ratio equal to 1.0%. Panels P1-GNU-16-1.0-1.5 and P2-GNU-16-1.0-2.5 have a c_c / d_b of 1.5 and 2.5, respectively. Both panels are subjected to uniaxial tension. Panel P3-GNB-16-1.0-2.5 is similar to P2-GNU-16-1.0-2.5 except that it is subjected to biaxial tension.

- Series II consists of three GFRP-RC panels made of NSC with a reinforcement ratio of 0.7%. The reinforcement ratio is achieved by using a 16 mm bar diameter at bar spacing equal to 300 mm for panels P5-GNU-16-0.7-2.5 and P10-GNB-16-0.7-2.5, which are tested under uniaxial and biaxial tension, respectively. However, for panel P7-GNU-13-0.7-2.5, there are six bars that have a size of 13 mm and spaced at 150 mm. This panel is subjected to uniaxial tension. The c_c / d_b is fixed to 2.5 for this series.

- Series III consists of two GFRP-RC panels made of HSC, with a reinforcement ratio of 1.0%. Panels P4-GHU-16-1.0-2.5 and P6-GHB-16-1.0-2.5 are both reinforced with six GFRP bars that have a size of 16 mm, spaced at 150 mm, and subjected to uniaxial and biaxial tension loading, respectively. The c_c / d_b is fixed to 2.5 for both panels.

- Series IV consists of two GFRP-RC panels made of HSC, with a reinforcement ratio of 0.7%. Panels P8-GNU-13-0.7-1.5 and P9-GNB-13-0.7-2.5 are reinforced with six GFRP bars that have a size of 13 mm, spaced at 150 mm, and subjected to uniaxial and biaxial tension loading, respectively. Panel P8-GHU-13-0.7-1.5 has a c_c / d_b of 1.5 and panel P9-GHB-13-0.7-2.5 has a c_c / d_b of 2.5.

- Series V consists of two steel-RC panels made of NSC with a reinforcement ratio of 1.0%. Panels P11-SNU-16-1.0-2.5 and P12-SNB-16-1.0-2.5 are reinforced with six GFRP bars that have a size of 16 mm, spaced at 150 mm and subjected to uniaxial and biaxial tension loading, respectively. The c_c / d_b is fixed to 2.5 for both panels.

4.4 Properties of Materials

4.4.1 Concrete mix properties

Several trial batches were conducted to establish the proportions of the concrete mixes required for the experimental program. Two types of concrete mixes were designed to obtain a target cylinder compressive strength of 40 MPa for NSC and 75 MPa for HSC at 28 days.

The cement used for the NSC mix was a normal Portland cement Type 10 while for the HSC mix, blended hydraulic cement (Type 10E-SF - normal Portland cement with silica fume at 8% addition – by weight) was utilized. This type of cement complies with the CSA Standard A3000 (2003).

The coarse and fine aggregate were local available materials. The coarse aggregate used was mostly crushed granite. A sieve analysis of the fine and coarse aggregates was conducted according to ASTM C136 (2006). The results of the sieve analysis for both types of aggregate are given in Table 4-2. The water/cementitious ratios are 0.45 and 0.30 for NSC and HSC mixes, respectively. A superplasticizer of sulphonated naphthalene phormaldehyde base, conforming to ASTM C494/C494M (2005) Type F, was used in the production of HSC. A small dosage of a retarding agent was used to delay the setting time of the HSC mix. The concrete mix proportions for 0.1 m^3 are listed in Table 4-3.

A minimum of three standard cylinders (100 mm in diameter by 200 mm in height) were prepared, per ASTM C192/C192M (2005) standard, from each mix to determine the compressive strength. The concrete cylinders were prepared on the day of casting for testing on

the same day that the corresponding panel was tested. The concrete cylinders were tested according to ASTM C39/C39M (2003) standard. The concrete cylinders were capped using sulphur capping layers. A compression machine (Figure 4-2) with a maximum capacity of 3000 kN was used to test the concrete cylinders. The average compressive strength for the NSC panels is 43.6 MPa, with a standard deviation of 5.1 MPa, and a coefficient of variation (C.O.V.) of 11.7%. The average compressive strength for the HSC panels is 77.3 MPa, with a standard deviation of 1.9 MPa, and a C.O.V. of 2.55%. The tensile properties of the concrete mixes were initially estimated by measuring the tensile splitting strength, f_{sp} and modulus of rupture, f_r. For the NSC mix, the average f_{sp} and f_r was found to be 3.5 MPa and 3.8 MPa, respectively. For HSC, the average f_{sp} and f_r was found to be 4.2 MPa and 5.2 MPa, respectively.

4.4.2 GFRP and steel reinforcement properties

Figure 4-3 shows a close up of the reinforcement bars used. The GFRP bars used in the experiments are commercially known as 'Aslan-100'. These bars were sand coated with helical lengthwise indentations. The selected bar sizes of 13 and 16 had actual bar diameters of 12.7 mm and 15.88 mm, respectively. The ultimate tensile strength was 690 and 655 MPa for the 13 and 16 mm bars, respectively. Both bars had a modulus of elasticity equal to 40.8 GPa and average bond strength of 11.6 MPa from pullout tests according to the bar manufacturer data (Hughes Brothers 2006). The steel reinforcement bars were deformed CSA grade 400 of 16 mm in diameter. The steel bars had a modulus of elasticity of 200 GPa. The properties of the GFRP and steel reinforcement bars are summarized in Table 4-4.

4.5 The Formwork of the Specimens

In the experimental investigation, a typical specimen size was 600 × 600 × 190 mm. The design of the setup required that the test specimens to be cast and kept in place until the time of testing. Therefore, a special formwork was designed to allow stripping without moving the specimen.

As shown in Figure 4-4, the formwork consisted of four sides made of plexiglass sheets that were 15 mm in thickness, and stiffened by wooden bars all around the form. Each side of the formwork had three slots that were 30 mm in width, to facilitate the passing of the GFRP bars through them to the corresponding slots in the fixed frame and moving walls. The bottom of the form was made of a plexiglass square sheet that had a side dimension of 600 mm and thickness of 15 mm. The form was mounted by screws to a rigid wooden seat placed over the structural floor at the center of the fixed frame. Special care was taken to properly align the formwork and wooden seat with respect to each other and to the outer fixed RC frame and moving walls of the test setup.

Additional wooden formwork moulds that were 19 mm in thickness, made of stiffened-plywood sheets, were used to cast the concrete around the gripping cage to form the gripping blocks at each side of the test setup.

4.6 Preparation of the Reinforcement Cage

The GFRP and steel reinforcing bars were cut into lengths of 4300 mm as required. This length was suitable for extending between the end fittings of the gripping concrete blocks.

Before setting up the bars inside the formwork, electrical strain gauges were attached to selected locations on the bars. As shown in Figure 4-5, the strain gauges were typically oriented within three main regions; the edge region of the specimen (location 1) and middle regions (locations 2 and 3). The figure shows typical alternate locations of strain gauges attached to the top and bottom reinforcing bars in both loading directions. Typically, in each specimen, eight to twelve strain gauges were attached according to the designated specimen configuration. As the experiments were conducted, a few additional strain gauges were attached to capture some extra data that could be used in further interpretation of the test results. The orientation of the strain gauges is selected to capture the strain variations in the reinforcement. These variations could arise from the changes in the test parameters and loading cases.

The installation of electrical strain gauges required preparation of the GFRP bar surface. This preparation consisted of carefully removing the sand coated layer to expose the surface of fibres without damaging them. This was done by softly grinding the bar surface. Next, a special solvent for GFRP was used to remove any traces of oil or dust, and the surface was etched with an appropriate acid. Finally, the clean surface was neutralized by using a basic solution to give a proper chemical affinity for the adhesive. The gauge location was then marked on the bar and positioned by using rigid transparent tape. The tape maintained the position and orientation of the gauge as the adhesive was applied. The gauge was then pressed firmly into position by squeezing out the excess adhesive. To provide an additional confinement to the gauge during the glue-drying stage, additional plastic tape was firmly wrapped around the location of the gauge, and then the gauge was left for at least 24 hours,

which was found to be a suitable length of time to ensure a complete curing. Then, the plastic tape was removed for electrical wire connections. The wires were connected to the gauge and the proper resistance was checked. To protect the strain gauges from any possible water damage during casting, water proofing materials were applied for coating, such as M-coat chemical material, flammable toluene and rubber splicing tape.

The GFRP bars were placed in two layers, top and bottom. For the case of uniaxial tension loading, transverse bars of the same diameter were used. The transverse bars were cut into lengths of 700 mm just to extend outside of the formwork. Steel wires were used to tie the GFRP bars of each layer together and keep the spacing and orientation of the GFRP bars as required. The concrete cover was adjusted using wooden and steel spacers outside the boundaries of the formwork.

4.7 Placement of Concrete

The specimens were cast in a horizontal position inside the test setup. Prior to casting, appropriate placing and adjustment of the concrete cover of the bars inside the form were done. The bars extended outside of the formwork through the fixed frame slots, into moving wall slots until they reached the gripping blocks.

The concrete was mixed using a concrete mixer at a rate of 18 rpm in the concrete laboratory at MUN. The mixer has a capacity of 0.12 m^3. One to two batches were required to cast each test specimen. Extra batches were needed to cast the gripping blocks on the same day of casting each panel. The surface of each specimen was finished and the specimen was covered for curing.

Polyethylene sheets were placed on the top surface for 12 hours. Wet burlap was then placed over the specimen and surrounded by polyethylene sheets. The specimens were allowed to cure by maintaining wetness of the burlap which was sprayed with water daily for at least two weeks. Afterwards, the formwork was removed and the specimen stayed at ambient room temperature until testing.

4.8 Test Procedure and Loading Sequence

Each specimen was painted white to facilitate the monitoring of cracks. Attaching and calibrating the instrumentation was carried out before testing. As shown in Figure 4-6, four LPDTs with a 50 mm maximum displacement, are attached orthogonally on the surface of the test specimen. Two LPDTs were attached in each direction. The fifth LPDT, which has a 100 mm maximum displacement, was attached diagonally over the test specimen surface. An aluminum bar was connected to each LPDT in order to extend the gauge length over which the deformations were measured.

The panels subjected to uniaxial tension were loaded in the EW direction; while specimens subjected to biaxial tension were simultaneously loaded in the EW and NS directions. During testing, the load was gradually increased until the first crack was observed. The average loading rate was about 2.5 - 5 kN/min per jack. Once a developed crack was observed, the loading was paused using the hydraulic system valves. The crack pattern was marked on the specimen, and photographs were taken.

The load was then increased, and the above procedure for crack and load monitoring, and recording was repeated at each loading stage until complete failure of the GFRP bars, at which

the test ended. After completing the test, the final crack spacing was measured. Any further observations about the specimens were recorded.

The dismantling of each test specimen included removing the attached instrumentations, cutting the GFRP bars at a distance between the specimen and the moving walls. The specimen was then lifted out of the test setup using an overhead crane, and the cracks on the bottom surface were also recorded and compared with the cracks on the top surface. Finally, the gripping concrete blocks were taken out for dumping by using the overhead crane.

4.9 Experimental Measurements

The main measurements that were of concern for monitoring and recording during the experimental investigation were the displacements, and the strains developed under different loading cases. The crack pattern, widths, and spacings were major variables for measurements.

4.9.1 Deformations and strains measurements

If several cracks exist in a reinforced member, then it is reasonable to use the average stresses and strains. The average stress is the average value of local stresses. The average composite strain, ε_m, is the total deformation (over a certain gauge length) divided by the gauge length. This is assumed to be equal to the average reinforcement strain, $\varepsilon_{b,avg}$, which is the average of local reinforcing bars strains $\varepsilon_b(x)$, over the gauge length, l_g.

However, the average composite strain is not equal to the average local concrete strains, $\varepsilon_c(x)$, over the gauge length l_g. This is due to the presence of cracks and the fact that it is not

possible to define a strain quantity at a crack location. Thus, to define an average concrete strain that includes all crack widths, Wallrob et al. (1996) proposed the following definition:

$$\varepsilon_{c,avg} = \frac{1}{l_g}\left[\int_0^{l_g} \varepsilon_c(x)\cdot dx + \sum_{i=1}^{n_{cr}} w_i\right] \tag{4.1}$$

where, n_{cr} is the total number of cracks; and w_i are the crack widths. With this definition, Wollrab et al. (1996) assumed that the average strains in the reinforcement $\varepsilon_{s,avg}$, the concrete strain $\varepsilon_{c,avg}$, and the composite strain $\varepsilon_{m,avg}$ are identical.

In this experimental program, electric resistance strain gauges and LPDTs are simultaneously used to measure the strains and deformations. The concept of an average stress-strain relationship can be better introduced by taking the results of the LPDTs, since the strain gauges reflect local strains in the reinforcement. The tensile strains are obtained and averaged from two or four LPDTs that are attached to the specimen with different gauge lengths. In an identical concept, the strain values obtained from many strain gauges attached in the same direction could be averaged to offset the asymmetric behaviour of the panel specimen in the lateral and vertical directions.

As a result of the variations in crack patterns and the direction of crack development from one panel to the other, it was found that using only the LPDT readings may not be enough to reflect the observed cracking behaviour. Thus, an approach is adopted here to define the average tensile strain of the panel. The approach assumes that the readings obtained from LPDTs and strain gauges are explicitly representative of the overall behaviour of the panel for

the entire loading stages, i.e., from the uncracked stage up to complete failure. Hence, the average tensile strain, ε_m (member strain) is determined as:

$$\varepsilon_m = \frac{1}{2}\left(\frac{1}{n_{LPDT}} \cdot \sum_{i=1}^{n_{LPDT}} \frac{\delta_i}{l_{gi}} + \frac{1}{n_{SG}} \sum_{j=1}^{n_{SG}} \varepsilon_{bj} \right) \tag{4.2}$$

where n_{SG} is the total number of strain gauges per direction and ε_{bj} are the local strains obtained from the strain gauges in the loading direction (excluding strain gauges within the end regions of the specimen); δ_i are the individual readings of LPDTs, n_{LPDT} is the number of LPDTs used in the same loading direction, and l_{gi} is the individual gauge length of the LPDT.

4.9.2 Crack spacing and crack width measurements

An RC member subjected to an axial tensile monotonic load usually experiences several stages of cracking until complete failure. As the load is increased, the development of the primary cross cracks normal to the loading direction can be first observed. Then, under a higher load, axial cracks, due to concrete splitting failure, may take place from the primary crack. A secondary transverse network of cracks can grow from the splitting crack. Finally, a complete failure is reached under increasing the load.

The mean crack spacing determined from classical theories (mainly derived for steel-RC) is usually calculated from the mathematical explanation of the crack formation mechanism due to the bar to concrete bond. However, only the primary network of cracks is due to this phenomenon. Consequently, to assume a unique basis for comparison between the tested panels, only the primary major cracks were considered for measuring the experimental mean crack spacing. The crack pattern observation that leads to the minimal (S_{rmin}), mean (S_{rm}), and

maximal (S_{rmax}) values of crack spacing are presented. For the biaxial loaded panels, the results shown are based on measurements for both directions and then taking the mean value for S_{rm} while S_{rmin} and S_{rmax} are the minimal and maximal values for any of the orthogonal directions, respectively. The measured crack spacings were based on the assumption that the ends of the panel act as the location for cracks.

The determination of the mean crack width at a given level of stress is obtained from Eq. (4.3) and simultaneously cross-checked at different locations during experiments using a crack monitoring manual device.

$$w_m = \sum_{i=1}^{n} \frac{w_i}{n_{cr}} \tag{4.3}$$

where, n_{cr} is the number of cracks at a given GFRP stress level, w_i is the crack width locally measured by an LPDT by neglecting the concrete elongation, and w_m is the mean crack width.

4.9.3 Shrinkage effects

Few researchers have taken into account the effect of concrete shrinkage on the tensile response of RC (Abrishami and Mitchell 1996; and Bischoff 2001). It was deemed that restraint to shrinkage from the reinforcement puts the reinforcing bars into compression and adds tension to the concrete at the same time. Subsequently, such action reduces the cracking load of the member. Moreover, the restraint to shrinkage causes an offset in a bare bar response. This might lead to underestimation of the tension stiffening.

Since plastic shrinkage cracking is due to differential volume changes in the plastic concrete, several steps were taken to prevent a rapid moisture loss. This included full moisture

saturation and the use of plastic sheeting to cover the surface for more than two weeks until the preparation stage of the testing of panels. By applying such a procedure, there was no evidence that any cracks due to plastic shrinkage appeared in any of the tested specimens.

The drying shrinkage is caused by the loss of moisture from the cement paste constituent. In fact, the drying shrinkage, which is a common cause of cracking in restrained concrete, could be more important than plastic shrinkage. The shrinkage effects may be of paramount importance in the case of steel-RC members, where there is large difference between the steel bar stiffness (modulus of elasticity) and concrete stiffness (Kaklauskas et al. 2007). However, shrinkage effects should be negligible for the members reinforced with GFRP bars, which have modulus of elasticity relatively comparable to concrete. This should lead to reduced restraint action of reinforcement. Moreover, it was previously found that granite based aggregates greatly reduce the amount of shrinkage compared to other types of aggregates (Carlson 1938). Coarse and fine aggregates used in the experimental program were mostly crushed granite.

A preliminary estimation for the strain due to shrinkage was conducted. This prediction was based on Bazant and Baweja (1995) and Gardner (2000) shrinkage models, to include into account the specimen size, concrete strength, cement type, curing method, age of testing, and relative humidity. The prediction of both models showed an insignificant shrinkage strain to be induced in the specimens.

Based on this discussion, it could be concluded that shrinkage strains have negligible effects on the test results and hence it was not considered in the experimental measurements.

Table 4-1: Details of test specimens

Series No.	Specimens Designation*	Concrete Type		Bar Size (mm)		Bar type		ρ%	Loading type		c_c / d_b		Bar Spacing, b_s (mm)	
		NSC	HSC	16	13	GFRP	Steel		Uniaxial	Biaxial	1.5	2.5	150	300
I	P1-GNU-16-1.0-1.5	•		•		•		1.00	•		•		•	
	P2-GNU-16-1.0-2.5	•		•		•		1.00	•			•	•	
	P3-GNB-16-1.0-2.5	•		•		•		1.00		•		•	•	
II	P5-GNU-16-0.7-2.5	•		•		•		0.70	•			•		•
	P7-GNU-13-0.7-2.5	•			•	•		0.70	•			•	•	
	P10-GNB-16-0.7-2.5	•		•		•		0.70		•		•		•
III	P4-GHU-16-1.0-2.5		•	•		•		1.00	•			•	•	
	P6-GHB-16-1.0-2.5		•	•		•		1.00		•		•	•	
IV	P8-GHU-13-0.7-1.5		•		•	•		0.70	•		•		•	
	P9-GHB-13-0.7-2.5		•		•	•		0.70		•		•	•	
V	P11-SNU-16-1.0-2.5	•		•			•	1.00	•			•	•	
	P12-SNB-16-1.0-2.5	•		•			•	1.00		•		•	•	

**Specimen Designation: (Panel code according to testing order)-(bar type-concrete type-loading type)-(bar size)-(reinforcement ratio)-(cover/bar diameter ratio)*

Table 4-2: Grading of aggregates

Coarse Aggregate		Fine Aggregate	
Sieve Size	Cumulative Passing %	Sieve Size	Cumulative Passing %
25.00 mm	100.0	4.75 mm	97.21
19.00 mm	95.9	2.36 mm	81.64
12.50 mm	55.0	1.18 mm	62.12
9.50 mm	27.3	600 μm	41.53
4.75 mm	4.1	300 μm	19.45
Remainder	0.0	150 μm	6.84
		Pan	0.0

Table 4-3: Mix proportions of 0.1 m^3 of concrete

	NSC mix	HSC mix
Cement	40 kg	40 kg*
Coarse aggregate	125 kg	107 kg
Fine aggregate	83 kg	65 kg
Water	18 litre	12 litre
Superplasticizer	-	1200 ml
Water reducer	-	200 ml
Retarder	-	40 ml
Mix density	2380 kg/m^3	2410 kg/m^3

*Type 10 cement blended with silica fume (8% of cement weight).

Table 4-4: Properties of the GFRP and steel reinforcement bars

Bar type	Bar diameter, (mm)	Nominal diameter, (mm)	Cross sectional area, (mm^2)	Yield stress, (MPa)	Tensile strength, (MPa)	Elastic modulus, (GPa)
GFRP	13	12.70	144.85	-	690	40.8
GFRP	16	15.88	220.64	-	655	40.8
Steel	15	16.00	200.00	400	600	200

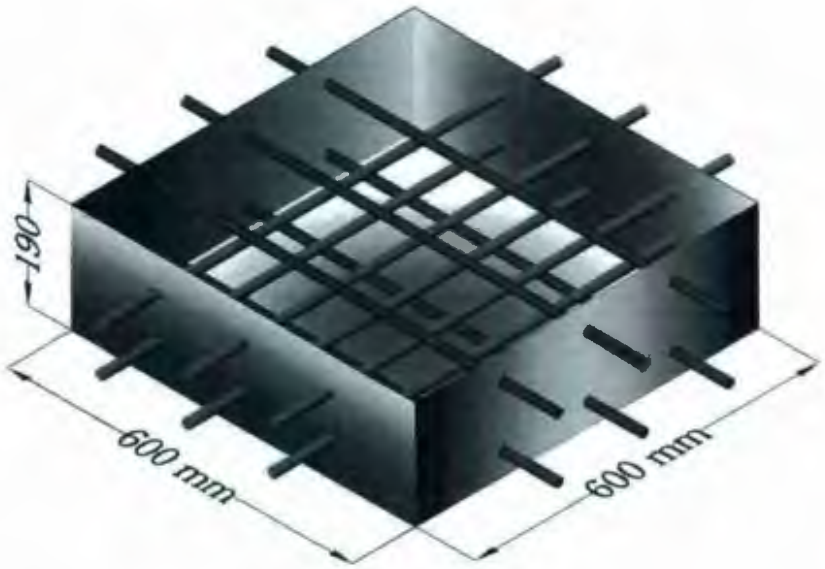

Figure 4-1: The orientation and dimensions of a typical test specimen

Figure 4-2: Compression testing machine used to test concrete cylinders

Figure 4-3: Close up to the GFRP and steel reinforcement bars

Figure 4-4: The formwork used in the experimental program

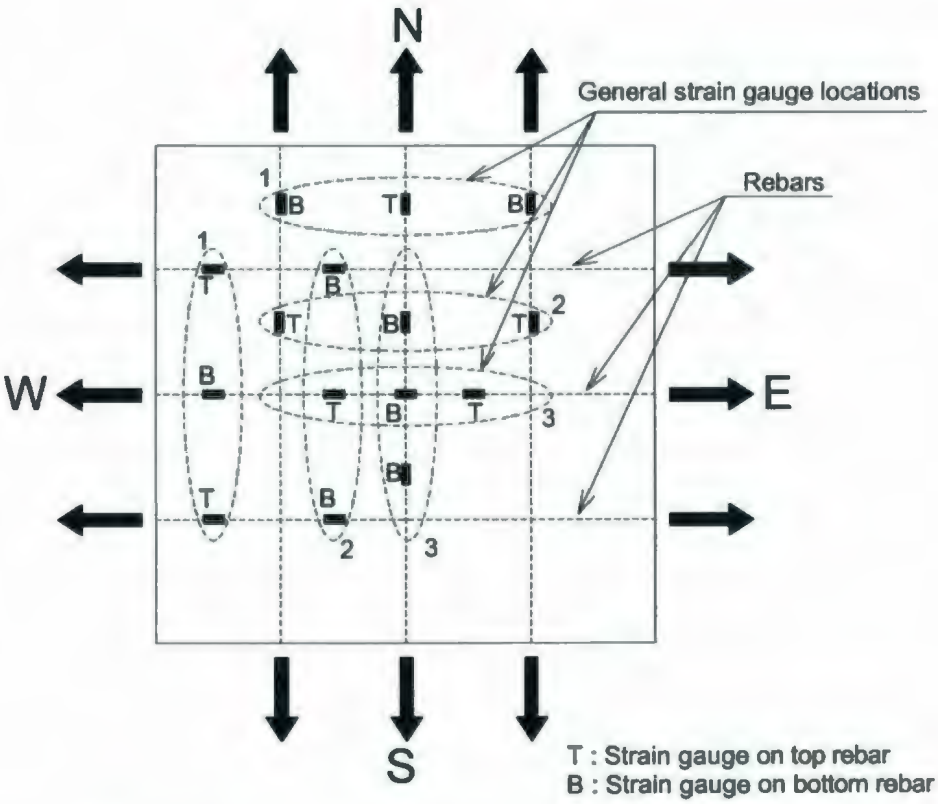

Figure 4-5: Typical locations of strain gauges mounted on the reinforcement

Figure 4-6: LPDTs attached to a test specimen

Chapter 5

CRACKING BEHAVIOUR OF GFRP-RC PANELS

5.1 Introduction

In this chapter, the experimental results and the cracking behaviour of the GFRP-RC tested panels are presented. A total of twelve panels are tested under uniaxial and biaxial tension to study their cracking characteristics. Six GFRP-RC panels are made with NSC (Series I and II). The effect of compressive strength is investigated by testing four GFRP-RC panels made of HSC (Series III and IV). In order to compare the cracking behaviour of GFRP-RC to steel-RC, two steel-reinforced NSC panels (Series V) are also tested.

The effects of the different test parameters on the cracking behaviour of the panels are discussed. The cracking behaviour is presented in terms of development of cracks, crack patterns and spacings, and cracking loads and stresses.

5.2 Development of Cracks in GFRP-RC Panels

The cracking behaviour and relevant observations were recorded through the entire loading stages up to failure. To assist in understanding the crack formation sequences and their mechanism, the progress of cracks was marked on the specimens along with corresponding applied loads during the experiments. These marked patterns along with photographs taken during the experiments were then used to re-produce the marked crack patterns for

presentation purposes. Computer aided design (CAD) software was used in the reproduction of these crack patterns to scale. The crack patterns were used to verify the crack spacings as directly measured from the specimens during the experiments. Figures 5-1 to 5-12 show the stabilized crack patterns of the panels. Two main types of cracks developed in the panels; namely, primary and secondary cracks. The primary ones are those major cracks that penetrated through the full thickness of the panels; while the secondary cracks are defined as those that penetrated for only some distance through the thickness. Splitting cracks (i.e. parallel to the loading over the bar) are considered as secondary cracks. It should be noted that Broms (1965) defined primary cracks as those that are visible and show on the surface of the concrete. Broms also defined secondary cracks as those that do not progress to the concrete surface (i.e. not visible). To avoid conflict with Broms' definition, the latter type of cracks will be referred as 'internal cracks' in the ensuing discussion. Since the internal cracks are non-visible, they are not reported in the crack pattern results. In the presentation of the crack patterns, primary cracks are presented by using a relatively thicker line than minor or secondary cracks.

Table 5-1 summarizes the main test results recorded for the tested panels. The test results are reported as per the loading direction (i.e. EW and/or NS). For each panel, the table shows the experimental results of:

- Initial cracking load N_{cr}, which is the load at which the first initial crack(s) occurs;
- Loads for subsequent cracks; and
- The concrete cracking strength f_{cr} is defined as the maximum tensile stress that can be sustained by concrete under the imposed N_{cr}.

5.2.1 Cracking under uniaxial direct tension

The development of cracks in the GFRP-reinforced panels tested under uniaxial direct tension loads follows an almost typical cracking sequence. However, some differences between the tested panels are noticed which depend on the properties of the panels as discussed later.

Figure 5-13 shows the recorded stages of failure for panel P1-GNU-16-1.0-1.5 as a typical illustration. The GFRP-RC panels transfer from a normal uncracked stage to a stage of cracking where initial and subsequent cracks form. The development of cracks starts with primary major crack(s); followed by development of secondary cracks (if any). The stabilized cracking stage is then reached, beyond which the ultimate failure is accomplished by rupturing of the GFRP bars. For most of the panels, the GFRP bars rupture within the free distance between the specimen and any of the moving walls of the test setup.

In general, the final crack patterns developed under uniaxial tension show that the primary cracks form perpendicular to the loading direction (i.e. perpendicular to the direction of principal stresses). For instance, the crack pattern of panel P1-GNU-16-1.0-1.5 (Figure 5-1) shows that the first and second cracks, respectively develop at 216 and 249 kN. Both cracks are directly perpendicular to the loading direction. Eventually, they both propagate through cracks that cross the full thickness of the panel. As the load increases, splitting cracks (parallel to the loading direction) develop at nearly 481 kN, which is nearly 76% of the ultimate load (627 kN). Similar observations are noticed for other panels tested under uniaxial tension, such

as panels P2-GNU-16-1.0-2.5, and P7-GNU-13-0.7-2.5 as shown in Figures 5-2 and 5-5, respectively. The only difference is the stage of developing splitting cracks as discussed later.

In general, the commencement of cracking is influenced by the transverse bar locations. In many instances, cracks initially develop near a transverse bar location. The progress of cracks afterwards depends on the configuration of the panel and applied tension loading case.

5.2.2 Cracking under biaxial direct tension

The GFRP-RC panels subjected to biaxial tension follow a cracking sequence that is relatively different from panels subjected to uniaxial tension. For the latter, cracks form through different stages of loading which include uncracked, crack formation, stabilized, and then GFRP rupture. During the crack formation stage, one crack formed, followed by another, until reaching the stabilized cracking stage. However, under biaxial tension, two or three cracks developed together (i.e. multiple cracks) in both of the orthogonal directions. These cracks develop close to the same initial cracking loading stage. This results in no significant changes in the final cracking pattern beyond this initial cracking stage. In other words, the stabilized stage is achieved almost as early as the first initial crack formation. For example, the stabilized crack pattern of panel P3-GNB-16-1.0-2.5 (Figure 5-3) shows that most of the cracks develop at an initial tension load of 100 ~ 120 kN and a few secondary and minor cracks develop at a higher load of 207 kN. Such a difference in the crack formation sequence is attributed to the type and equal magnitude of biaxial tension loads applied. Therefore, all cracks occur at almost the same time in both directions. Such cracks are also influenced by the locations of the reinforcing bars, which in most cases, act as crack initiators. The other relevant

observation is that cracks are almost identical in both directions; which can also be attributed to the equal loading and equal bar spacing in the biaxial direction.

Where most of the cracks developed and converged towards the orthogonal reinforcing bar locations, it is noted that at certain locations, the cracks tend to follow relatively inclined patterns. This can be shown by the crack pattern of panel P3-GNU-16-1.0-2.5 (Figure 5-3) and it is even more pronounced for panel P10-GNB-16-0.7-2.5 (Figure 5-6). The crack directional angle; the angle between the crack and the direction of the reinforcement, was measured. In general, most of the inclined cracks have a directional angle between 45° and 60°, and in particular, within the middle regions between the GFRP bars. Since equal biaxial tension was applied to the panels, this range of crack directional angles is found to be reasonable. The change in the crack direction is attributed to the variation in principal stresses with the development of cracks under loading. In addition, as the cracks progress away from the influence of the effective concrete volume surrounding the GFRP bars (effective RC tension zone), cracks tend to progress through the weakest path across the concrete cross-section. This can be observed, in particular, towards the boundaries of the specimen, and midway between the bar locations. The effect of the specimen boundaries and equilibrium of forces at the locations of intersection of the GFRP bars could be another reason for this trend of crack inclination in some regions.

One of the direct effects of crack inclinations is that they affect the overall resistance of the biaxially tensioned panels, in terms of cracking loads and stresses. As shown in Table 5-1, the cracking and failure loads recorded for GFRP-RC under biaxial tension are generally lower than those subjected to uniaxial tension. For instance, panel P3-GNB-16-1.0-2.5 experiences

an N_{cr} = ~ 126 kN, which is nearly 22% lower than the corresponding panel P2-GNU-16-1.0-2.5 that is subjected to uniaxial tension. This decrease is also reflected on the f_{cr}, which decreases by almost 40% due to the biaxial loading effect. Using a lower reinforcement ratio of 0.7%, the cracking load for panel P10-GNB-16-0.7-2.5 is 31% and 47% lower than panels P5-GNU-16-0.7-2.5 and P7-GNU-13-0.7-2.5, respectively. The average concrete cracking stress of panel P10-GNB-16-0.7-2.5 is also nearly 30% and 44% less than that for P5-GNU-16-0.7-2.5 and P7-GNU-13-0.7-2.5, respectively. Hence, for NSC panels, the concrete cracking strength under biaxial tension is nearly 22% to 30% less than that for the corresponding panels subjected to uniaxial tension. A decrease of 20% to 30% in the ultimate tension load carried by GFRP-RC panels under biaxial tension can also be observed.

A similar observation is noticed for HSC panels. For instance, panel P6-GHB-16-1.0-2.5, which was subjected to biaxial tension, experiences an N_{cr} that is 23% less than the corresponding load of panel P4-GHU-16-1.0-2.5 that was subjected to uniaxial tension. There is also a reduction in the concrete cracking stress by almost 24%. Similar reductions are observed for panel P9-GHB-13-0.7-2.5 compared to panel P8-GHU-13-0.7-1.5 for the same reinforcement ratio as the cracking load is reduced by nearly 22%, while the cracking stress of concrete is reduced by 7%.

The above experimental observations are in good agreement with the findings of Aoyagi and Yamada (1983), which showed that there is a reduction factor in the tensile strength of RC shell elements in the tension-tension domain as a result of a continuum fracture of concrete. The researchers explained that in a steel-RC element subject to membrane forces, a

degradation of bond between concrete and steel proceeds more rapidly than in ordinary RC beams or slabs.

The crack development under biaxial tension affects the magnitude of stresses in the GFRP-RC panels through a general decrease in cracking loads and stresses. This decrease is mainly attributed to the effect of tensile stresses in the transverse direction where multiple orthogonal internal cracks form simultaneously. These internal cracks then develop to be major surface cracks in the initial cracking stage. Then, parts of these cracks develop in an arbitrary inclined pattern as a result of the variation in principal stresses with the progression of cracks. This is more noticeable within the regions relatively farther away from the location of the bars. Therefore, there is a dependence of stresses on the crack inclinations, which results from the applied biaxial tension.

According to an investigation by Aoyagi and Yamada (1985), about a 25% reduction in the uniaxial tensile strength is experienced by specimens subjected to equal biaxial tension. This reduction is in reasonable agreement with the general reduction of cracking loads and stresses recorded for the GFRP-RC panels, which confirms the experimental findings and the explanation discussed above.

5.2.3 Effect of concrete strength

The effect of HSC on the behaviour of GFRP-RC can be evaluated through examining the behaviour of the specimens tested within Series I and III. These include panels P2-GNU-16-1.0-2.5, and P4-GHU-16-1.0-2.5 which are subjected to uniaxial loading; and panels P3-GNB-16-1.0-2.5 and P6-GHB-16-1.0-2.5 which are subjected to biaxial tension.

There are some similarities in the cracking behaviour for both types of concrete. The crack development in the GFRP-RC panels made of HSC and subjected to uniaxial tension follows a sequence that is nearly similar to those recorded for NSC panels. Under uniaxial tension, the HSC panels typically transfer from the uncracked stage to crack formation stage once the tensile strength is reached. Through the crack formation stage, initial and subsequent cracks develop. Similar sequences of crack formation are also observed for HSC panels subjected to biaxial tension; for which all cracks form in both of the orthogonal directions, and nearly at the same initial cracking loading stage. The crack patterns of the HSC panels also show that primary cracks typically form perpendicular to the loading direction, i.e. perpendicular to the direction of the principal stresses.

Similar to NSC panels, the HSC panels subjected to biaxial tension have a final number of cracks that is almost identical in both loading directions. This can be attributed to the equal biaxial tension and equal bar spacings in the orthogonal directions. All cracks form in both of the orthogonal directions nearly at the same initial cracking loading stage and there is no significant change in the cracking pattern that has been formed until the stabilized stage is reached. This means that the stabilized cracking stage is accomplished at the same time or with a longer time and slightly higher load after the initial cracking load is reached.

Although there are similarities between NSC and HSC panels in some cracking aspects, there are also some important differences that should be highlighted as follows:

- In general, the test observations revealed that the HSC panels show a more brittle cracking mechanism compared to NSC. In particular, this is noticed with respect to the mechanism

of crack development and progression through concrete. For NSC panels, the primary or major cracks form gradually and at a slower rate to achieve full penetration either through the panel thickness or across the panel width while for HSC panels, the commencement of cracks occur 'immediately' as major cracks penetrate sharply through the full thickness of the panel. The cracks also form directly and instantly across the panel width. In fact, such a cracking response was never observed for panels made of NSC. The brittle nature of HSC is considered one of the main reasons for such behaviour in which cracks open directly, losing the interfacial bond and aggregate interlock at the crack mouth opening interface region. For NSC panels, cracks usually develop around the aggregate, i.e. at the interfacial surface between the aggregates and cementitious paste or through the cementitious paste itself. This results in a gradual progression in the development of cracks across the panel.

- For HSC panels, cracks follow a relatively sharper line across the panel compared to NSC panels. This means that once a crack starts, it is a one path progression across the width of the panel and through its thickness. This path is perpendicular to the loading direction. Cracks develop through the weakest paths. Thus, cracks directly develop through the cementitious paste and coarse aggregate, causing sharp and immediate cracking once the cracking strength of concrete panel f_{cr} is reached. This behaviour is related to the nature of HSC, as fractures occur through both cementitious paste and aggregate at the same time, and thus reflects its brittleness. Such behaviour reflects on the development of the secondary cracks for the tested HSC panels. The use of HSC eliminates the development of secondary cracks compared to NSC at the same level of stress.

- Similar to NSC, crack patterns are influenced by the locations of the reinforcement grid. Cracks tend to start and/or converge toward the bar locations. Bars act as crack initiators, and because cracks progress immediately and sharply across the panel width and thickness, there is no significant deviation from the locations of the bars. This can be noted in the crack pattern of panel P4-GHU-16-1.0-2.5 (Figure 5-7).

- Few insignificant crack inclinations from the reinforcing bar axes are observed in the crack patterns of biaxially loaded panels. Compared to NSC panels, such inclinations are not significant enough to follow, since most of them progress sharply across the panel.

- The results shown in Table 5-1 reveal that there is a significant improvement in the cracking loads and stresses due to the use of HSC. Panel P4-GHU-16-1.0-2.5 made of HSC is compared to panel P2-GNU-16-1.0-2.5 made of NSC. Both panels are subjected to uniaxial tension. Due to the use of HSC, the N_{cr} and concrete cracking strength increase by 45% and 43%, respectively. For the panels subjected to biaxial tension; namely, P3-GNB-16-1.0-2.5 (NSC) and P6-GHB-16-1.0-2.5 (HSC), similar increases in the N_{cr} and concrete cracking strength are recorded. The N_{cr} and concrete cracking strength increase by 45.6% and 44%, respectively. The change in the ultimate loads carried by the panels subjected to uniaxial tension is not significantly changed due to the increase in the concrete compressive strength. However, under biaxial tension, a 32% increase in the ultimate load is recorded for panels due to the use of HSC.

- The average concrete compressive strength of HSC panels is 77.3 MPa, which is nearly 44% higher than NSC (f'_c = 43.6 MPa). Therefore, the initial crack loading and concrete

cracking stress increase nearly proportional to the increase in the concrete compressive strength. This is valid for uniaxial and biaxial tension loading cases.

5.2.4 Effect of concrete cover to bar diameter ratio

The effect of cover to bar diameter ratio c_c / d_b on the cracking behaviour of GFRP-RC panels can be discussed by comparing NSC panels P1-GNU-16-1.0-1.5 and P2-GNU-16-1.0-2.5, with c_c / d_b = 1.5 and 2.5, respectively. The HSC panel P8-GHU-13-0.7-1.5 has a c_c / d_b = 1.5 and can be compared with other HSC panels which have c_c / d_b = 2.5.

The direction of cracks is not significantly influenced by the change in the c_c / d_b ratio. The cracks normally develop perpendicular to the principal stresses or loading directions for both uniaxial and biaxial tension cases.

The crack patterns show that the total number of primary cracks for panel P1-GNU-16-1.0-1.5 (Figure 5-1) is only two, compared to three primary cracks that developed in panel P2-GNU-16-1.0-2.5. A similar observation is noted for the HSC panels, as the total number of primary cracks for panel P8-GHU-13-0.7-1.5 is two compared to three primary cracks developed in panels P4-GHU-16-1.0-2.5, P6-GHB-16-1.0-2.5 and P9-GHB-13-0.7-2.5. As shown in Figures 5-1 and 5-9, one of the two cracks develops independently from the bar location influence. This means that cracks are not influenced by the transverse bar locations, which could be a result of using a low c_c / d_b.

The reduction in the final number of cracks developed where c_c / d_b = 1.5 can only be explained by discussing its confining effect on the GFRP reinforcing bar, and consequently, its

effect on the bond stress and mechanism of load transfer between the GFRP bar and surrounding concrete volume. When a crack forms in a RC member, the stress in concrete must be zero at the edge of the crack (Figure 2-4). With increasing distance away from the crack, the concrete stress will increase until at some distance, l_t, the stress distribution remains unaffected by the crack. As explained earlier, the length l_t is often referred as 'transfer length'; which is defined as the distance at which there is a significant change in the bar strain distribution. This means that the crack influence on the stresses in the concrete is within a distance $\pm l_t$ of the crack location. Hence, the next crack to develop should form outside the l_t. The shape of the strain or stress curve over the l_t is arbitrary, as it will depend upon the distribution of bond stress along the bar. This l_t is characterized by a large variation in the bar strain or stress distribution. As the bond stress distribution is usually affected by the amount of concrete confinement around the bar, which arises from the concrete cover, hence, the effect of c_c / d_b appears. The new crack will not form within a distance l_t of the first crack since the stress in the concrete within l_t has been reduced to below the tensile strength. However, the new crack can form anywhere else and hence the spacing between cracks cannot be less than l_t. Further cracks can successively form until there remains no part of the member where the stress has not been reduced by cracking. When this occurs, the resulting pattern is known as a 'stabilized crack pattern'. It should be clear that where the spacing is marginally above $2l_t$ then there will be some parts where the stress is still above tensile cracking strength and more cracks can form whereas if a crack is marginally at a distance less than $2l_t$ from another crack, then the stress will be reduced below the tensile cracking strength at all points between the two cracks.

In fact, it is difficult to experimentally measure the l_t (Beeby and Scott 2005). However, the strain gauges attached to the bars are used to construct the strain profiles along the length of the panel. These strain profiles can give an approximate indication of the overall changes in strains and thus the deformational response due to applied tension and location of cracks. Hence, the l_t can be roughly estimated from the bar strain distribution profiles. Figures 5-14 to 5-16 show the changes in the strain distribution along the GFRP bars for panels P1-GNU-16-1.0-1.5, P2-GNU-16-1.0-2.5, and P8-GHU-13-0.7-1.5, respectively. The strain distributions are approximate interpolation between the readings of strain gauges that are attached to the GFRP bars at different locations parallel to the loading direction. Examining such a plot along with the crack patterns can show the changes in the strain distribution at the crack vicinities. As the strain distribution is plotted for different loading stages up to nearly failure, it can be noticed that the strain variation is directly related to the sequence of the recorded cracking and location of cracks.

From these profiles, the l_t for panel P1-GNU-16-1.0-1.5 is almost 60 to 100 mm adjacent to the crack (Figure 5-14). The l_t for panel P8-GHU-12-0.7-1.5 is approximately 60 to 100 mm adjacent to the crack (Figure 5-16). These are compared to the l_t from the GFRP strain distribution for panel P2-GNU-16-1.0-2.5 which has an l_t of ~ 70 mm (Figure 5-15). This indicates that the load carried by panel P1-GNU-16-1.0-1.5 requires a longer l_t to be transferred and thus creates another crack due to the reduction of the concrete cover. However, for panel P2-GNU-16-1.0-2.5, the l_t is shorter, and thus, has the opportunity to develop an extra major crack within the panel length.

ACI 224.2 (1992) states that the number of visible cracks can be reduced at a given tensile force by simply increasing the concrete cover. ACI 224.2 (1992) further discusses that with a larger concrete cover, a larger percentage of the cracks remain as internal cracks at a given tensile force. In order to discuss these statements, consideration is given to the experimental observations and the interpretations discussed above. Hence, it should be noted that ACI 224.2 (1992) defines the visible cracks as primary cracks and internal cracks as secondary cracks. This is based on Broms' (1965) research work. Hence, the experimental observations may suggest that the final number of primary cracks can be decreased by decreasing the c_c / d_b, which contradicts the ACI 224.2 statement. In fact, this is not completely true, because the stage of developing secondary and splitting cracks is significantly influenced by using a low c_c /d_b. For instance, the splitting cracks in panel P1-GNU-16-1.0-1.5 developed as early as 60% to 70% of the ultimate failure load while for panel P2-GNU-16-1.0-2.5, there was no sign of splitting cracks until nearly 97% of the ultimate failure load. For panel P8-GHU-13-0.7-1.5, there was no evidence of splitting or secondary cracks developing until failure, which is a result of using HSC. Therefore, by considering the splitting cracks as visible cracks (according to the ACI 224.2 (1992) or Broms' (1965) definition), it can still be concluded that the number of visible cracks can be reduced at a given tensile force by simply increasing the concrete cover.

Based on an earlier pullout tests conducted by Ehsani et al. (1996), a splitting failure is more likely to occur when the concrete cover is less than or equal to 2 d_b. However, a pullout failure is more likely to occur if the concrete cover exceeds 2 d_b. Hence, the ACI 440.1 (2002) design guide for FRP-RC recommends the use of a concrete cover that is not less than the d_b.

In order to calculate the development length of the FRP reinforcement, a modification factor of 1.5 should be used as a multiplier of the basic development length when c_c equal d_b. This modification factor can take a value of 1.0 when c_c exceeds 2 d_b (ACI 440.1 2002).

In general, the presented experimental evidence confirms that GFRP-RC is more vulnerable of the development of splitting cracks when the concrete cover is less than or equal to $2d_b$, which confirms the findings of Ehsani et al. (1996). Therefore, to improve the structural aesthetics and delay the stage of development of splitting cracks, it can be recommended that GFRP-RC members subjected to direct tensile stresses should be designed for a serviceability limit not greater than 50% of the ultimate load and the c_c / d_b should not be less than 2.5. This should reduce the excessive cracking and thus preserve the integrity of the GFRP-RC structures.

The experimental results show that panel P2-GNU-16-1.0-2.5, which has a c_c / d_b = 2.5, experience an N_{cr} = 163 kN, which is 32% less compared to N_{cr} = 216 kN for panel P1-GNU-16-1.0-1.5. However, the ultimate tension load of P2-GNU-16-1.0-2.5 is nearly 20% higher. This is a result of the relatively early development of splitting cracks in panel P1-GNU-16-1.0-1.5, which affects the ultimate resistance of the panel. For HSC panel P8-GHU-13-0.7-1.5, N_{cr} and stress is 15.9% and 16% less respectively, compared to panel P4-GHU-16-1.0-2.5. However, this is not be directly related to the change in the c_c / d_b, but could be related to the change in the reinforcement ratio.

Thus, due to changing of the c_c / d_b, the differences in cracking loads and stresses are relatively scattered. Since a small c_c / d_b = 1.5 was employed in only one panel, P1-GNU-16-

1.0-1.5, from the NSC series in order to assess the development of splitting cracks, there is no clear effect of the c_c / d_b on the N_{cr} and stresses that can be deduced. Thus, further tests are recommended for future research.

5.2.5 Effect of bar spacing

As previously mentioned, transverse bars generally act as crack initiators, and thus force the cracks to develop at certain locations across the panel. This observation is similar to the experimental findings of Rizkalla et al. (1983). However, this behaviour is not completely observed in panels P5-GNU-16-0.7-2.5 and P10-GNB-16-0.7-2.5, which have a larger bar spacing of 300 mm. The cracks in these specimens do not exactly follow the reinforcement grid. Cracks appear to start and then progress relatively through the weakest path influenced by high local stresses at the specimen boundaries. It can be argued that they progress relatively randomly. It should be noted that there is a difference between the commencement of cracks and their progression. For specimens with relatively small bar spacings, cracks tend to start at or close to the bar locations and their progression are more likely to be at the same locations. However, for larger bar spacings, cracks commence relatively independent of the bar locations, and then tend to progress according to the weakest concrete material path or converging to a bar location. This observation is valid for all specimens with $c_c / d_b = 2.5$.

Nawy and Blair (1971) observed a similar phenomenon in two-way slabs reinforced with steel grid. The researchers explained that there are stress concentrations that initially develop at the points of intersection of the reinforcing bars. These stress concentrations cause plastic deformations of the concrete at these locations as a result of the energy imposed by the external

load per unit area of slab. The bond between the bar or wire and the concrete at these locations is destroyed and active cleavages start to generate fracture lines towards the paths of least resistance.

Similarly, when the GFRP reinforcing bar spacings are relatively large, such as in the case of panels P5-GNU-16-0.7-2.5 and P10-GNB-16-0.7-2.5, the magnitude of the stress concentrations are too low to initiate cracks along the bars. This results in the primary cracks following the weakest path by adjusting the local stress concentrations at the specimen boundaries where the GFRP reinforcing bars are pulled. For smaller bar spacings, the magnitude of stress concentrations is relatively higher, and thus the commencement of cracks is more influenced by the reinforcement grid location.

There is no significant change in the cracking loads and stresses due to the increase of bar spacing from 150 mm to 300 mm. Since there is overlapping between the change in the bar spacings, and the change in the d_b and reinforcement ratio, it is difficult to separate the test parameters without changing the specimen cross section dimensions. Future tests are recommended.

5.2.6 Effect of reinforcement ratio

There is no significant influence on the cracking formation sequence and stabilized crack patterns due to changes in the d_b and/or reinforcement ratio for GFRP-RC panels of Series I and II. For panels P2-GNU-16-1.0-2.5 (ρ = 1.0%) and P7-GNU-13-0.7-2.5 (ρ = 0.7%), where they both have 150 mm bar spacing, the final number of primary cracks is almost the same.

From Table 5-1, it can be noticed that there is no significant change in the cracking loads and stresses due to the decrease in the reinforcement ratio from 1.0% to 0.7%. For instance, for the GFRP-RC panels P3-GNB-16-1.0-2.5 and P10-GNB-16-0.7-2.5 subjected to biaxial tension, the differences in N_{cr} and average concrete cracking stress are less than 1%. Since N_{cr} is almost equal and a smaller reinforcement area is used, these results in a 32% increase in the GFRP stress at the N_{cr}. Due to decreasing the reinforcement ratio, the ultimate load only decreases 10 - 15%, which can be attributed to a smaller reinforcement area (smaller d_b) placed in the same concrete cross-section.

The main change that can be noticed is between panels P7-GNU-13-0.7-2.5 and P2-GNU-16-1.0-2.5, which were subjected to uniaxial tension. The use of a smaller d_b, and thus less reinforcement ratio, results in a higher N_{cr} by nearly 30%. There is also an increase in average concrete cracking stress by 27%. Since for the same d_b, the reinforcement ratio does not significantly affect the N_{cr} and stresses, such an increase could be attributed to a smaller d_b used. The increase in the N_{cr} and cracking stress could be attributed to the improved GFRP-concrete bond characteristics associated with using the smaller d_b of 13 mm. A smaller d_b means fewer effects of the shear-lag that will be experienced in the GFRP bar. The shear-lag effect, which occurs in larger diameters between fibres in the core and the fibres in the outer diameter of the bar, appears more influential as the GFRP d_b becomes larger (Benmokrane et al. 1996a; Tighiouart et al. 1998). However, there is a 42% decrease in the ultimate tension load of P7-GNU-13-0.7-2.5 compared to P2-GNU-16-1.0-2.5 due to the decrease in the reinforcement area used, thus the overall tension capacity is smaller as expected.

5.3 Crack Spacings

In general, the variation in crack spacings is a result of considerable variation in stress distribution until the crack stabilization stage. The variability in the tensile strength of concrete, bond integrity of the bar, and proximity of previous primary cracks which tend to decrease the local tensile stress in the concrete, are the main causes of this variation in crack spacing (ACI 224.2 1992).

Table 5-2 shows the spacings of primary cracks and the total number as recorded for the tested panels, from which the following points can be summarized:

- There is an increase of about 14% in the average crack spacings of NSC panels due to the change in the loading from uniaxial tension (panel P2-GNU-16-1.0-2.5) to biaxial tension (panel P3-GNB-16-1.0-2.5).

- There is about a 10% increase in the average crack spacing recorded for HSC panels under biaxial tension compared to uniaxial tension cases. Similar increases in the maximum and minimum crack spacings are also recorded. It can also be noticed that the number of primary cracks developed at the stabilized stage is nearly the same for NSC and HSC panels. However, the use of HSC improves the final number of cracks by eliminating the development of secondary and splitting cracks. There is no significant influence on the average crack spacing due to the use of HSC. Nevertheless, there is no large variation between the values of the minimum, mean, and maximum crack spacings for HSC panels compared to the NSC panel recorded spacings. This can be attributed to the better homogenous material properties of HSC. Thus, the crack progresses sharply, taking a

straight-line path directly through the concrete matrix once it has started. This is not the case for NSC, where cracks start and progress randomly across the weakest path through the panel. Therefore, HSC is recommended for improving the structural aesthetics of GFRP-RC.

- There is not significant variation in crack spacings due to the change in reinforcement ratio. It appears that the bar spacing has more influence on the crack spacing than the reinforcement ratio. A larger bar spacing means larger maximum crack spacing. This observation matches with the findings of Williams (1986). Also, a larger transverse bar spacing means a larger crack spacing. This is attributed to the effect of the bar location in starting a crack in its proximity.

- The use of a relatively small c_c / d_b results in a larger spacing of primary cracks. On the other hand, it results in the development of more splitting cracks at a given level of tension load.

5.4 GFRP-RC Cracking Behaviour Compared to Steel-RC

The specimens of Series V are two reference specimens made of NSC and reinforced with traditional steel bars. Panels P11-SNU-16-1.0-2.5 and P12-SNB-16-1.0-2.5 were tested under uniaxial and biaxial tension loading, respectively. Both panels correspond to GFRP-RC panels P2-GNU-16-1.0-2.5 and P3-GNB-16-1.0-2.5, respectively.

5.4.1 Development of cracks

Figures 5-11 and 5-12 show the crack patterns of steel-RC panels P11-SNU-16-1.0-2.5 and P12-SNB-16-1.0-2.5, respectively. For panel P11-SNU-16-1.0-2.5, which is tested under uniaxial tension, the cracking behaviour is relatively different from panel P2-GNU-16-1.0-2.5. A single primary crack develops at a load of 317 kN, which corresponds to a concrete cracking strength of 2.4 MPa. However, an analysis of the data showed that this crack could have developed internally at a load equal 269 kN, which corresponds to an average concrete stress of about 2.27 MPa. As the load was increased, no further major cracks developed. At a load of 420 – 430 kN, the load was relatively stable, indicating that yielding of the steel reinforcement bars occurred. Only some cracks appear on the side faces of the specimens (Figure 5-19). Beyond yielding, the load was then increased up to 590 kN at which it was decided that the test to be terminated. To better analyze the cracking behaviour of panel P11-SNU-16-1.0-2.5, the strain gauges attached to the bars were used to construct the steel strain profile along the length of the panel. These strain profiles give an indication of the changes in strains and thus the deformational response to the application of load and cracks locations. An analysis of the strain distribution (Figure 5-17) of this specimen indicates that the yielding strain (~2000 με) occurs at the proximity of the middle major crack.

Similar to GFRP-RC panels, the final crack patterns developed under uniaxial tension show that the primary cracks form perpendicular to the loading direction. Under biaxial tension, all cracks also develop at almost the same time in both directions. These cracks are influenced by the locations of the reinforcing bars, which act as crack initiators. The other relevant observation is that cracks are almost identical in both directions; which can be also

attributed to the equal loading and equal bar spacing in the biaxial direction. Therefore, the effect of the bar type on the development of cracks is similar.

Under uniaxial tension, the recorded cracking characteristics showed that the steel-RC (panel P11-SNU-16-1.0-2.5) experiences only one primary crack compared to about three major cracks that developed in the GFRP-RC (panel P2-GNU-16-1.0-2.5). Such behaviour can be explained from the cracking and bond stress transfer mechanism. The bond stress transfer mechanism of deformed steel bars is inherently three dimensional, resulting from the bearing stress that arises when the lugs of deformed bars push against the surrounding concrete, which results in conical compression struts as shown in Figure 5-18. The conical bond actions between the bar and concrete can be resolved into radial and tangential components. The tangential component per unit surface area of the reinforcing bar is the bond stress whereas the radial one causes the confining stress. The bond stress can lead to primary cracks if its summation over a certain length exceeds the concrete tensile strength. When the tensile ring stress (radial stress) exceeds the cracking strength, then splitting cracks will form (Maekawa et al. 2003). Due to bonding, local stresses in concrete and reinforcement are not uniform, but vary along the bar axis. In front of the steel bar lugs, internal cracks develop, causing another variation in the stresses between the primary cracks.

From the average distribution of the steel strain in panel P11-SNU-16-1.0-2.5 (Figure 5-17), it can be noticed that there is a large variation in the steel strain within a distance that varies from 90 mm to more than 250 mm around the primary crack location. This distance is equivalent to the l_b in which there is a large variation in the bar strains. The large variation in the steel strains could be attributed to the internal cracks that developed in front of the steel bar

lugs within the l_t adjacent to the primary visible crack. Beyond this length, another crack may develop at another location outside the l_t. However; this l_t is relatively large compared to the panel length, which could be a reason for the development of only one crack until steel yielding occurred. This explains that the number of cracks developed within the same panel specimen is influenced by the length required to transfer the loads from the bar to the concrete.

Also, by comparing the steel strain distribution in panel P11-SNU-16-1.0-2.5 (Figure 5-17) to the GFRP strain distribution in panel P2-GNU-16-1.0-2.5 (Figure 5-15), it can be noticed that the latter has a relatively smoother variation in the strains. This could be attributed to the smaller number of internal cracks that develop at the interface between the GFRP bar and concrete. The smaller number of internal cracks is a result of the smaller surface deformations (height of bar lugs) of the GFRP bars. However, it can be noticed that steel-RC panels experience much fewer strains to achieve its stabilized cracking stage compared to the GFRP-RC panels. This is due to the difference in the modulus of elasticity between the two types of reinforcing bars. If the steel-RC panel is required to develop more number of cracks, this would have required more tensile strains to be induced within the panel length. However, this is not the case, as the average distribution of steel strain (Figure 5-17) shows relatively high local strains around the major crack location developed in panel P11-SNU-16-1.0-2.5. This can be interpreted that beyond this stage of initial cracking, there are no signs of other major cracks developing. The main issue is that more cracks developed in the GFRP-RC panel as a result of the larger tensile strains induced in the GFRP.

The stabilized crack patterns are fairly similar for panels P3-GNB-16-1.0-2.5 (Figure 5-3) and P12-SNB-16-1.0-2.5 (Figure 5-12) subjected to biaxial tension. The difference in number

of primary cracks between both panels is not as significant as the panels subjected to uniaxial tension. This is a result of the effect of biaxial tension causing a general reduction in the N_{cr} and concrete stresses as previously discussed. This allows the reinforcement grid to act as crack initiators and thus cracks converge to the locations of these reinforcing bars. However, because of the low modulus of elasticity of GFRP, more secondary cracks develop in panel P3-GNB-16-1.0-2.5.

Table 5-2 shows that there is comparable crack spacing between steel- and GFRP-RC panels. Others observed similar differences (Joh et al. 1997). Bischoff and Paixao (2004) observed that the spacing between cracks probably depends on the surface characteristics for the steel and GFRP bars. This observation is found applicable to the present experimental results. The bar surface characteristics should affect the bond-stress transfer mechanism, which should be considered in a cracking model.

5.4.2 Cracking loads and stresses

In general, the N_{cr} and cracking stress for steel-RC panels are higher than the corresponding GFRP-RC panels. Under uniaxial tension, Table 5-1 shows that panel P11-SNU-16-1.0-2.5 has an N_{cr} of 317 kN, which is ~ 93% higher than the N_{cr} of the corresponding GFRP-RC panel P2-GNU-16-1.0-2.5. Under biaxial tension, Table 5-1 shows that the N_{cr} of panel P12-SNB-16-1.0-2.5 is higher by ~ 81% than the N_{cr} of panel P3-GNB-16-1.0-2.5. The average concrete cracking strength of the steel-RC panel is 76% higher than the cracking strength recorded for the GFRP-RC panel. These differences can be directly attributed to the

difference in the modulus of elasticity of the GFRP and steel, and also the different surface characteristics of the steel bar compared to the GFRP.

Figures 5-19 and 5-20 compare the mechanical behaviour of GFRP-RC panels made of HSC and NSC under uniaxial and biaxial tension, respectively. The results of the corresponding steel-RC panels of Series V made of NSC are included in the figure for comparison. As previously mentioned, due to the lower modulus of elasticity of GFRP compared to the steel, there are reductions in cracking loads and concrete stresses. Figures 5-19 and 5-20 show that such reductions are recovered by the use of HSC. The use of HSC compensates for the reduction in the cracking loads and stresses due to the use of GFRP bars combined with NSC. The HSC improves the overall resistance of the GFRP-RC, thus it almost reaches the same cracking loads and stresses of NSC panels reinforced with traditional steel bars.

Accordingly, changing the concrete type for HSC is recommended. The use of HSC with GFRP will lead to significant improvements when it is compared to GFRP reinforced NSC and steel reinforced NSC. Such changes include: (1) an increase of the N_{cr} and initial cracking strain; (2) a rise of the average concrete cracking strength load due to the higher tensile strength of HSC; and (3) reduction in the total number of visible cracks; especially the secondary splitting cracks.

5.4.3 Effective RC tension zones

An important phenomenon was observed for most of the tested panels, steel-RC and GFRP-RC where cracks form on the sides of the panels. These cracks form around the bars.

Figures 5-21 and 5-22 show typical crack formation on the sides of steel-RC and GFRP-RC panels, respectively. These side cracks are more noticeable in specimens tested under uniaxial tension. However, it can be noticed that the cracks develop on a larger scale or diameter around steel bars compared to similar GFRP-RC panels. This results in an overlapping between the cracked regions around each steel bar. The same cracked zones are observed for panel P12-SNB-16-1.0-2.5, also with a similar larger cracked diameter compared to the corresponding GFRP-RC panel.

Such phenomenon was observed earlier by MacGregor et al. (1980) for steel-RC panels. The researchers related such a phenomenon to the mechanism of the transferring of force from the reinforcing bar to concrete. Thus, it was assumed that the transfer of force is accomplished primarily by the bearing of the bar deformations on the concrete around the bar. This results in a wedging action which leads to splitting cracks that isolate wedge shaped pieces of concrete. At very high strains, prior to failure, these pieces could come loose from the surface and fall. The GFRP bars used in the experiments have much less surface deformations compared to the traditional steel bars. However, such a mechanism could be also assumed as one of mechanisms of force transfer.

In the same context, the influence of effective RC tension zones should also be considered for explaining such a phenomenon of side cracks. The concept of effective tension zones was introduced earlier for steel-RC (Chi and Kirstein 1958) and later was adopted by several design codes (CEB-FIP 1990; NBR 1992). The approach is based on theoretically dividing to the RC members into a series of cylinders or prisms, each around a single bar of the tension reinforcement. The effective tension zone is defined as the area of concrete that surrounds the

bar and has the same centroid of the tension bars. Thus, this effective zone contributes 'significantly' in resisting tension. Beyond this zone, the influence of bond interaction between the concrete and reinforcing bar decreases relatively. Thus, the cracked regions around the bars can be reasonably assumed as representative of the influence of the effective tension zones around the bars.

The region of the RC tension zone indicates a maximum volume of concrete that the effect of bonding can reach. The size of the RC effective tensile zone should be governed by the crack control ability of reinforcement, which depends on the reinforcement ratio and the d_b (Maekawa et al. 2003). For a single reinforcing bar, Maekawa et al. (2003) showed that the maximum size of the concrete is limited by the yielding of the reinforcing bar f_y. Hence, the largest effective zone area can be calculated as follows:

$$A_{ec,max} = \frac{A_s f_y}{f_t'} \tag{5.1}$$

where A_s is the cross-sectional area of the reinforcing bar; $A_{ec,max}$ is the possible largest area of the bond effective zone in concrete; and f_y and f_t' are the yield strength of the reinforcing bar and the tensile strength of concrete, respectively.

For two-dimensional applications or in case of multi-layered reinforcing bars, the RC tension zone is calculated according to each layer. Since part of the zone may fall outside the structure boundary and there may be an overlapping effect between the bars, Maekawa et al. (2003) showed that the height of the RC effective zone can be calculated by using the following relation:

$$h_{eff} = \frac{h_{max}^2 n_{bars}}{b} \tag{5.2}$$

where h_{eff} is the equivalent height of the RC tension zone; n_{bars} is the number of steel bars; b is the length of the RC member where the bars are spaced; and h_{max} is the maximum height of the effective tension zone which is limited by the yielding strength of steel reinforcement, and calculated as follows:

$$h_{max} = \frac{\sqrt{\pi}}{2} . d_b . \sqrt{\frac{f_y}{f_t'}} \tag{5.3}$$

Using the above relations, the effective tension zone height can be estimated for the steel-RC panels P11-SNU-16-1.0-2.5 and P12-SNB-16-1.0-2.5 as 164.8 mm (~ 10.4 d_b) and 211.7 mm (~ 13.3 d_b), respectively. These values are in good agreement with the research work of Chi and Kirstein (1958), it was suggested that 16 d_b be used for steel bars. Moreover, the calculated values match with the 15 d_b used in the CEB-FIP (1990) and NBR (1992) codes to calculate the effective reinforcement ratio.

For specimens that clearly showed cracks on their sides, the dimensions of the crack regions were measured. This is done in order to confirm the above interpretation that the cracks which develop on the sides of the specimens are mainly due to the load-transfer mechanism and influence of the effective tension zones. Such cracked regions are assumed to be presented by effective diameters D_{eff} equivalent to the effective height h_{eff} (Eq. 5.2). The recorded D_{eff} of the cracked regions around the steel and GFRP bars are shown in Table 5-3. For steel-RC panels, D_{eff} / d_b varies from 10 to 12, with an average ratio of 11. These values match fairly well with the above calculated values for steel-RC panels. The agreement

confirms the interpretation that such cracks that are developed around the bars can show the size of the effective tension zone.

For the GFRP-RC panels, D_{eff} / d_b varies from 4.0 to 8.0 with an average ratio of 6.4. It should be noted that there is no significant difference between the D_{eff} of tension zones measured for HSC and NSC panels.

Therefore, the diameter of the effective tension zones are found to be dependent on the bar type used for reinforcement. By comparing the recorded sizes for the tested panels with the same reinforcing d_b, it can be concluded that the size of the effective tension zones for GFRP-RC is almost half the size of those developed around the traditional steel reinforcing bars.

5.5 Summary and Conclusions

In this chapter, the development of cracks in GFRP-RC panels is discussed. Based on the discussion, it can be concluded that the development of cracks and final crack patterns are dependent on the loading type, reinforcing bar spacings, c_c / d_b, and concrete strength. Crack patterns are found to be less dependent on other factors, such as d_b and/or reinforcement ratio providing that the same bar spacing is used. From this discussion, the following main conclusions can be summarized:

1. Under uniaxial tension, the GFRP-RC panels transfer from a normal uncracked stage to a stage of cracking where initial and subsequent cracks form. The development of cracks starts with primary major crack(s); followed by development of secondary cracks (if any). The stabilized cracking stage is then

reached, beyond which the ultimate failure is reached by rupture of the GFRP bars.

2. Under biaxial tension, cracks develop together in the form of two or three cracks (i.e. multiple cracks) in both of the orthogonal directions. These cracks develop nearly at the same initial cracking loading stage. This observation shows that there is no significant change in the final cracking pattern beyond this initial cracking stage.

3. The final crack patterns that are developed under uniaxial tension show that the primary cracks form perpendicular to the loading direction (i.e. perpendicular to the direction of principal stresses) whereas under biaxial tension and at certain locations, cracks tend to follow relatively inclined patterns. The change in the crack direction is attributed to the variation of principal stresses with the development of cracks under biaxial tension loading.

4. For NSC panels, the f_{cr} varied from 3.0% to 3.85% of f_c' under uniaxial tension, and from 2.24% to 3.04% of f_c' under biaxial tension. For HSC panels, the f_{cr} varied from 2.68% to 3.23% of f_c' under uniaxial tension, and from 2.44% to 3.52% of f_c' under biaxial tension. The crack development under biaxial tension affects the magnitude of stresses in the GFRP-RC panels through a general decrease in cracking loads and stresses. This decrease is mainly attributed to the effect of tensile stresses in the transverse direction where multiple orthogonal

internal cracks form simultaneously. These internal cracks then develop to be major surface cracks at the initial cracking stage. Then, parts of these cracks develop in an arbitrary inclined pattern as a result of the variation in principal stresses with the progression of cracks. This results in about 25% reduction in the initial cracking loads and concrete crack strength compared to panels subjected to uniaxial tension.

5. The brittle nature of HSC affects the development of the cracks with respect to two main aspects: (a) the commencement of cracks occurs 'immediately' as major cracks, penetrating sharply through the full thickness of the panel; and (b) cracks follow a relatively sharper line across the panel compared to NSC panels. This behaviour is related to the nature of HSC, as fracture occurs through both the cementitious paste and aggregate at the same time, and thus reflects its brittleness.

6. In order to improve the structural aesthetics and delay the development of splitting cracks, it is recommended that GFRP-RC members subjected to direct tensile stresses should be designed for a serviceability limit not greater than 50% of ultimate load and the c_c / d_b should not be less than 2.5. This should reduce the excessive cracking and thus preserve the integrity of the GFRP-RC structures.

7. The development of cracks is more likely to start at reinforcing bar locations for closer bar spacings and large concrete covers. This could be attributed to the

magnitude of the stress concentration and the energy absorbed per unit bar grid. This stress concentration can be too low to generate cracks along the bars for wider bar spacings.

8. The number of cracks developed with the RC member is dependent on the mechanism of bond stress transfer from the reinforcing bar to the surrounding concrete. The bond stress transfer mechanism of deformed steel bars is inherently three dimensional, resulting from the bearing stress that arises when the lugs of deformed bars push against the surrounding concrete. The internal cracks that develop in front of the bar lugs result in a large variation in stress distribution. For GFRP-RC, a relatively smoother variation in the strains is recorded. This can be attributed to the reduction in internal cracking mechanism as a result of the smaller deformations and different surface characteristics of the GFRP bars.

9. Steel-RC panels experience much less strains in achieving its stabilized cracking stage compared to the GFRP-RC panels. This is due to the difference in modulus of elasticity between the two types of reinforcing bars. This result means that GFRP-RC experiences more cracks once stabilized cracking is achieved, which is normally reached at a tensile strain of nearly two to four times that of steel-RC.

10. Due to the lower bar modulus of elasticity of GFRP compared to steel bars, there are significant reductions in cracking loads and concrete stresses. GFRP-RC panels cracked at N_{cr} nearly 10% to 20% that recorded for steel-RC panels.

11. The use of HSC compensates for the reduction in the cracking loads and stresses as compared to the use of GFRP bars combined with NSC. HSC improves the overall resistance of the GFRP-RC, thus it almost reaches the same cracking loads and stresses of NSC panels reinforced with traditional steel bars. Accordingly, changing the concrete type to HSC is recommended. The initial crack loading and concrete cracking stress increase nearly proportional to the increase in the concrete compressive strength. This is found to be valid for uniaxial and biaxial tension loading cases. The use of HSC with GFRP will lead to significant improvements when comparing GFRP reinforced NSC and steel reinforced NSC. Such changes include: (a) an increase of the N_{cr} and initial cracking strain; (b) a rise of the average concrete cracking strength load due to the higher tensile strength of HSC; and (c) reduction in the total number of visible cracks, especially the secondary splitting cracks if a small concrete cover is employed.

12. The size of the effective tension zones are found to be dependent on the bar type used for reinforcement. The size of the effective tension zones for GFRP-RC is almost half the size of those that develop around traditional steel reinforcing bars. Therefore, the diameter of the effective tension zones for this type of

GFRP bars can not be taken as the steel bars of the same diameter. The experimental evidence suggests that the size of an effective tension zone for GFRP-RC is about six to seven times the bar diameter ($6 \sim 7\ d_b$). This behaviour should be considered in the development of a cracking model.

Table 5-1: Cracking loads and stresses at initial crack occurrences

S	Specimen	f_c', (MPa)	Loading direction	Initial cracking load, N_{cr} (kN)	2nd crack load (kN)	3rd crack load (kN)	4th crack load (kN)	Ultimate load (kN)	Concrete cracking stress, f_{cr} (MPa)
I	P1-GNU-16-1.0-1.5	48.1	EW	216.4	250	481(1)	—	637	1.86
	P2-GNU-16-1.0-2.5	46.9	EW	163.6	183	290	—	786	1.41
	P3-GNB-16-1.0-2.5	34.8	EW	126.5	207(2)	300(3)	—	390	1.06
			NS	126.2	207	300	—		1.07
II	P5-GNU-16-0.7-2.5	47.2	EW	180.8	204	220	380	430	1.55
	P7-GNU-13-0.7-2.5	43.6	EW	235.9	290(4)	290	320(1)	455	1.94
	P10-GNB-16-0.7-2.5	46.1	EW	124.9(5)	155	315(6)	—	395	1.08
			NS	127.9					1.11
III	P4-GHU-16-1.0-2.5	76.9	EW	299.5	385	410	—	748	2.49
	P6-GHB-16-1.0-2.5	74.9	EW	232.6	—	—	—	578	1.92
			NS	233.7	—	—	—		1.89
IV	P8-GHU-13-0.7-1.5	77.5	EW	251.7	332	—	—	506	2.08
	P9-GHB-13-0.7-2.5	79.7	EW	223.6	—	—	—	490	1.95
			NS	225.0	—	—	—		1.96
V	P11-SNU-16-1.0-2.5	43.7	EW	317.0	—	—	—	590	2.40
	P12-SNB-16-1.0-2.5	38.4	EW	243.0	280	—	—	500	1.87
			NS	228.5					1.88

(1) Splitting Crack developed parallel to the loading direction.
(2) Initial Crack propagation in both loading directions.
(3) Secondary/Minor Cracks.
(4) Two transverse cracks developed simultaneously.
(5) Two cracks developed.
(6) Propagation of initial cracks.

Table 5-2: Experimental crack spacing

S	Specimen	Direction	S_{rm}, (mm)	S_{rmin} (mm)	S_{rmax} (mm)	Total no. of cracks
I	P1-GNU-16-1.0-1.5	EW	200	140	290	2
	P2-GNU-16-1.0-2.5	EW	150	92	220	3
	P3-GNB-16-1.0-2.5	EW	172	53	304	2 - 3
		NS	150	75	220	3
II	P5-GNU-16-0.7-2.5	EW	184	71	319	2-3
	P7-GNU-13-0.7-2.5	EW	149	100	218	3
	P10-GNB-16-0.7-2.5	EW	168	33	369	3 - 4
		NS	191	60	396	2 - 3
III	P4-GHU-16-1.0-2.5	EW	151	137	167	3
	P6-GHB-16-1.0-2.5	EW	171	52	451	3
		NS	167	92	315	2 - 3
IV	P8-GHU-13-0.7-1.5	EW	199	146	236	2
	P9-GHB-13-0.7-2.5	EW	172	60	320	2 - 3
		NS	149	80	225	3
V	P11-SNU-16-1.0-2.5	EW	300	282	318	1
	P12-SNB-16-1.0-2.5	EW	160	116	277	2 - 3
		NS	175	102	304	1 - 3

Table 5-3: Cracked zones measured around the GFRP and steel reinforcing bars

S	Panel No.	Range of diameters of effective tension zones, D_{eff} (mm)	Average D_{eff} (mm)	d_b (mm)	D_{eff}/d_b
GFRP-RC Panels					
I	P1-GNU-16-1.0-1.5	70 – 150	114	16	7.0
	P2-GNU-16-1.0-2.5	70 - 130	100	16	6.4
	P3-GNB-16-1.0-2.5	-	-	16	-
II	P5-GNU-16-0.7-2.5	70 – 120	94	16	5.8
	P7-GNU-13-0.7-2.5	70 - 90	82	13	6.4
	P10-GNB-16-0.7-2.5	-	-	16	-
III	P4-GHU-16-1.0-2.5	30 – 100	66	16	4.0
	P6-GHB-16-1.0-2.5	-	-	16	-
VI	P8-GHU-13-0.7-1.5	66 – 140	102	13	8.0
	P9-GHB-13-0.7-2.5	40 – 170	80	13	6.4
			Average for GFRP bars		**6.4**
Steel-RC Panels					
V	P11-SNU-16-1.0-2.5	80 – >190 480 – 500(1)	190	16	12.0
	P12-SNB-16-1.0-2.5	140 – 180	160	16	10.0
			Average for steel bars		**11.0**

(1) On one side there were overlapping between cracks around the bars; thus the total width of cracks were 480 ~ 500 mm. Thus, the diameter of effective tensile zone per bar was assumed larger than 180 mm.

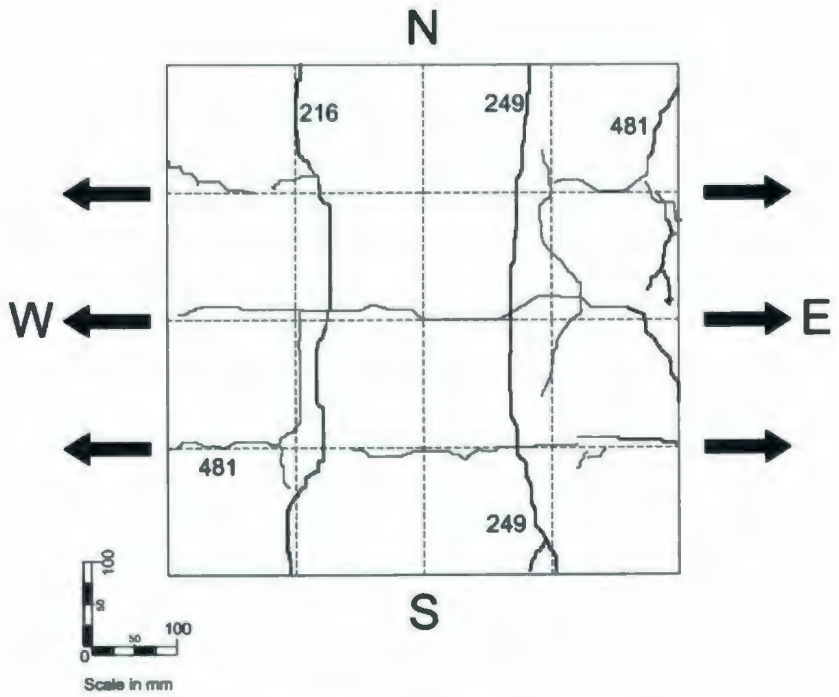

Figure 5-1: Stabilized crack pattern of panel P1-GNU-16-1.0-1.5
(Cracking loads shown are in kN)

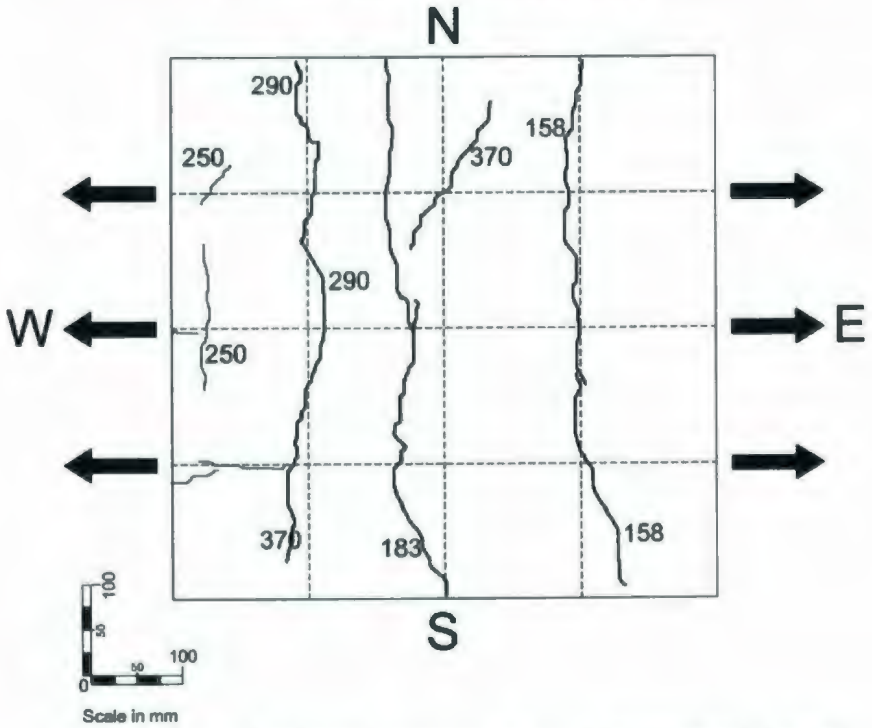

Figure 5-2: Stabilized crack pattern of panel P2-GNU-16-1.0-2.5
(Cracking loads shown are in kN)

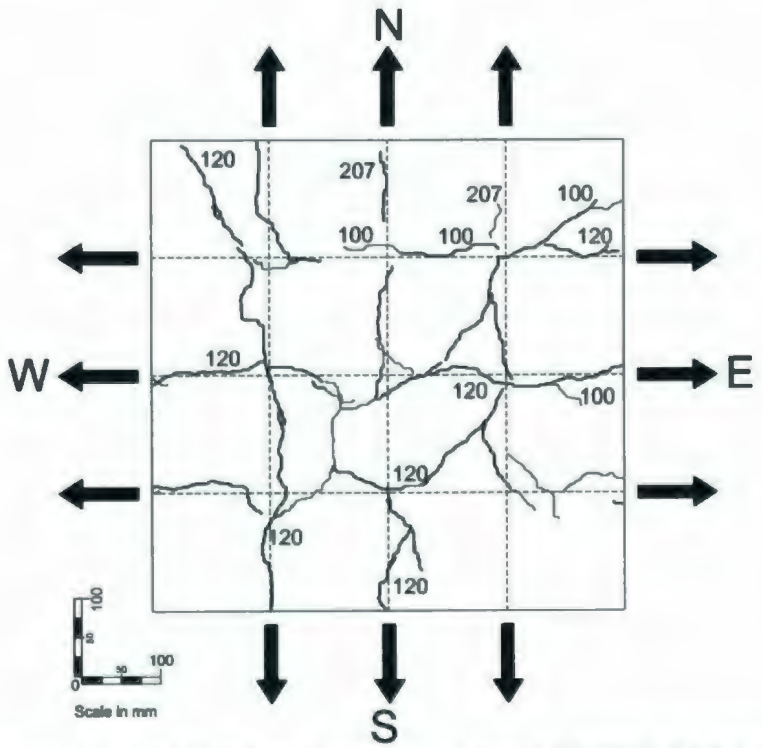

Figure 5-3: Stabilized crack pattern of panel P3-GNB-16-1.0-2.5
(Cracking loads shown are in kN)

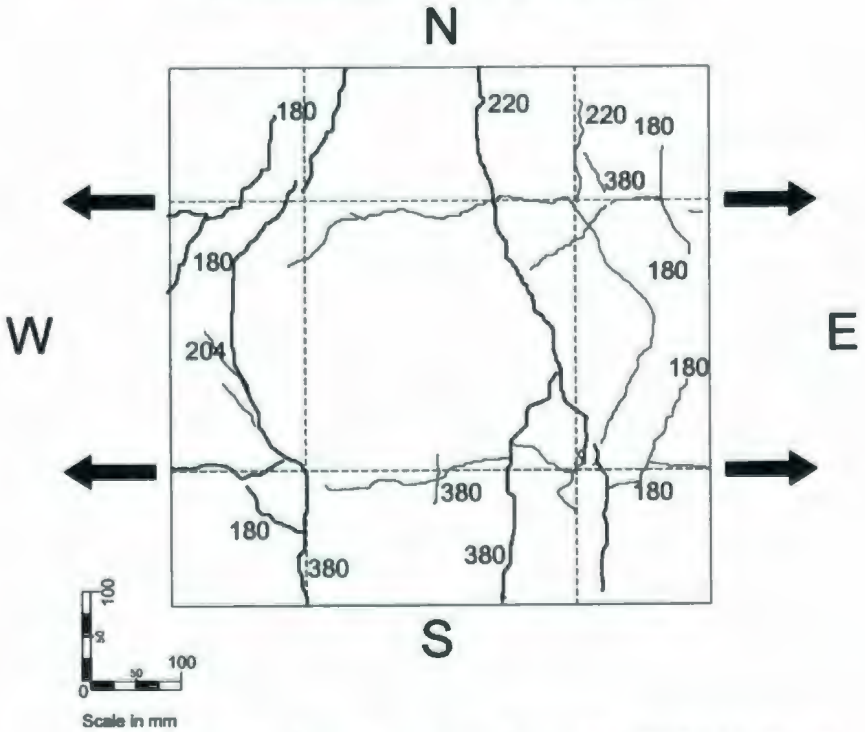

Figure 5-4: Stabilized crack pattern of panel P5-GNU-16-0.7-2.5
(Cracking loads shown are in kN)

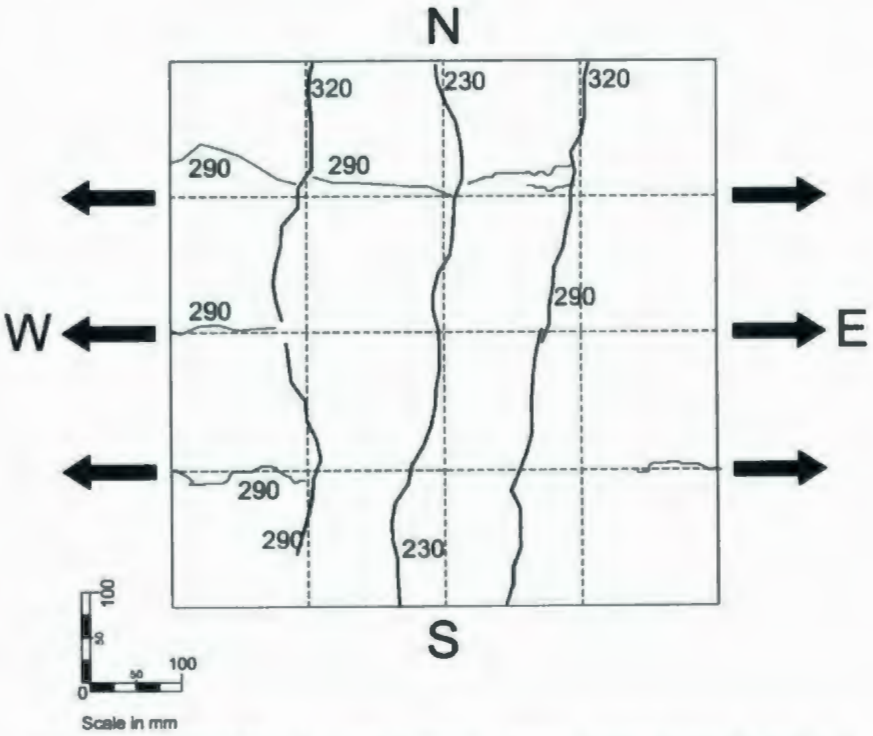

Figure 5-5: Stabilized crack pattern of panel P7-GNU-13-0.7-2.5
(Cracking loads shown are in kN)

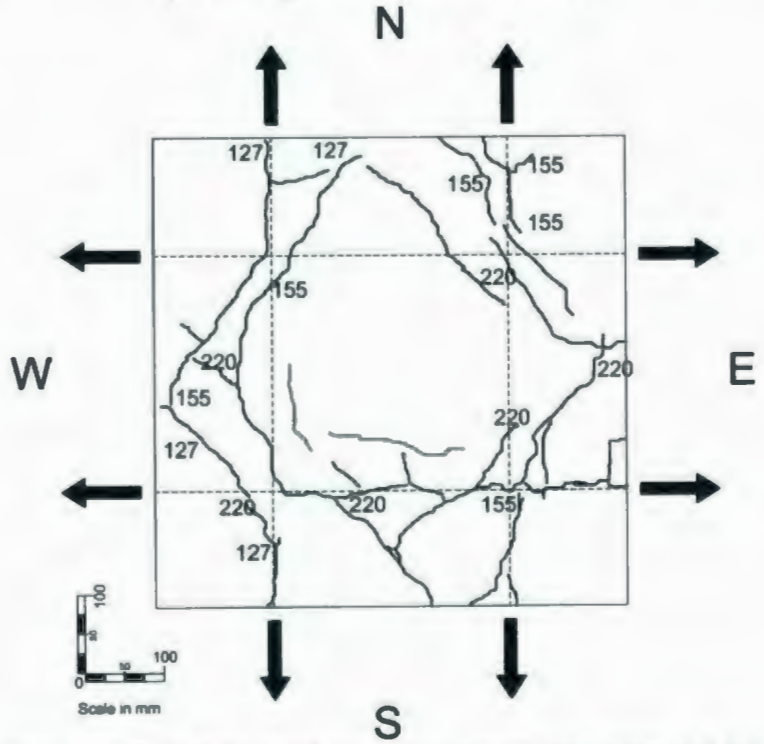

Figure 5-6: Stabilized crack pattern of panel P10-GNB-16-0.7-2.5
(Cracking loads shown are in kN)

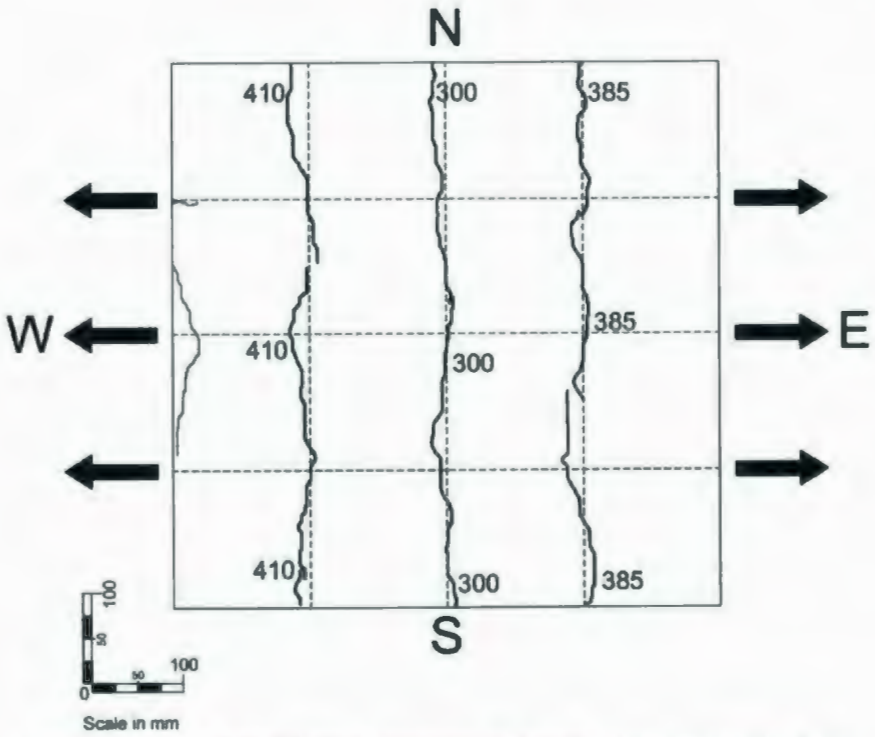

Figure 5-7: Stabilized crack pattern of panel P4-GHU-16-1.0-2.5
(Cracking loads shown are in kN)

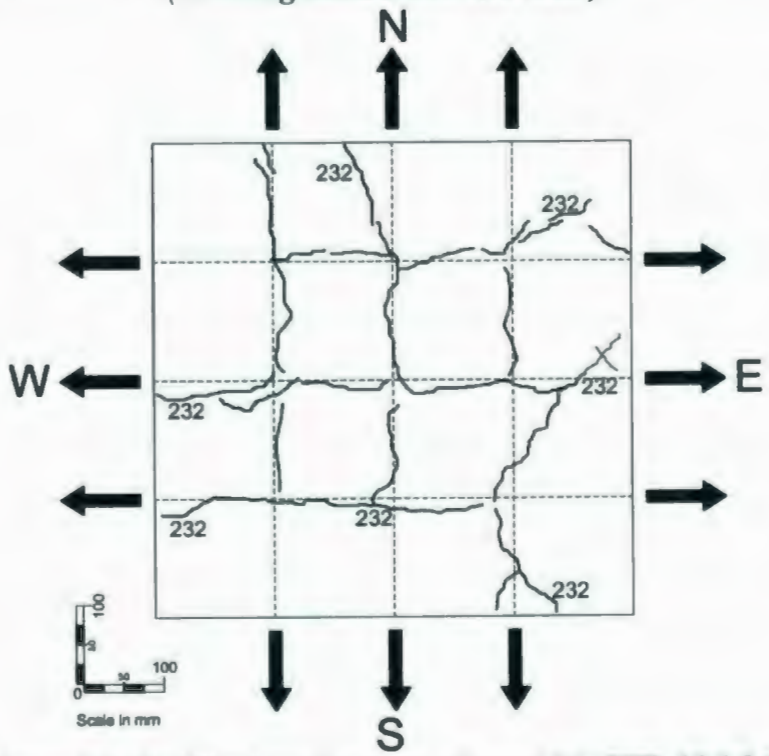

Figure 5-8: Stabilized crack pattern of panel P6-GHB-16-1.0-2.5
(Cracking loads shown are in kN)

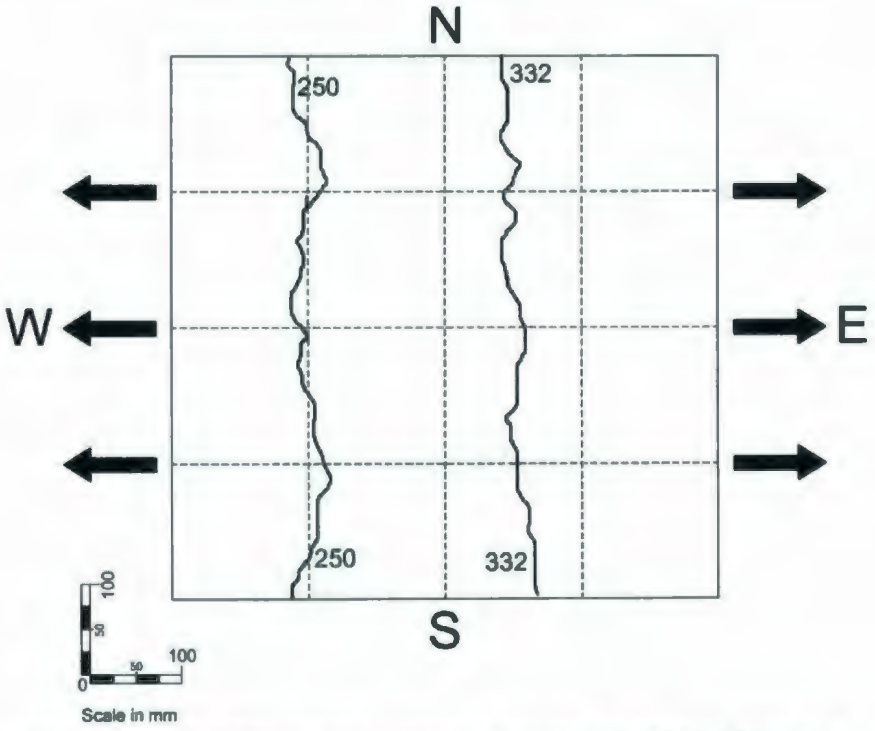

Figure 5-9: Stabilized crack pattern of panel P8-GHU-13-0.7-1.5
(Cracking loads shown are in kN)

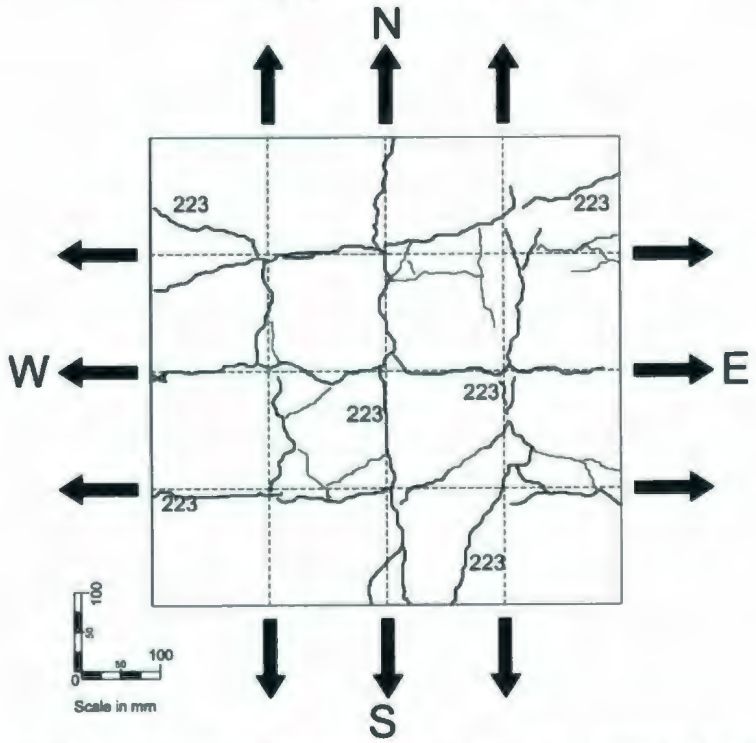

Figure 5-10: Stabilized crack pattern of panel P9-GHB-13-0.7-2.5
(Cracking loads shown are in kN)

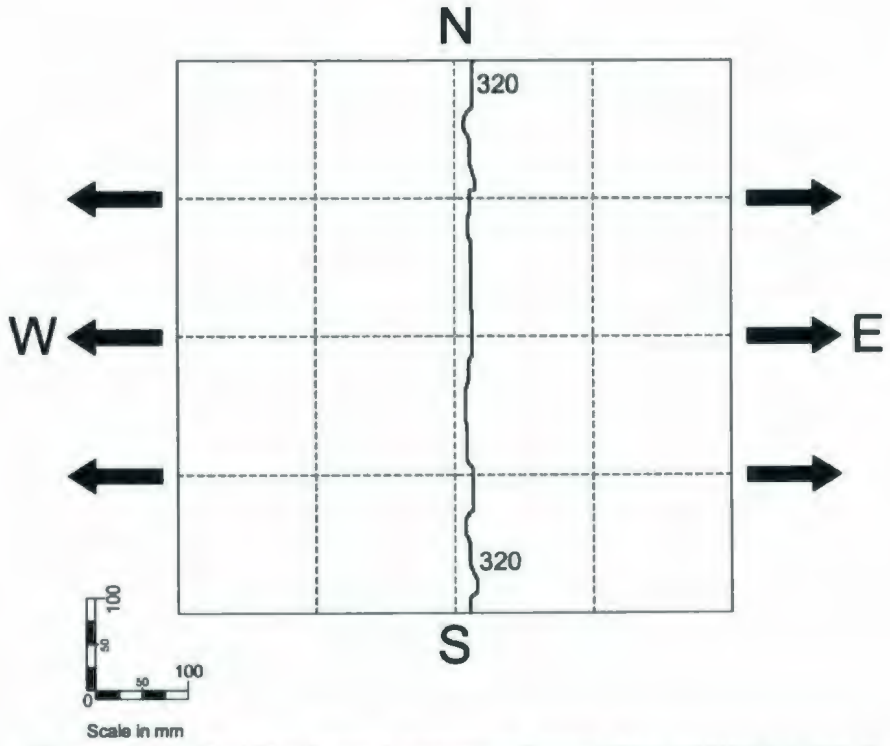

Figure 5-11: Stabilized crack pattern of panel P11-SNU-16-1.0-2.5
(Cracking loads shown are in kN)

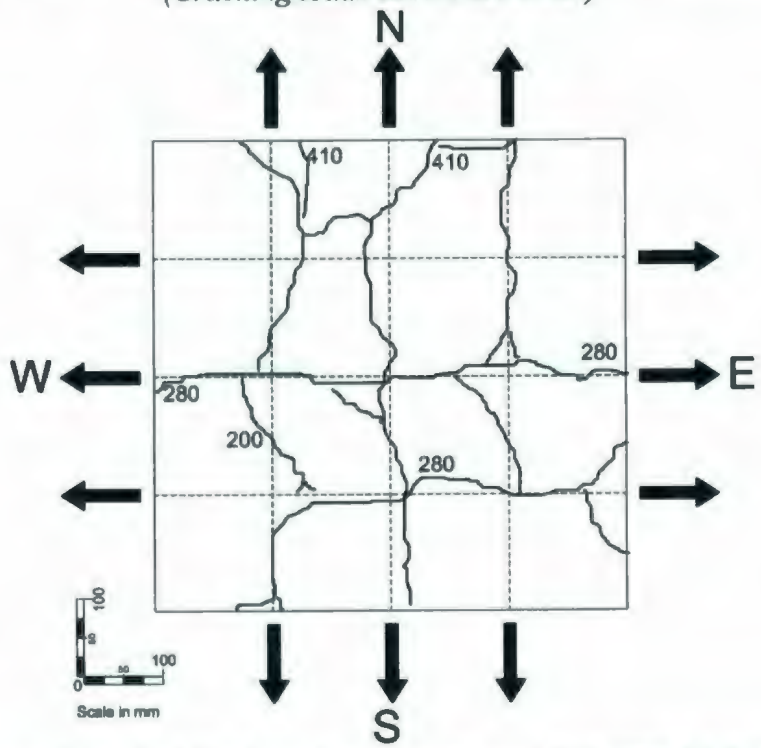

Figure 5-12: Stabilized crack pattern of panel P12-SNB-16-1.0-2.5
(Cracking loads shown are in kN)

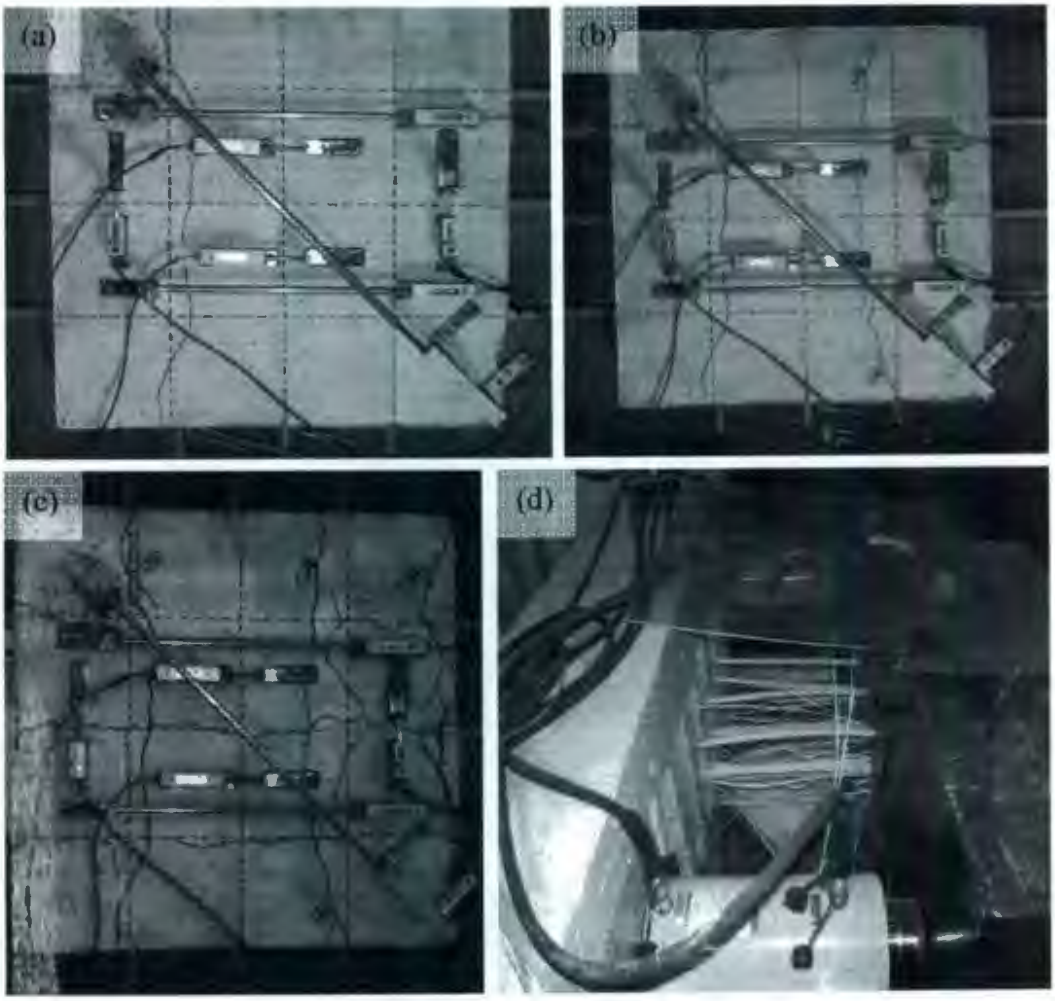

Figure 5-13: Typical stages of failure for panel P1-GNU-16-1.0-1.5
(a) first crack, (b) second crack, (c) stabilized crack pattern, and (d) GFRP rupture

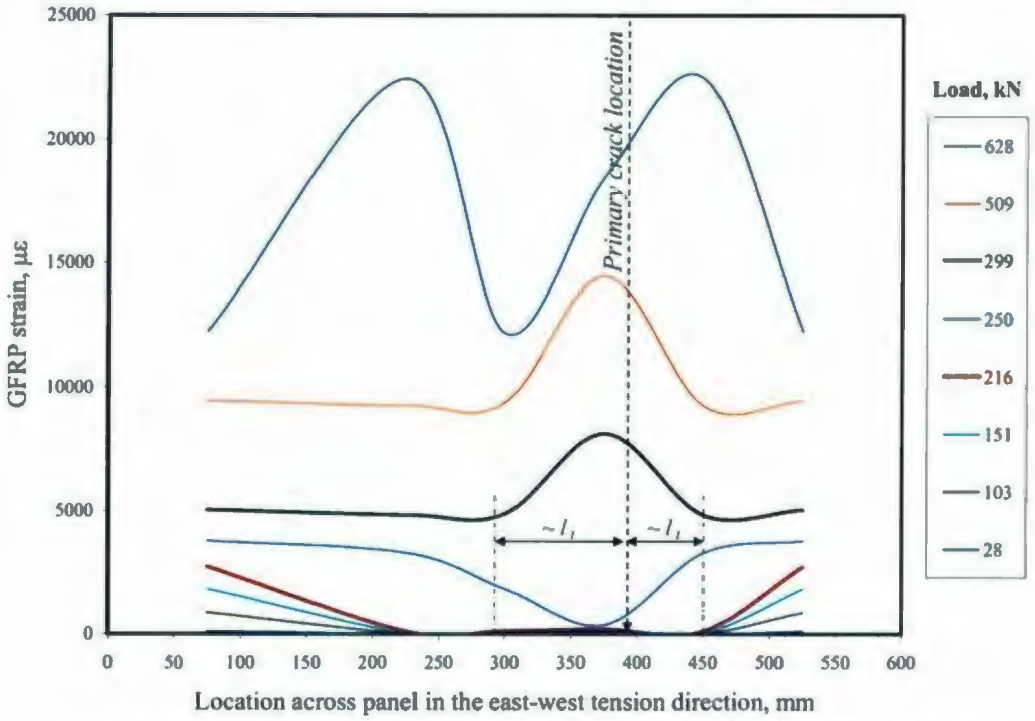

Figure 5-14: Change in GFRP-strain distribution in panel P1-GNU-16-1.0-1.5

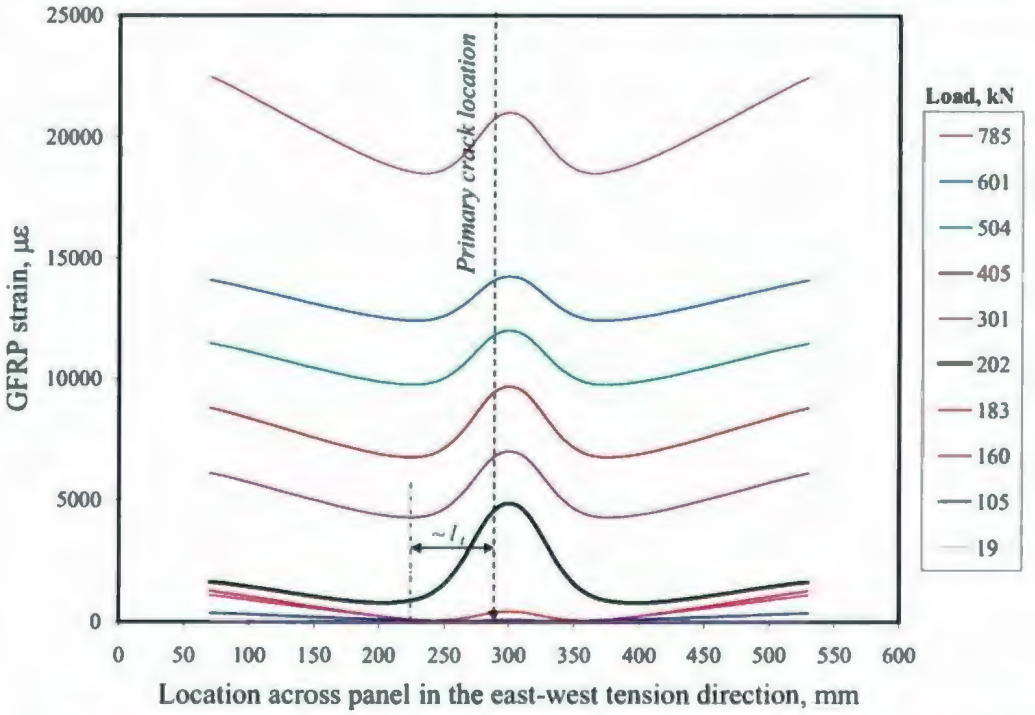

Figure 5-15: Change in GFRP-strain distribution in panel P2-GNU-16-1.0-2.5

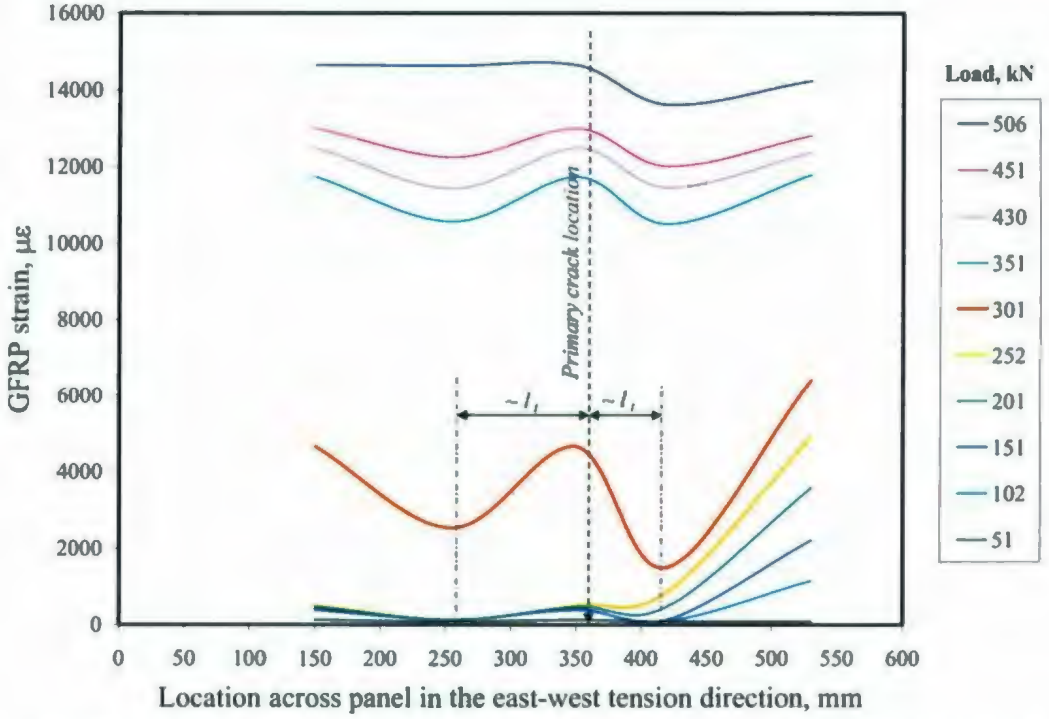

Figure 5-16: Change in GFRP-strain distribution in panel P8-GNU-13-1.0-1.5

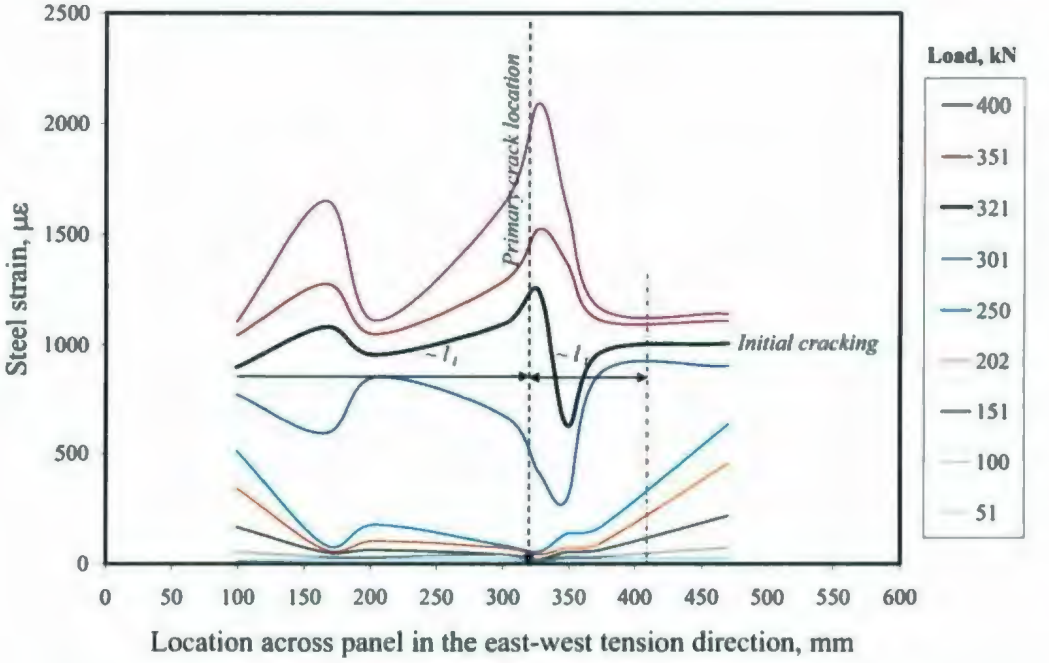

Figure 5-17: Change in steel-strain distribution in panel P11-SNU-16-1.0-2.5

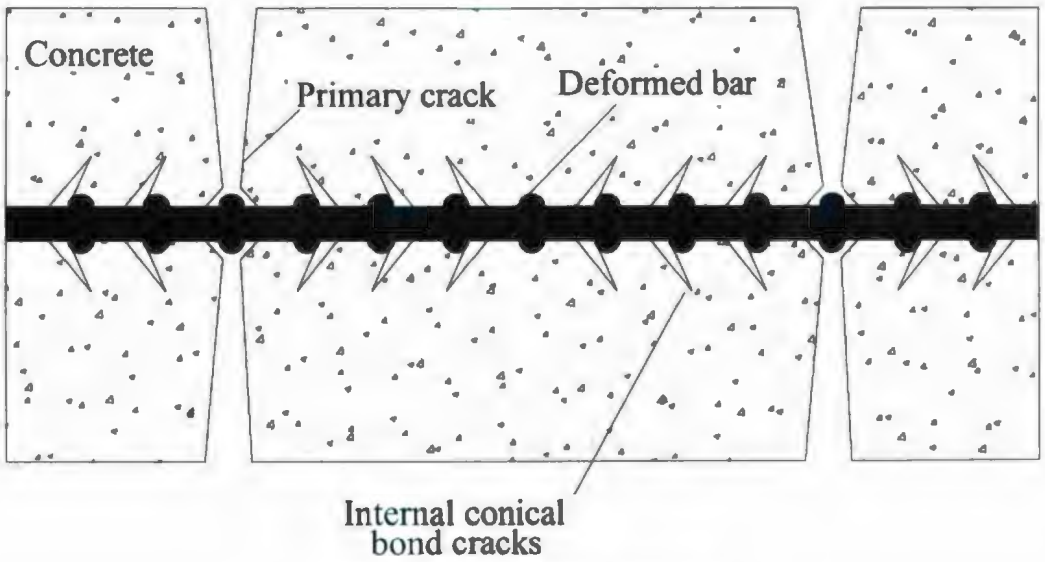

(a) Primary and internal cracks

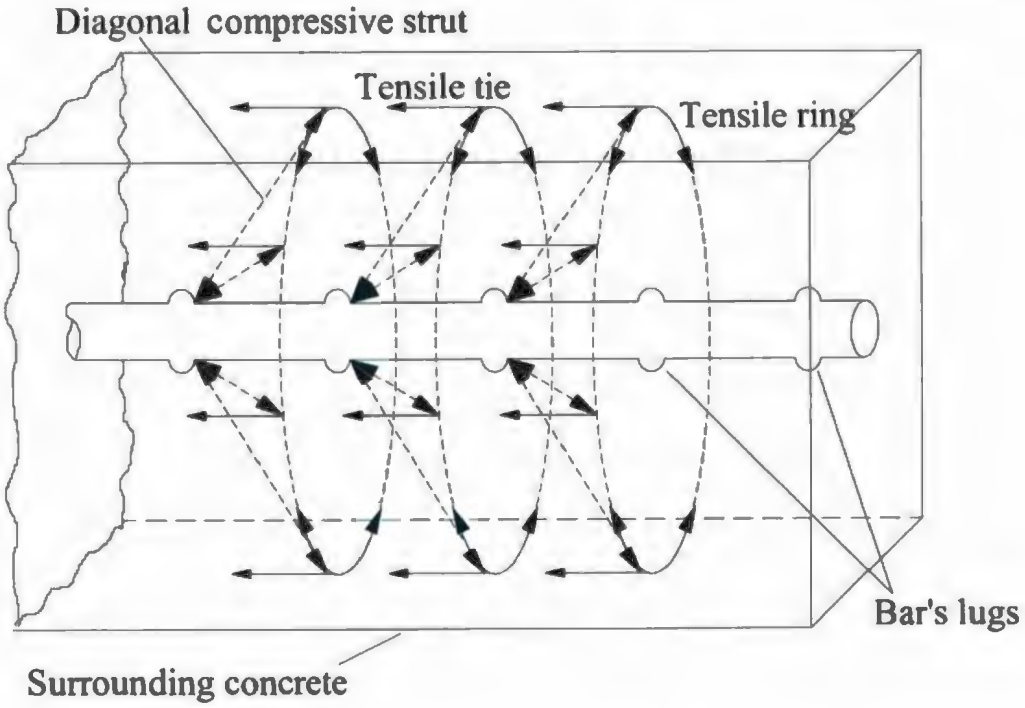

(b) Bond actions at bar's lug of deformed steel bar

Figure 5-18: Mechanisms of bonding and formation of tensile cracks

(Adapted from Maekawa et al. 2003)

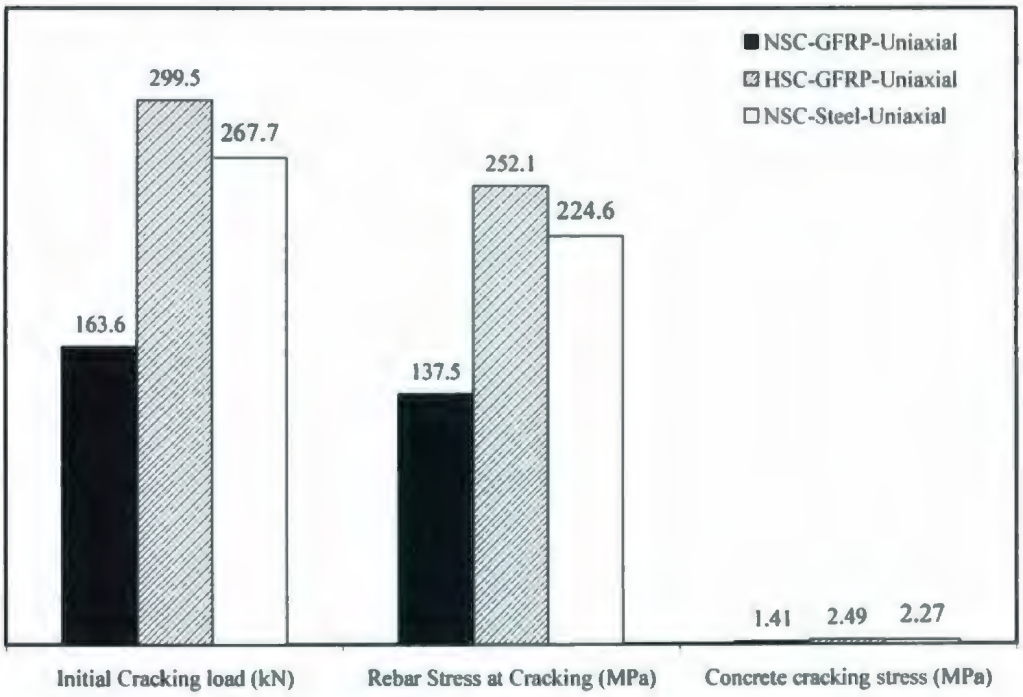

Figure 5-19: Influence of HSC on the cracking behaviour under uniaxial tension

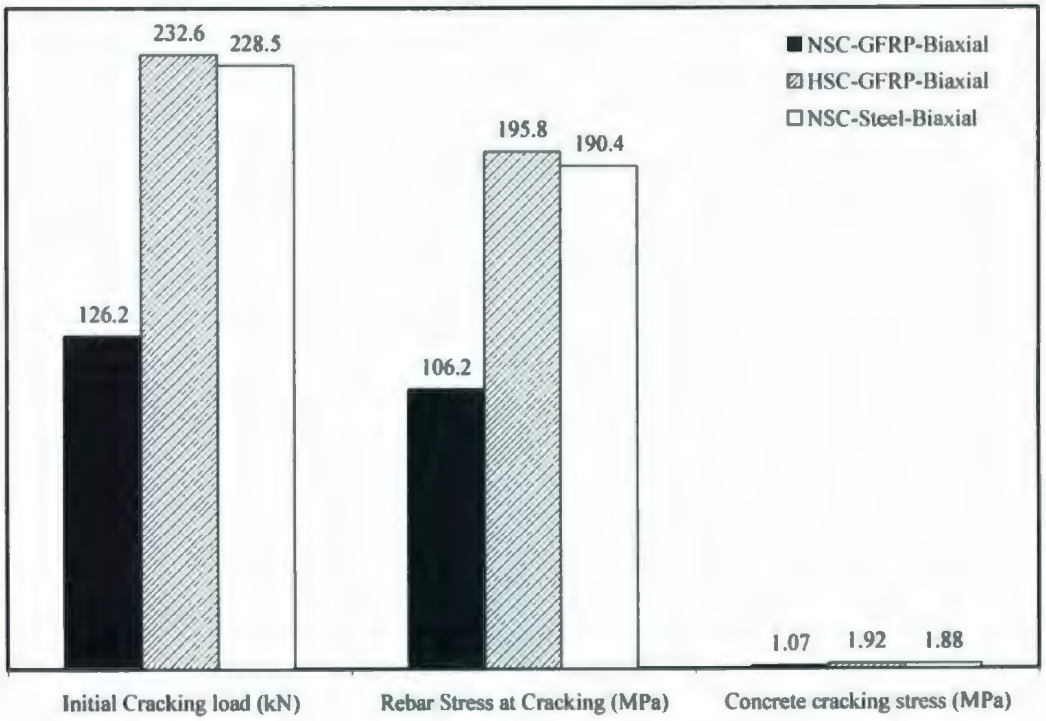

Figure 5-20: Influence of HSC on the cracking behaviour under biaxial tension

Figure 5-21: Typical cracks developed on the sides of steel-RC panels

(a) Panel P1-GNU-16-1.0-1.5

(b) Panel P7-GNU-13-0.7-2.5

Figure 5-22: Typical cracks developed on the sides of GFRP-RC panels

Chapter 6

STRESS-STRAIN RELATIONSHIP AND CRACK WIDTH

6.1 Introduction

In the present chapter, the tensile stress-strain relationships of GFRP-RC under uniaxial and biaxial tension are investigated. The stress-strain relationships are compared and discussed in light of the cracking behaviour discussed in the previous chapter. The discussion focuses on the changes in the tension-stiffening behaviour of the tested panels due to the different test parameters. The main differences between the tensile relationships of GFRP-RC and steel-RC are discussed. Moreover, the changes in the mean crack width, w_m, due to the different test parameters are discussed.

The experimental results are used to develop an appropriate constitutive law for the tensile stress-strain relationship of GFRP-RC. The constitutive law is proposed to reflect the experimental results. The main purpose of the proposed model is for usage in calculations of serviceability requirements (crack control) and non-linear analysis of GFRP-RC structures.

6.2 Tensile Response of GFRP-RC Panels

The load-strain relationships of Series I and II GFRP-RC panels are shown in Figures 6-1 and 6-2, respectively. In order to estimate the concrete contribution in resisting the tensile stresses, the relationships are plotted along with the theoretical bare bar response. The load-

strain relationships of Series III and IV GFRP-RC panels that are made with HSC are shown in Figures 6-3 and 6-4, respectively.

In general, the load-strain relationships are characterized by an ascending portion, which is almost linear elastic up to N_{cr}, once this load is reached, an abrupt change in the tensile strain occurs as the first crack develops. The magnitude of this change varies according to the specimen details, and loading case; that is, whether it is uniaxial or biaxial tension. The relationship then becomes less steep as the tensile force increases. Further abrupt changes in the tensile strain are recorded with the development of new cracks until the stabilized cracking stage is reached. Finally, the GFRP bars rupture.

The test data is used to determine the average tensile stress f_{ct} carried by the concrete after cracking, as well as the cracking strength f_{cr}. The tensile contribution of the concrete for any given value of tensile strain is obtained by subtracting the bare bar response from the measured load response, which is then divided by the net concrete area ($A_c = A_g - A_b$) to give the tensile response of the cracked concrete. For panels subjected to biaxial tension, the stress-strain relationships in the biaxial directions are found to be close to each other. This is attributed to the equal biaxial tension applied. Therefore, it is reasonably valid to take an average curve of the stress-strain relationships of the two-orthogonal directions to be used in the analysis of data.

6.2.1 Effect of loading type

From the load-strain relationship (for example, Figure 6-1), the maximum difference between the average tensile strain and bare bar response at the initial cracking load, $\Delta\varepsilon_{m,cr}$.

represents the maximum tension stiffening contribution that occurs through the entire loading. Table 6-1 shows the values of $\Delta\varepsilon_{m,cr}$ deduced from the load-strain relationships. Under biaxial tension, panel P3-GNB-16-1.0-2.5 exhibits a $\Delta\varepsilon_{m,cr}$ = 2427 ~2434 με, which is nearly 26% lower than the $\Delta\varepsilon_{m,cr}$ recorded for panel P2-GNU-16-1.0-2.5. Similarly, the HSC panel P6-GHB-16-1.0-2.5 has a $\Delta\varepsilon_{m,cr}$ = 4559 ~ 4563 με, which is nearly 23% lower than the $\Delta\varepsilon_{m,cr}$ recorded for panel P4-GHU-16-1.0-2.5. Figure 6-5 could also be used to compare the effect of changing the loading type from uniaxial (panel P2-GNU-16-1.0-2.5) to biaxial tension (panel P3-GNB-16-1.0-2.5) on the average concrete stress-average strain relationship. The figure clearly shows that under biaxial tension, the GFRP-RC panel experiences less tension stiffening contribution.

The general reduction in the tension stiffening contribution under biaxial tension is attributed to the reduction in the initial cracking loads and f_{cr} under biaxial tension. More importantly is that under biaxial tension, most of the cracks develop as early as the initial cracking load or at a higher load. This results in no major time difference between the occurrence of initial and stabilized cracking stages. This behaviour significantly reduces the concrete contribution as a result of reaching the full cracking stage at an early stage of loading.

The stress-strain relationships under uniaxial and biaxial tension are characterized by a sharp drop in the tensile stress sustained by concrete, accompanied by a jump in the tensile strain after a crack forms. Under uniaxial tension, the concrete stress after this drop reaches nearly 25 - 40% of the f_{cr} of concrete. Under biaxial tension, the concrete stress drops to nearly 15 - 25% of the f_{cr} of concrete.

6.2.2 Effect of concrete strength

The use of HSC can influence the tension stiffening behaviour due to the increase in the cracking loads of the specimens. The other influence is a result of a better bond between concrete and reinforcement, which allows the mechanism of stress transfer between the reinforcing bars and concrete to be more uniform. This is attributed to the increase in the average stress contribution. Figure 6-6 illustrates the effect of using HSC on the load-strain relationships compared to similar panels made of NSC. The figure clearly shows the better mechanical strength of embedding concrete on the load-strain relationship of the GFRP-RC panels. This phenomenon is valid for both loading cases, and uniaxial and biaxial tension.

Under uniaxial tension load, Table 6-1 shows that panel P4-GNU-16-1.0-2.5 has a $\Delta\varepsilon_{m,cr}$ = 5943 με, which is about 80% higher than the corresponding $\Delta\varepsilon_{m,cr}$ of panel P2-GNU-16-1.0-2.5 whereas under biaxial tension, the $\Delta\varepsilon_{m,cr}$ for panel P6-GNB-16-1.0-2.5 is ~ 87% higher compared to the $\Delta\varepsilon_{m,cr}$ recorded for panel P3-GNB-16-1.0-2.5. Hence, it can be concluded that the difference between the panel and bare bar responses increases nearly proportional to the increase in the concrete compressive strength. This means that HSC results in a higher tension-stiffening contribution, due to higher cracking loads and reduction in tensile strain at the same level of loading.

However, it is noted that a significant jump in the tensile strain occurs at the crack initiation in the HSC panels. This significant change is observed more often than that recorded for NSC specimens. This agrees with previous test observations of Alavi-Fard and Marzouk (2004) and Mitchell et al. (1996) for traditional steel reinforcement. This significant change in

the tensile strain results in a rapid loss of the tension stiffening contribution. This is significantly observed for panels subjected to biaxial tension, where there is no gradual development of cracks until stabilization. The significant jump in the tensile strains is attributed to the brittle nature of HSC, in addition to the local slip of the GFRP bars. The local-slips that develop at crack vicinities could be an important reason for the large changes in the tensile strain. From the established bond stress transfer mechanism for steel-RC, the steel-concrete bond failure is commonly caused by crushing in front of the bar lugs. In order to check if there is a similar failure, a close visual examination of the interfacial surface between the GFRP bars and surrounding concrete was conducted after completing the tests. For NSC panels, the examination showed that the interfacial local bond failure occurred on the surface between the concrete and GFRP bar due to failure in the sand coating surface (Figure 6-7). However, for HSC panels, the failure occurred on the surface between the concrete and glass-fibres (Figure 6-8). This indicates that not only does the sand coating fail, but also a delamination of the glass fibres at different local locations occurs. This phenomenon agrees with an experimental study conducted by Lee et al. (2007), which showed similar types of interfacial bond failures at the interface between GFRP bars and HSC. Such a bond stress transfer mechanism could explain the nature of the large abrupt change in the tensile strain at the time of developing a new crack. Once this delamination of fibres is created, a large amount of force carried by the HSC is transferred directly to the embedded GFRP reinforcing bar. The sudden mobilization of the reinforcing bar causes a sudden crack opening and a relatively large change in the tensile strain.

Since GFRP and HSC experience brittle failures, the combination of both materials may not be desirable from the design point of view. However, the design of GFRP-RC is usually governed by serviceability limits, in order to control excessive cracking and deflection. Therefore, the improvement in mechanical performance of concrete allows a significant increase in the initial cracking loads, stresses and strains. Also, a significant improvement in the tension stiffening contribution $\Delta\varepsilon_m$ compared to NSC is achieved. Therefore, it can be recommended that HSC be utilized in GFRP-RC, and thus should improve the general characteristics required to control cracking and deflection limits. This is in addition to the general improvement in the durability of GFRP-RC due to the use of HSC.

6.2.3 Effect of concrete cover to bar diameter ratio

Figure 6-9 shows the f_{ct} normalized with respect to f_{cr} versus the average tensile strains for panels P1-GNU-16-1.0-1.5 and P2-GNU-16-1.0-2.5, where panel P2-GNU-16-1.0-2.5 experiences an N_{cr} that is nearly 25% less than panel P1-GNU-16-1.0-1.5. However, the initial cracking strain for panel P2-GNU-16-1.0-2.5 is lower by almost 40%. This results in only a 9% increase in the initial stiffness (curve slope) in the pre-cracking stage when a $c_c / d_b = 2.5$ is used.

Table 6-1 shows that panel P1-GNU-16-1.0-1.5 ($c_c / d_b = 1.5$) has a $\Delta\varepsilon_{m,cr} = 4334$ με, which is nearly 25% higher than that recorded for panel P2-GNU-16-1.0-2.5 ($c_c / d_b = 2.5$). The difference in $\Delta\varepsilon_{m,cr}$ can only be related to the difference in the initial cracking load of both panels. For the post-cracking stage, the degradation of the descending curve slope remains lower for panels with $c_c / d_b = 2.5$ up to about 2000 με. Beyond 2000 με, panel P1-GNU-16-

1.0-1.5 loses its concrete contribution at a faster rate once its f_{cr} is reached. Beyond 4000 με, there is an apparent increase in the tension stiffening contribution of panel P1-GNU-16-1.0-1.5 compared to panel P2-GNU-16-1.0-2.5, which could be attributed to the fewer numbers of primary cracks developed in panel P1-GNU-16-1.0-1.5. Abrishami and Mitchell (1996) showed that there is a reduction in the tension stiffening of steel-RC uniaxial tension members due to the development of splitting cracks. However, for the tested GFRP-RC panels, there is no evidence of a similar reduction in the tension stiffening due to the development of splitting cracks. This is in good agreement with the experimental findings of Bischoff and Paixao (2004).

From the above discussion, it is concluded that the c_c / d_b has an insignificant effect on the tensile stress-strain relationship of GFRP-RC under direct tension up to ~ 4000 με. Few differences are noticed in the initial cracking loads and stresses and in the tensile stress-strain relationship beyond 4000 με, which can not be exclusively attributed to the effect of c_c / d_b. However, it is recommended that a separate experimental investigation to be conducted that focuses on the c_c / d_b effect and further examines the effect of splitting cracks on the tension stiffening contribution.

6.2.4 Effect of reinforcement ratio

The reinforcement ratio is an important parameter that can significantly affect the tensile stress-strain relationship. The reinforcement ratio changes by means of changing the d_b for the same bar spacing, b_s or vice versa. Therefore, the influence of the reinforcement ratio is discussed in light of changing in d_b and b_s.

Figure 6-10 shows the effect of changes in the reinforcement ratio on the tension stiffening response under uniaxial tension. The figure compares panels P2-GNU-16-1.0-2.5, P5-GNU-16-0.7-2.5, and P7-GNU-13-0.7-2.5. The difference between the average load-strain response and bare bar response is significantly higher as the reinforcement ratio is decreased. This increase occurs in spite of the similarity in the final number of primary cracks developed in panels P2-GNU-16-1.0-2.5 and P7-GNU-13-0.7-2.5. Table 6-1 shows that panel P5-GNU-16-0.7-2.5 has a $\Delta\varepsilon_{m,cr}$ = 5421 με, which is 65% higher than that recorded for panel P2-GNU-16-1.0-2.5. The increase in $\Delta\varepsilon_{m,cr}$ is even higher due to the change in d_b to a 13 mm size. Panel P7-GNU-13-0.7-2.5 has a $\Delta\varepsilon_{m,cr}$ = 7318 με, which is 122% and 35% higher than that recorded for panel P2-GNU-16-1.0-2.5 and P5-GNU-16-0.7-2.5, respectively.

The same phenomenon is observed for panels subjected to biaxial tension. Figure 6-11 shows the effect of changes in the reinforcement ratio on the load-strain relationship for panels P3-GNB-16-1.0-2.5 and P10-GNB-16-0.7-2.5. The figure clearly shows that there is a large difference between the panel and bare bar responses. However, it should be noted that part of this tensile contribution is attributed to the influence of the large b_s of panel P10-GNB-16-0.7-2.5. The larger b_s results in wider crack spacing and thus results in more tension stiffening contribution of the concrete between cracks. Table 6-1 shows that panel P10-GNB-16-0.7-2.5 has a $\Delta\varepsilon_{m,cr}$ = 3660 - 3749 με, which is ~ 50 % higher than that recorded for panel P3-GNB-16-1.0-2.5.

The increase in tension-stiffening due to decreasing the reinforcement ratio becomes even larger when combined with HSC. Table 6-1 shows that P8-GHU-13-0.7-1.5 has a $\Delta\varepsilon_{m,cr}$ =

7798 με, which is ~ 31 % and 43% higher than that recorded for panels P4-GHU-16-1.0-2.5 and P7-GNU-13-0.7-2.5, respectively. Figure 6-6 shows an increase in tension stiffening as recorded for HSC panels subjected to uniaxial and biaxial tension, respectively.

Therefore, it can be concluded that there is a general increase in the tension stiffening contribution due to the decrease in the reinforcement ratio. The tension stiffening behaviour is found to be sensitive to any changes in the reinforcement ratio, which is found valid for both loading cases. The increase in tension stiffening is attributed to two main factors: (1) with a low reinforcement ratio, there is a larger concrete area around the bar, which results in a greater tension stiffening contribution, and (2) the use of a smaller d_b that is 13 mm in diameter rather than 16 mm enhances the bond transfer mechanism of the GFRP-bar and thus the tension stiffening contribution. The combination of a low reinforcement ratio, small d_b and HSC results in significant increase in the tension-stiffening contribution of GFRP-RC.

6.2.5 Tensile response of steel-RC compared to GFRP-RC

Figure 6-12 shows the variation of the average tensile strain with the applied loads for the steel-RC panels of Series V. For panel P12-SNB-16-1.0-2.5, the load-strain relationships are plotted for the EW and NS tension directions.

It can be noticed that for panel P11-SNU-16-1.0-2.5 the load-strain relationship remains linear up to N = 237 kN, which corresponds to a tensile strain of ~37 με. The primary crack develops as surface crack at N_{cr} = 317 kN which corresponds to a ε_{cr} = 202 με. The small change recorded in the tensile strain at N = 237 kN suggests that an internal crack could have been developed as early as 37 με. Beyond this change in the strain with the crack opening, the

load-strain relation becomes less steep up to f_y at N = 437 kN. The yielding strain that is recorded around 2000 με occurs at the vicinity of the primary crack (Figure 5-17).

The main differences in the behaviour between GFRP- and steel-RC panels are evaluated by comparing GFRP-RC panels P2-GNU-16-1.0-2.5 and P3-GNB-16-1.0-2.5 of Series 1 with the corresponding steel-RC panels P11-SNU-16-1.0-2.5 and P12-SNB-16-1.0-2.5 of Series V, respectively.

As shown in Table 6-1, there is a significant difference in the initial cracking strain observed. The concrete cracking strain of the GFRP-RC panels are almost 41% and 43% less than the corresponding steel-RC panels subjected to uniaxial and biaxial tension, respectively. The significant difference in cracking strains can be directly attributed to the difference in the modulus of elasticity of GFRP and steel, which significantly affects the initial cracking strain. The tension stiffening contribution is limited by f_y, which occurs at a yielding strain around 2000 με at the vicinity of the crack as shown in Figure 5-17. The tensile strains of the steel-RC are much less compared to GFRP-RC.

Figure 6-13 is used to compare the load versus average tensile strains for steel-RC and GFRP-RC panels subjected to uniaxial and biaxial tension. The bare bar responses for both steel and GFRP are also illustrated to show the differences under tensile load. The stress-strain relations recorded for the steel-RC panels are nearly similar in curve profile to those recorded in a previous study by Cho et al. (2004b). Similar to GFRP-RC, there is an abrupt change in the tensile load versus strain response which typically occurs once a new crack forms.

However, these abrupt changes in the tensile strains are much less in magnitude for steel-RC compared to those recorded for GFRP-RC panels. This could be attributed to:

- The different mechanism of force transfer between the GFRP bar and concrete compared to the steel-RC. The nature of the surface characteristics of the GFRP-bars may result in a larger relative slip from the surrounding concrete; especially at the crack vicinities until the end of l_t.

- GFRP experiences much higher strains than steel at the same level of loading. This explains that the amount of stress relief developed should be relatively higher once a new crack develops.

Figure 6-14 shows the average concrete stress normalized with respect to the cracking stress versus the average tensile strains for specimens subjected to uniaxial and biaxial tension. It can be noticed that there is a significant difference in behaviour under uniaxial tension. Although there are fewer numbers of cracks developed for steel-RC panel, GFRP bars contribute more in resisting tension at the same level of loading. This could be explained by comparing the area under the curve which reflects the tension stiffening contribution. A larger area means a higher tension stiffening contribution. Table 6-1 also confirms that panel P2-GNU-16-1.0-2.5 has a $\Delta\varepsilon_{m,cr}$ = 3286 με, which is 168% higher than that recorded for panel P11-SNU-16-1.0-2.5.

Table 6-1 also confirms that panel P3-GNB-16-1.0-2.5 has a $\Delta\varepsilon_{m,cr}$ = 2434 με, which is 167 ~ 195% higher than that recorded for panel P12-SNB-16-1.0-2.5. As shown in Figure 6-14, the

GFRP-RC panel P3-GNB-16-1.0-2.5 subjected to biaxial tension experiences more tension stiffening than panel P12-SNB-16-1.0-2.5. However, it appears from Figure 6-13, that for both panels, the rate of loss in tension stiffening contribution is relatively higher than the uniaxial tension case. This can be interpreted by the difference in the development of crack mechanisms under biaxial tension in which multiple cracks initiate directly and instantly in both directions when N_{cr} is reached. Therefore, the panels reach their stabilized cracking stage just after the crack formation stage. This explains why the panels under biaxial tension lose more of their concrete contribution at early stages of loading.

Therefore, it can be presumed that GFRP-RC under uniaxial tension experiences a significant increase in the tension stiffening contribution compared to steel-RC at the same level of stress, which confirms the findings of Bischoff and Paixao (2004). However, tension stiffening is not as significant under biaxial tension, due to the different cracking mechanism, which results in faster degradation in the tension-stiffening contribution under biaxial tension.

6.3 Change in Mean Crack Width

Table 6-2 shows the w_m recorded at the stabilized cracking stage of the tested panels. It is noticed from this table that the average tensile strain at the stabilized cracking stage for GFRP-RC panels varies between 2000 to 8000 με, which is nearly 10 to 40 times the ε_{cr}, while for steel-RC, the stabilized strain is in the range of 1700 με, which is about 8 to 15 times the ε_{cr}.

Each panel reaches its stabilized cracking stage at different tension loads according to the properties of each panel. Therefore, the changes in the w_m are plotted against the ε_m as shown later.

6.3.1 *Effect of loading type*

Figure 6-15 shows the effect of biaxial tension on the changes in w_m. For panel P2-GNU-16-1.0-2.5 under uniaxial tension, and up to a tensile strain ~ 2000 με, there is no significant effect on the w_m at the same level of ε_m. Beyond 2000 με, the w_m is relatively lower under biaxial tension for the same level of tensile strain by nearly 42% at ε_m ~ 4000 με. The w_m decreases further beyond this stage. Such a reduction in the w_m could be attributed to the reduction in the GFRP-strains under biaxial tension relative to the uniaxial tension at the same level of loading. As previously discussed, this reduction is attributed to the effect of some crack inclinations due to the variation in the principal stresses under biaxial tension. Also, the reduction in w_m could be due to the effect of tensile force in the transverse direction which affects the mechanism of opening cracks.

6.3.2 *Effect of concrete strength*

Figure 6-16 shows the effect of changing the concrete strength on the w_m. Under uniaxial tension, there is a minor difference in the w_m due to the use of HSC. This is valid up to ε_m 4000 to 5000 με. Beyond this change, w_m is reduced by nearly 20 ~ 30%, which could be attributed to the higher concrete compressive strength.

Under biaxial tension, HSC shows a reduction in w_m by nearly 45% up to the stabilized cracking stage, which corresponds to ε_m ~ 4700 με and 5401 με for panels P3-GNB-16-1.0-2.5 and P6-GHB-16-1.0-2.5, respectively.

Therefore, the use of HSC could cause a reduction in w_m. This could improve the margin of safety and allow more tolerance in the serviceability requirements that usually control the GFRP-RC design.

6.3.3 Effect of concrete cover to bar diameter ratio

The effect of c_c / d_b on the change in w_m is shown in Figure 6-17 in which panels P1-GNU-16-1.0-1.5 and P2-GNU-16-1.0-2.5 are compared. Prior to ε_m = 2000 – 3000 με, a wider w_m is experienced due to the increased c_c / d_b. However, beyond ε_m = 3000 με, it appears that using a c_c / d_b = 2.5 significantly reduces the w_m, at the same level of tensile strain compared to c_c / d_b = 1.5, as higher tensile strains are experienced. For instance, the w_m is reduced from about 30% less to 60% less for ε_m = 4000 με to ε_m = 8000 με. Such a difference can be related to the difference in the stabilized cracking stage achieved for each panel.

Table 6-2 compares the recorded w_m at the stabilized cracking stage for panels P1-GNU-16-1.0-1.5 and P2-GNU-16-1.0-2.5, which have c_c / d_b of 1.5 and 2.5, respectively. It appears that w_m increases by almost three times when c_c / d_b = 2.5 is used. Hence, it should be noted that there is a delay in the stage of stabilized cracking as a result of increasing the c_c / d_b from 1.5 to 2.5. In the stabilized cracking stage for P2-GNU-16-1.0-2.5, the stabilized ε_m is 5512 με, which is nearly 150% higher than the stabilized ε_m of panel P1-GNU-16-1.0-1.5.

6.3.4 Effect of reinforcement ratio

Figures 6-18 and 6-19 show the effect of changing the reinforcement ratio on the change in w_m under uniaxial and biaxial tension, respectively. Under uniaxial tension, Figure 6-18 shows

that panel P5-GNU-16-0.7-2.5 experiences a reduction in w_m by nearly 75%, on average, compared to panel P2-GNU-16-1.0-2.5. This reduction in w_m is valid up to ε_m = ~ 7000 με, which is directly attributed to the higher tension stiffening contribution recorded for panel P5-GNU-16-0.7-2.5 as shown in Figure 6-10. Panel P7-GNU-13-0.7-2.5 also shows a reduction in w_m by nearly 34% on average compared to P2-GNU-16-1.0-2.5.

Figure 6-19 also shows that under biaxial tension, there is a minor change in w_m up to ε_m = ~ 2000 με. Some variation in w_m is observed between 2000 με to 6000 με. Beyond that, w_m is almost equal. In general, the overall change in w_m is considered minor under biaxial tension. Such a minor change is not only dependent on the reinforcement ratio, but can also be related to changes in bar spacings and thus the total number of cracks developed within the panel.

6.3.5 Effect of bar type

The stabilized w_m values are shown in Table 6-2. Similar to GFRP, panel P12-SNB-16-1.0-2.5 under biaxial tension shows a 9% reduction in w_m compared to panel P11-SNU-16-1.0-2.5.

Figure 6-20 shows the effect of the bar type on the changes in w_m under uniaxial tension. Up to 2000 με, the GFRP-RC apparently experiences a smaller crack width compared to steel-RC. However, this can be misleading since the stabilized cracking stage for GFRP-RC is not yet achieved. The steel-RC panel reaches its stabilized cracking stage at about 1700 με (just below steel yielding) while the GFRP-RC panel reaches its stabilized cracking stage at nearly 4000 to 6000 με. This means that GFRP-RC still experiences a much higher w_m once it reaches

its stabilized cracking stage. A similar observation can be noted for the panels subjected to biaxial tension as shown in Figure 6-21.

Therefore, for a given level of stress, crack widths are obviously greater for GFRP-RC because of the lower modulus of elasticity of the GFRP bar, which results in larger panel strains. This means that in spite of the greater tension stiffening contribution of GFRP-RC, there is no great reduction in w_m, which is more influenced by the level of strain in the member. However, it should be noted that up to 2000 με, which is considered a serviceability design limit (ISIS 2001), the difference in w_m between steel-RC and GFRP-RC is still considered minor.

6.4 Constitutive Modelling of Tensile Stress-Strain Relationship

From the above discussion, it can be concluded that the tensile-stress relationship of GFRP-RC is significantly influenced by three main factors, which are (1) loading type (uniaxial or biaxial tension), (2) concrete strength, and (3) reinforcement ratio.

The experimental results are used to formulate a constitutive relationship that defines the tensile response of GFRP-RC under direct tension loads. The proposed model accounts for the pre-cracking and post-cracking failure through idealization of the ascending and descending curves, respectively. The f_{cr} of GFRP-RC panels under uniaxial and biaxial tension is incorporated in the proposed constitutive model as discussed later.

6.4.1 Cracking strength of RC-panels under uniaxial tension

Test methods for determining the tensile strength of plain concrete include the third point loading method (ASTM C78-09), center point loading method (ASTM C293-08), and splitting method of cylinder (ASTM C496/C486M-04). These tests methods result in various tensile strength for the same concrete. For instance, the tensile strength given from a flexural tensile test is 40% to 80% higher than that from the splitting tensile test (Neville 1971). A reliable tensile strength can be obtained from direct tension tests, but it is not easy to apply pure tension to plain concrete specimens as previously mentioned. Therefore, a more reasonable method to acquire the cracking stress and stress-strain curve of RC is the direct test using RC panels (Cho et al. 2004b). In the present investigation, the load applied to reinforcement is transferred to the concrete by bond along the reinforcement embedded length, and then the cracking stress is predicted.

In fact, the actual distribution of concrete stress in the transverse and longitudinal direction of the RC panels is non-uniform. This results in a difference between the cracking strength f_{cr} of the RC panel and the tensile strength f_t' of plain concrete. The f_{cr} is defined as the stress level of concrete in a RC panel (member) at which cracking takes place corresponding to initial cracking load N_{cr}. The f_t' is a material property for plain concrete that can be experimentally measured from direct tension tests. Similar to the present investigation, many investigators observed a difference between f_t' and f_{cr} (Blackman et al. 1958; Somayaji and Shah 1981; Cho et al. 2004b). Chan et al. (1992) explained that the f_{cr} of a RC member increases with a decrease of the ratio of segment length to cross-sectional areas with an increase of the strain

gradient in the transverse or longitudinal directions. This means that the size effect may play a role in creating such a difference. Other investigators showed that the loading history probably causes some differences (Chan et al. 1992; Aoyagi and Yamada 1983). However, it is difficult to establish any criteria that consider such a variation of cracking strength according to the specimen length found in the literature. If a rational relation for the size effect of a specimen is introduced, better numerical results can be expected (Kwak and Song 2002).

Meanwhile, Eq. (6.1) is proposed to estimate the f_{cr} of the RC panels under uniaxial direct tension:

$$f_{cr} = \alpha_o \cdot f_t^{'} \tag{6.1}$$

where α_o is a material constant to be determined from the test data. The α_o is assumed to be in the range of 0.65 ~ 0.85. The $f_t^{'}$ can be experimentally estimated from direct tension test of plain concrete specimens. Also, it can be estimated from any of the available equations in the literature. The ACI 224.2 (1992) equation: $f_t^{'} = 0.33\sqrt{f_c^{'}}$ can be used. For HSC, Alavi-Fard and Marzouk (2002) recommended that $f_t^{'}$ is better expressed in terms of the cubic root of $f_c^{'}$ instead of the square root of $f_c^{'}$. This is to account for the more nonlinear and brittle behaviour of HSC compared to NSC.

6.4.2 Cracking strength of RC-panels under biaxial tension

Concrete under a combination of biaxial stress exhibits different strength and stress-strain behaviours from those under uniaxial loading conditions through the effects of Poisson's ratio

and micro-crack confinement. To define the change of material properties according to the biaxial tensile stress state, the biaxial strength envelope in the tension-tension region is defined.

A general expression (Eq. 6.2) is proposed to define the biaxial failure envelope in the tension-tension region. This expression was originally proposed by Aoyagi and Yamada (1983). However, a modification is made to the original model by replacing $f_t^{'}$ with the term: $\alpha_o f_t^{'}$, which is f_{cr} of the concrete panel under uniaxial tension (Eq. 6.1). Figure 6-22 shows the biaxial strength envelope of concrete under biaxial tension based on Eq. (6.2).

$$f_{cr} = \alpha_o f_t^{'} \left(1 - 0.25 \left(\frac{f_2}{f_1} \right)^2 \right) \tag{6.2}$$

where, f_1 and f_2 are the principal stresses. The f_{cr} in the primary direction (f_1) decreases with increasing tensile stress in the other principal stress direction, and failure basically takes place by cracking in the primary direction. However, when cracking occurs, the principal tensile stress and strain in the other direction still remain in the ascending curve of the concrete stress-strain relation. Therefore, the concrete stress-strain relation in the other direction (f_2 direction in Figure 6-22) can be assumed to be the same as that of uniaxial loading and does not change with the variation of tensile stress in the primary direction before cracking. In Figure 6-22, the envelope points between the two loading ratios being investigated, (i.e. between $f_2 / f_1 = 0$ and $f_2 / f_1 = 1$) are assumed to be valid by using Eq. (6.2). Hence, by using the f_{cr} determined from Eq. (6.2), the stress-strain relation of concrete in the tension part can

finally be defined on the basis of uniaxial tension-stiffening and the cracking model. Using this concept, the two-dimensional problem is reduced to a simple uniaxial problem.

Table 6-3 summarizes the experimental f_{cr} of the GFRP-RC specimens under uniaxial tension and the predicted values using Eq. (6.2). A good agreement is found, as the ratio of the experimental to the predicted f_{cr} has a mean value of 1.06, standard deviation of 0.16, and a C.O.V. of 14.9%. The predicted f_{cr} results are based on an average value of 0.75 for the material constant α_0 (Eq. 6.1).

6.4.3 Proposed tensile stress-strain constitutive model

Reinforced concrete panels which crack under in-plane tensile forces are governed by many factors, such as the size and distribution of the reinforcing mesh, bar surface characteristics, reinforcement ratio, etc. The tensile forces perpendicular to an open crack are carried by the reinforcing bars at the crack. Some of theses forces are transferred by bond to the intact concrete between the cracks. Therefore, the stress distribution in the concrete varies from a zero value at the crack to a higher value between the cracks (Figure 2-2). Consequently, the average stress in the concrete is nonzero. As previously discussed, this behaviour defines the tension stiffening. Thus, tension stiffening is a method of retaining some amount of stress which is not released when cracking occurs.

Most of the current models appear to use a gradual reduction of stress. However, this is not observed in most of the test results of GFRP-RC panels. The experimental evidence suggests that a sudden drop in load occurs accompanied by a jump in the tensile strain after crack forms, so it would seem realistic to include this effect. In this investigation, the load sharing approach

is adopted to define the average concrete stress-strain relationship. The idealization of the tension characteristics of GFRP-RC, including post-cracking tension-stiffening behaviour, is shown in Figure 6-23. The proposed model assumes a linear relation in the pre-cracking range (Eq. 6.3) and a bi-linear relation (Eqs. 6.4 and 6.5) for the post-cracking descending branch as follows:

$$f_{ct1} = E_c \varepsilon_{cr} = \frac{E_b}{n_b} \varepsilon_{cr} \qquad \varepsilon_m \le \varepsilon_{cr} \qquad (6.3)$$

$$f_{ct2} = \alpha_1 f_{cr} + \frac{f_{cr}(1-\alpha_1)(\alpha_2 \varepsilon_{cr} - \varepsilon_m)}{\varepsilon_{cr}(\alpha_2 - 1)} \qquad \varepsilon_{cr} \le \varepsilon_m \le \alpha_2 \varepsilon_{cr} \qquad (6.4)$$

$$f_{ct3} = \frac{\alpha_1 f_{cr}\left(\alpha_3 - \frac{\varepsilon_m}{\varepsilon_{cr}}\right)}{(\alpha_3 - \alpha_2)} \qquad \alpha_2 \varepsilon_{cr} \le \varepsilon_m \le \alpha_3 \varepsilon_{cr} \qquad (6.5)$$

where:

E_c and E_b Concrete and bar modulus of elasticity, respectively

n_b = modular ratio E_b / E_c

f_{cr} cracking strength of concrete panel

ε_{cr} – cracking strain

ε_m – member tensile strain normal to the crack directions

f_{ct} tensile stress normal to the crack directions

α_1, α_2, α_3 = material constants that depend on concrete strength, loading type (uniaxial or biaxial), and reinforcement ratio. Table 6-4 shows the proposed range for these constants calibrated using the experimental data.

6.5 Comparison between the Proposed Model, Test Results and Other Models

The proposed model is compared with some typical experimental results, shown in Figures 6-24 to 6-27. These figures also include the predictions of the proposed model in this investigation and the predictions of another four tension stiffening models from the literature. The other four models are models proposed by: Bischoff and Paixao (2004) (Eq. 2.40), Okamura et al. (1985) (Eq. 2.30), Vecchio and Collins (1986) (Eq. 2.25), and Marzouk and Chen (1993) (Eq. 2.29).

The model proposed by Bischoff and Paixao (2004) is the only one that was obtained based on test results of GFRP-RC members subjected to uniaxial tension. The models proposed by Vecchio and Collins (1986) and Okamura et al. (1985) were obtained from the results of shear tests of steel-RC panels. Marzouk and Chen (1993) adopted the concept of converting the tension softening into tension stiffening by changing the parameters α and β in their proposed model. According to Marzouk and Chen (1993), the parameter α was found in the range from 1.00 to 4.00 for steel-reinforced HSC slabs, while parameter β has a suggested value equal to 1.6655. In the shown comparisons, the parameter α is assumed to be equal to 1.00.

In general, the Bischoff and Paixao (2004), Vecchio and Collins (1986), and Okamura et al. (1985) models vary in their agreement with the experimental results. Out of these models,

the Bischoff and Paixao (2004) model may be better in its prediction for GFRP-RC under uniaxial tension. In general, the three models overestimate the tension-stiffening response. This overestimation appears to be significant for the GFRP-RC panels subjected to biaxial tension.

In general, the Marzouk and Chen (1993) model underestimates the tensile response for most of the uniaxial members. However, both Figures 6-26 and 6-27 demonstrate that this model performs better for HSC. This model has a good advantage in calibrating its incorporated parameters (α and β) to accommodate various tensile stress-strain relationships for different types of reinforcement. Therefore, in order to account for the tension stiffening contribution of GFRP-RC, it is recommended that the parameter α incorporated in this model be changed to $0.1 \sim 0.2$ for a better fitting for the uniaxial tension case of GFRP-RC.

In comparison with other tension-stiffening models, the proposed model in this investigation performs satisfactorily. The main feature of the suggested model is the inclusion of both the partial sudden drop of stress and sudden jump in the tensile strain after the tensile (cracking) strength has been exceeded. This feature reasonably reflects the experimental evidence. Thus, a reasonable agreement is found between the proposed tension-stiffening model and experimental results. This is valid for both loading cases of uniaxial and biaxial, and also for the GFRP-RC panels made of NSC and HSC. The material constants (α_1, α_2, and α_3) incorporated in the proposed model give the advantage of calibration to accommodate the changes in the tensile behaviour due to changes in concrete strength, loading type (uniaxial or biaxial), and reinforcement ratio.

6.6 Summary and Conclusions

In this chapter, the tensile stress-strain characteristics of GFRP-RC under uniaxial and biaxial tension are presented and discussed. The discussion focuses on the changes in the tension-stiffening behaviour of the tested panels due to different test parameters. The main differences between the tensile relationships of GFRP-RC and steel-RC are investigated. The changes in the w_m due to different test parameters are also discussed. Moreover, a constitutive law is proposed to idealize the tensile stress-strain relationships of GFRP-RC panels. The proposed model is further compared with other constitutive models. Based on the discussion presented in this chapter, the following conclusions can be summarized:

1. Under biaxial tension, the GFRP-RC panels experience much less tension stiffening contribution than those under uniaxial tension. This reduction is attributed to the reduction in the initial cracking loads and cracking strength under biaxial tension. This is in addition to the differences in the mechanism of crack development under biaxial tension.

2. The stress-strain relationships under uniaxial and biaxial tension are characterized by a sharp drop in the tensile stress sustained by concrete, accompanied by a jump in the tensile strain after a crack forms. Under uniaxial tension, the concrete stress after this drop reaches nearly 25 - 40% of the f_{cr} of concrete. Under biaxial tension, the concrete stress drops to nearly 15 - 25% of the f_{cr} of concrete.

3. The use of HSC results in a higher tension-stiffening contribution, due to higher cracking loads and reduction in tensile strain at the same level of loading. The

difference between the panel tensile response and bare bar response is found to be increasing nearly proportional to the increase in the concrete compressive strength.

4. A significant jump in the tensile strain is found to occur at the crack initiation in the HSC panels. This abrupt change in the tensile strain has a higher magnitude than NSC panels. This is attributed to the brittle nature of HSC and due to the local slip between the GFRP bars and surrounding concrete at the cracks' vicinities.

5. In general, there is an increase in the tension stiffening contribution due to the decrease in reinforcement ratio. The increase in tension stiffening is attributed to two main factors: (a) for a low reinforcement ratio, there is a larger concrete area around the bar, which results in a greater tension stiffening contribution, and (b) the use of a smaller d_b enhances the bond transfer mechanism of the GFRP-bar and thus the tension stiffening contribution.

6. GFRP-RC under uniaxial tension experiences a significant increase in the tension stiffening contribution compared to steel-RC at the same level of stress, which is due to the lower modulus of elasticity of the GFRP. However, the tension stiffening is not as significant under biaxial tension, due to the different cracking mechanism, which results in faster degradation in the tension-stiffening contribution under biaxial tension.

7. The tensile strain at which the stabilized cracking stage is achieved for GFRP-RC panels varies between 2000 to 8000 με, which is nearly 10 to 40 times the ε_{cr}, while

for steel-RC, the stabilized strain is in the range of 1700 με, which is about 8 to 15 times the ε_{cr}. Up to 2000 με, which is considered a serviceability design limit, the difference in w_m between steel-RC and GFRP-RC is considered minor. Beyond the steel-RC stabilized cracking stage, crack widths are evidently greater for the GFRP-RC because of the lower modulus of elasticity of the GFRP bar.

8. Compared to the uniaxial tension case, w_m is relatively lower under biaxial tension for the same level of tensile strain by nearly 42%. Such a reduction in w_m could be attributed to the reduction in the GFRP-strains under biaxial tension.

9. In general, HSC causes a reduction in w_m. Under uniaxial tension, there is a minor difference in w_m due to the use of HSC up to ε_m = 4000 to 5000 με. Beyond that, w_m is reduced by nearly 20 ~ 30%, which can be attributed to the higher concrete compressive strength. Under biaxial tension, HSC allows a reduction in w_m by nearly 45% up to the stabilized cracking stage.

10. Under uniaxial tension, a reduction in w_m by nearly 75% on average due to the decrease in the reinforcement ratio from 1% to 0.7%, which is directly attributed to the higher tension stiffening contribution recorded for the lower reinforcement ratio. However, under biaxial tension, the overall change in w_m is considered minor.

11. A tensile stress-strain constitutive relationship (Eqs. 6.3 to 6.5) is proposed for GFRP-RC. The main feature of the suggested model is the inclusion of both the partial sudden drop of stress and change in the tensile strain after the f_{cr} is exceeded.

This feature reasonably reflects the experimental evidence. The f_{cr} of concrete is incorporated in the proposed model to account for the biaxial tension strength envelope (Eq. 6.2). Using this concept, the two-dimensional relationship is reduced to a simple uniaxial expression.

Table 6-1: Test results

S	Specimen	f_c', (MPa)	N_{cr} (kN)	f_{crs} (MPa)	$\varepsilon_{cr,\,avg}$ (με)	At initial crack load, N_{cr}		
						Bare bar stress, (MPa)	Bare bar strain, (με)	$\Delta\varepsilon_{m,\,cr}$ (με)
I	P1-GNU-16-1.0-1.5	48.1	216.4	1.86	128.9	182.5	4463	4334
	P2-GNU-16-1.0-2.5	46.9	163.6	1.41	89.2	137.5	3375	3286
	P3-GNB-16-1.0-2.5	34.8	126.5	1.06	175.4	106.5	2610	2434
			126.2	1.07	174.8	106.2	2603	2427
II	P5-GNU-16-0.7-2.5	47.2	180.8	1.55	173.9	228.3	5595	5421
	P7-GNU-13-0.7-2.5	43.6	235.9	1.94	286.4	310.3	7605	7318
	P10-GNB-16-0.7-2.5	46.1	124.9	1.08	206.9	157.8	3867	3660
			127.9	1.11	205.5	161.4	3955	3749
III	P4-GHU-16-1.0-2.5	76.9	299.5	2.49	253.5	252.1	6179	5943
	P6-GHB-16-1.0-2.5	74.9	232.6	1.92	236.5	195.8	4799	4562
			233.7	1.89	263.9	196.8	4823	4559
IV	P8-GHU-13-0.7-1.5	77.5	251.7	2.08	318.7	331.2	8117	7798
	P9-GHB-13-0.7-2.5	79.7	223.6	1.95	62.8	294.1	7208	7145
			225.0	1.96	43.9	295.9	7252	7208
V	P11-SNU-16-1.0-2.5	43.7	317.0	2.40	202	285	1425	1223
	P12-SNB-16-1.0-2.5	38.4	243.0	1.87	107	186.3	931	824
			228.5	1.88	45.4	190.4	952	906

Table 6-2: Mean crack width at stabilized cracking stage

Series	Specimen	$N_{stab.}$, (kN)	Bar stress, (MPa)	$\varepsilon_{m,\ stab}$, (με)	w_m, (mm)
S-I	P1-GNU-16-1.0-1.5	250	210	2199	0.40
	P2-GNU-16-1.0-2.5	290	245	5512	1.20
	P3-GNB-16-1.0-2.5	207	175	5401	0.93
S-II	P5-GNU-16-0.7-2.5	336	424	6932	1.20
	P7-GNU-13-0.7-2.5	280	368	6580	0.66
	P10-GNB-16-0.7-2.5	302	380	6253	1.06
S-III	P4-GHU-16-1.0-2.5	415	350	8004	0.93
	P6-GHB-16-1.0-2.5	230	194	4723	0.58
S-IV	P8-GHU-13-0.7-1.5	336	442	3942	1.09
	P9-GHB-13-0.7-2.5	251	332	8534	1.11
S-V	P11-SNU-16-1.0-2.5	433	361	1630	0.85
	P12-SNB-16-1.0-2.5	420	350	1756	0.77

Table 6-3: Prediction of cracking strength of GFRP-RC panels

Series	Specimen	$f_{cr(experimental)}$, (MPa)	$f_{cr\ (predicted)}$, (MPa)	$\frac{f_{cr(experimental)}}{f_{cr(predicted)}}$
I	P1-GNU-16-1.0-1.5	1.86	1.66	1.12
	P2-GNU-16-1.0-2.5	1.27	1.65	0.77
	P3-GNB-16-1.0-2.5	1.06	1.06	1.00
II	P5-GNU-16-0.7-2.5	1.55	1.61	0.96
	P7-GNU-13-0.7-2.5	1.94	1.52	1.28
	P10-GNB-16-0.7-2.5	1.09	1.21	0.90
III	P4-GHU-16-1.0-2.5	2.49	2.11	1.18
	P6-GHB-16-1.0-2.5	1.77	1.56	1.13
IV	P8-GHU-13-0.7-1.5	2.09	2.11	0.99
	P9-GHB-13-0.7-2.5	1.96	1.61	1.22
			Mean	1.06
			St. Deviation	0.16
			C.O.V. %	14.9

Table 6-4: Proposed material constants for tension stiffening model

Concrete Type	Loading Type	α_1	α_2	α_3
NSC	Uniaxial tension	0.25 – 0.40	20 – 30	60 – 100
	Biaxial tension	0.20 – 0.25	10 – 15	15 – 20
HSC	Uniaxial tension	0.15	15 – 20	25 – 35
	Biaxial tension	0.10		

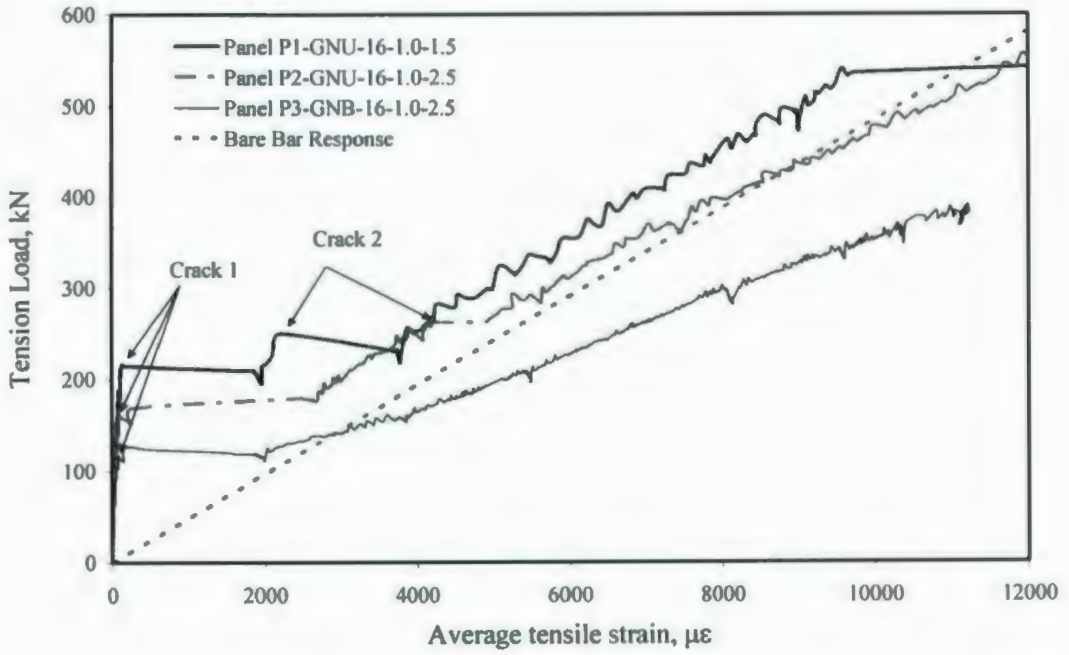

Figure 6-1: Load-strain relationships of GFRP-RC panels of Series I

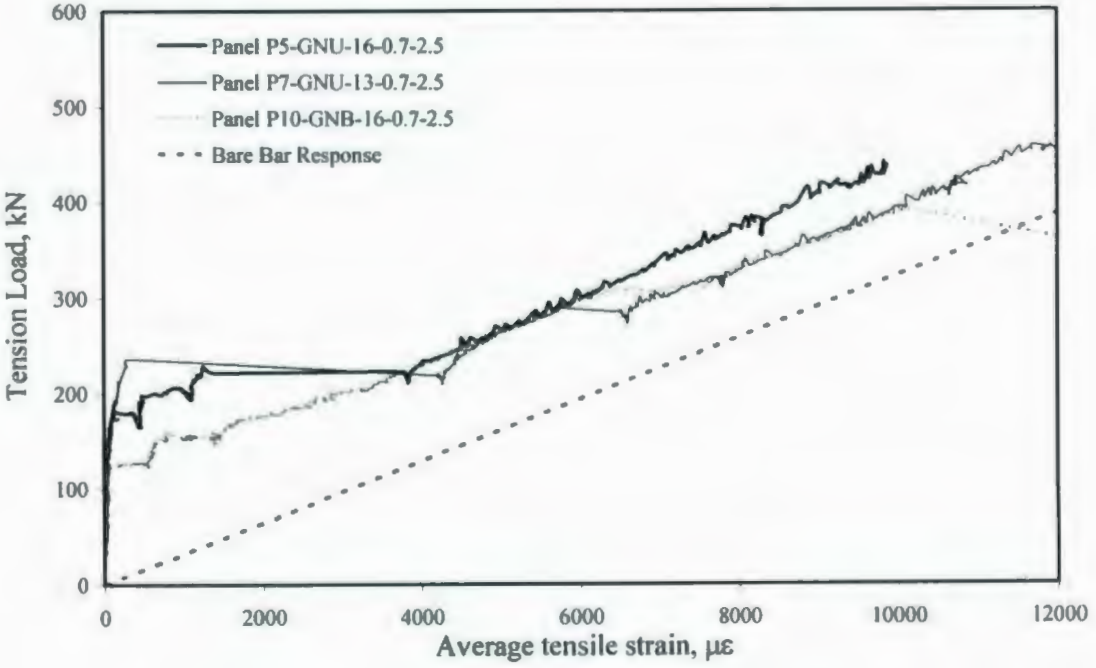

Figure 6-2: Load-strain relationships of GFRP-RC panels of Series II

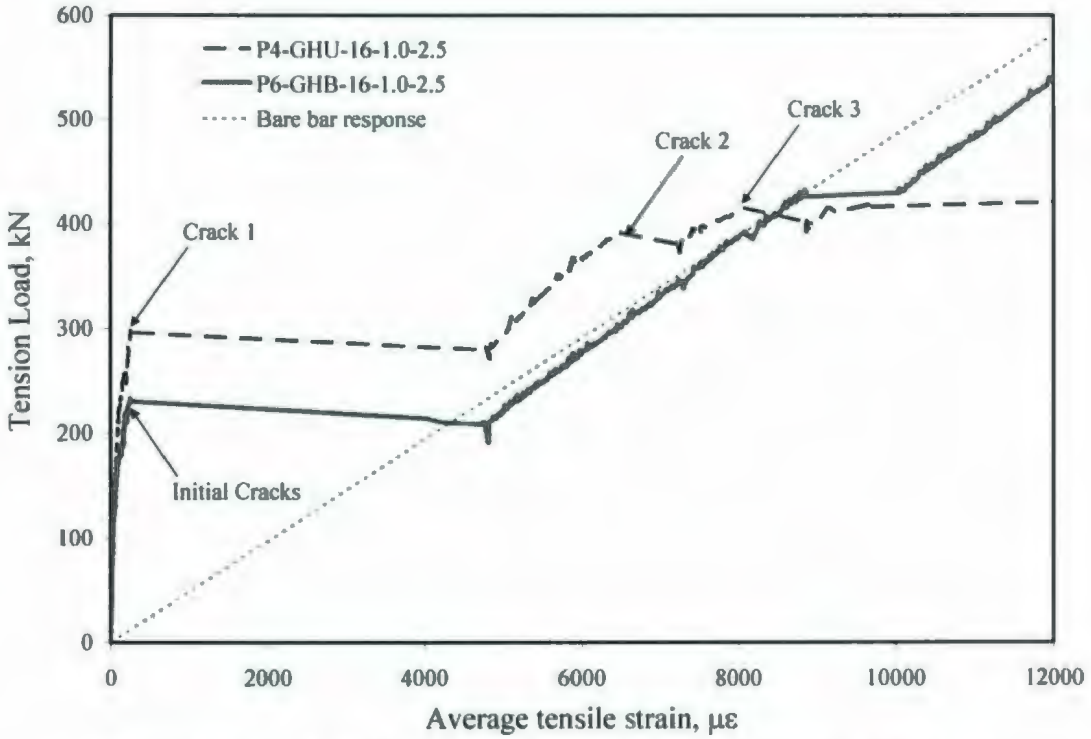

Figure 6-3: Load-strain relationships of GFRP-RC panels of Series III

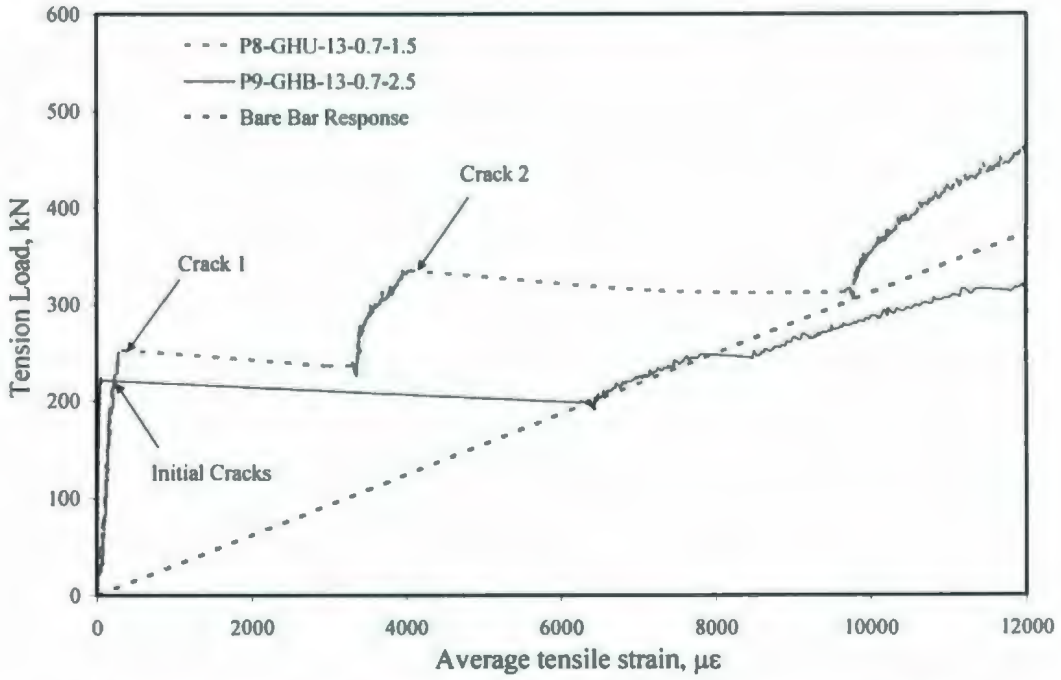

Figure 6-4: Load-strain relationships of GFRP-RC panels of Series IV

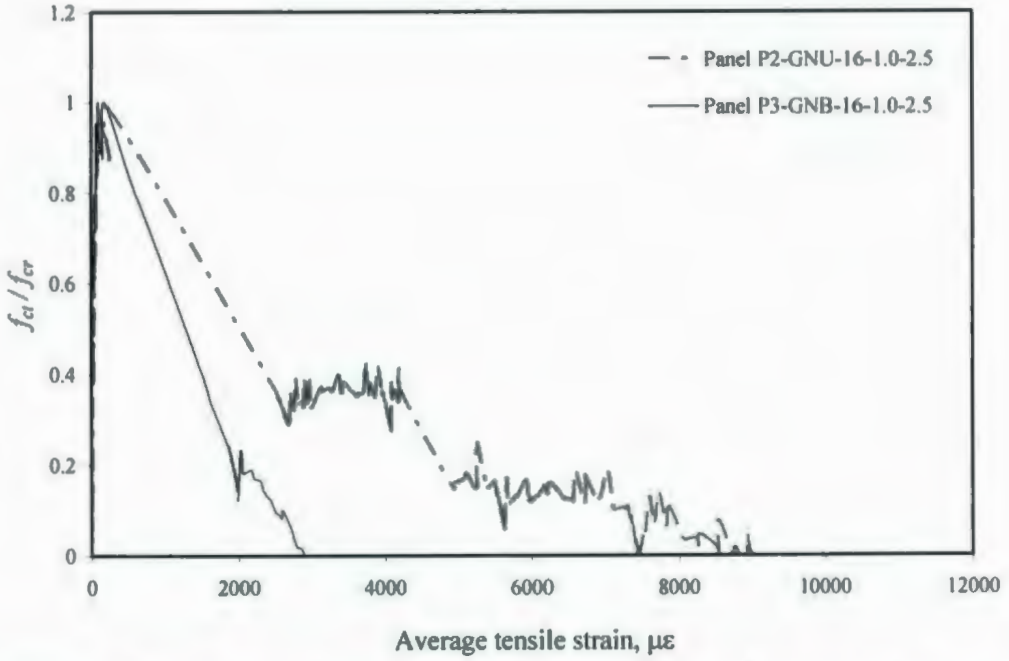

Figure 6-5: Effect of loading type on the concrete normalized stress-strain relationship

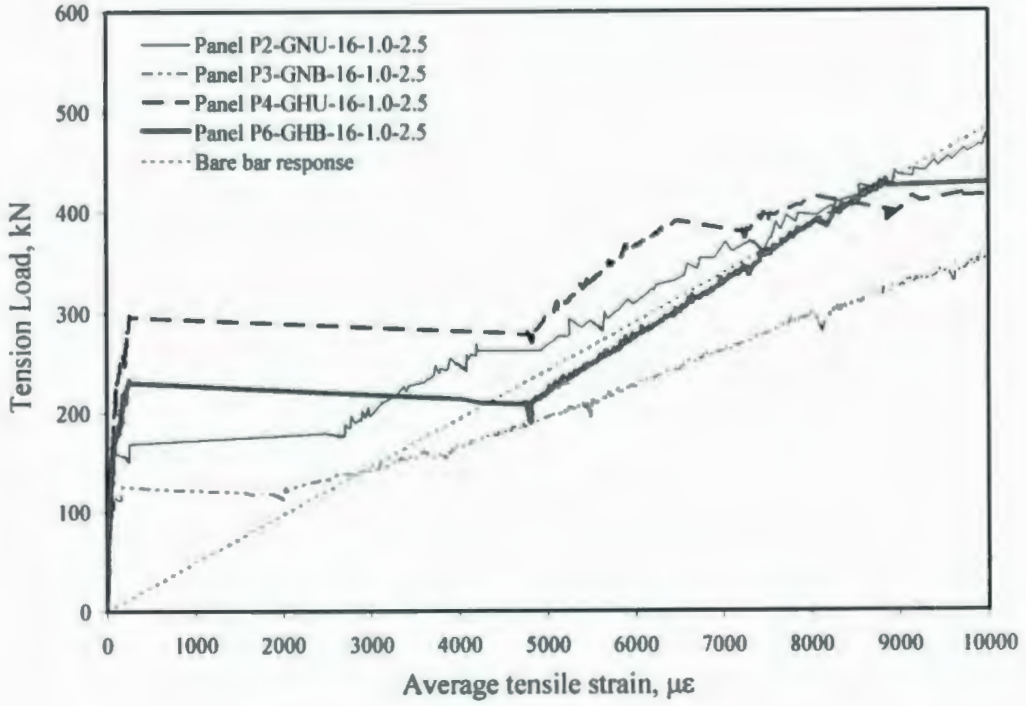

Figure 6-6: Effect of HSC on the change in load-strain relationship

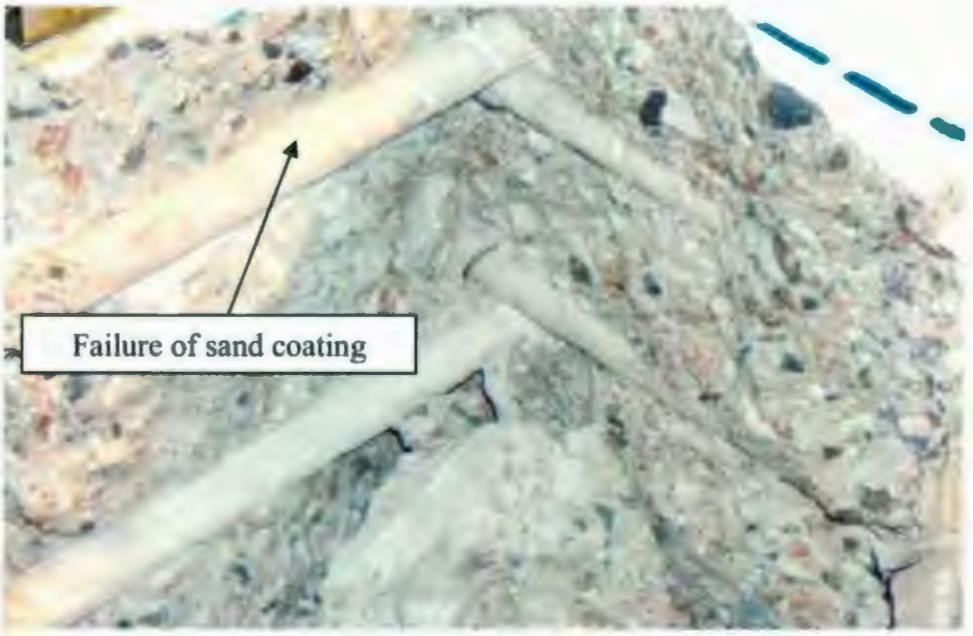

Figure 6-7: A close up on the interfacial bond failure between GFRP and NSC

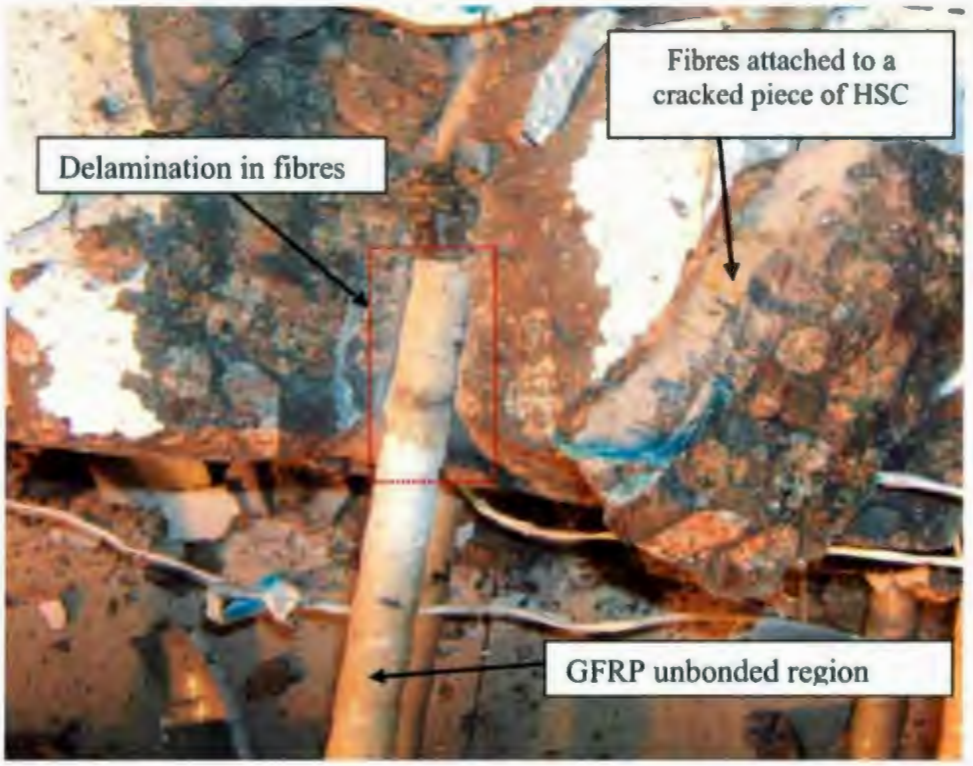

Figure 6-8: A close up on the interfacial bond failure between GFRP and HSC

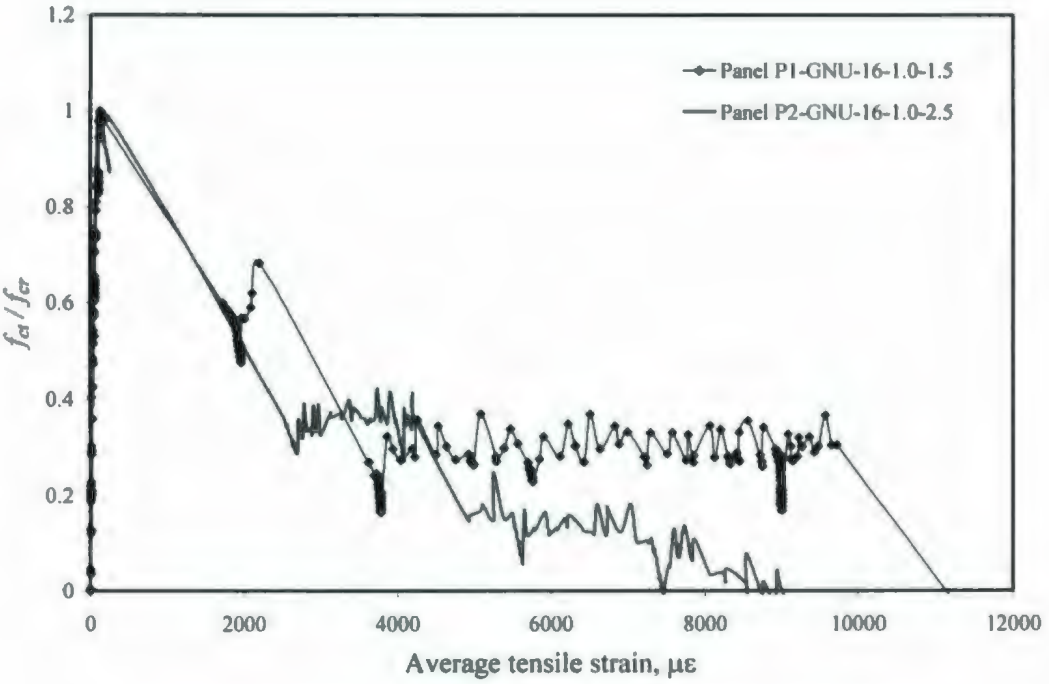

Figure 6-9: Effect of c_c / d_b on tensile stress-strain relationship

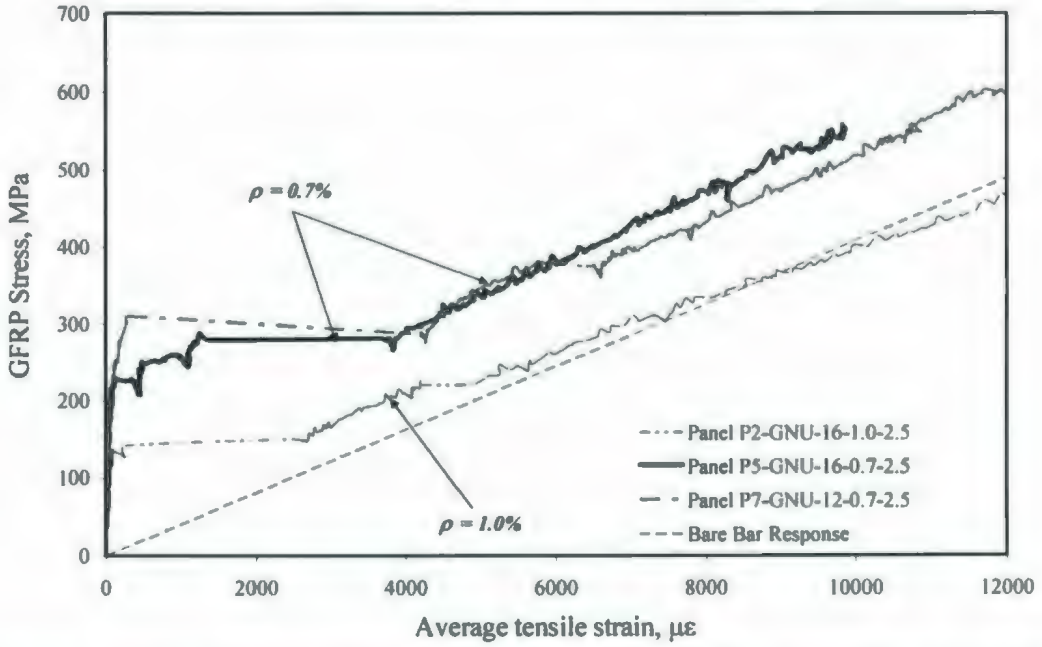

Figure 6-10: Effect of reinforcement ratio on GFRP-stress strain relationships under uniaxial tension

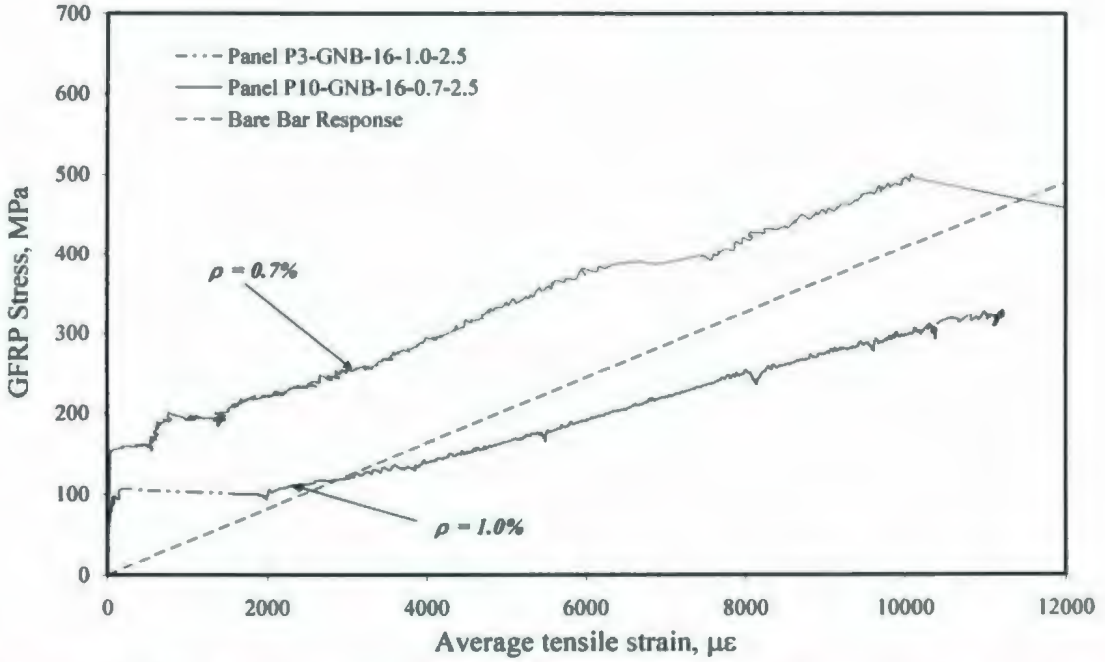

Figure 6-11: Effect of reinforcement ratio on GFRP-stress strain relationships under biaxial tension

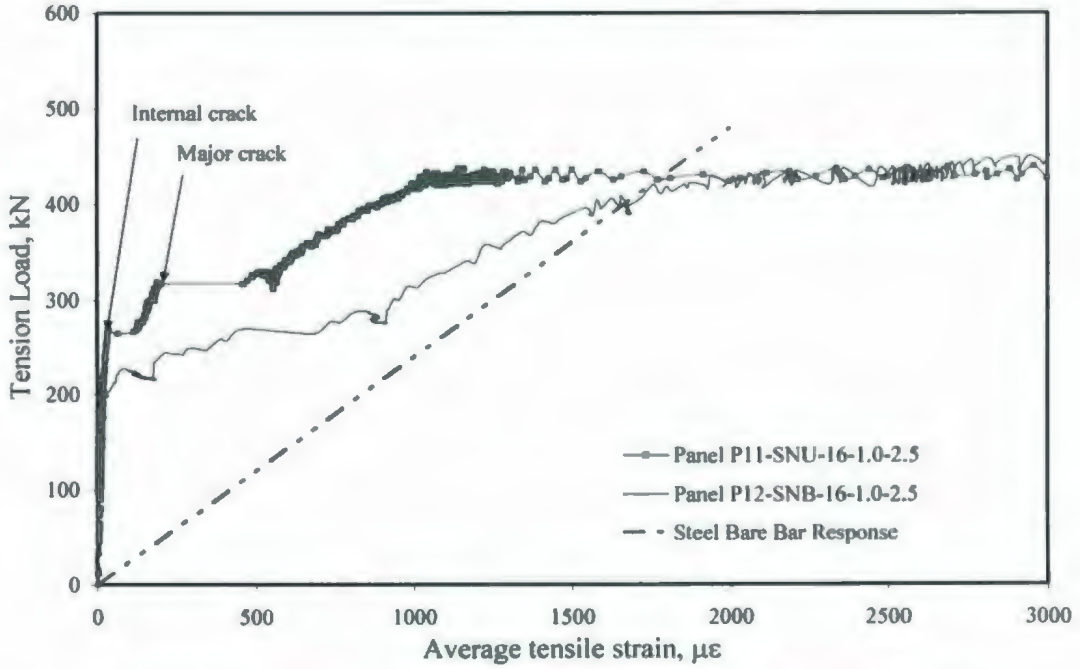

Figure 6-12: Load-strain relationships of steel-RC panels of Series V

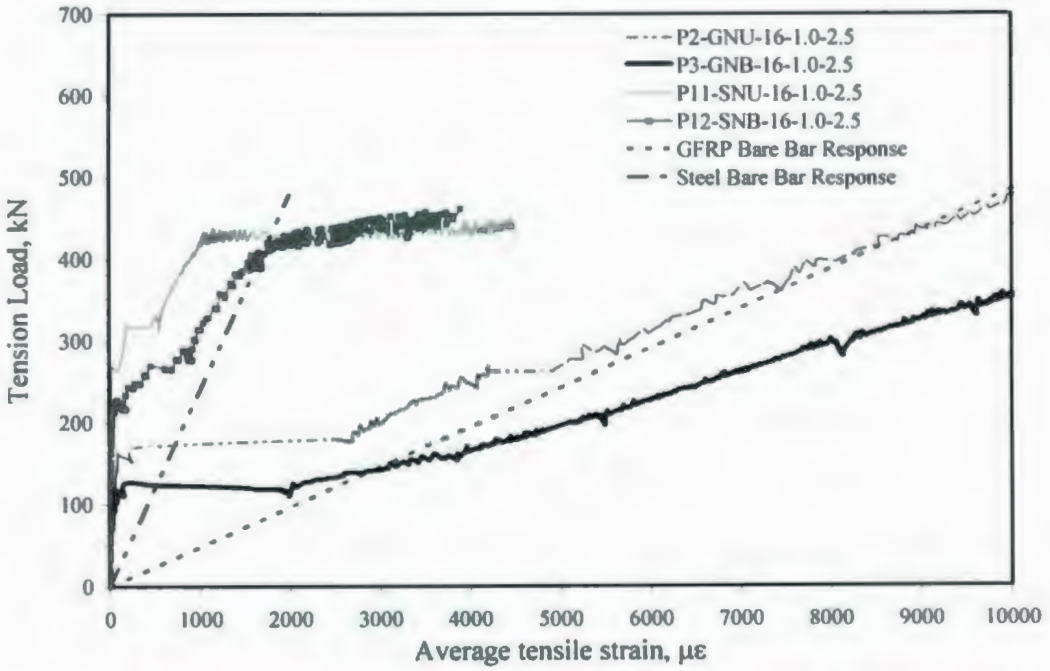

Figure 6-13: Load-strain relationship GFRP- and steel RC-panels

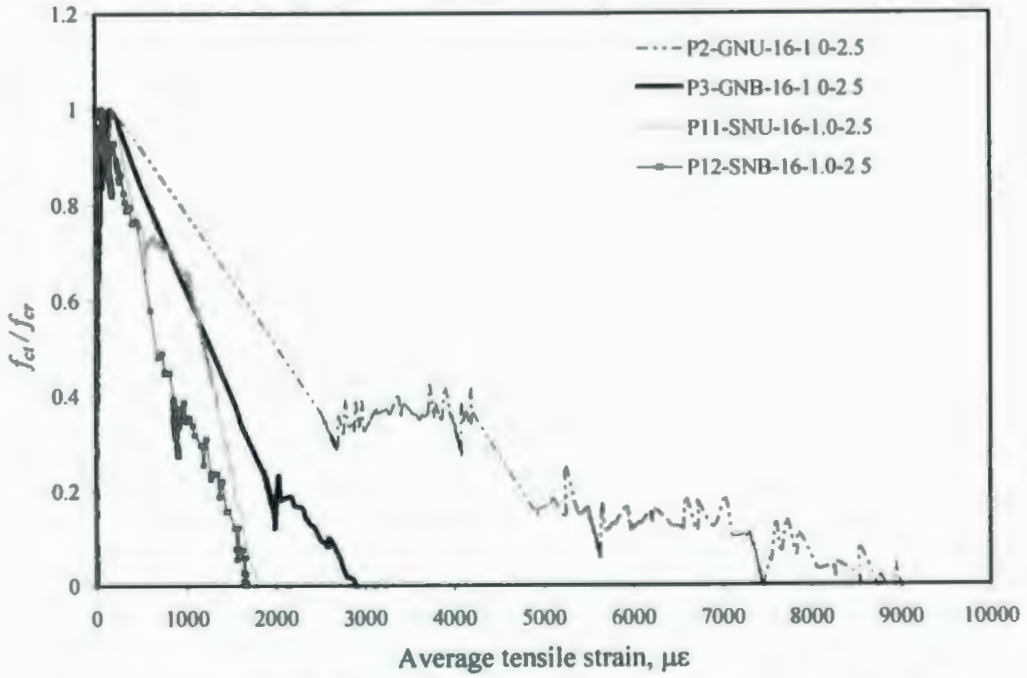

Figure 6-14: Effect of bar type on concrete normalized stress-strain relationship

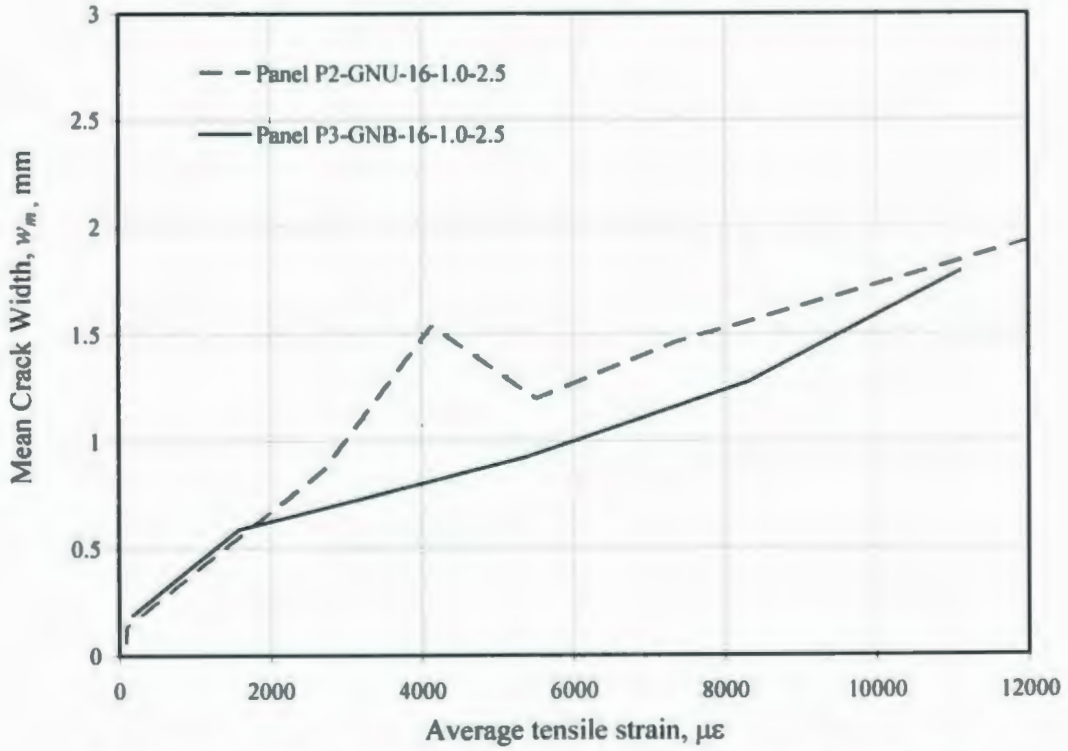

Figure 6-15: Effect of loading type on the change in mean crack width

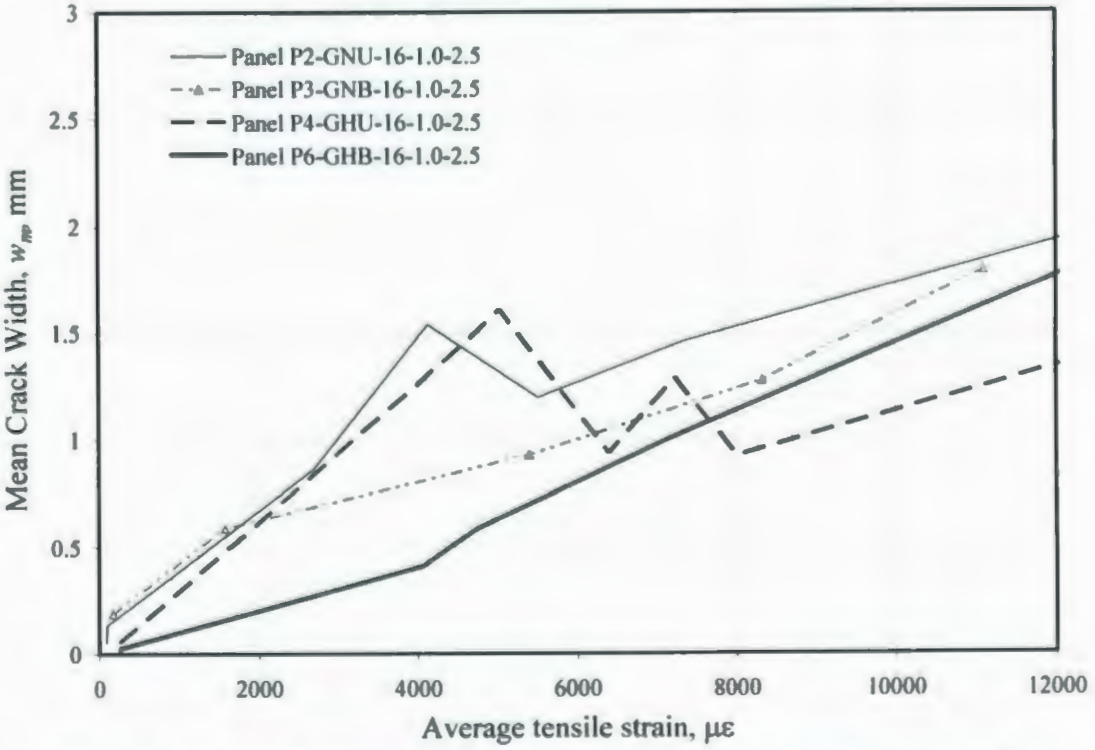

Figure 6-16: Effect of concrete strength on the change in mean crack width

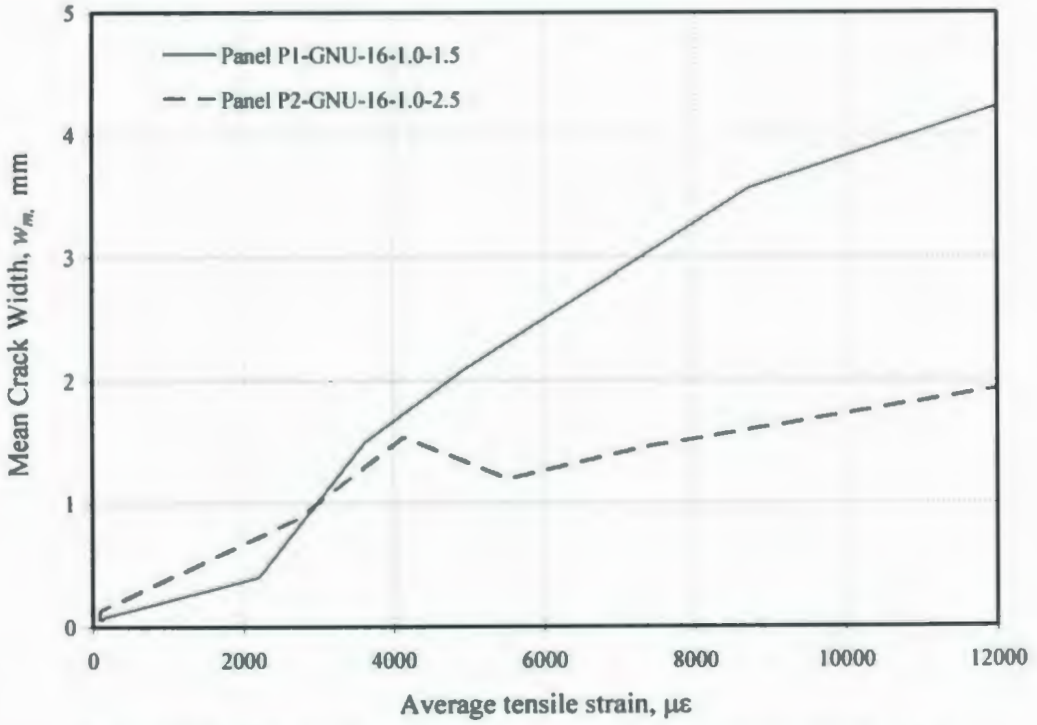

Figure 6-17: Effect of c_c / d_b ratio on the change in mean crack width

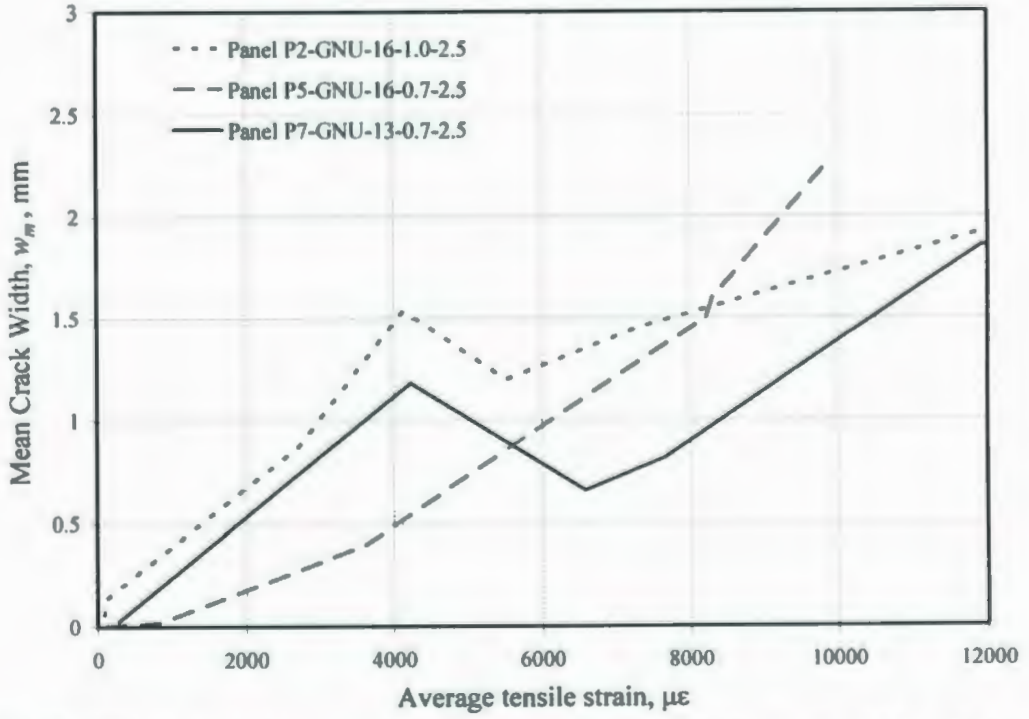

Figure 6-18: Effect of reinforcement ratio on the change in mean crack width under uniaxial tension

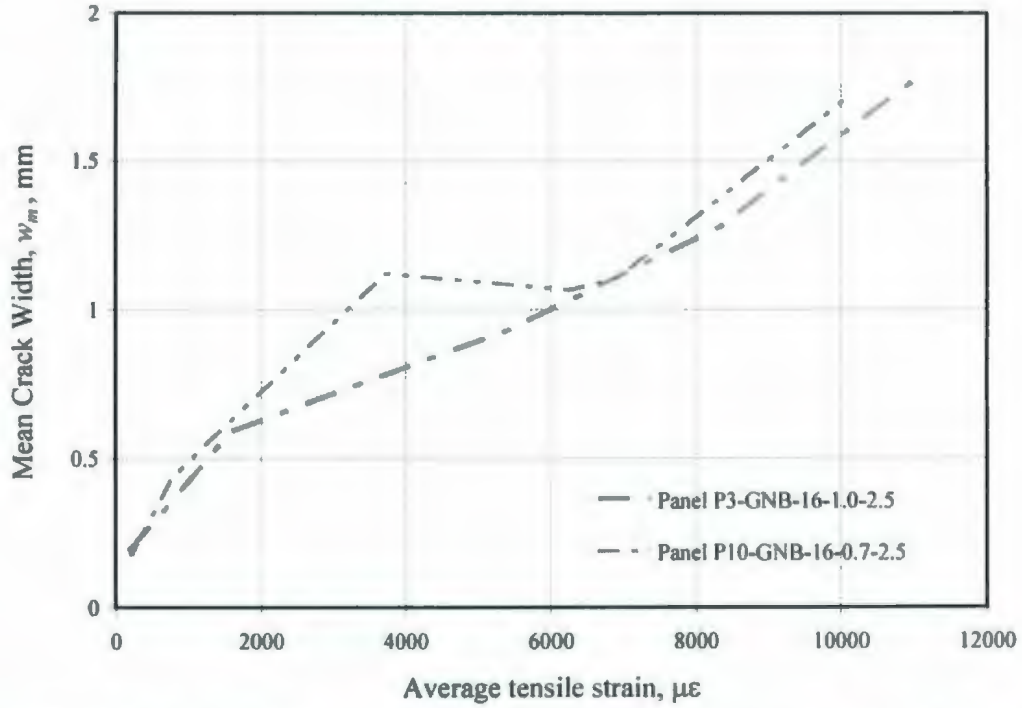

Figure 6-19: Effect of reinforcement ratio on the change in mean crack width under biaxial tension

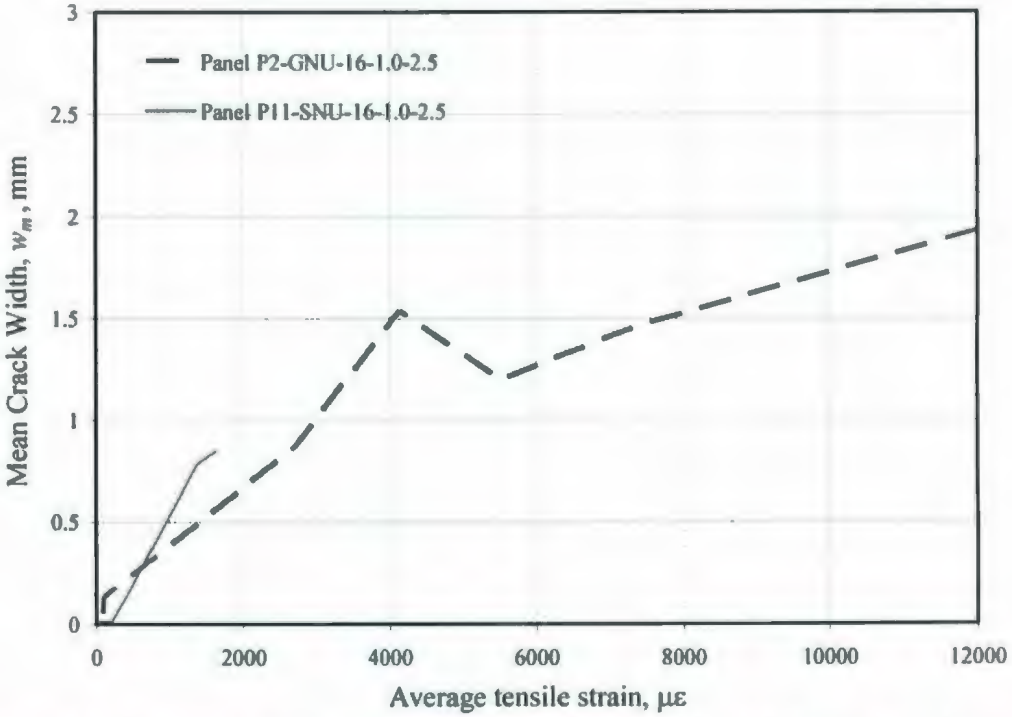

Figure 6-20: Change in mean crack width for GFRP- and Steel-RC panels under uniaxial tension

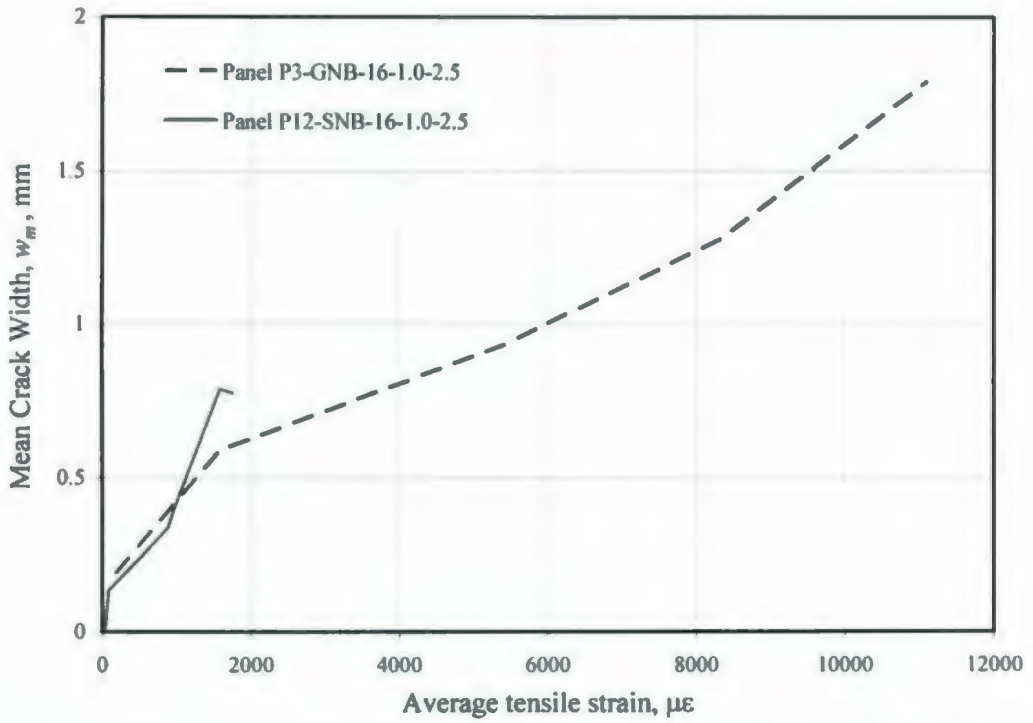

Figure 6-21: Change in mean crack width for GFRP- and steel-RC panels under biaxial tension

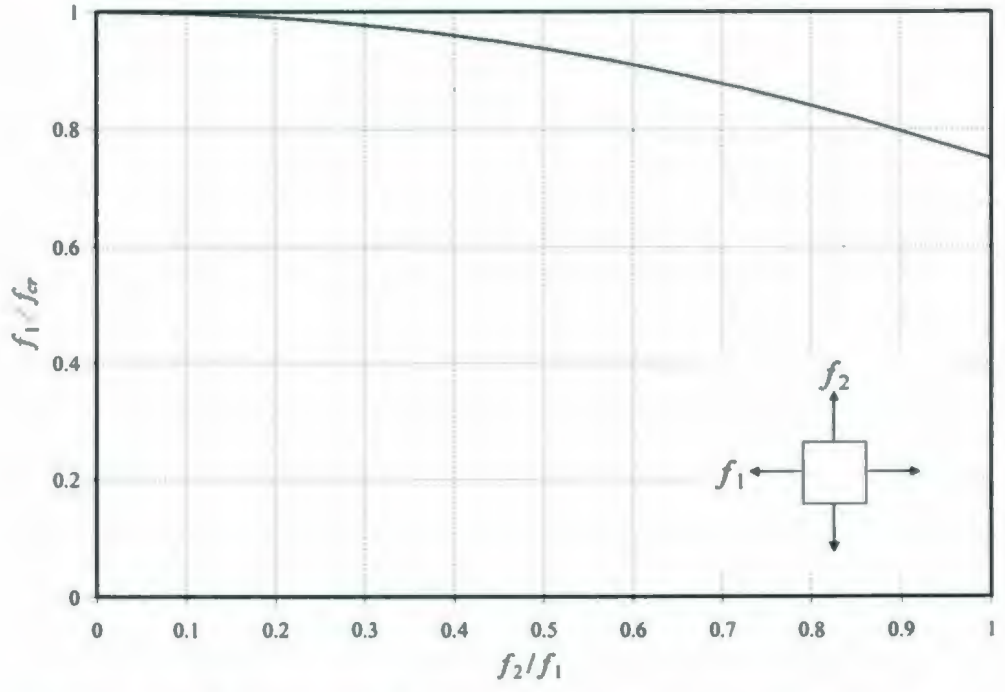

Figure 6-22: Biaxial strength envelope of concrete under biaxial tension

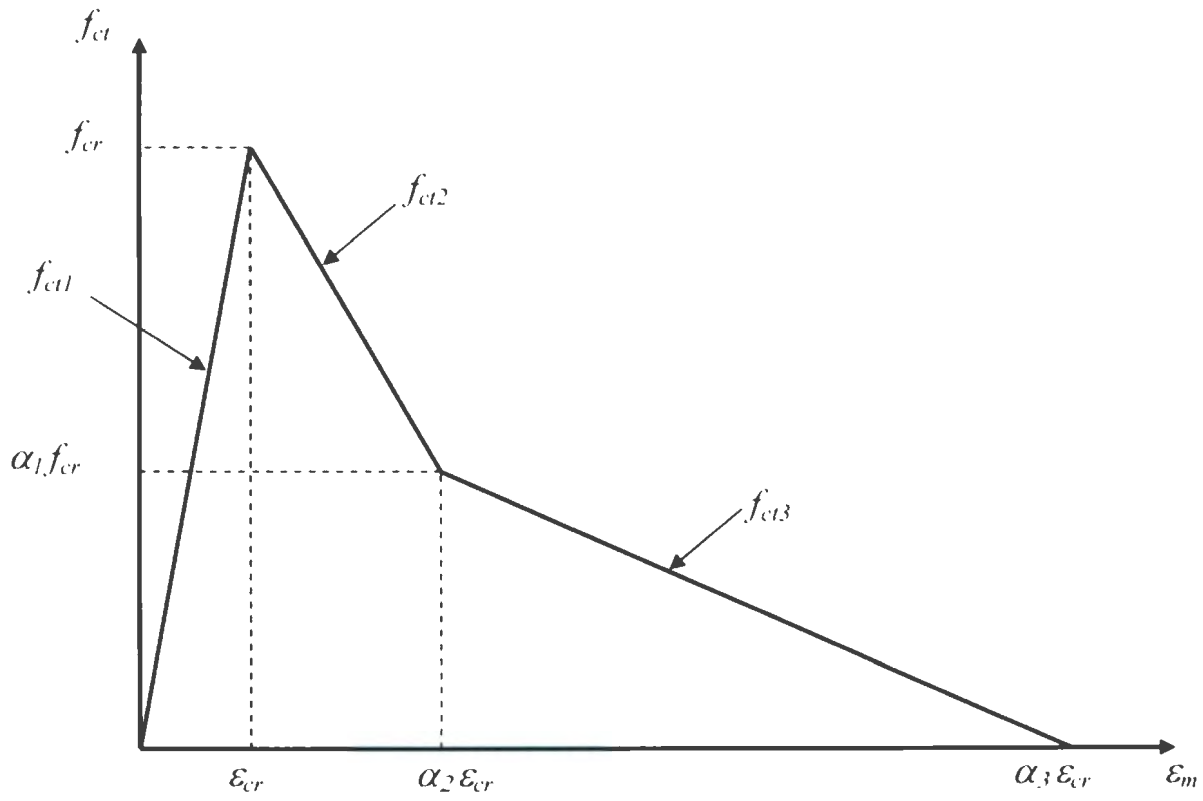

Figure 6-23: Proposed model of tensile stress-strain relationship of GFRP-RC

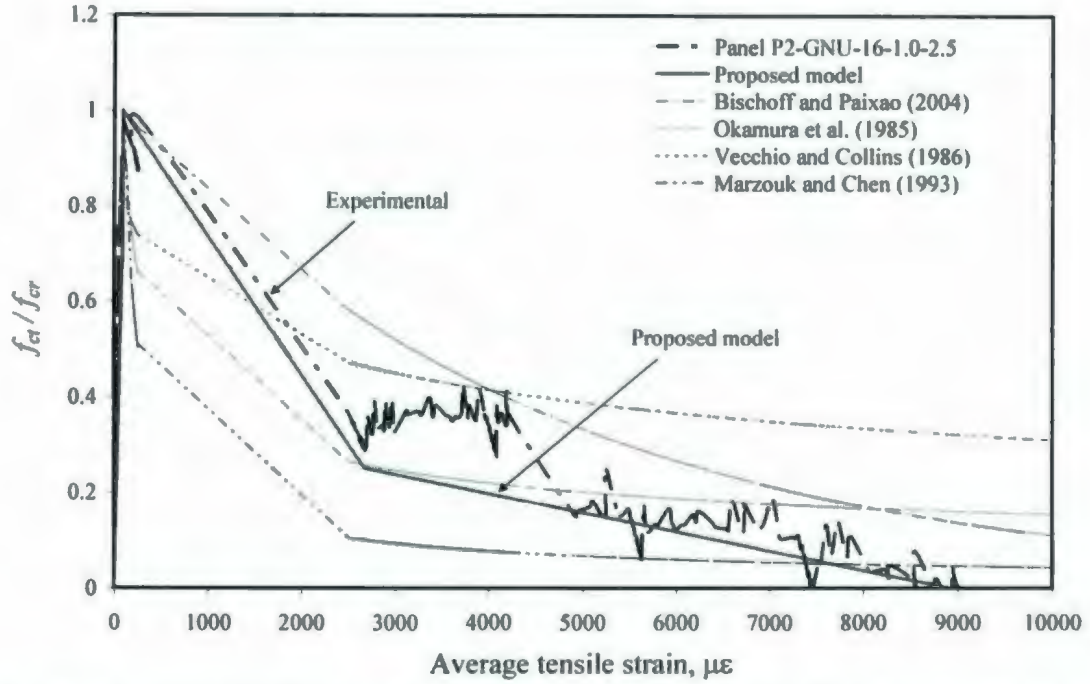

Figure 6-24: Proposed tension stiffening model compared to test result of P2-GNU-16-1.0-2.5 and other models

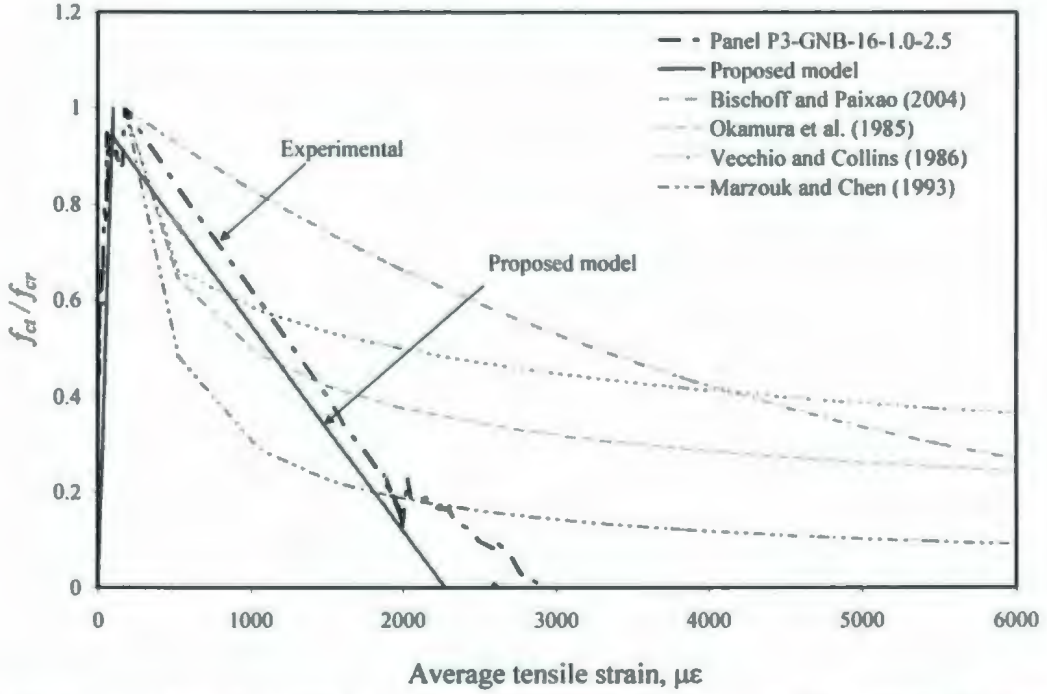

Figure 6-25: Proposed tension stiffening model compared to test result of P3-GNB-16-1.0-2.5 and other models

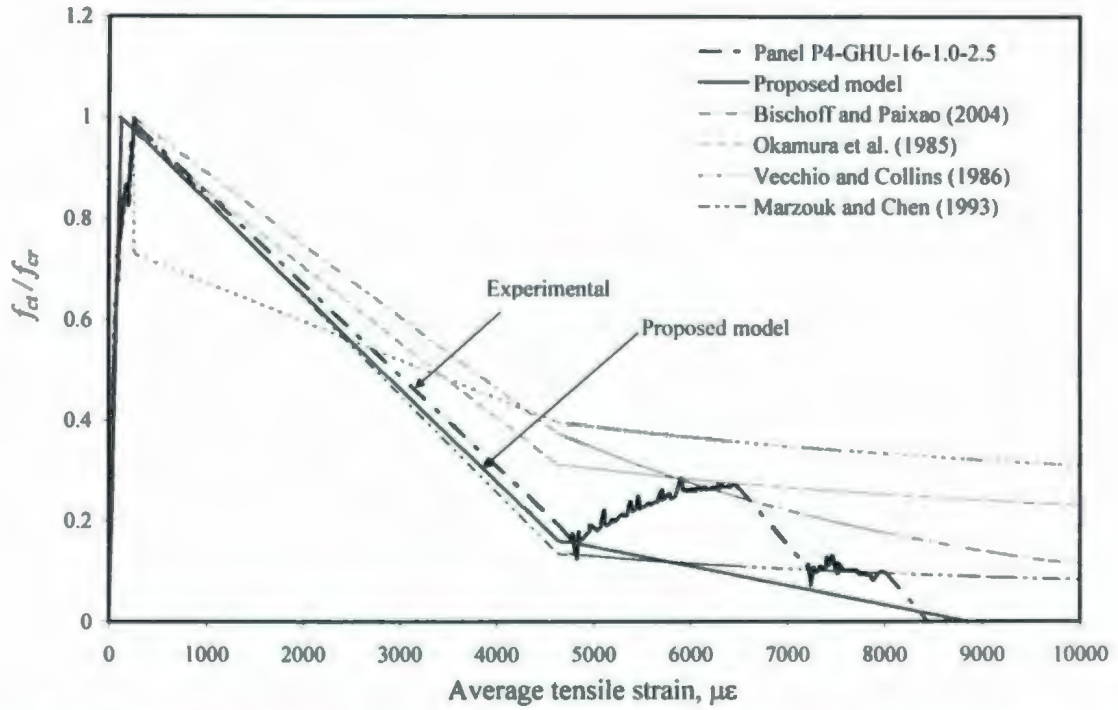

Figure 6-26: Proposed tension stiffening model compared to test result of P4-GHU-16-1.0-2.5 and other models

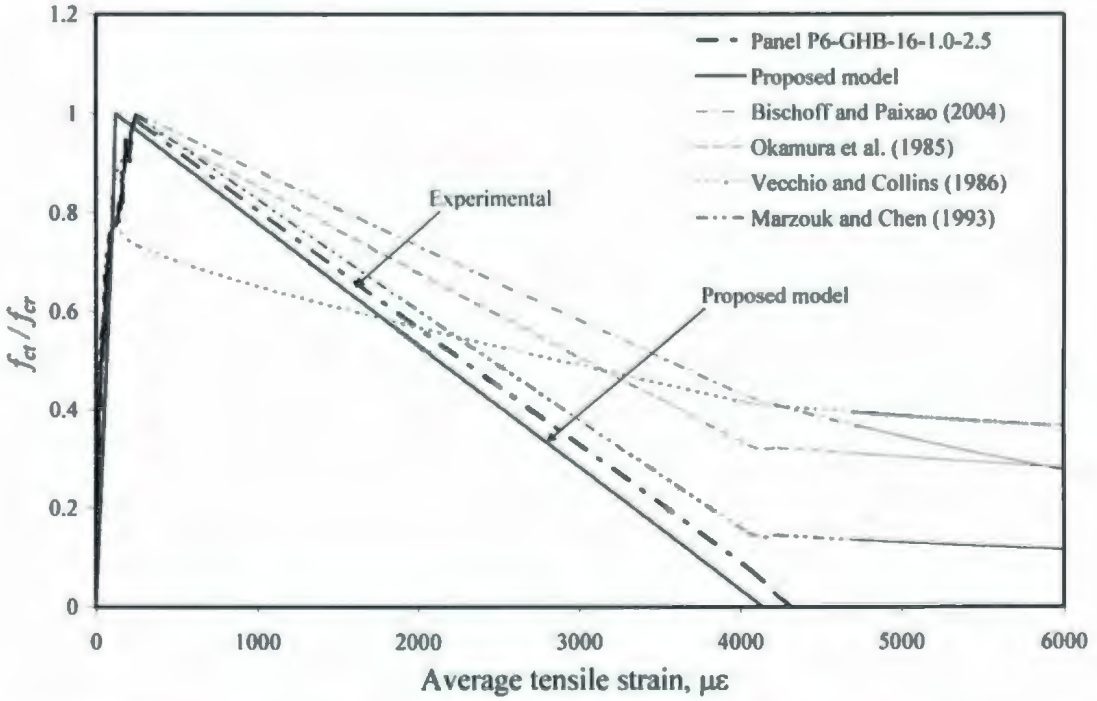

Figure 6-27: Proposed tension stiffening model compared to test result of P6-GHB-16-1.0-2.5 and other models

Chapter 7

CRACKING MODEL FOR GFRP-RC

7.1 Introduction

An analytical investigation is carried out to develop a crack spacing model for GFRP-RC panels under direct tension. The main details of this investigation are presented in this chapter.

The first part of this chapter discusses an approach to develop a constitutive relation to predict the crack spacing of GFRP-RC panels under direct uniaxial and biaxial tension. The cracking mathematical model is developed by adopting the classical stress transfer approach based on equilibrium, strain compatibility, and bond-slip relations. The proposed model explicitly accounts for the bond characteristics of the GFRP bar type, and its effect on the stabilized crack spacing. The model also considers an analytical approach to account for the biaxial tensile stress problem. The model takes into account the effect of concrete contribution on crack width through a proposed idealization for the tension-stiffening behaviour of GFRP-RC, thus reflecting the experimental observations. The proposed tension-stiffening constitutive model includes the pre- and post-cracking properties of concrete.

The verification and validation of the proposed approach for cracking constitutive modelling is presented in the second part of this chapter. A comparison between the predictions of the cracking model and some of the available experimental data on GFRP-RC panels is presented. The model is also compared to other relevant crack spacing equations

available in the literature. Finally, the cracking model is validated using some experimental data of other relevant research investigations found in the literature.

7.2 Classical Stress-Transfer Approach

The cracking model is developed by adopting the classical stress transfer approach based on equilibrium, strain compatibility, and bond-slip relations. The basis of the mathematical formulation is reviewed in this section.

Reinforcing bars transfer tensile stresses to concrete through the bond stresses located along the interface between the reinforcement and the surrounding volume of concrete. This can be explained by considering a portion of RC panel subjected to uniaxial tension as a free body diagram to obtain the equilibrium equations for concrete and reinforcement (Figure 7-1). When a crack is developed in the RC member, the stress in the concrete must be zero at the edge of the crack. Thus, the distribution of the tensile stress in the concrete, f_{ct} after the formation of the first crack, or just before the formation of the second crack, will appear as shown in Figure 2-4. With increasing distance from the crack, the surface stress will increase until the end of transfer length, l_t. Beyond this length, the stress distribution will not be affected by the crack. As previously mentioned, the l_t is the embedment length required to satisfy the condition where the strains in the reinforcing bar and the surrounding concrete are equal to each other as shown in Figure 7-1. The crack affects the stresses in the concrete within a distance $\pm l_t$ of the crack. The next crack will form outside this region.

When the tensile force N is applied, the far ends represent the fully cracked state (state 2) with a reinforcement strain ε_{b2}. The tensile force N is first transferred from the bar to the

concrete by the bond stress τ_b, and the net value of the bond stress can be assumed equal to zero at the inner part (S - $2l_t$). This means that there is no bond-slip within the central region bounded by the l_t. Thus, it can be reasonably assumed that the strains in the reinforcement and concrete are equal to each other at $x = l_t$ and the strain value corresponds to ε_{b1}.

From the strain distribution (Figure 7-1), the local slip $s(x)$ can be defined as the total difference in elongations between the reinforcement and surrounding concrete measured over the length between distance x from a crack face and the center of the segment ($x = S/2$). Thus:

$$s(x) = \int_{x}^{S/2} \left(\varepsilon_b(x) - \varepsilon_c(x)\right) dx \tag{7.1}$$

where S is the spacing between two adjacent cracks (crack spacing); and $\varepsilon_b(x)$ and $\varepsilon_c(x)$ are the strain distributions of reinforcement and concrete, respectively.

The applied N is distributed partly between the concrete volume F_c and the reinforcement bar F_b, then by force equilibrium, N can be defined as: $N = F_c + F_b$. The force variations between the concrete and reinforcement can be derived in terms of τ_b using a free body diagram of an axial member as shown in Figure 7-2, thus:

$$\frac{dF_b}{dx} = A_b E_b \frac{d\varepsilon_b}{dx} = n_{bars} p_b \tau_b \tag{7.2}$$

$$\frac{dF_c}{dx} = A_c E_c \frac{d\varepsilon_c}{dx} = -n_{bars} p_b \tau_b \tag{7.3}$$

where n_{bars} is the number of bars placed within length dx; p_b is the perimeter of a reinforcing bar; τ_b is the bond stress at the bar-concrete interface; A_b and A_c are the cross-section area of

the reinforcing bar and concrete, respectively; while E_b and E_c are the elastic modulus of the reinforcing bar and concrete, respectively.

On the basis of the bond-slip $s(x)$, as defined in Eq. (7.1), the second order differential equation of the $s(x)$ with respect to x leads to:

$$\frac{d^2 s(x)}{dx^2} = \frac{-d}{dx}\left(\varepsilon_b(x) - \varepsilon_c(x)\right) \tag{7.4}$$

By substituting Eqs. (7.2) and (7.3) into Eq. (7.4), the following governing differential equation is obtained:

$$\frac{d^2 s(x)}{dx^2} - \frac{\left(1 + n_b \rho_b\right)}{E_b A_b} \tau_b(x) = 0 \tag{7.5}$$

where $n_b = E_b / E_c$ is the modular ratio.

Equation (7.5) represents the basic relationship between the second derivative of $s(x)$ and local τ_b. The general solution of this equation has to be determined using boundary conditions and assuming a relationship between local τ_b and $s(x)$ (Edwards and Picard 1972; Nilson 1972). This approach requires a series of complex integration and derivation procedures. Determination of the bond characteristics along the member should make it possible to obtain a unique distribution of slip and stresses between two adjacent cracks. However, it may be experimentally difficult to find an explicit mathematical model to define the local bond-local slip relationship. In addition, this relationship must satisfy all boundary conditions of the RC-specimen. Thus, it is recommended that a simple assumption is used for the bond stress distribution.

7.3 Basic Assumptions for Mathematical Formulation

7.3.1 Cracking strength

The proposed cracking strength prediction equations discussed in Chapter 6 are adopted. Equation (6.1) is used to estimate the cracking strength f_{cr} of the RC panels under uniaxial direct tension. The general expression (Eq. 6.2) is used to define the failure envelope in the tension-tension region.

7.3.2 Effective reinforcement ratio

It was concluded in Chapter 5 that the effective tension zones around the GFRP bars are relatively smaller than those developed for deformed steel bars. This is attributed to the different bond properties of reinforcement between both types of bars. This finding will be considered when calculating the effective reinforcement ratio ρ_{eff} in the cracking equations. It is common to assume that the ρ_{eff} for steel-RC members is based on 15 times the bar diameter d_b (15 d_b) (NBR 1992).

The presented experimental evidence for GFRP-RC suggests that it would be realistic to assume a lower value than 15 d_b. Thus, it is recommended that a typical value is used for the diameter of effective tension zones around the GFRP bars as 7 d_b measured from the centre of the bar. This is schematically shown in Figure 7-3.

7.3.3 Tension stiffening constitutive model

The tension stiffening constitutive model is taken as proposed in Chapter 6. The proposed model assumes a bi-linear relation (Eqs. 6.4 and 6.5) for the post-cracking descending branch.

7.4 Maximum Crack Spacing Mathematical Formulation

As shown in Figures 2-2, 2-4, and 7-1, at the end of the l_t distance away from the crack, the force carried by concrete must be equal to the area of concrete A_c multiplied by the f_{ct}. This force must be transferred from the reinforcement, which carries the total N at a crack to the concrete by bond over the l_t. Thus:

$$A_c f_{ct} = \pi d_b \int \tau_x dx \tag{7.6}$$

As the load increases up to the N_{cr}, the crack will open to a width w. At sections containing primary cracks, there is no effective concrete area in tension, i.e. $A_c = 0$, and thus the axial load N is carried by the total area of GFRP bar at crack A_f. Therefore, the GFRP stress at the crack location can be given by:

$$f_{f2} = \frac{N}{A_f} \tag{7.7}$$

Away from the crack, the concrete stress is less than the f_{cr} (Figure 2-4). The A_c in tension is assumed to carry the concrete tensile stress f_{ct}, which develops due to the τ_b that exists between the GFRP and the surrounding concrete. The stress in the GFRP and f_{ct} at location x, where $0 \le x \le S/2$, may be expressed by:

$$f_{ft,x} = \frac{N}{A_f} - \frac{4\tau_b x}{d_b} \tag{7.8}$$

$$f_{ct,x} = \frac{4\tau_b \rho_f x}{d_b} \tag{7.9}$$

The new crack will not form with a distance l_t of the first crack since the stress in the concrete within l_t of a crack has been reduced to below the f_{cr}. However, the new crack can form anywhere else and so, the spacing between cracks cannot be less than l_t. Further successive cracks can form until there remains no part of the member where the stress has not been reduced by cracking. When this occurs, the resulting pattern is the so called the 'stabilized crack pattern'. It should be clear that where the spacing is marginally above $2l_t$, then there will be some length where the stress is still above f_{cr} and a further crack can form. Whereas if a crack is marginally at a distance less than $2l_t$ from another crack, then the stress will be reduced below f_{cr} at all points between the two cracks.

Midway between the cracks at distance $x = S/2$, the stresses are:

$$f_{ft1} = \frac{N}{A_f} - \frac{2\tau_b S}{d_b} \tag{7.10}$$

$$f_{ct1} = \frac{2\tau_b \rho_f S}{d_b} \tag{7.11}$$

The maximum crack spacing $S = S_{rmax}$ will occur when f_{ct} equals the cracking tensile strength f_{cr} and from Eq. (6.2), S_{rmax} is calculated as follows:

$$S_{rmax} = \frac{f_{cr} d_b}{2\tau_b \rho_{eff}} \tag{7.12}$$

Here, the bond stress, τ_b, is the bond stress between the GFRP bar and effective tension zone of concrete around the bar. Thus, the effective reinforcement ratio, ρ_{eff} is defined as:

$$\rho_{eff} = \frac{n_{bars} \cdot A_f}{A_{ceff}} \tag{7.13}$$

where, n_{bars} is the total number of bars in the cross section; A_f is the GFRP reinforcing bar cross section; and A_{ceff} is the effective concrete tensile zone around each reinforcing bar calculated as discussed in Section 7.3.2.

There is no unique solution for τ_b as it may vary according to RC element conditions. It is affected by several parameters such as bar type, bar stress, concrete cover, bar spacing, transverse reinforcement, lateral pressure, degree of compaction, and size of bar deformations (Gilbert 2005).

Marti et al. (1998) assumed for steel-RC, a rigid-plastic bond stress-slip relationship, $\tau_b = 2f_t'$ at all values of slip, where f_t' = direct tensile strength of concrete. This approach simply assumes a direct proportionality relation between the τ_b and tensile strength of concrete f_t'. However, a similar assumption may not be valid for the GFRP bars. A preliminary analysis using this relation resulted in overestimating the measured experimental crack spacing.

A simple yet reasonably accurate and computationally convenient approach is to assume equivalent τ_b distribution for GFRP-RC under direct tension as shown in Figure 7-4. The τ_b is assumed to be a general function of the f_{cr} of the member, thus

$\tau_b = f_n(f_{cr})$. This function depends on the properties and conditions of the GFRP-RC element, and therefore, can be deduced from experimental data.

The following quadratic polynomial equation is found to have the best fit with the experimental results of the GFRP-RC tested panels as shown in Figure 7-5.

$$\tau_b = 0.85 f_{cr}^2 + 0.1 f_{cr} \tag{7.14}$$

where f_{cr} is calculated from Eq. (6.2). Figure 7-5 also shows the Marti et al. (1998) relationship compared to the proposed expression.

7.5 Determination of Average Crack Spacing

The stabilized crack pattern has the characteristic:

$$l_t \le S_{rm} \le 2l_t \tag{7.15}$$

where, S_{rm} is the average crack spacing in a stabilized crack pattern.

In the literature, there are several assumptions for the relation between the minimum and maximum crack spacings. The most common is $S_{rmin} = S_{rmax}/2$. Thus, the average crack spacing S_{rm} may be expressed as:

$$S_{rm} = \lambda . S_{rmax} \tag{7.16}$$

where λ is an arbitrary parameter commonly assumed to be in the range of 0 to1.0 (Marti et al. 1998).

Since λ relates the average and maximum crack spacings, it can be assumed that this parameter depends on the mechanism of transferring the load between the GFRP bar and surrounding concrete, and consequently on the mechanism of developing new cracks until a stabilized crack pattern is reached. Thus, it may be reasonable to assume that λ is a function in the l_t. The parameter of the l_t implicitly reflects the surface characteristics of the reinforcing bar and thus the load transfer within that length, which will be discussed next.

7.5.1 Determination of transfer length l_t

There are a number of ways by which the values of l_t can be determined. The most obvious is from experimental results, where the distribution of strain or stress in the reinforcing bars has been measured. Hence, l_t can be obtained directly from the distribution. However, this requires some care and may really only be possible at early load stages before the cracks are sufficiently closely spaced to interfere with each other. In addition, the measurement of strains requires a relatively large number of strain gauges attached at small increments along the bar, which is practically difficult and could affect the bond between the bar and the concrete.

An empirical relationship (Eq. 7.17) was proposed earlier by Favre et al. (1983) and others for a concrete member containing steel deformed bars or welded wire mesh.

$$l_t = \frac{d_b}{10\rho_s} \tag{7.17}$$

Another approach is to assume that the relationship between the transfer load and l_t is linear. Based on this assumption, Somayaji and Shah (1981) proposed the following linear relationship on the basis of experimental data from pull-out tests:

$$l_t = K_p \frac{F_c}{p_b} \tag{7.18}$$

where F_c is the transfer load; p_b is the circumferential perimeter of the bar; and K_p is a constant to be determined from pullout tests. Somayaji and Shah (1981) observed a K_p value equal to 0.55 mm^2/ N for steel wires. An experimental study by Mirza and Houde (1979) indicates that the value of K_p is in the range of 0.183 - 0.493 mm^2/ N for steel bars.

The K_p value is not yet known for GFRP bars. Thus, there is a need to calibrate the K_p value based on the GFRP type of bars used in the experimental investigation.

7.5.2 Calibration of constant K_p

Published experimental results on similar types of GFRP Aslan bars are used to calibrate the constant K_p. Tastani and Pantazopoulou (2007) conducted an experimental investigation to identify the bond-slip behaviour using direct tension pullout bond tests. The experiments were conducted on 15 specimens reinforced with GFRP Aslan-100 types of bars. The Aslan bars were sand coated and wrapped with helical lengthwise indentations, which means that they are similar to the bar type used in the current research investigation. Three different bar sizes of each bar type were tested with nominal diameters of 12.70, 15.88 and 19.05 mm, with elasticity modulus equal to 40.8 GPa. The pullout specimens, made of concrete, had a uniaxial cylinder compressive strength of 40 MPa at the time of testing. The embedment length of the GFRP bar was ~5 d_b. Moreover, the researchers investigated another type of sand coated bars known as fibre-glass CPP bars.

Using the researchers' data, the observed peak pullout load divided by the circumference of bars is plotted against the embedment length as shown in Figure 7-6. The inverse slope of the line gives the value of the constant K_p. The K_p value obtained is (1/7.74 = 0.129 mm^2/N), which is exclusive to the GFRP Aslan bar type used.

Similarly, the above calibration process is applied to more test results found in the literature in order to compare the K_p values for other different types of bars. Table 7-1 shows that the calibrated value of K_p for the GFRP Aslan bar is reasonably comparable to other GFRP bar types with different surface treatments. It can also be noted that the K_p values range from 0.129 ~ 0.158 mm^2/N for different GFRP bar types. This range is relatively less compared to the K_p values calculated for deformed steel bars (K_p = 0.2 mm^2/N) or steel wires (K_p = 0.55 mm^2/N) as reported by Somayaji and Shah (1981).

7.5.3 Transfer length l_t and parameter λ relationship

Using Eq. (7.18) and the estimated value of K_p parameter, the l_t for the tested GFRP-RC panels can be determined. Table 7-2 shows the calculated values of the l_t in comparison with the prediction of expression (Eq. 7.17) of Favre et al. (1983). The shown calculated values are based on the initial cracking load recorded for the tested panels.

In addition, Table 7-2 shows the ratio between the experimental mean and maximum crack spacings, which is $\lambda_{exp} = S_{rm} / S_{rmax}$ and the ratio between l_t and λ_{exp}. Since l_t is a factor of the specimen length L_{sp}, the following relationship between l_t and λ_{exp} is proposed in terms of L_{sp}:

$$\lambda = \frac{\psi l_t}{L_{sp}} \tag{7.19}$$

where ψ is a dimensionless factor between 2 and 4, which depends on the boundary conditions of the RC under tension. A value of 3.5 is found to be in good agreement with the experimental results.

Using the above proposed expression, the λ values are predicted in Table 7-2. It can be seen that the mean values of the predicted λ (i.e. λ_{pred}) are in good agreement with the experimental λ_{exp}. The following observations can be deduced from the analysis of Table 7-2:

- The Favre et al. (1983) expression (Eq. 7.17) may overestimate the l_t for GFRP-RC by nearly 70% on average if it is used in its present form.

- Equation (7.17) determines l_t as a constant value for some panels having the same d_b and reinforcement ratio regardless of their different final stabilized crack patterns. Since the stabilized crack patterns of the tested GFRP-RC are different, it is expected that the values of l_t should be different. Hence, the proposed expression succeeds in estimating the different values of l_t, which is more realistic and reflects the different variation in the crack patterns.

- While Eq. (7.17) determines the l_t based on only the d_b and reinforcement ratio, the proposed expression (Eq. 7.18) explicitly accounts for the bar type used and its bond behaviour expressed in the constant K_p.

- As observed in the experiments, the specimens with c_c / d_b ratio equal to 1.5; namely, P1-GNU-16-1.0-1.5 and P8-GHU-13-0.7-1.5, had fewer cracks (2 cracks) compared to other panels with a c_c / d_b = 2.5. Both specimens have a larger l_t that is required over all other specimens. This confirms the interpretation shown in the discussion of the effect of the c_c / d_b ratio on the number of cracks developed within the L_{sp}. A larger l_t means that fewer cracks will develop within the same panel length.

- For the purpose of comparison, the last two rows of Table 7-2 show the l_t values calculated for the two tested steel-RC panels within Series V. The l_t values are calculated based on a value of K_p = 0.2 mm^2/N for steel bars (Table 7-1). The steel-RC panel P11-SNU-16-1.0-2.5 experienced a single major crack. This panel has a calculated l_t that is equal to 210 mm. This value is much higher than any other GFRP-RC tested panels. Once this single crack developed, the panel would require almost double the predicted l_t value (i.e. 210 mm on each side of the crack) to develop another crack beyond this range. This is difficult to occur within the 600 mm L_{sp}. In addition to that, the yielding limit is reached at the vicinity of the major crack before developing any other crack. Therefore, the use of the l_t concept confirms the interpretation of the experimental behaviour.

7.6 Predictions of Proposed Crack Spacing Model

Figure 7-7 shows a schematic flow chart of the main sequence that is used for calculating the cracking characteristics of GFRP-RC panels under direct tension. Table 7-3 shows a comparison between the prediction of the proposed model and experimental results. In general,

the proposed approach shows a reasonable prediction of the maximum and average crack spacings.

7.7 Analytical Comparison of the Proposed Model to Other Models

As mentioned in the literature review, most of the existing crack spacing models are exclusively developed for steel-RC based on various experimental and analytical approaches. The proposed crack spacing model is verified by comparing the predicted values with the test results of the GFRP-RC panels presented in the current investigation. The recorded crack spacings for the panels are also compared to some cracking models that are available in the literature. The objective of this comparison is to evaluate the proposed model with respect to other existing models and to verify the accuracy of these models in predicting the crack spacing of GFRP-RC under direct tension.

For the purpose of this comparison, five cracking models are selected: (1) Rizkalla et al. (1983) (Eq. 2.16); (2) Haqqi (1983) (Eq. 2.18); (3) NBR (1992) (Eq. 2.19); (4) EC2 (2004) (Eq. 2.20); and (5) Desayi and Kulkarni (1976) (Eq. 2.8).

The predictions of the proposed model are compared with the predictions of other models as shown in Table 7-4. It can be noted that the proposed crack spacing model gives reasonable predictions. Both the Rizkalla et al. (1983) and Haqqi (1983) models are able to reasonably predict the mean crack spacing. The Desayi and Kulkarni (1976) model overestimates the predicted values. However, the results of this model could be improved if the incorporated bond parameters (k_t and k_b) are calibrated for the GFRP bar type. The calculations show that the term B: ($d_{b2} f_{bb}/b_{s2}$) in the Desayi and Kulkarni (1976) model, which accounts for the

bearing stress exerted by transverse bars, does not exceed 5% of the total value of the sum of terms A and B (Eq. 2.8).

The EC2 (2004) and NBR (1992) models can significantly overestimate the mean crack spacing of GFRP-RC by almost three to five times if they are used in their present format. The NBR (1992) model can give better predictions if ρ_{eff} is based on 7 d_b for GFRP bars instead of the 15 d_b that is currently used for steel. Using such a modification, this NBR-modified model provides a prediction of the mean crack spacing values that are almost 1.5 times higher, on average, than the observed test values.

Therefore, it can be concluded that the proposed model is able to give reasonable predictions of the experimental results compared to other existing models found in the literature.

7.8 Numerical Validation of the Proposed Crack Spacing Model

To validate the proposed crack spacing model, it is applied to the experimental work carried out by Bischoff and Piaxio (2004) and Mahmood (2002) on GFRP-RC members subjected to uniaxial tension. Unfortunately, there is no other related published research on members subjected to biaxial tension that could be used for validation.

Bischoff and Piaxio (2004) reported the test results of three uniaxial members reinforced with a single GFRP-bar (C-bar type). The member dimensions were 1100 mm in length with a typical cross-section of 100 × 100 mm. The effective length used for taking the measurements was 900 mm. Three bar diameters were tested; namely, 12.7, 15.9, and 19.0 mm. The reported

experimental mean crack spacings are presented in Table 7-5. The K_p value used in the proposed model calculations for the C-bar type is based on the calibration carried out in Section 7.6.2 as shown in Table 7-1. The average f_{cr} is taken as 2.6 MPa as reported by the researchers, since the values were not reported for each specimen. As shown in Table 7-5, the proposed model gives reasonable predictions of the S_{rm} in comparison with other models. The models of Rizkalla et al. (1983) and Desayi and Kulkarni (1976) are also found to give reasonable predictions for average crack spacings. The Haqqi (1983) model underestimates the mean crack spacing while the EC2 (2004) and NBR (1992) models significantly overestimate the crack spacings in comparison with recorded values.

Mahmood (2002) tested six concrete specimens reinforced with GFRP-bars (C-bar type) as shown in Figure 2-10. The material properties and recorded f_{cr} values for the tested specimens are taken as reported by the researcher.

The reported experimental mean crack spacings are shown in Table 7-6. Similarly, the K_p value used in the proposed model calculations for the C-bar type is as shown in Table 7-1. As shown in Table 7-6, the proposed model gives reasonable predictions of the S_{rm} in comparison with other models. The models of Rizkalla et al. (1983), Haqqi (1983), and Desayi and Kulkarni (1976) are found to give reasonable predictions for S_{rm} as well. The other models overestimate the crack spacing.

Therefore, it can be concluded that the proposed crack spacing model is able to give reasonable predictions with other experimental results found in the literature; and compared to other existing models found in the literature. Hence, the proposed model is suitable for GFRP-

RC under direct tension, providing that enough material properties are available and accurate calibration of the bar bond characteristics is conducted.

7.9 Prediction of Mean Crack Width

The mean crack width can be predicted from Eq. (7.20) using the crack spacing values predicted from the above shown model and taking into account, the defined tension-stiffening response in terms of the average tensile strain ε_m. Reiterating the crack spacing values predicted are based on the stabilized cracking stage, where:

$$w_m = \varepsilon_m S_{rm} \tag{7.20}$$

Table 7-7 compares the calculated mean crack width to the experimental results. In general, the predicted mean crack widths are in reasonable agreement with the recorded experimental results, which demonstrate that the proposed cracking model performs satisfactorily.

7.10 Summary and Conclusions

A constitutive model is proposed to predict the crack spacing of GFRP-RC panels under direct tensile stresses. The mathematical formulation of the proposed cracking model is presented in this chapter. The proposed model is based on the stress transfer approach, adopting the laws of force equilibrium and implicitly accounts for the bond-slip relationship. From the presented analytical investigation, the following main conclusions can be summarized:

1. A quadratic polynomial expression is proposed to describe the relation between the τ_b and f_{cr} of concrete. It is also proposed to calculate the effective reinforcement ratio for GFRP-RC based on an effective tension zone size of 7 d_b around reinforcing bar. Both assumptions are found to be in good agreement with the experimental evidence.

2. The proposed crack spacing model (Eq. 7.16) explicitly accounts for the bond and surface characteristics of the reinforcing bar. This is included through the calibration of the factor K_p deduced from pullout tests and the proposed expression (Eq. 7.18). Hence, establishing a relation (Eq. 7.19) between l_t and L_{sp} from which the average stabilized crack spacing is determined. For different GFRP bar types, the recommended values for K_p vary from 0.129 to 0.158 mm^2/N.

3. The Favre et al. (1983) expression (Eq. 7.17) may overestimate the l_t for GFRP-RC by nearly 70% on average if it is used in its present form. The proposed expression (Eq. 7.18) to estimate different values of l_t according to specimen configuration is more realistic and reflects the different variation in the crack patterns.

4. The proposed crack spacing model is compared to five crack spacing models from the literature. The comparison shows that the proposed model is as good as other models developed by Rizkalla et al. (1983), Haqqi (1983), and Desayi and Kulkarni (1976). In general, the EC2 (2004), and NBR (1992) models are found to overestimate the crack spacing for GFRP-RC.

5. Furthermore, the proposed crack spacing model is validated using limited experimental data found in the literature. The proposed model is applied on experimental data reported by Bischoff and Paixao (2004) and Mahmood (2002). The calculations show that the proposed model gives reasonable predictions compared to the experimental crack spacings recorded by other researchers.

Table 7-1: Results of calibration of bond factor K_p

Pullout Test Reference	Bar Type (Product name)	Bar Surface Treatment	Bar diameters tested (mm)	K_p (mm^2/N)
Tastani and Pantazopoulou (2007)	GFRP (Aslan 100)	Wrapped and sand coated	12.7; 15.9; 19.05	0.129
	GFRP (Fibreglass CPP)	Sand coated		0.133
Cosenza et al. (1999)	GFRP (C-Bar)	Deformed	12.7	0.144
Tighiourut et al. (1998)	GFRP Type A- (ISOROD)	Smooth surface with helical winding	12.7; 15.9; 19.1; 25.4	0.158
	Steel	Deformed bars		0.20
Somayaji and Shah (1981)	Steel	Plain wires	0.794; 1.19; 1.588	0.55

Table 7-2: Prediction of transfer length l_t and parameter λ

Series	Specimen	Proposed l_t (mm) Eq. (7.18)	Favre et al. (1983) l_t (mm) Eq. (7.17)	λ_{exp}	l_t / λ_{exp}	$\lambda_{pred.}$ Eq. (7.19)	$\lambda_{exp} / \lambda_{pred.}$
I	P1-GNU-16-1.0-1.5	93	151	0.69	136	0.54	1.28
	P2-GNU-16-1.0-2.5	70	151	0.68	103	0.40	1.69
	P3-GNB-16-1.0-2.5	55	151	0.53	103	0.31	1.69
II	P5-GNU-16-0.7-2.5	117	227	0.58	203	0.67	0.86
	P7-GNU-13-0.7-2.5	127	189	0.68	186	0.73	0.94
	P10-GNB-16-0.7-2.5	81	227	0.42	191	0.46	0.91
III	P4-GHU-16-1.0-2.5	129	151	0.90	143	0.74	1.22
	P6-GHB-16-1.0-2.5	101	151	0.37	269	0.58	0.65
IV	P8-GHU-13-0.7-1.5	135	189	0.84	161	0.78	1.08
	P9-GHB-13-0.7-2.5	121	189	0.50	242	0.69	0.72
V	P11-SNU-16-1.0-2.5	210	150	0.94	223	—	—
	P12-SNB-16-1.0-2.5	149	150	0.55	270	—	—
						Mean	**1.10**
						St. deviation	**0.37**
						C.O.V. %	**33.2**

Table 7-3: Proposed model predictions of crack spacings

Series	Specimen No.	Experimental		Proposed Model Prediction						
		$S_{rm,\,exp}$ (mm)	$S_{rmax,\,exp}$ (mm)	f_{cr} (predicted), (MPa) Eq. (6.2)	$\lambda_{predicted.}$ Eq. (7.19)	τ_b (N/mm^2) Eq. (7.14)	$S_{rmax,\,pred.}$ (mm) Eq. (7.12)	$\frac{S_{rmax,exp}}{S_{rmax,pred.}}$	$S_{rm,\,pred.}$ (mm) Eq. 7.16	$\frac{S_{rm,exp}}{S_{rm,pred.}}$
I	P1-GNU-16-1.0-1.5	200	290	1.66	0.54	2.52	258	0.89	140	0.70
	P2-GNU-16-1.0-2.5	150	220	1.65	0.41	2.47	308	1.40	126	0.84
	P3-GNB-16-1.0-2.5	161	304	1.06	0.32	1.07	459	1.51	146	0.91
II	P5-GNU-16-0.7-2.5	184	319	1.61	0.68	2.36	314	0.98	214	1.17
	P7-GNU-13-0.7-2.5	149	218	1.52	0.74	2.11	265	1.22	197	1.32
	P10-GNB-16-0.7-2.5	168	396	1.21	0.47	1.36	409	1.03	193	1.15
III	P4-GHU-16-1.0-2.5	151	167	2.11	0.75	3.98	244	1.46	184	1.22
	P6-GHB-16-1.0-2.5	169	451	1.56	0.59	2.22	324	0.72	190	1.12
IV	P8-GHU-13-0.7-1.5	199	236	2.11	0.79	4.01	164	0.69	130	0.65
	P9-GHB-13-0.7-2.5	160	320	1.61	0.70	2.35	252	0.79	177	1.11
	Mean	**168.9**	**292.1**	**1.6**	**0.6**	**2.4**	**299.6**	**1.07**	**169.8**	**1.02**
	St. deviation	**19.08**	**86.40**	**0.33**	**0.16**	**0.95**	**84.95**	**0.31**	**31.42**	**0.23**
	C.O.V. %	**11.3**	**29.6**	**20.4**	**26.8**	**38.7**	**28.4**	**28.9**	**18.5**	**22.4**

Table 7-4: Comparison between the predictions of the proposed model and experimental data

Series	Specimen No.	Experimental	Proposed Model	Prediction of other cracking models				
		$S_{rm,\ exp}$ (mm)	$S_{rm,\ pred.}$	Rizkalla et al. (1983)	Haqqi (1983)	NBR (1992)	EC2 – (2004)	Desayi & Kulkarni (1976)
			Eq. (7.16)	Eq. (2.16)	Eq. (2.18)	Eq. (2.19)	Eq. (2.20)	Eq. (2.8)
I	P1-GNU-16-1.0-1.5	200	140	155	166	655	560	222
	P2-GNU-16-1.0-2.5	150	126	176	166	748	848	214
	P3-GNB-16-1.0-2.5	161	146	176	166	748	848	127
II	P5-GNU-16-0.7-2.5	184	214	233	250	778	1233	189
	P7-GNU-13-0.7-2.5	149	197	192	208	604	833	247
	P10-GNB-16-0.7-2.5	168	193	233	250	778	1233	137
III	P4-GHU-16-1.0-2.5	151	184	176	166	748	848	294
	P6-GHB-16-1.0-2.5	169	190	176	166	748	848	271
IV	P8-GHU-13-0.7-1.5	199	130	175	208	528	546	246
	P9-GHB-13-0.7-2.5	160	177	192	208	604	833	296

Note: Crack spacings are in mm.

Table 7-5: Comparison between predicted crack spacing and experimental test results by Bischoff and Paixao (2004)

Reference	Specimen No.	Bar type	Experimental	Proposed Model	Prediction of other crack models				
			$S_{rm,\ exp}$ (mm)	$S_{rm,pred.}$	Rizkalla et al. (1983)	Haqqi (1983)	NBR (1992)	EC2 – (2004)	Desayi & Kulkarni (1976)
				Eq. (7.16)	Eq. (2.16)	Eq. (2.18)	Eq. (2.19)	Eq. (2.20)	Eq. (2.8)
Bischoff and Paixao (2004)	S1	GFRP ribbed (C-bar)	133	175	143	110	642	1089	151
	S2		140	119	127	87	730	885	120
	S3		144	76	117	71	819	747	99

Note: Crack spacings are in mm.

Table 7-6: Comparison between predicted crack spacing and experimental test results by Mahmood (2002)

Reference	Specimen No.	Bar type	Experimental	Proposed Model	Prediction of other crack models				
			$S_{rm,\ exp}$ (mm)	$S_{rm,pred.}$	Rizkalla et al. (1983)	Haqqi (1983)	NBR (1992)	EC2 – (2004)	Desayi & Kulkarni (1976)
				Eq. (7.16)	Eq. (2.16)	Eq. (2.18)	Eq. (2.19)	Eq. (2.20)	Eq. (2.8)
Mahmood (2002)	A3-4	GFRP ribbed (C-bar)	144	362	209	248	452	794	281
	A3-6		156	160	149	165	440	543	204
	A3-8		130	89	119	124	432	417	127
	A5-4		128	127	142	147	646	544	148
	A5-6		134	57	106	97	634	376	103
	A5-8		127	32	88	73	626	292	72

Note: Crack spacings are in mm.

Table 7-7: Comparison of predicted mean crack widths to experimental results

Series	Specimen	w_m (mm) Experimental	w_m (mm) Predicted	$\frac{w_{m,exp}}{w_{m,pred}}$
I	P1-GNU-16-1.0-1.5	0.40	0.41	0.98
	P2-GNU-16-1.0-2.5	1.20	0.80	1.50
	P3-GNB-16-1.0-2.5	0.93	0.77	1.20
II	P5-GNU-16-0.7-2.5	1.20	1.15	1.04
	P7-GNU-13-0.7-2.5	0.66	0.87	0.76
	P10-GNB-16-0.7-2.5	1.06	1.07	0.99
III	P4-GHU-16-1.0-2.5	0.94	1.11	0.84
	P6-GHB-16-1.0-2.5	0.58	0.58	1.00
IV	P8-GHU-13-0.7-1.5	1.09	1.10	0.99
	P9-GHB-13-0.7-2.5	1.11	1.11	1.00
			Mean	**1.03**
			St. Deviation	**0.20**
			C.O.V.%	**19.8**

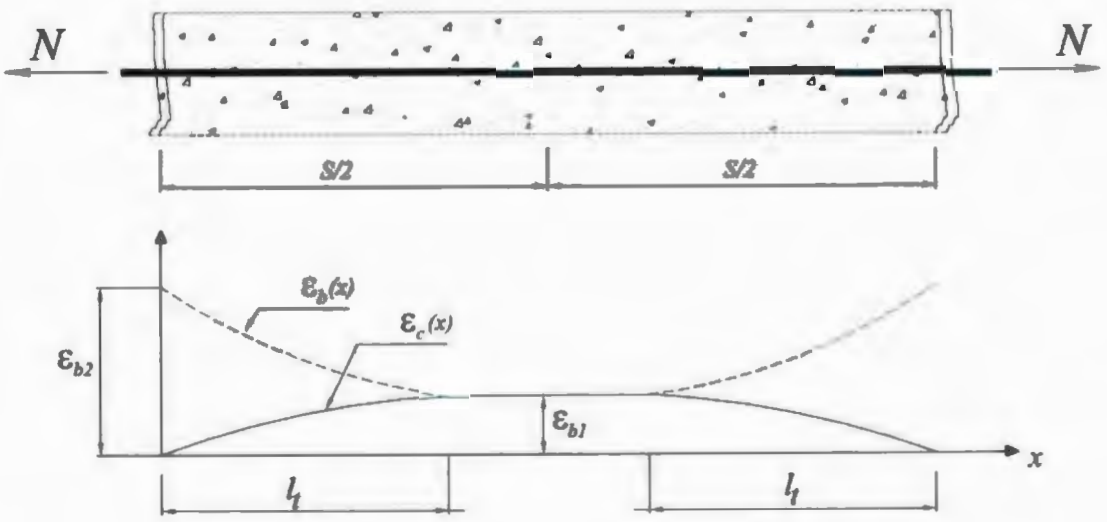

Figure 7-1: Behaviour under direct tension

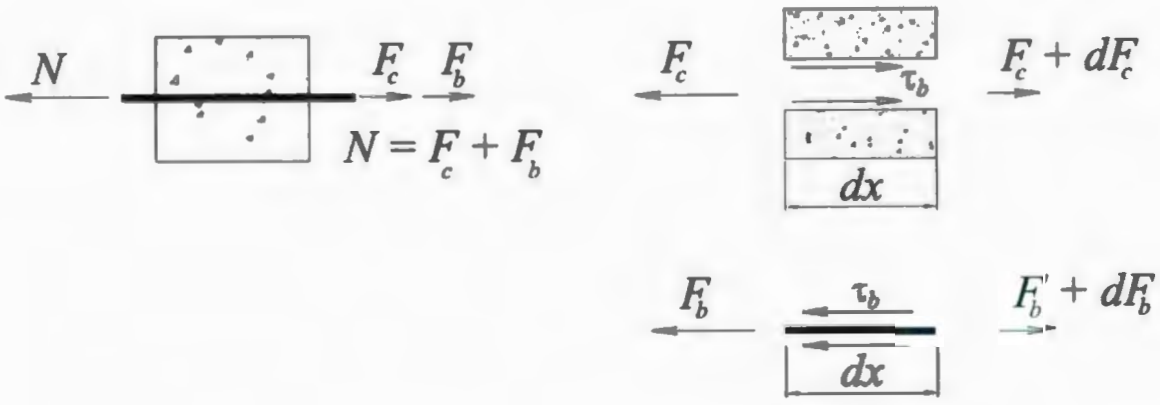

Figure 7-2: Free body diagram for a RC member

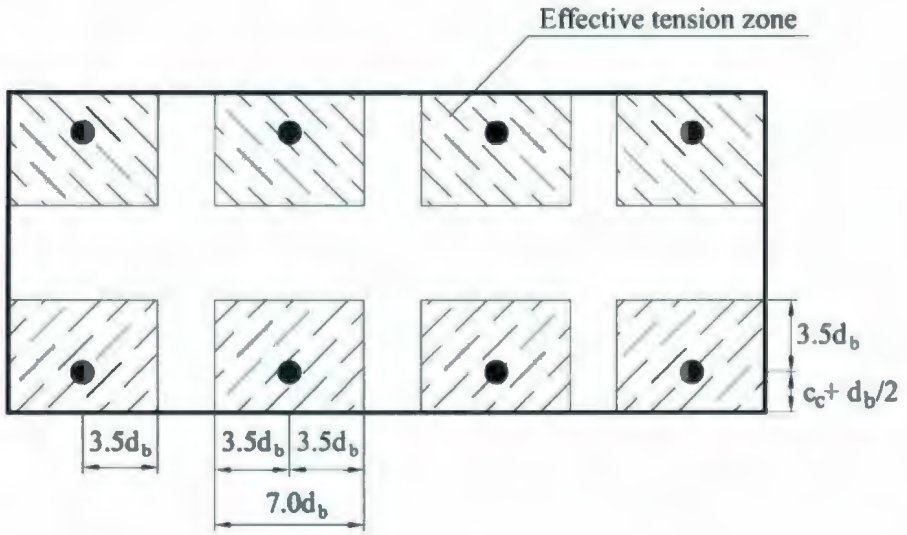

Figure 7-3: Proposed effective tension zone for GFRP-RC tension member

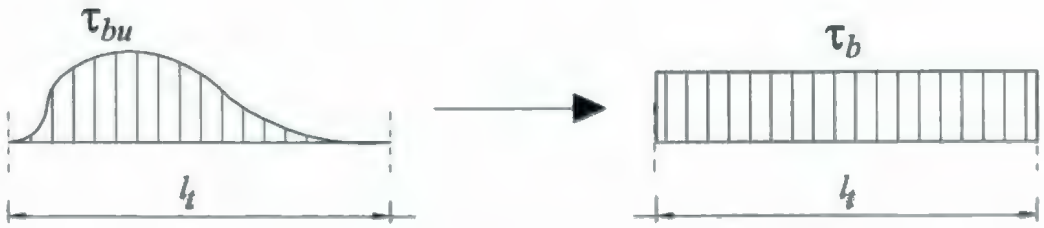

Figure 7-4: Equivalent bond stress distribution

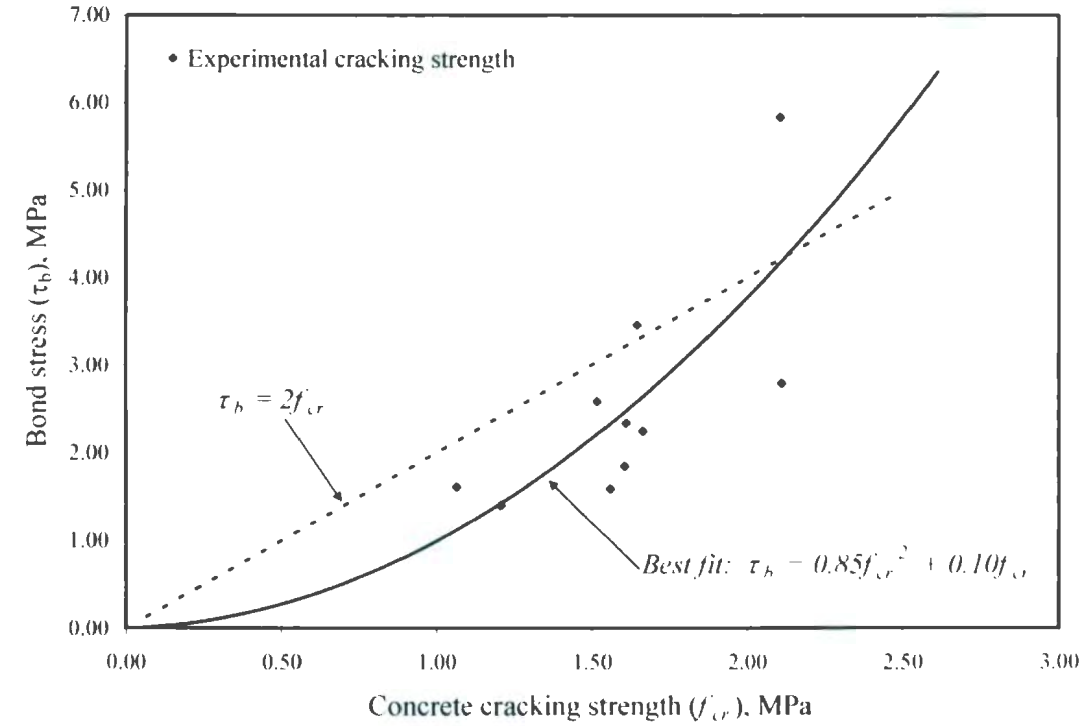

Figure 7-5: Relationship between bond stress and experimental cracking strength

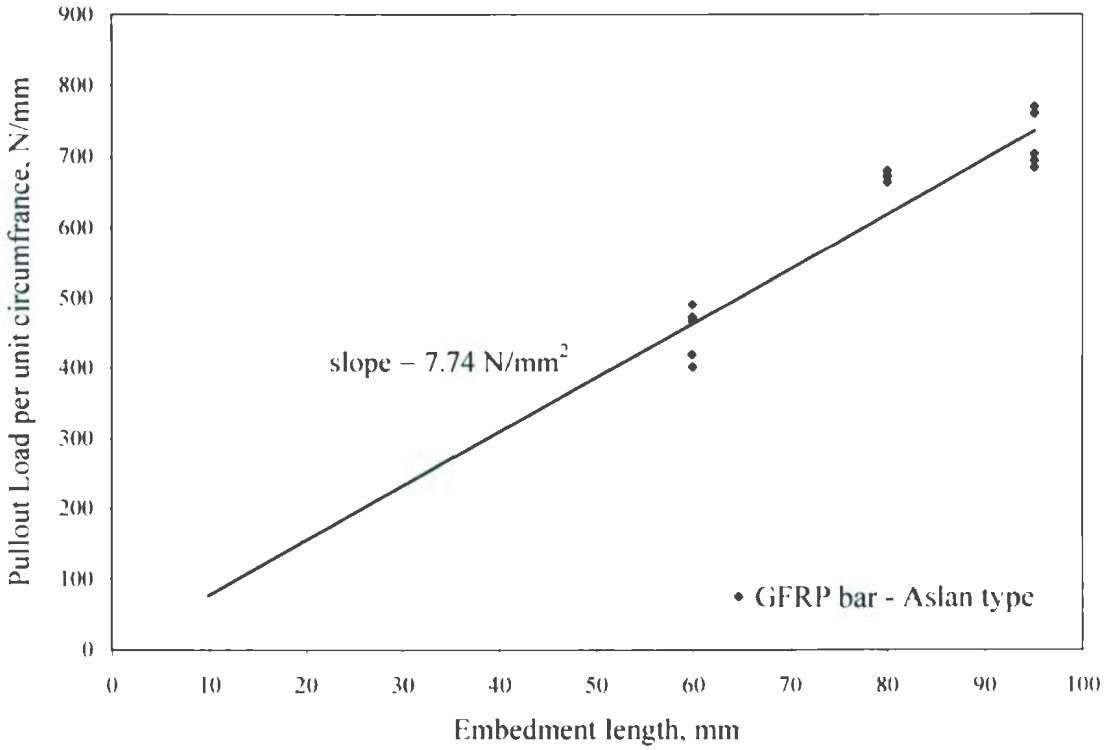

Figure 7-6: Determination of K_p for Aslan bar type

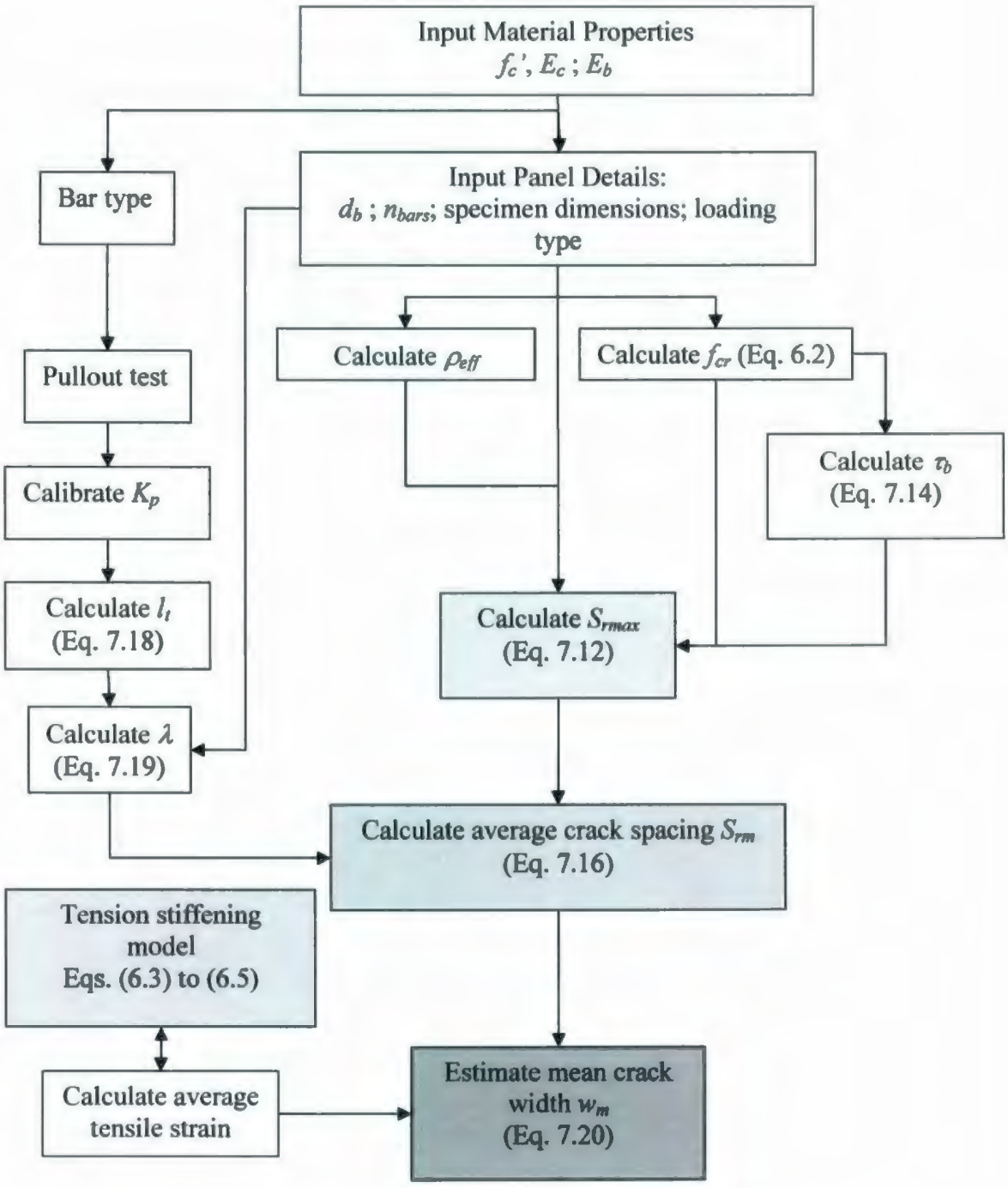

Figure 7-7: Outline of proposed cracking model main calculation steps

Chapter 8

FINITE ELEMENT ANALYSIS OF GFRP-RC PANELS

8.1 Introduction

The growing interest in GFRP-RC for different structural applications requires the identification of the key issues for successful numerical material modelling. In order to achieve reasonable predictions of the structural response, a material model that can adequately reflect the behaviour of the concrete response should be adopted.

In this chapter, the calibration of a finite element model for GFRP-RC is presented. A plasticity-based concrete model is used. The local energy release and interface between the reinforcing GFRP and concrete cracking is modelled by introducing a suitable tension stiffening to simulate the load transfer across cracks. A tension-stiffening idealization is proposed and calibrated for the finite element modelling.

The model is implemented in a finite element analysis (FEA) code that could be used to carry out a numerical analysis. The finite element model is developed based on the smeared cracking approach. The validity of the proposed model is established through comparison with the test results of GFRP-RC panels. The recommended numerical model can be used to predict the behaviour of GFRP-RC with reasonable accuracy.

8.2 Inelastic Concrete Constitutive Model

The incremental elastic-plastic concrete model used in this analysis is based on the classical concepts of the theory of plasticity (ABAQUS 2006). The model is defined by considering the following concepts: strain rate decomposition in elastic and inelastic rates, elasticity, yield, flow, and hardening, which allow for strain softening after both cracking and crushing.

8.2.1 Concrete in compression

When concrete is loaded in compression, it initially exhibits an elastic response. As the stress is increased, some non-recoverable (inelastic) straining occurs, and the response of the material softens. An ultimate stress is reached, after which the material softens until it can no longer carry any stress.

The concrete model under compression is elastic until the initial yield surface limit is reached as shown in Figure 8-1, which shows the compression surface in the p - q plane, where p and q are the effective pressure stress and the Mises equivalent deviatoric stress, respectively. The initial yield surface defines the elastic limit at which the linear-elastic constitutive relationships are valid. Further stressing of the concrete cause an expansion of the initial yield surface so that new yield surfaces develop. Moreover, stresses beyond the initial yield surface formation cause further 'irrecoverable' strain. The strain rate is then composed into elastic and plastic strain rates. The strain rate decomposition is:

$$d\varepsilon_c = d\varepsilon_c^{el} + d\varepsilon_c^{pl} \tag{8.1}$$

where $d\varepsilon_c$ is the total compressive strain rate; $d\varepsilon_c^{el}$ is the compressive elastic strain rate; and $d\varepsilon_c^{pl}$ is the compressive plastic strain rate.

The yield stage is followed by flowing of the material, then hardening. The equation of the compression surface is defined using the following relationship:

$$f_c = q - 3\left(\frac{1-\overline{f}_{bc}}{1-2\overline{f}_{bc}}\right)p - \sqrt{3}\tau_c = 0 \tag{8.2}$$

The compression stress in concrete is expressed in terms of the effective pressure stress p, the Mises equivalent deviatoric stress q, and a hardening parameter τ_c. The p is expressed as:

$$p = -\frac{1}{3}(f_1 + f_2 + f_3) \tag{8.3}$$

where f_1, f_2, and f_3 are the principal normal stresses.

The q is expressed as:

$$q = \sqrt{\frac{2}{3}\left(\frac{1}{3}\right)\left(S_1^2 + S_2^2 + S_3^2\right)} \tag{8.4}$$

where S_1, S_2, and S_3 are the principal stress deviators. Hence the amount q^2 is equivalent to 3/2 times the mean of the square of principal-stress deviations. The deviatoric stress components S_{ij} are correlated to the normal stresses components f_{ij}, using the following formula:

$$S_{ij} = f_{ij} + p\delta_{ij} \tag{8.5}$$

where δ_{ij} is equal to:

$$\delta_{ij} = \begin{pmatrix} 1 & 0 & 0 \\ 0 & 1 & 0 \\ 0 & 0 & 1 \end{pmatrix} \tag{8.6}$$

The factor $\overline{f}_{bc}^{'}$ in Eq. (8.2) defines the ratio between the equal biaxial compressive strength $f_{bc}^{'}$ and the uniaxial cylinder strength $f_c^{'}$ through the equation:

$$\overline{f}_{bc}^{'} = \frac{f_{bc}^{'}}{f_c^{'}}, \quad \left(f_c^{'} > 0\right) \tag{8.7}$$

In addition, the model accounts for associated flow and isotropic hardening response as illustrated in Figures 8-1 and 8-2.

8.2.2 Concrete in tension

Cracking is considered the most significant factor of the material behaviour in tension. In general, cracks in the finite element simulation may be defined as smeared, discrete, or fracture. Cracking is assumed to occur when the stresses reach the crack detection surface that is defined by the Coulomb line written in the first two stress invariants p and q. Crack occurrence is determined using the crack detection plasticity surface in stress space. In the crack detection model, the strain rate decomposition in tension is governed by the following equation:

$$d\varepsilon_t = d\varepsilon_t^{el} + d\varepsilon_t^{pl} \tag{8.8}$$

where $d\varepsilon_t$ is the total tensile strain rate, $d\varepsilon_t^{el}$ is the tensile elastic strain rate, and $d\varepsilon_t^{pl}$ is the tensile plastic strain rate associated with the crack detection surface. The equation of the crack detection surface is the Coulomb line as follows:

$$f_t = q - \left(3 - b_0 \frac{f_t}{f_t^u}\right)\hat{p} - \left(2 - \frac{b_0}{3}\frac{f_t}{f_t^u}\right)\sigma_t = 0 \tag{8.9}$$

where f_t^u is the uniaxial tensile strength of concrete (= f_t'). The factor b_0 is used to define the ratio between the biaxial and uniaxial tensile strengths. In Eq. (8.9), f_t is the equivalent uniaxial tensile stress. The crack detection model uses the associated flow rule assumption that states:

$$d\varepsilon_t^{pl} = \begin{cases} d\lambda_t \dfrac{\partial f_t}{\partial f} & \sigma_t = 0 \text{ and } d\lambda_t > 0 \\ 0 & \text{otherwise} \end{cases} \tag{8.10}$$

where λ_t is a factor to measure the hardening.

8.3 Finite Element Analysis of GFRP-RC Panels

The material model described earlier is implemented in the general-purpose finite element program ABAQUS (2006). The program has several well described material models, and a general interface for user specification of material behaviour. The program also has a graphical user interface (GUI) with different sub-routine modules to develop the finite element model, apply loads, and post-processing. These features make the program attractive in the development of user defined material behaviour.

8.3.1 Smeared cracking approach

A smeared crack concrete modelling approach is adopted for the FEA. The smeared crack model uses the concept of oriented damaged elasticity (smeared cracking) and isotropic compressive plasticity to represent the inelastic behaviour of concrete. The smeared crack

modelling approach does not track individual "macro" cracks. Constitutive calculations are performed independently at each integration point of the finite element model. The presence of cracks enters into these calculations by the way in which the cracks affect the stress and material stiffness associated with the integration point.

The behaviour of direct straining across cracks is modelled with tension stiffening, which allows a definition of the strain-softening behaviour for cracked concrete. This behaviour also allows for the effects of the reinforcement interaction with concrete to be simulated in a simple manner. Tension stiffening is required in the concrete smeared cracking model. Specification of strain softening behaviour in RC generally means specifying the post-peak stress as a function of strain across the crack. In cases where there is little or no reinforcement, this specification often introduces mesh sensitivity in the analysis results and that the finite element predictions do not converge to a unique solution as the mesh is refined because mesh refinement leads to narrower crack bands. This problem typically occurs if only a few discrete cracks form in the structure, and mesh refinement does not result in the formation of additional cracks. If cracks are evenly distributed (either due to the effect of rebar or the presence of stabilizing elastic material, as in the case of plate bending), mesh sensitivity is less of a concern.

In practical calculations for RC, the mesh is usually such that each element contains reinforcing bars. The interaction between the reinforcing bars and concrete tends to reduce the mesh sensitivity, provided that a reasonable amount of tension stiffening is introduced in the concrete model to simulate this interaction.

8.3.2 Geometric modelling

The RC panel is modelled using its full dimensions (600 × 600 × 190 mm). A four-node quadrilateral doubly curved shell element is used in the analysis. Five Simpson-type integration points are used along the thickness of each shell element. In addition, a reduced integration rule is used over the X-Y plane of the elements.

In order to evaluate the finite element model sensitivity to mesh size, an investigation is carried out using different meshes. The mesh sizes are 150, 75, and 37.5 mm for 4 × 4, 8 × 8, and 16 × 16 mesh elements, respectively. A minor difference is observed in the tensile-strain relation as shown in Figure 8-4. Based on this investigation, it is found that mesh size has a minor effect on the FEA results for the present case. To acquire better stress distribution contours across the elements, mesh size 37.5 mm (16 × 16 mesh elements) is used in the present investigation.

Reinforcement in concrete structures is typically provided by means of reinforcing bars, which are one-dimensional strain theory elements (rods) that can be defined singly or embedded in oriented surfaces. Reinforcing bars are typically used with metal plasticity models and superposed on a mesh of standard element types used to model the concrete.

With this modelling approach, the concrete behaviour is considered independently of the reinforcing bar. Effects associated with the reinforcing bar/concrete interface, such as bond slip and dowel action, are modelled approximately by introducing "tension stiffening" into the concrete modelling to simulate load transfer across cracks through the reinforcing bar. The

tension stiffening effect must be estimated. The finite element code allows the tension stiffening parameter to be calibrated for a particular case.

The definition of reinforcing bars in shell elements is based on three geometric properties: the cross-sectional area of each individual reinforcing bar, spacing between the bars, and orientation of the reinforcing bar with respect to the local coordinate system of the element. For shell elements, the rebar definition also requires the distance from the mid-surface to the rebar. Therefore, the reinforcement of the panel in each direction is treated as smeared unidirectional layers. These layers are embedded in concrete and located at the center line of the actual reinforcing bars in the panels. The layers are smeared with a constant thickness that is equal to the area of each reinforcing bar divided by the reinforcing bar spacings.

8.3.3 Implementation of proposed tension stiffening model

The choice of tension stiffening parameters is important since generally, more tension stiffening makes it easier to obtain numerical solutions. Too little tension stiffening will cause the local cracking failure in the concrete to introduce temporarily unstable behaviour in the overall response of the model. Few practical designs exhibit such behaviour, so that the presence of this type of response in the analysis model usually indicates that the tension stiffening is unreasonably low. Therefore, the effects associated with the reinforcing bar/concrete interface are modelled through the proposed tension stiffening idealization for the GFRP-RC as described in Chapter 6. The proposed tension-stiffening idealization includes the post-cracking failure behaviour assuming a bi-linear relation (Eqs. 6.4 and 6.5) as shown in Figure 8-3.

For steel-RC, ABAQUS (2006) assumes that after failure (cracking) the stress linearly reduces to zero at a total strain about ten times the strain at failure. However, this parameter should be calibrated to each particular case. The experimental investigation shows that, in general, GFRP-RC has a greater tension stiffening contribution compared to steel-RC. Therefore, a relatively high value of ultimate tensile strain value (50 ~ 100 times the cracking strain) is incorporated in the tension stiffening curve for GFRP-RC. This range is relatively higher than the recommended values for steel-RC in ABAQUS (2006). However, it is important to note that realistic results can not be achieved without the proper idealization of: (1) tensile (cracking) strength; (2) ultimate tensile strain; and (3) descending degradation curve of the concrete stress. These parameters would inherently result in a proper model for the bond-slip interaction of the GFRP-RC.

8.3.4 Material properties

The properties of the materials are either known from the experimental results or given by the manufacturer's specification. Poisson's ratio is assumed as 0.15 for NSC and 0.24 for HSC as reported by Chen (1982). The complete uniaxial compressive stress-strain relation with the secant modulus of elasticity at $0.4 f_c^{'}$ is used. The concrete stress-strain relationship (Eq. 8.11) is implemented in the model as proposed by Thorenfeldt et al. (1987) and adopted by ISIS (2001).

$$\frac{f_c}{f_c^{'}} = \frac{n\left(\frac{\varepsilon_c}{\varepsilon_o}\right)}{n-1+\left(\frac{\varepsilon_c}{\varepsilon_o}\right)^{nk}} \qquad (8.11)$$

where ε_o = concrete strain at f_c'; n = curve fitting factor; $E_c = f_c'/\varepsilon_o$; E_c = tangent stiffness at zero strain; and k is the stress decay factor, taken as 1.0 for ($\varepsilon_c / \varepsilon_o < 1.0$) and as a number greater than 1.0 for ($\varepsilon_c / \varepsilon_o > 1.0$).

The cracking strength of concrete is evaluated based on Eq. (6.2). In general, for the range of concrete compressive strengths in the current experimental results, the cracking strength varies from 2.5% to 3.5% of the standard cylinder compressive strength.

8.3.5 Solution strategy

A general static solution algorithm is used to effectively obtain the static equilibrium solution. This static stress procedure is one in which inertia effects are neglected. The analysis is assumed nonlinear and ignores time-dependent material effects, such as creep, swelling, and viscoelasticity.

The automatic loading incrementation scheme is selected to perform the nonlinear analysis of the panels. The computation is conducted at each loading increment. The load is assumed to be distributed along the boundaries of the panel-model. The finite element model is incrementally loaded up to the ultimate strength of the GFRP reinforcement or closer. A direct equation solver with a full Newton solution technique is utilized.

8.4 Comparison of Finite Element Analysis to Test Results

The measured and computed loads, cracking strengths and strain values are shown in Table 8-1. The ratio of predicted-to-measured cracking load ranges from 0.89 to 1.21, with an average of 1.004 and standard deviation of 0.14, while the average ratio of cracking strength

and standard deviation are 1.06 and 0.20, respectively, with the predicted values varying between 0.86 and 1.36 of the experimental results.

The results show that the model performs satisfactorily. The load-strain diagrams obtained with the model reasonably follow the test measurements. Figures 8-4 to 8-9 show typical comparisons between experimental and predicted load-strain relations for some panels.

Figures 8-10 to 8-17 show samples of stresses and crack patterns developed in the panels models. Crack patterns are represented herein as symbols indicating the directions of the minimum in-plane principal stresses. The stress distribution and cracking patterns reflect the experimental cracking behaviour. For example, comparing Figures 8-11 and 8-13 indicates that the observed final crack pattern of panel P1-GNU-16-1.0-1.5 (c_c / d_b = 1.5) shows the presence of more cracks compared to panel P2-GNU-16-1.0-2.5 (c_c / d_b = 2.5). This reflects the influence of a smaller c_c / d_b in developing more cracks to include main, secondary and splitting cracks at the ultimate stage. Also, comparing Figures 8-13 and 8-15, indicates the influence of HSC (panel P4-GHU-16-1.0-2.5) on decreasing the number of cracks compared to those develop in NSC panel P2-GNU-16-1.0-2.5.

8.5 Summary and Conclusions

In this chapter, the calibration and implementation of a tension stiffening model for finite element applications is presented. Based on the comparison between the model numerical prediction and the experimental results of the GFRP-RC panels, it is concluded that the incremental elastic plastic concrete model implemented in the finite element program is capable of predicting the behaviour of the tested panels. The proposed tension-stiffening

idealization realistically reflects the experimental behaviour of GFRP-RC panels. Based on the presented numerical analysis, the following main conclusions can be summarized:

1. GFRP-RC has a greater tension stiffening contribution compared to steel-RC. Therefore, it is recommended that a typical value of the ultimate tensile strain (around 50 ~ 100 times the initial cracking strain) be incorporated in the tension stiffening curve for GFRP-RC.

2. Adequate numerical results can only be achieved with the implementation of realistic stress-strain characteristics. The post-cracking behaviour has a significant effect on the entire panel response. In addition, the proper geometric modelling and suitable load simulation are key aspects in achieving solution convergence in nonlinear analysis of concrete.

3. The smeared cracking modelling approach is successfully utilized in modelling the GFRP-RC panels. The two-dimensional crack pattern representations, calculated load strain relationships, and stress contours generally reflect the experimental behaviour observed for the tested panels. Therefore, the analysis results recommend such a numerical modelling approach, so that it can be used to predict the behaviour of GFRP-RC with reasonable accuracy. Nonetheless, it should be noted that the local effect of reinforcing mesh in initiating a discrete crack cannot be noticed using the smeared crack method.

Table 8-1: A sample of FEA results

Specimen	Cracking Load, N_{cr} (kN)			Cracking Strength, f_{cr} (MPa)			Ultimate Load, N_{ult} (με)		
	Exp.	*FEA*	$\frac{N_{cr\_FEA}}{N_{cr\_Exp}}$	*Exp.*	*FEA*	$\frac{f_{cr\_FEA}}{f_{cr\_Exp}}$	*Exp.*	*FEA*	$\frac{N_{ult\_FEA}}{N_{ult\_Exp}}$
P1-GNU-16-1.0-1.5	216.4	198	0.91	1.86	1.61	0.86	627	771	1.22
P2-GNU-16-1.0-2.5	163	198	1.21	1.41	1.68	1.19	786	771	0.98
P3-GNB-16-1.0-2.5	126.5	113	0.89	1.06	1.05	0.99	390	360	0.92
P4-GHU-16-1.0-2.5	299.5	273	0.91	2.49	2.30	0.92	747	774	1.03
P6-GHB-16-1.0-2.5	233.2	258	1.10	1.77	2.41	1.36	575	480	0.83

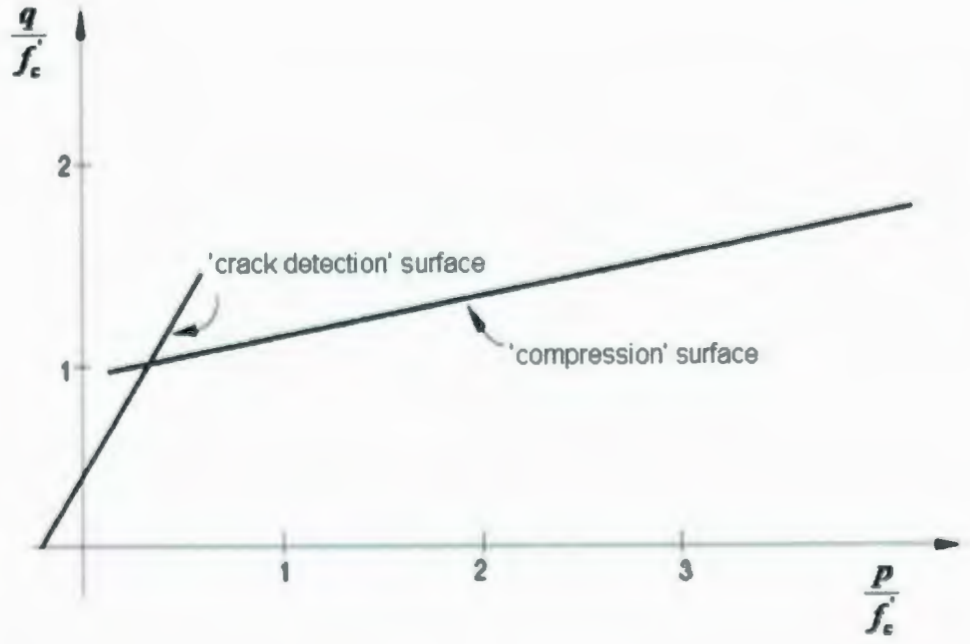

Figure 8-1: Concrete failure surfaces in the p-q plane (ABAQUS 2006)

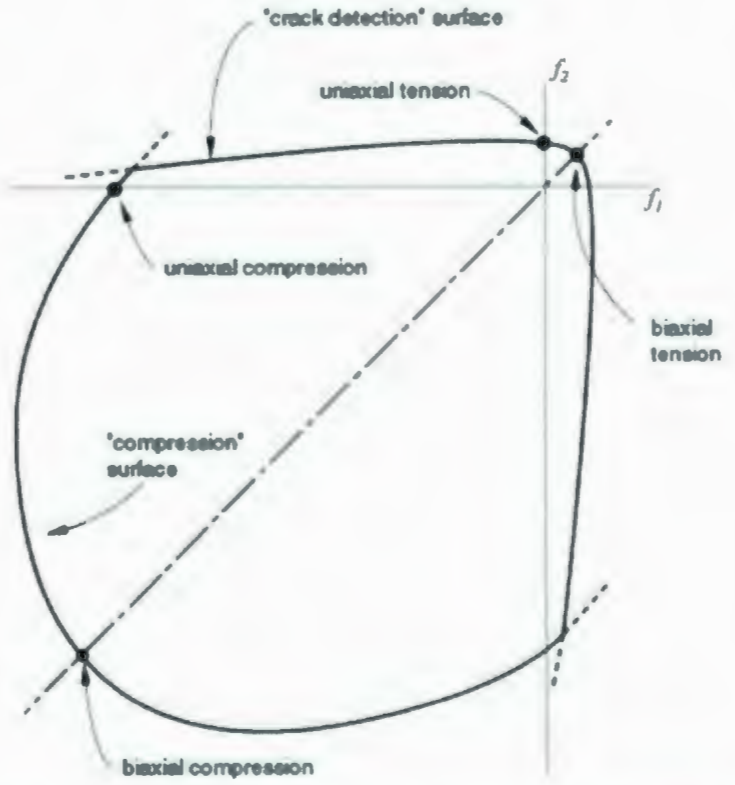

Figure 8-2: Concrete failure surfaces in plane stresses (Kupfer et al. 1969)

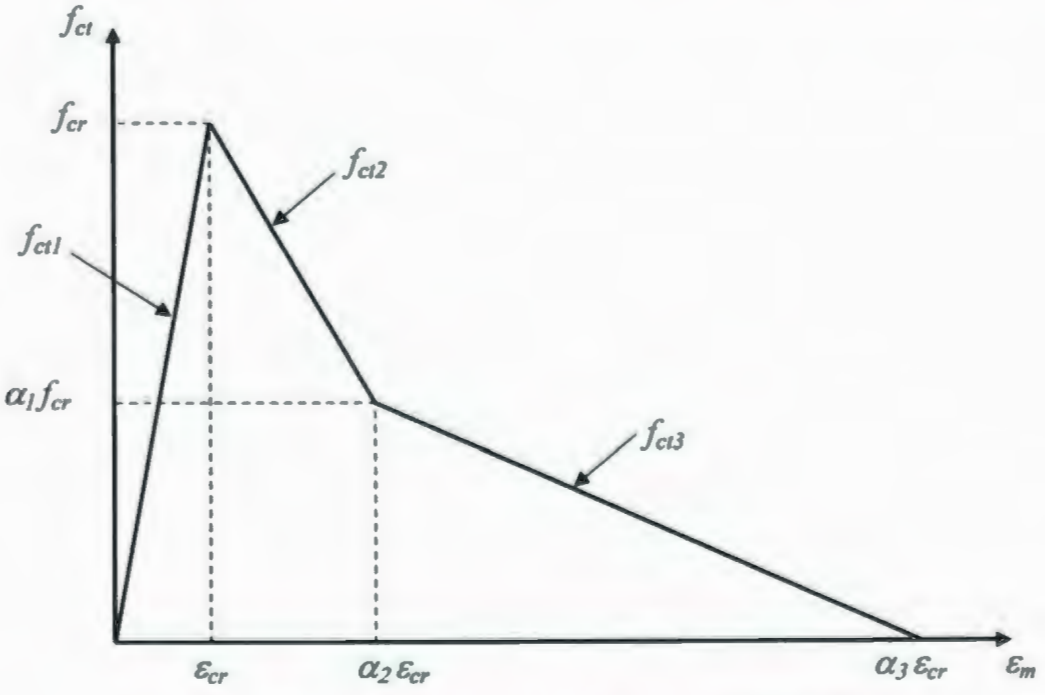

Figure 8-3: Idealization model of tension-stiffening response

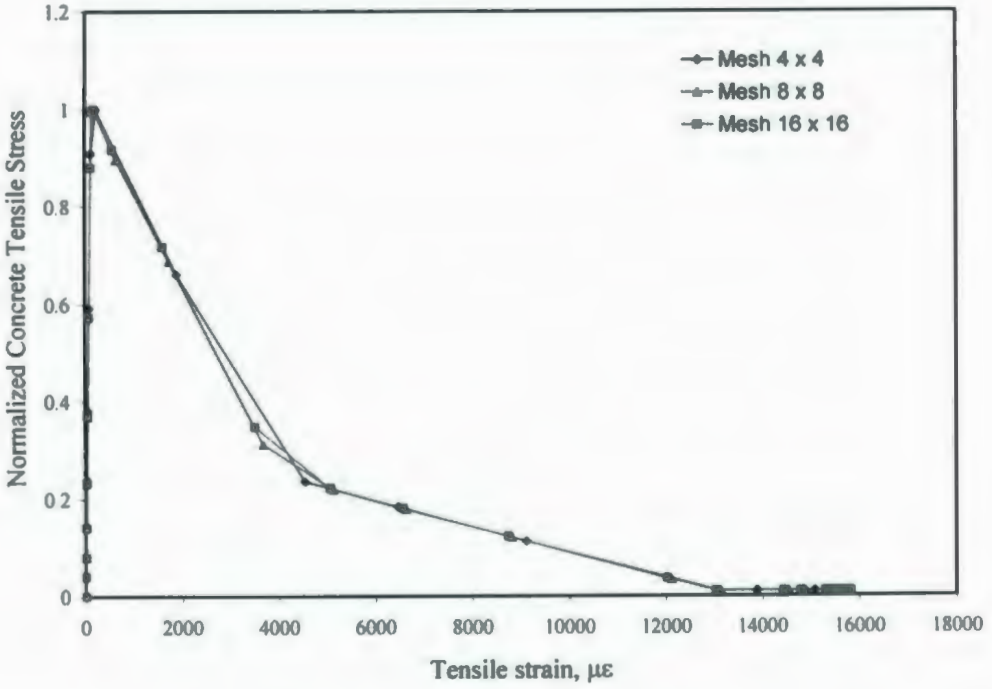

Figure 8-4: Mesh sensitivity effect on the tension stiffening response

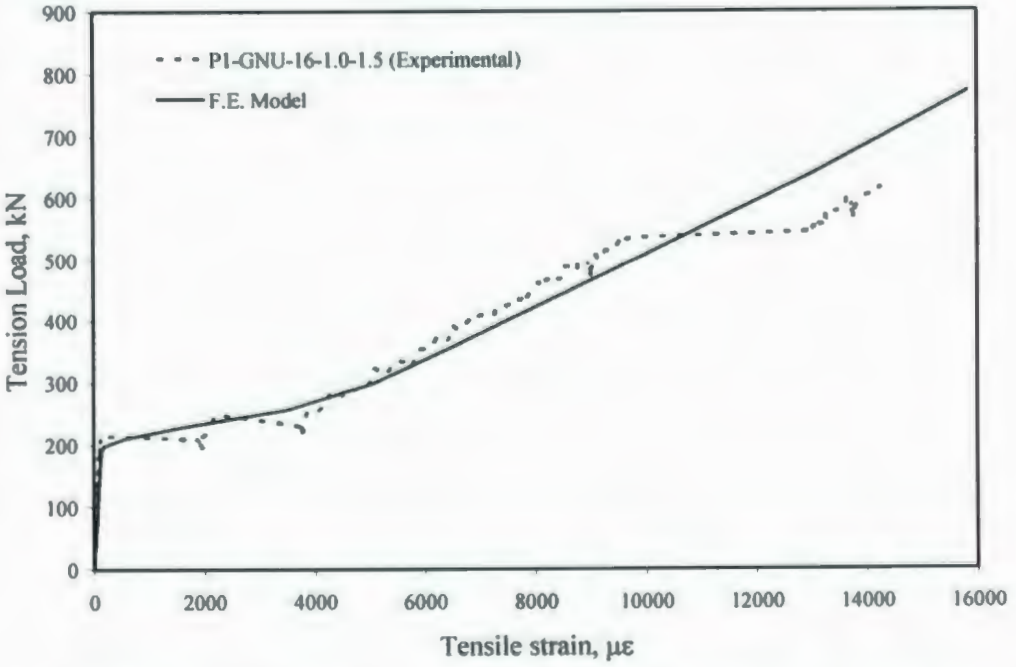

Figure 8-5: Comparison of model prediction to test result, P1-GNU-16-1.0-1.5

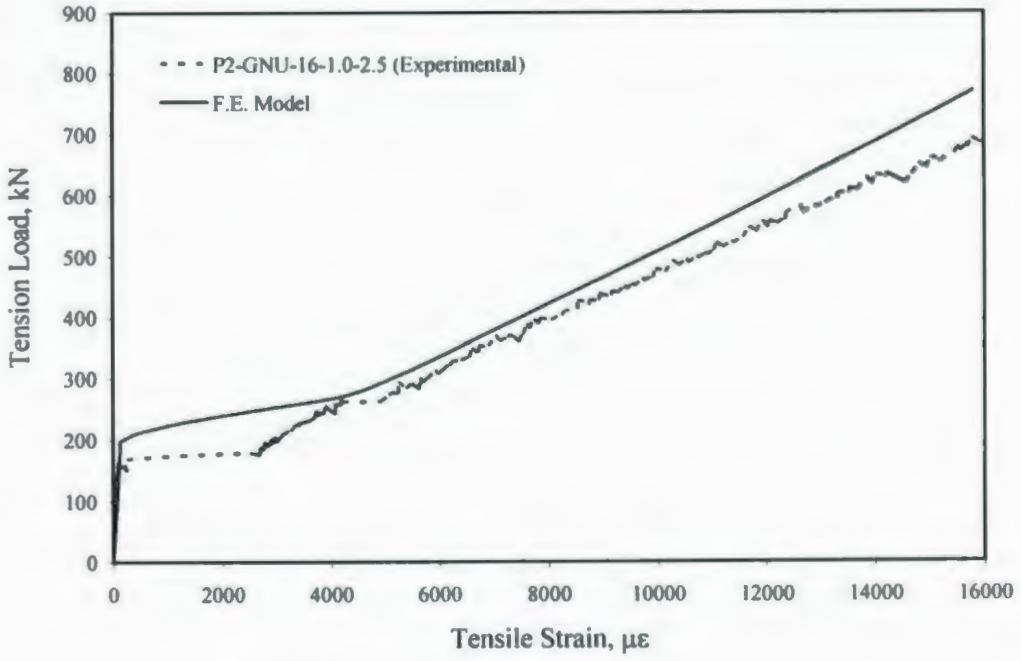

Figure 8-6: Comparison of model prediction to test result, P2-GNU-16-1.0-2.5

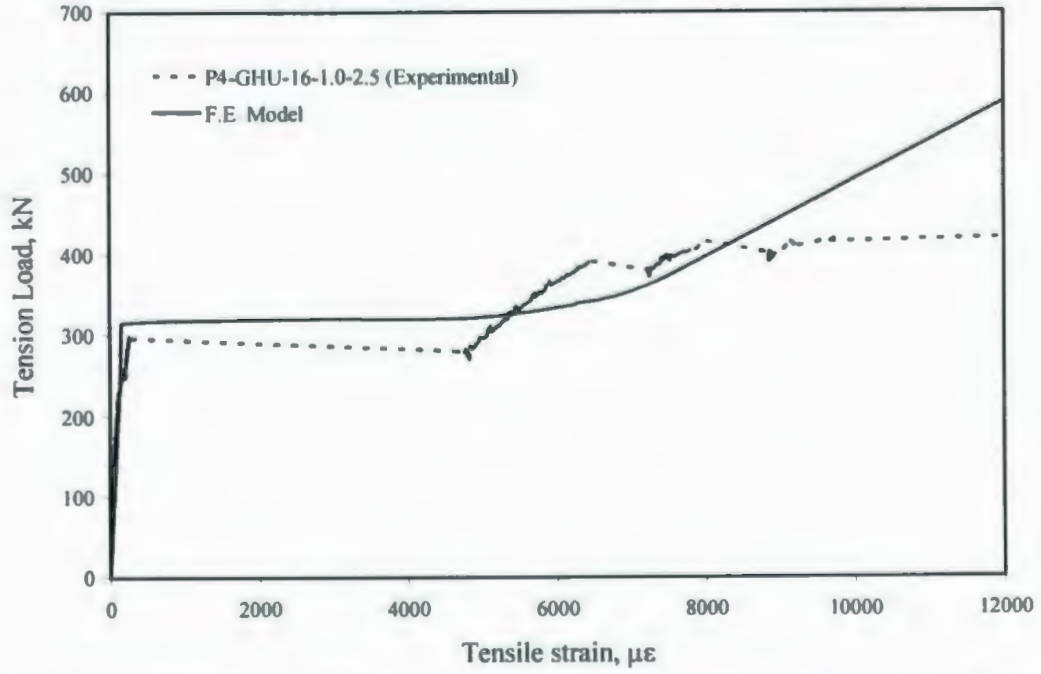

Figure 8-7: Comparison of model prediction to test result, P4-GHU-16-1.0-2.5

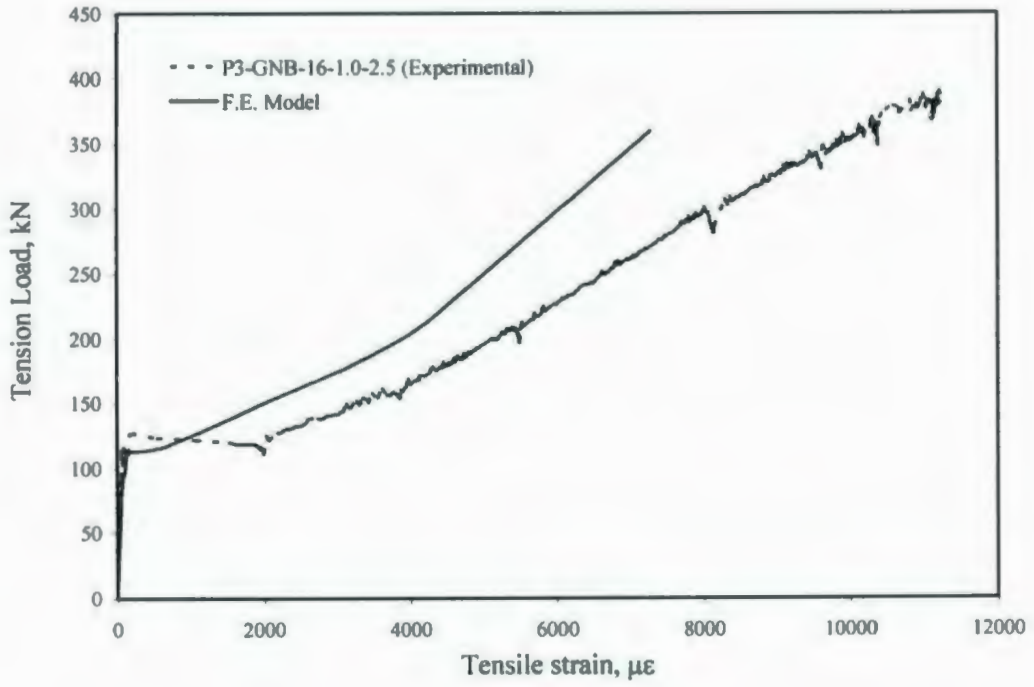

Figure 8-8: Comparison of model prediction to test result, P3-GHB-16-1.0-2.5

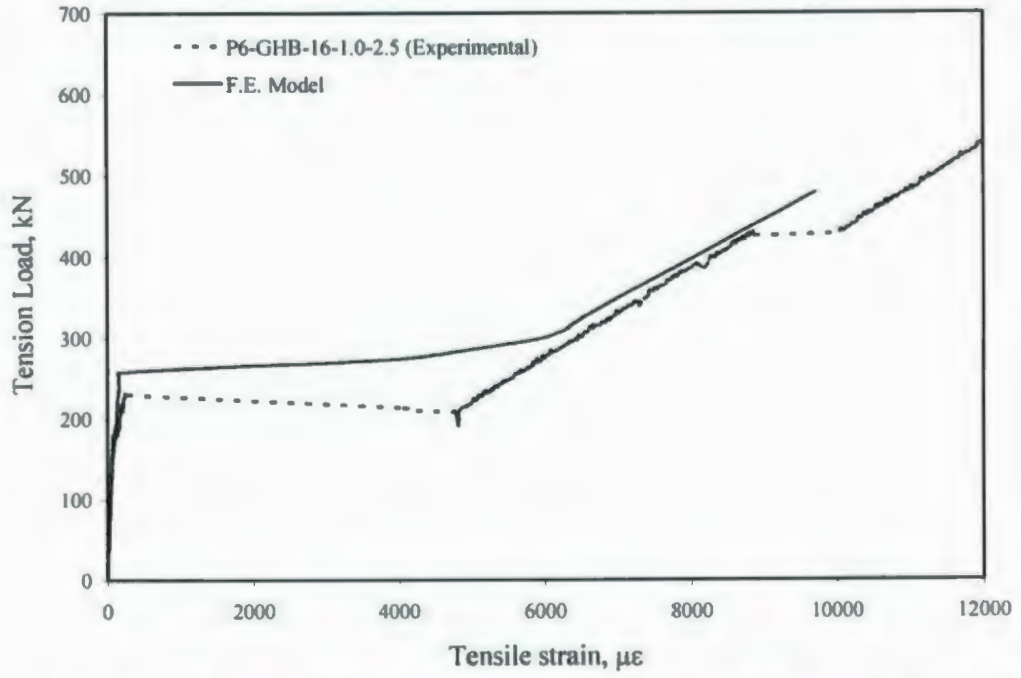

Figure 8-9: Comparison of model prediction to test result, P6-GHB-16-1.0-2.5

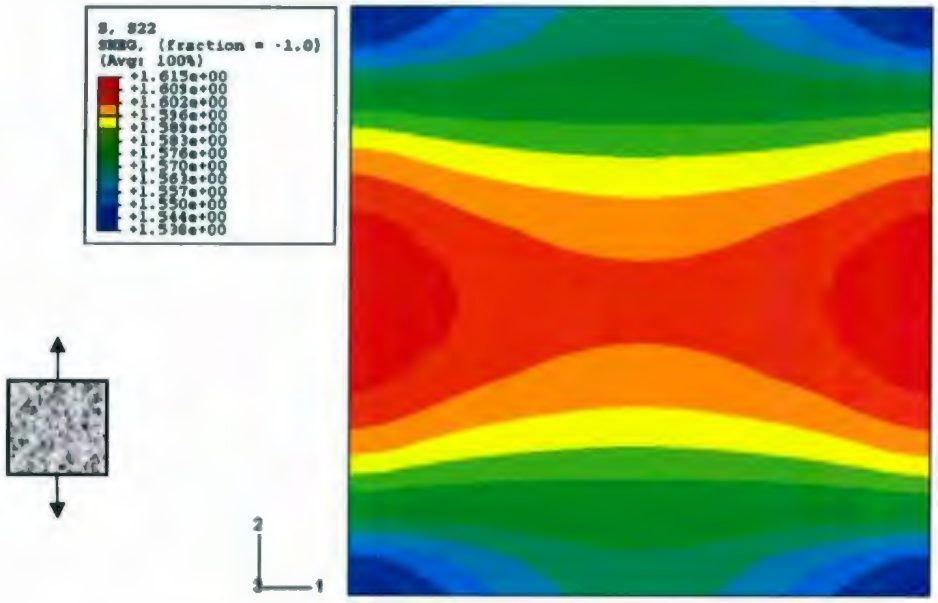

Figure 8-10: Stresses, S22 at initial cracking load for panel P1-GNU-16-1.0-1.5 (at N_{cr} = 198 kN)

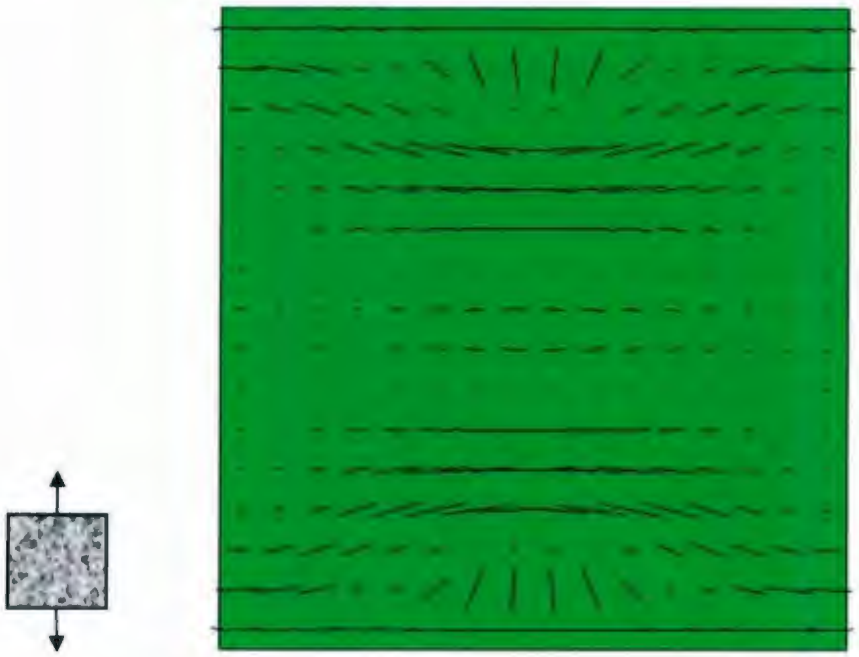

Figure 8-11: Final cracks for panel P1-GNU-16-1.0-1.5 (at N_{ult} = 771 kN)

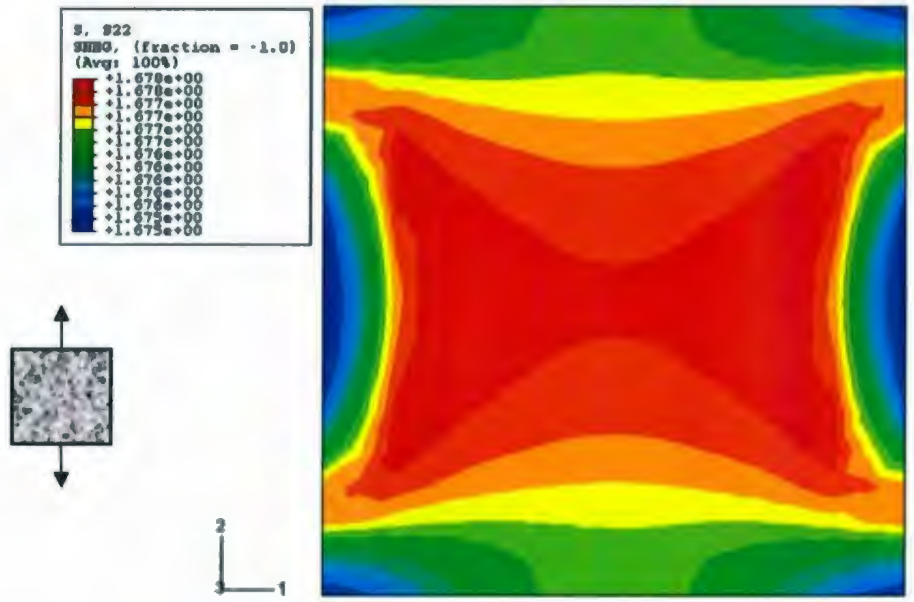

Figure 8-12: Stresses, S22 at initial cracking load for panel P2-GNU-16-1.0-2.5 (at N_{cr} = 198 kN)

Figure 8-13: Final cracks for panel P2-GNU-16-1.0-2.5 (at N_{ult} = 771 kN)

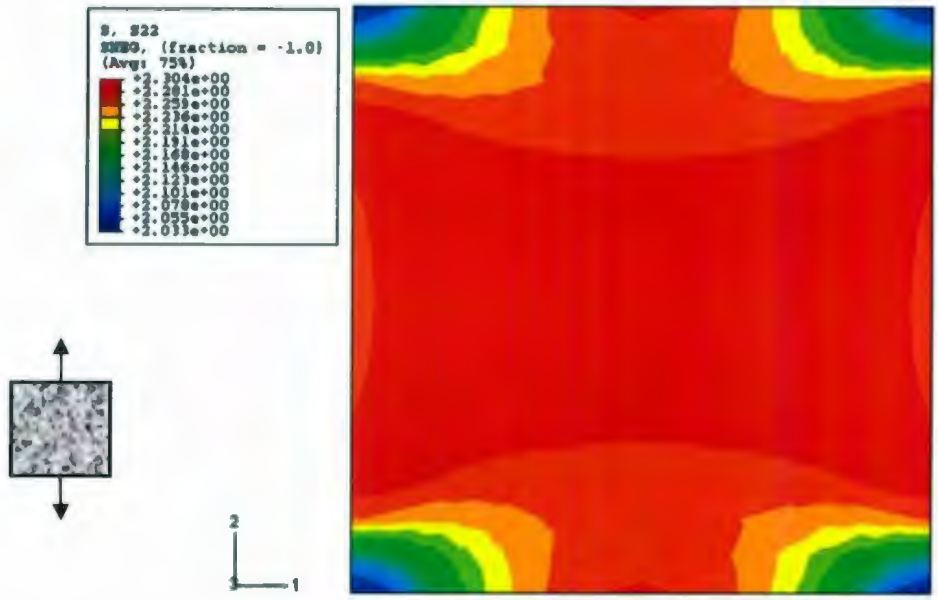

Figure 8-14: Stresses, S22 at initial cracking load for panel P4-GHU-16-1.0-2.5 (at N_{cr} = 273 kN)

Figure 8-15: Final cracks for panel P4-GHU-16-1.0-2.5 (at N_{ult} = 774 kN)

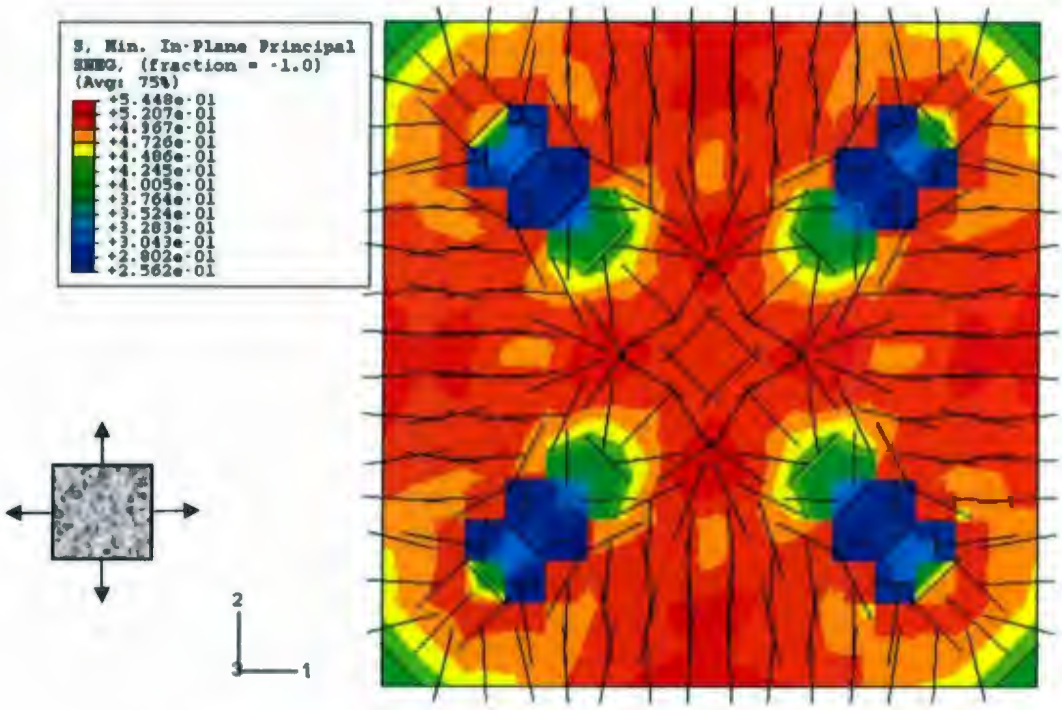

Figure 8-16: Initial cracks for panel P3-GNB-16-1.0-2.5 (at N_{cr} = 113 kN)

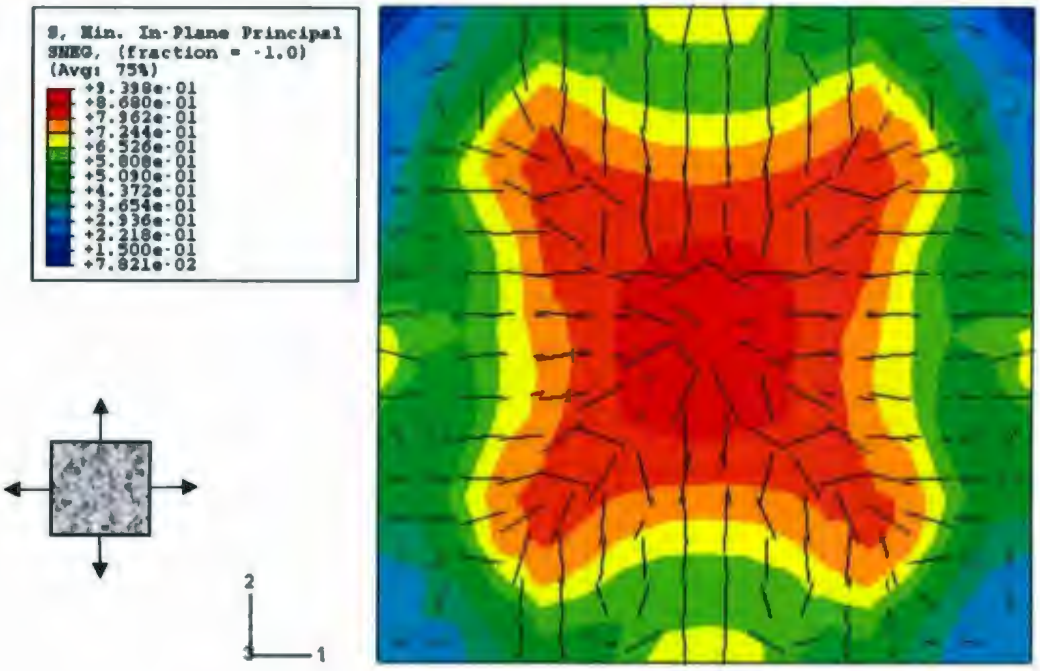

Figure 8-17: Initial cracks for panel P6-GHB-16-1.0-2.5 (at N_{cr} = 258 kN)

Chapter 9

SUMMARY AND CONCLUSIONS

9.1 Summary

In the presented research investigation, the behaviour of GFRP-RC panels under uniaxial and biaxial tension was studied. For that regard, an experimental program was carried out, which required a special test setup to be designed and constructed. The test setup included five main components; namely, an RC reaction frame, four moving walls, hydraulic system, gripping system, and measuring instrumentations. The test setup can accommodate FRP and steel reinforcing bars. The test setup design provided a simple solution to the common gripping problems of FRP bars. The test setup is designed to accommodate different specimen sizes, bar diameters, various bar spacing and loading conditions.

Several parameters were investigated, namely, loading type (uniaxial or biaxial tension), concrete strength, concrete cover to bar diameter ratio, bar spacing, reinforcement ratio, and bar type (GFRP or steel). A total of twelve specimens were tested during the experimental investigation. This included six GFRP-RC panels made of NSC. The effect of the compressive strength was investigated by testing four GFRP-RC panels made of HSC. Moreover, the behaviour of GFRP-RC panels was compared to the corresponding panels reinforced with steel reinforcing bars.

The measurements during the experimental program included the load, displacements and the strains developed under different loading cases. The changes in crack patterns, crack widths, and crack spacings were investigated. The stress-strain relationships, and thus the tension stiffening behaviour were also studied.

A theoretical approach was proposed to predict the cracking characteristics of GFRP-RC under tensile stresses. The proposed cracking model is based on the stress transfer approach, adopting the laws of force equilibrium and implicitly accounts for the bond-slip relationship. A comparison between the proposed cracking model and the experimental data of GFRP-RC panels was presented. The proposed model was also compared to other relevant crack spacing equations available in the literature. Finally, the suggested cracking model was further validated through applying its solution strategy on experimental data of other relevant research investigations found in the literature.

Based on the experimental results, a constitutive law was proposed to idealize the tensile stress-strain relationships of GFRP-RC panels under uniaxial and biaxial tension. The proposed model was further compared with other constitutive models in the literature. The model was implemented in a general finite element program. The finite element model was developed based on the smeared cracking approach. The validity of the proposed model was established by comparison with the test results of the GFRP-RC panels.

9.2 Findings of Experimental Investigation

The main findings of the experimental investigation are summarized as follows:

1. Under uniaxial tension, the GFRP-RC panels transferred gradually from the uncracked stage to the stabilized cracking stage. Beyond which the ultimate failure was reached by rupturing of the GFRP bars. Under biaxial tension, cracks developed simultaneously in both orthogonal directions and in the form of two or three cracks (i.e. multiple cracks). This resulted in a faster transition from the initial cracking to the stabilized cracking stage. There was no significant change in the final cracking pattern beyond the initial cracking stage.

2. Under biaxial tension, some cracks tended to follow relatively inclined patterns that were not observed in uniaxial tension. The change in the crack direction was attributed to the variation of principal stresses with the development of cracks under biaxial tension loading.

3. The crack development under biaxial tension affected the magnitude of stresses in the GFRP-RC panels. There was a decrease in cracking loads and stresses by almost 25%. This decrease was mainly attributed to the effect of tensile stresses in the transverse direction and due to cracks developed in an arbitrary inclined pattern as a result of variation of principal stresses with the progress of cracking.

4. Under biaxial tension, the GFRP-RC panels experienced much less tension stiffening contribution than those under uniaxial tension. This reduction was attributed to the

reduction in the initial cracking loads and cracking strength under biaxial tension. This reduction was also attributed to the differences in the mechanisms of crack development under biaxial tension, which resulted in a fast transition from initial to stabilized cracking.

5. Under uniaxial tensile stresses, once the cracking strength was exceeded, the concrete stress dropped to nearly 25 - 40% of the cracking strength. Under biaxial tension, the concrete stress dropped to nearly 15 - 25% of the cracking strength of concrete.

6. Due to the lower bar modulus of elasticity of GFRP compared to steel bars, there were significant reductions in cracking loads and concrete stresses. GFRP-RC panels cracked at N_{cr} nearly 10% to 20% of that recorded for steel-RC panels. Moreover, the tensile strain at which the stabilized cracking stage was achieved for GFRP-RC panels varied between 2000 to 8000 με, which is nearly 10 to 40 times the initial cracking strain. For steel-RC, the stabilized strain was in the range of 1700 με, which is about 8 to 15 times the initial cracking strain. Therefore, GFRP-RC reached its stabilized cracking stage at a tensile strain of nearly two to four times that of steel-RC

7. Up to the serviceability design limit, which is commonly taken around 2000 με (ISIS 2001), the difference in mean crack width between steel-RC and GFRP-RC was found to be minor. Beyond the steel-RC stabilized cracking stage, crack widths were obviously greater for the GFRP-RC because of the lower modulus of elasticity of the GFRP bar.

8. The size of the effective tension zones were found to be dependent on the bar type used for reinforcement. The size of the effective tension zones for GFRP-RC was almost half the size of those that develop around traditional steel reinforcing bars. For the GFRP type used, the experimental evidence showed that the size of an effective tension zone for GFRP-RC is about six to seven times the reinforcing bar diameter ($6 - 7\ d_b$).

9. GFRP-RC under uniaxial tension experienced a significant increase in the tension stiffening contribution compared to steel-RC at the same level of stress, which is due to the lower modulus of elasticity of the GFRP. However, the tension stiffening was not as significant under biaxial tension due to the different cracking mechanism, which resulted in faster degradation in the tension-stiffening contribution under biaxial tension.

10. The brittle nature of HSC affected the development of the crack. The initiation of major-through cracks was occurring at a faster rate compared to NSC. Also, there were significant jumps in the tensile strain at the crack initiation in the GFRP-RC panels made of HSC. These abrupt changes in the tensile strain had a higher magnitude than those occurred in NSC panels. This was attributed to both the brittle nature of HSC and due to the local slip between the GFRP bars and surrounding concrete.

11. The use of HSC compensated for the reduction in the cracking loads and stresses due to the use of GFRP bars when used with NSC. The HSC improved the overall

resistance of the GFRP-RC. It almost reached the same cracking loads and stresses of the corresponding NSC panels reinforced with traditional steel bars.

12. The initial crack loading and concrete cracking stress increased nearly proportional to the increase in the concrete compressive strength. This was found to be valid for uniaxial and biaxial tension loading cases.

13. The use of HSC allowed a reduction in the total number of visible cracks; especially the secondary and splitting cracks. Thus, the use of HSC could enhance the cracking characteristics of GFRP-RC.

14. The use of HSC resulted in a higher tension-stiffening contribution, due to higher cracking loads and reduction in tensile strain at the same level of loading. The difference between the panel tensile response and bare bar response was found to be increasing nearly proportional to the increase in the concrete compressive strength.

15. In general, the use of HSC caused a reduction in mean crack width. Under uniaxial tension, there was a minor difference in the mean crack width due to the use of HSC up to ε_m = 4000 to 5000 με. Beyond that, the mean crack width was reduced by nearly 20 ~ 30%, which could be attributed to the higher concrete compressive strength. Under biaxial tension, HSC allowed a reduction in w_m by nearly 45% up to the stabilized cracking stage. Hence, the compressive strength of concrete has a minimal influence on the change in mean crack width within the practical serviceability limits (~ up to 2000 με).

16. In order to improve the structural aesthetics and delay the stage of development of splitting cracks, it is recommended that for GFRP-RC members subjected to direct tensile stresses should be designed for a serviceability limit not greater than 50% of the ultimate load and the c_c / d_b ratio should not be less than 2.5.

17. There was an increase in the tension stiffening contribution due to the decrease in reinforcement ratio. The increase in tension stiffening could be attributed to two main factors: (a) with a low reinforcement ratio, there is a larger concrete area around the bar, which results in a greater tension stiffening contribution, and (b) the use of a smaller d_b enhances the bond transfer mechanism of the GFRP-bar and thus the tension stiffening contribution.

9.3 Conclusions of Theoretical Investigation

The main conclusions and recommendations of the theoretical investigation are summarized as follows:

1. The crack spacing developed within the RC panels was found to dependent on the mechanism of bond stress transfer from the reinforcing bar to the surrounding concrete. Therefore, a mathematical approach was suggested to predict the crack spacing in GFRP-RC. The proposed model accounted for the bond stress transfer mechanism and surface characteristics of the reinforcing bar, through the calibration of the bond factor K_p deduced from pullout tests. The results of such calibration were used to estimate the transfer length and thus to deduce the average crack spacing.

2. The proposed crack spacing model was validated using additional experimental data from the literature. The analysis showed that the proposed cracking model provided reasonable predictions. Hence, the proposed approach is suitable for predicting the cracking characteristics of GFRP-RC.

3. A tensile stress-strain constitutive relationship was proposed for GFRP-RC. The main feature of the model was the inclusion of both the partial sudden drop of stress and the change in the tensile strain after the cracking strength is exceeded. This was performed by assuming a bi-linear relation in the post-cracking range.

4. The proposed tension stiffening model reasonably reflected the experimental behaviour. The cracking strength of concrete panels was incorporated in the proposed model to account for the biaxial tension strength envelope. Using this concept, the two-dimensional problem was reduced to a simple uniaxial problem.

5. The proposed tension-stiffening model was implemented in a finite element program to examine the behaviour of GFRP-RC panels through the nonlinear finite element analysis. The finite element analysis adopted the smeared cracking approach. The analysis results recommend such a numerical modelling approach can be used to predict the behaviour of GFRP-RC with reasonable accuracy.

9.4 Contribution

To the best of author's knowledge, it is the first time to investigate the behaviour of GFRP-RC panels under uniaxial and biaxial direct tension. Also, it is the first time to design and

construct a test-setup that can be used to carry out experimental tests on GFRP-RC panels under biaxial tension. Thus, this thesis presents an original research topic in the field of FRP-RC.

The thesis presented a comprehensive investigation on the cracking behaviour of concrete panels that were reinforced with multi-layers of GFRP bars. The investigation showed, in detail, the experimental cracking behaviour and the tensile response. To the author's knowledge, this thesis is the first to examine the effect of reinforcing bar type on the size of effective tension zone.

The investigation was further extended to propose a theoretical and numerical approach to analyze the cracking and tensile behaviour under uniaxial and biaxial tension. A cracking model was proposed to calculate the crack spacing for GFRP-RC under direct tension. The model exclusively incorporates the bond stress transfer mechanism through accounting for surface characteristics of the GFRP reinforcing bar.

Furthermore, a constitutive relationship was proposed to idealize the complete tensile stress-strain relationship of GFRP-RC. A non-linear finite element analysis of GFRP-RC panels was conducted to identify the key parameters for a successful numerical computation. The proposed tension-stiffening idealization was incorporated in a finite element program to demonstrate its validity.

9.5 Recommendations for Further Research

1. It is recommended to carry out further experimental studies on the influence of other test parameters such as different bar spacings, and aggregate size, and other types of

FRP reinforcing bars. These studies will help in improving the understanding of the cracking characteristics of FRP-RC.

2. Further experimental studies are required to include the shear effects along with different loading ratios in biaxial tension. It may also be recommended to further investigate the effect of specimen size on the tensile properties of RC, and thus establish a generic rationale that can be used in calculations.

3. The use of HSC with GFRP reinforcing bars is found to be promising in overcoming some of the cracking problems of GFRP-RC. However, the brittle nature of HSC may suggest carrying out a separate study to investigate the influence of fibre-reinforced concrete (FRC) mix type on the cracking mechanism of HSC reinforced with GFRP bars.

4. The finite element method is a powerful tool that can be used to provide insight into the behaviour of concrete structures. Further experimental studies can help in refining the existing models so that they can be used to predict the behaviour FRP-RC structures.

Bibliography

ABAQUS (2006), "ABAQUS User's Manual," Hibbitt, Kalrsson and Sorensen Inc., Providence, R.I., version 6.5 edition.

Abrishami, H. and Mitchell, D. (1996), "Influence of Splitting Cracks on Tension Stiffening," ACI Structural Journal, Vol. 93, No. 6, pp. 703-710.

Achillides, Z. and Pilakoutas, K. (2004), "Bond Behaviour of Fibre Reinforced Polymer Bars under Direct Pullout Conditions," Journal of Composites for Construction, ASCE, Vol. 8, No. 2, pp.173-181.

ACI 222 (2001), "Protection of Metals in Concrete against Corrosion," ACI Manual of Concrete Practice, American Concrete Institute, ACI Committee 222, Farmington Hills, MI.

ACI 222.3 (2003), "Design and Construction Practices to Mitigate Corrosion of Reinforcement in Concrete Structures," ACI Manual of Concrete Practice, American Concrete Institute, ACI Committee 222, Farmington Hills, MI.

ACI 224 (2001), "Control of Cracking in Concrete Structures," ACI Manual of Concrete Practice, American Concrete Institute, ACI Committee 224, Farmington Hills, MI.

ACI 224 (1992), "Cracking of Concrete Members in Direct Tension," ACI Manual of Concrete Practice, American Concrete Institute, ACI Committee 224, Farmington Hills, MI, (Reapproved 2004).

ACI 318 (2005), "Building Code Requirements for Reinforced Concrete and Commentary," ACI Manual of Concrete Practice, ACI Committee 318, Farmington Hills, MI.

ACI 440R (1996), "State-of-the-Art Report on Fibre-Reinforced Polymer (FRP) Reinforcement for Concrete Structures," ACI Manual of Concrete Practice, ACI Committee 440, Reapproved 2002, Farmington Hills, MI.

ACI 440R (2007), "Report on Fibre-Reinforced Polymer (FRP) Reinforcement for Concrete Structures," ACI Manual of Concrete Practice, ACI Committee 440, Farmington Hills, MI.

ACI 440.1 (2001), "Guide for the Design and Construction of Concrete Reinforced with FRP bars," American Concrete Institute, ACI Committee 440, Farmington Hills, MI.

ACI 440.1 (2003), "Guide for the Design and Construction of Concrete Reinforced with FRP bars," American Concrete Institute, ACI Committee 440, Farmington Hills, MI.

ACI 440.1 (2006), "Guide for the Design and Construction of Concrete Reinforced with FRP bars," American Concrete Institute, ACI Committee 440, Farmington Hills, MI.

ACI 440.3 (2004), "Guide Test Methods for Fiber-Reinforced Polymers (FRPs) for Reinforcing or Strengthening Concrete Structures," American Concrete Institute, ACI Committee 440, Farmington Hills, MI.

ACI 446.1 (1991), "Fracture Mechanics of Concrete: Concepts, Models and Determination of Material Properties," ACI Manual of Concrete Practice, American Concrete Institute, ACI Committee 446, Farmington Hills, MI, (Reapproved 1999).

ACMA (2008), http://www.mdacomposites.org, American Composites Manufacturers Association (ACMA), (Accessed Dec. 2008).

Aiello, M.A., Leone, M.A., and Ombres, L. (2002), "Cracking Analysis of FRP Reinforced Concrete Tension Members," Advanced Polymer Composites for Structural Applications in Construction, Southampton, U.K.

Alavi-Fard, M. and Marzouk, H. (2004) "Bond Behaviour of High Strength Concrete," Magazine of Concrete Research, Vol. 56, No. 9, pp 545-557.

Al-Sunna, R., Pilakoutas, K., Waldron, P., and Al-Hadeed, T. (2006), "Tension Stiffening in GFRP Reinforced Concrete Beams," Measuring, Monitoring and Modelling Concrete Properties, M.S. Konsta-Gdoutos (ed.), Springer.

Aoyagi, Y. and Yamada, K. (1983), "Strength and Deformation Characteristics of Reinforced Concrete Shell Elements Subjected to In-plane Forces," Proc. JSCE, Vol. 331, pp. 167-180.

ASTM C39/C39M (2003), "Standard Test Method for Compressive Strength of Cylindrical Concrete Specimens," Annual Book of ASTM Standards, Vol. 04.02.

ASTM C78-09 (2009), "Standard Test Method for Flexural Strength of Concrete (Using Simple Beam with Third-Point Loading)," Annual Book of ASTM Standards, Vol. 04.02.

ASTM C136 (2006), "Standard Test Method for Sieve Analysis of Fine and Coarse Aggregates," Annual Book of ASTM Standards, Vol. 04.02.

ASTM C192/C192M (2005), "Standard Practice for Making and Curing Concrete Test Specimens in the Laboratory," Annual Book of ASTM Standards, Vol. 04.02.

ASTM C293-08 (2008), "Standard Test Method for Flexural Strength of Concrete (Using Simple Beam with Center-Point Loading)," Annual Book of ASTM Standards, Vol. 04.02.

ASTM C494/C494M (2005), "Standard Specification for Chemical Admixtures for Concrete," Annual Book of ASTM Standards, Vol. 04.02.

ASTM C496/C496M (2004), "Standard Test Method for Splitting Tensile Strength of Cylindrical Concrete Specimens," Annual Book of ASTM Standards, Vol. 04.02.

ASTM D3916 (2002), "Test Method for Tensile Properties of Pultruded Glass Fibre Reinforced Plastic Rod," Annual Book of ASTM Standards, Vol. 08.02.

Base, R.D., Read, J.B., Beeby, A.W., and Taylor, H.P.J. (1966), "An Investigation of the Crack Control Characteristics of Various Types of Bar in Reinforced Concrete Beams," Research Report No. 18, Parts I and II, Cement and Concrete Association, London.

Bažant, Z.P. and Baweja, S. (1995), "Creep and Shrinkage Prediction Model for Analysis and Design of Concrete Structures – Model B3," Materials and Structures, RILEM, Paris, Vol. 28, pp. 357-365, 415-430, 488-495.

Bažant, Z.P. and Oh, B. H. (1983), "Crack Band Theory for Fracture of Concrete," Materials and Structures Research and Testing, Vol. 16, No. 93, pp. 155-177.

Bedard, C. (1992), "Composite Reinforcing Bars: Assessing their Use in Construction," Concrete International, January, pp. 55-59.

Beeby, A.W. (1972), "A Study of Cracking in Reinforced Concrete Members Subjected to Pure Tension," Technical Report 42.468, Cement and Concrete Association, London.

Beeby, A.W. (1979), "The Prediction of Crack Widths in Hardened Concrete," The Structural Engineer, Vol. 57A, No. 1, pp. 9-17.

Beeby, A.W. and Scott, R.H. (2005), "Insights into the Cracking and Tension Stiffening Behaviour of Reinforced Concrete Tension Members Revealed by Computer Modelling," Magazine of Concrete Research, Vol. 5/Iss. 3, pp. 179-190.

Belarbi, A. and Hsu, T.T. (1994), "Constitutive Laws of Concrete in Tension and Reinforcing Bars Stiffened by Concrete," ACI Structural Journal, Vol. 91, No. 4, pp. 465-474.

Benmokrane, B., Chaallal, O., and Masmoudi, R. (1995), "Glass Fibre Reinforced Plastic (GFRP) Rebars for Concrete Structures," Constructions and Building Materials, Vol. 9, No. 6, pp. 353-364.

Benmokrane, B., Tighiouart, B., and Chaallal, O. (1996a), "Bond Strength and Load Distribution of Composite GFRP Reinforcing Bars in Concrete," ACI Materials Journal, Vol. 93, No. 3, pp. 246-253.

Benmokrane, B., Challal, O., and Masmoudi, R. (1996b), "Flexural Response of Concrete Beams with FRP Reinforcing Bars," ACI Structural Journal, Vol. 93, No. 1, pp. 46-55.

Bischoff, P.H. (2001), "Effects of Shrinkage on Tension Stiffening and Cracking in Reinforced Concrete," Canadian Journal of Civil Engineering, Vol. 28, pp. 363-374.

Bischoff, P.H. (2005), "Reevaluation of Deflection Prediction for Concrete Beams Reinforced with Steel and Fibre Reinforced Polymer Bars," Journal of Structural Division, ASCE, Vol. 131, No. 5, pp. 752-767.

Bischoff, P.H. and Paixao, R. (2004), "Tension Stiffening and Cracking of Concrete Reinforced with Glass Fibre Reinforced Polymer (GFRP) Bars", Canadian Journal of Civil Engineering, 31, pp. 579-588.

Blackman, J.S., Smith, G., and Young, L.E. (1958), "Stress distribution affects ultimate tensile strength," ACI Journal, Proceedings Vol. 55, No.6, pp. 679-684.

Branson, D.E. (1977), *Deformation of Concrete Structures*, McGraw-Hill, New York.

Broms, B.B. (1965), "Crack Width and Crack Spacing in Reinforced Concrete," Journal of the American Concrete Institute, Vol. 62, No. 10, pp. 1237-1255.

Carlson, R.W. (1938), "Drying Shrinkage of Concrete as Affected by Many Factors," Proceedings, ASTM, V. 38, Part II, pp. 419-437.

Carreira, D.J. and Chu, K-H. (1986), "Stress-Strain Relation for Reinforced Concrete in Tension," ACI Journal, V. 82, No. 6, pp. 21-28.

CEB-FIP (1990), "CEB-FIP Model Code 1990 (MC-90), Design Code," Comité Euro-International du Béton (CEB), Thomas Telford Services Ltd., London.

Chaallal, O. and Benmokrane, B. (1993), "Physical and Mechanical Performance of an Innovative Glass-Fibre-Reinforced Plastic Rod," Canadian Journal of Civil Engineering, Vol. 20, No. 2, pp. 254-268.

Chan, H.C., Cheung, Y.K., and Huang, Y.P. (1992), "Crack Analysis of Reinforced Concrete Tension Members," Journal of Structural Engineering, ASCE, Vol. 118, No.1, pp. 2118-2132.

Chen, W.F. (1982), *Plasticity in Reinforced Concrete*, McGraw Hill, New York, 474 p.

Chi, M. and Kirstein, A.F. (1958), "Flexural Cracks in Reinforced Concrete Beams," Journal of the American Concrete Institute, title 54-48, pp. 865-878.

Cho, J.Y., Kim, N.S., Cho, N.S., and Choi, I.K. (2004a), "Cracking Behaviour of Reinforced Concrete Subjected to Biaxial Tension," ACI Structural Journal, Vol. 101, No. 1, pp. 202-208.

Cho, J.Y., Kim, N.S., Cho, N.S., and Choun, Y.S. (2004b), "Stress-Strain Relationship of Reinforced Concrete Subjected to Biaxial Tension," ACI Structural Journal, Vol. 101, No. 2, pp. 202-208.

Clark, A.P. (1956), "Cracking in Reinforced Concrete Flexural Members," Journal of American Concrete Institute, April, title 52-54, pp. 851-862.

Collins, M.P. and Mitchell, D. (1991), *Prestressed Concrete Structures*, Prentice-Hall, Inc., Englewood Cliffs, N. J., 766 p.

Cosenza, E., Manfredi, G., and Realfonzo, R. (1997), "Behaviour and Modelling of Bond of FRP Bars to Concrete," Journal of Composites for Construction, Vol. 1, No. 2, pp. 40-51.

Cosenza, E., Manfredi, M., Pecce, M., and Realfonzo (1999), "Bond between Glass Fibre Reinforced Plastic Reinforcing Bars and Concrete – Experimental Analysis," ACI SP 188-32, pp. 347-357.

CSA A3000 (2003), "Cementitious Materials Compendium," Canadian Standards Association, Toronto, Ontario, Canada.

CSA A23.3 (2004), "Design of Concrete Structures," Canadian Standards Association, Toronto, Ontario, Canada.

CSA S806 (2002), "Design and Construction of Building Components with Fibre-Reinforced Polymers," Canadian Standards Association, Toronto, Ontario, Canada.

CSA G40.20/G40.21 (2004), "General Requirements for Rolled or Welded Structural Quality Steel," Canadian Standards Association, Toronto, Ontario, Canada, (Reapproved 2009).

Damjanic, F. and Owen, D.R.J. (1984), "Practical Considerations for Modelling of Post-Cracking Concrete Behaviour for Finite Element Analysis of Reinforced Concrete Structures," Proc. Computer-Aided Analysis and Design of Concrete Structures, edited by N. Bicanic, and V. Simovic, Pineridge Press, Swansea, U.K, pp. 693-706.

Daniali, S. (1990), "Bond Strength of Fibre Reinforced Plastic Bars in Concrete," Proc. Serviceability and Durability of Construction Materials, ASCE, Boston, MA, USA.

Desayi, P. and Kulkarni, A.B. (1976), "Determination of Maximum Crack Width in Two-Way Reinforced Concrete Slabs," Proc. Institution of Civil Engineering, Part 2, Research and Theory, Vol. 61, No. 2, pp. 343-349.

Ebead, U. (2002), "Strengthening of Reinforced Concrete Two-Way Slabs," PhD Thesis, Memorial University of Newfoundland, St. John's, Newfoundland, Canada, 245 p.

EC2 (1994), "Eurocode 2: Design of Concrete Structures (BS EN 1992)," Comité Européen de Normalisation (CEN), Brussels.

EC2 (2004), "Eurocode 2: Design of Concrete Structures," Comité Européen de Normalisation (CEN), Brussels.

Edwards, A.D. and Picard, A. (1972), "Bond Proporties of ½ in. Diameter Strand," ACI Journal, Proceedings Vol. 69, No. 11, pp. 684-689.

Ehsani, M.R., Saadatmanesh, H., and Tao, S. (1996), "Design Recommendation for Bond of GFRP Bars to Concrete," Journal of Structural Engineering, Vol. 122, No. 3, pp. 247-257.

Elbadry, M., Mahmood, H. and Ghali, A. (2008), "Control of Displacement-Induced Cracking in FRP Reinforced Concrete ," In proceedings of 6th International Structural Specialty Conference, 37th Annual Conference for the Canadian Society for Civil Engineering, Quebec city.

Enerpac (2003), "ENERPAC – Hydraulic Power for all Industrial Applications," Products manual.

Engel, R.S., Croyle, M.G., Bakis, C.E., and Nanni, A. (1999), "Deflection of Reinforced Concrete Beams Reinforced by Fibre Reinforced Polymer Grid with Various Joint Designs," Fibre Reinforced Polymer Reinforcement for Reinforced Concrete Structures, SP-188, C.W. Dolan, S.H. Rizkalla, and A. Nanni, eds., American Concrete Institute, Farmington Hills, MI, pp. 75-85.

Favre, R. et al. (1983), "Fissuration et Deformations," Manual du Comite Euro International du Beton (CEB), Ecole Polytechnique Federale de Lausanne, Switzerland, 249 p.

Faza, S. S. (1991), "Bending and Bond Behaviour and Design of Concrete Beams Reinforced with Fibre Reinforced Plastic Bars," Ph.D. Dissertation, West Virginia University, Morgantown, West Virginia.

Faza, S.S. and GangaRao, H.V.S. (1993), "Glass FRP Reinforcing Bars for Concrete," Proceedings of International Symposium on Fibre Reinforced Plastic Reinforcement for Concrete Structures; ACI SP-138, A. Nanni and C. W. Dolan (editors).

Ferry-Borges, J. and Lima, J.A. (1960), "Crack and Deformation Similitude in Reinforced Concrete," RILEM Bulletin, No. 7, Paris, pp. 79-90.

Fields, K. and Bischoff, P.H. (2004), "Tension Stiffening and Cracking of High-Strength Reinforced Concrete Tension Members," ACI Structural Journal, Vol. 101, No. 4, pp. 447-456.

Frosch, R.J. (1999), "Another Look at Cracking and Crack Control in Reinforced Concrete," ACI Structural Journal, Vol. 96, No. 3, pp. 437-442.

GangaRao, H. and Vijay, P.V. (1997), "Aging of Structural Composites under Varying Environmental Conditions," Non-Metallic (FRP) Reinforcement for Concrete Structure: Proceeding of the Third International Symposium, Vol. 2, Japan Concrete Institute, Sapporo, Japan, pp. 91-98.

Gao, D., Benmokrane, B. and Masmoudi, R. (1998), "A Calculating Method of Flexural Properties of FRP-Reinforced Concrete Beam: Part 1: Crack Width and Deflection," Technical Report, Department of Civil Engineering, University of Sherbrooke, Sherbrooke, Quebec, Canada, 24 p.

Gardner, N.J. (2000), "Design Provisions for Shrinkage and Creep of Concrete," ACI SP194-3, American Concrete Institute, Detroit, pp. 101-134.

Gergeley, P. and Lutz, L.A. (1968), "Maximum Crack Width in Reinforced Flexural Members," Causes, Mechanism and Control of Cracking in Concrete, SP-20, American Concrete Institute, Detroit, pp. 87-117.

Ghali, A. and Favre, R. (1994), *Concrete Structures: Stresses and Deformations*, Second Edition, E & FN Spon, 444 p.

Giaccio, G., Rocco, C., and Zerbino, R. (1993), "The Fracture Energy (G_F) of High-Strength Concretes," Materials and Structures, Vol. 26, pp. 381-386.

Gilbert, R.I. (2005), "Time-Dependent Cracking and Crack Control in Restrained Concrete Structures," ACI SP-225: Serviceability of Concrete: A Symposium Honoring Dr. Edward G. Nawy, Ed. Barth, F., Co-Ed. Frosch, R, Nassif, H. and Scanlon, A., pp. 223-240.

Gopalaratnam, V.S. and Shah, S.P. (1985), "Softening Response of Plain Concrete in Direct Tension," ACI Journal, Proceedings Vol. 82, No. 3, pp. 310-323.

Goto (1971), "Cracks Formed in Concrete around Deformed Tension Bars," Journal of American Concrete Institute, Vol. 68, No. 4, pp. 244-251.

Guo, Z.H. and Zhang, X.Q. (1987), "Investigation of Complete Stress-Deformation Curves for Concrete in Tension," ACI Material Journal, Vol. 84, No. 4, pp. 278-285.

Haqqi, I.S. (1983), "Serviceability of Reinforced Concrete Subjected to Tension," Ph.D. Thesis, Council for National Academic Awards, London.

Hillerborg, A., Modeer, M., and Petersson, P.E. (1976), "Analysis of Crack Formation and Crack Growth in Concrete by Means of Fracture Mechanics and Finite Elements," Cement and Concrete Research, Vol. 6, pp. 773-782.

Hognestad, E. (1962), "High Strength Bars as Concrete Reinforcement, Part 2, Control of Flexural Cracking," Journal of PCA Research and Development Laboratories, Vol. 4, No. 1, pp. 46-63.

Houde, J. and Mirza, M.S. (1972), "A Study of Bond Stress-Slip Relationship in Reinforced Concrete," Structural concrete series no. 72-8, Montreal, Quebec: McGill University.

Hughes Brothers Inc. (2006), "Hughes Brothers Reinforcements" Product Guide Specification.

Hussein, A. and Marzouk, H. (2000), "Behaviour of High-Strength Concrete under Biaxial Stresses," ACI Materials Journal, Vol. 97, No.1.

Hsu, T.T., Belarbi, A., and Pang, X. (1995), "A Universal Panel Tester," Journal of Testing and Evaluation, ASTM, Vol.23, No.1, pp. 41-49.

Hsu, T.T. and Zhang, L.X. (1996), "Tension Stiffening in Reinforced Concrete Membrane Elements," ACI Structural Journal, Vol. 93, No. 1, pp. 108-115.

ISIS (2001), "Reinforcing Concrete Structures with Fibre Reinforced Polymers," Design Manual No. 3, ISIS Canada, Winnipeg, Manitoba.

Jaccoud, J.P. (1987), "Armature Minimale Pour le Contrôle de la Fissuration des Structures en Béton," Ph.D. Thesis, Départment de Génie Civil, École Polytechnique Fédérale de Lausanne, Lausanne, Switzerland.

Joh, O., Wang, Z., and Goto, Y. (1997), "Experimental Study of Bond Cracking Performance of FRP Reinforced Concrete," In Proceedings of the 3rd International Symposium on Non-metallic (FRP) Reinforcement for Concrete Structures (FRPRCS-3), Sapporo, Japan, Japan Concrete Institute, Tokyo, Japan, Vol. 2, pp. 431–438.

JSCE (1997), "Recommendation for Design and Construction of Concrete Structures Using Continuous Fibre Reinforcing Materials," Concrete Engineering Series No. 23, Japan Society of Civil Engineers, Tokyo, Japan, 325 pp.

Kaklauskas, G., Bacinskas, D., and Sokolov, A. (2007), "Discussion of 'Tension Stiffening Model for Concrete with Steel and FRP Bars' by Rim Nayal and Hayder Rasheed," Journal of Materials in Civil Engineering, ASCE, November.

Kanakubo, T., Yonemaru, K., Fukuyama, H., Fujisawa, M., and Sonobe, Y. (1993), "Bond Performance of Concrete Members Reinforced with FRP Bars," Proceedings of International Symposium on Fibre Reinforced Plastic Reinforcement for Concrete Structures; ACI SP-138, A. Nanni and C. W. Dolan (editors).

Kwak, H-G. and Kim, D-Y. (2006), "Implementation of Bond-Slip Effect in Analyses of RC Frames under Cyclic Loads using Layered Section Method," Engineering Structures, Vol. 28, pp. 1715–1727.

Kwak, H-G. and Kim, D-Y. (2006), "Cracking Behaviour of RC Panels Subject to Biaxial Tensile Stresses," Computers and Structures, Vol. 84, pp. 305–317.

Kwak, H-G. and Song, J-Y. (2002), "Cracking Analysis of RC Members using Polynomial Strain Distribution Function," Engineering Structures, Vol. 24, No. 4, pp. 455–68.

Kwak, H-G. and Kim, D-Y. (2001), "Nonlinear Analysis of RC Shear Walls Considering Tension-Stiffening Effect," Computers and Structures, Vol. 75, No. 5, pp. 499–517.

Kupfer, H., Hilsdorf, H., and Rusch, H. (1969), "Behaviour of Concrete under Biaxial Stresses," ACI Journal, Proceedings Vol. 66, No. 8, pp. 656-666.

Lee, J.Y., Kim, T.Y., Kim, T.J., Yi, C.K., Park, J.S., You. Y.C., and Park, Y.H. (2007), "Interfacial Bond Strength of Glass Fibre Reinforced Polymer Bars in High-Strength Concrete," Composites: Part B, 39, pp. 258-270.

Lee, S-K., Woo, S-K., and Song, Y-C. (2008), "Softening Response Properties of Plain Concrete by Large-Scale Direct Tension Tests," Magazine of Concrete Research, Vol. 60, No. 1, pp. 33-40.

Leonhardt, F. (1977), "Crack Control in Concrete Structures," IABSE Surveys No. S-4/77, International Association for Bridge and Structural Engineering, Zurich, 26 p.

Lin, C.S. and Scordelis, A.C. (1975), "Nonlinear Analysis of RC Shells of General Form," Journal of Structural Division, ASCE, 101 (ST3), pp. 523-538.

Link, R.A., Elwi, A.E., and Scanlon, A. (1989), "Biaxial Tension Stiffening due to Generally Oriented Reinforcing Layers," Journal of Engineering Mechanics, ASCE, Vol. 115, No. 8, pp. 1647-1662.

Lorrain M., Maurel O., and Seffo, M. (1998), "Cracking Behavior of Reinforced High-Strength Concrete Tension Ties," ACI Structural Journal, Vol. 95, No. 5, pp. 626-635.

MacGregor, J.G., Rizkalla, S.H., and Simmonds, S.H. (1980), "Cracking of Reinforced and Prestressed Concrete Wall Segments," University of Alberta, Department of Civil Engineering, Structural Engineering Report No. 82.

Maekawa, K., Pimanmas, A., and Okamura, H. (2003). *Nonlinear Mechanics of Reinforced Concrete*, Spon Press, London.

Makitani, E., Irisawa, I., and Nishiura, N. (1993), "Investigation of Bond in Concrete Member with Fibre Reinforced Polymer Bars," International Symposium Fibre-Reinforced-Plastic Reinforcement for Concrete Structures, ACI SP-138, pp. 315-331.

Mahmood, H. (2002), "Cracking of Concrete Members Reinforced with Glass Fibre Reinforced Polymer Bars," M.Sc. Thesis, Department of Civil Engineering, University of Calgary, Calgary, Canada, 139 p.

Malvar, L.J. (1994), "Bond Stress-Slip Characteristics of FRP Bars," Technical Report TR-2013-SHR, Naval Facilities Engineering Service Center, Port Hueneme, CA.

Malvar, L.J. (1995), "Tensile and Bond Properties of GFRP Reinforcing Bars," ACI Materials Journal, Vol. 92, No. 3, pp. 276-285.

Marti, P., Alvarez, M., Kaufmann, W. and Sigrist, V. (1998), "Tension Chord Model for Structural Concrete," Structural Engineering International, 4/98, pp. 287-298.

Masmoudi, R., Benmokrane, B., and Chaallal, O. (1996), "Cracking Behaviour of Concrete Beams Reinforced with Fibre Reinforced Plastic Rebars," Canadian Journal of Civil Engineering, Vol. 23, No. 6, pp. 1172-1179.

Marzouk, H. and Chen, Z. (1993), "Finite Element Analysis of High-Strength Concrete Slabs," ACI Structural Journal, Vol. 90, No. 5, pp. 505-513.

Marzouk, H. and Chen, Z. (1995), "Fracture Energy and Tension Properties of High-Strength Concrete," Journal of Materials in Civil Engineering, ASCE, Vol. 7, No. 2, pp. 108-116.

Mirza S.M. and Houde J. (1979), "Study of Bond Stress–Slip Relationships in Reinforced Concrete," ACI Journal, Vol. 76, No. 1, pp. 19–45.

Mitchell, D., Abrishami, H.H., and Mindess, S. (1996), "The Effect of Steel Fibres and Epoxy-Coated Reinforcement on Tension Stiffening and Cracking of Reinforced Concrete," ACI Structural Journal, Vol. 93, No. 1, pp. 61-68.

Nanni, A. (1993), "Flexural Behaviour and Design of Reinforced Concrete Using FRP Rods," Journal of Structural Engineering, ASCE, Vol. 119, No. 11, pp. 19-23.

Nanni, A., Bakis, C. E., and Boothby, T. E. (1995), "Test Method for FRP-Concrete Systems Subjected to Mechanical Loads: State-of-the-Art Report," Journal of Reinforced Plastic Composites, Vol. 14, pp. 524-558.

National Instruments (2003) "LabView 7 Express", National Instruments Corporation, Austin, Texas, USA, web site: http://www.ni.com.

Nawy, E.G. and Blair, K.W. (1971), "Further Studies on Flexural Crack Control in Structural Slab Systems," ACI SP 30-1, Vol. 30, p. 67.

Nawy, E.G. and Neuworth, G.E. (1977), "Fibreglass Reinforced Concrete Slabs and Beams," Journal of Structural Division, ASEC, February, pp. 421-440.

NBR (1992), "Concrete Structures – Design Rules," NS 3473 E, Norwegian Council for Building Standardization, 4th edition.

Nayal, R. and Rasheed, H.A. (2006), "Tension Stiffening Model for Concrete Beams Reinforced with Steel and FRP Bars," Journal of Materials in Civil Engineering," ASCE, Vol. 18, No. 6, pp. 831-841.

Newhook, J., Ghali, A., and Tadros, G. (2002), "Concrete Flexural Members Reinforced Concrete with Fibre Reinforced Polymer: Design for Cracking and Deformability," Canadian Journal of Civil Engineering, 29, pp. 125-134.

Nilson, A.H. (1972), "Internal Measurement of Bind Slip," ACI Journal, Proceedings V. 69, No. 7, pp. 439-441.

Oersterle, R.G. and Russell, H.G. (1980), "Shear Transfer in Large Scale Reinforced Concrete Containment Elements," Construction Technology Laboratories, Portland Cement Association (PCA), Skokie, IL, and Division of Reactor Safety Research, Washington, D.C. Report No. 1.

Ospina, C.E., Alexander, D.B., and Cheng, J.J.R. (2001), "Behaviour of Concrete Slabs with Fibre-Reinforced Polymer Reinforcement," Structural Engineering Report No. 242, Department of Civil and Environmental Engineering, University of Alberta, Edmonton, Canada, 355 p.

Ospina, C.E. and Bakis, C.E. (2006), "Indirect Crack Control Procedure for FRP-Reinforced Concrete Beams and One-Way Slabs," Third International Conference on FRP Composites in Civil Engineering (CICE 2006), Dec., Miami, Florida, USA.

Phillips, D.V. and Binsheng, Z. (1993), "Direct Tension Tests on Notched and Un-notched Plain Concrete Specimens," Magazine of Concrete Research, Vol. 45, No. 162, March, pp. 25-35.

Pickett, G. (1956), "Effect of Aggregate on Shrinkage of Concrete and Hypothesis Concerning Shrinkage," ACI Journal, Proceedings V. 52, No. 5, pp. 581-580.

Razaqpur, A.G., Svecova, D., and Cheung, M.S. (2000), "Rational Method for Calculating Deflection of Fibre Reinforced Polymer Reinforced Beams," ACI Structural Journal, Vol. 97, No. 1, pp. 175-184.

Reinhardt, H.W., Cornelissen, H.A., and Hordijk, D.A. (1986), "Tensile tests and failure analysis of concrete," Journal of Structural Engineering, Vol. 112, No. 11, 2462-2477.

Rizkalla, S.H. and Hwang, L.S. (1984), "Crack Prediction for Members in Uniaxial Tension," ACI Journal, Nov-Dec, pp. 572-579.

Rizkalla, S.H., Hwang, L.S., and El-Shahawi, M. (1983), "Transverse Reinforcement Effect on Cracking Behaviour of Reinforced Concrete Members," Canadian Journal of Civil Engineering, Vol. 10, No. 4, pp. 556-581.

Rossetti, V.A., Galeota, D., and Giammatteo, M.M. (1995), "Local Bond Stress-Slip Relationships of Glass Fibre Reinforced Plastic Bars embedded in Concrete," Materials and Structures Journal, Vol. 28, pp. 340-344.

Sabrah, T.B., Marzouk, H., and Hussein, A. (2006a), "Analysis of GFRP-Reinforced Concrete Panels under Direct Uniaxial and Biaxial Tension," In proceedings of 1st International Structural Specialty Conference, 34th Annual Conference for the Canadian Society for Civil Engineering, Calgary.

Sabrah, T.B., Marzouk, H., and Hussein, A. (2006b), "Utilisation of GFRP-Reinforced Concrete Panels for Box Girder Bridges," 7th International Conference on Short & Medium Span Bridges, Montreal, Canada.

Sabrah, T.B., Marzouk, H., and Hussein, A. (2007), "Cracking of GFRP-Reinforced Concrete Panels Under Direct Tension," Proceedings of the 8th International Symposium on Fibre Reinforced Polymers for Concrete Structures, Patras, Greece.

Sabrah, T.B., Marzouk, H., and Hussein, A. (2008), "Tensile Response of High Strength Concrete Panels Reinforced with GFRP," 5th International Conference on Advanced Composite Materials in Bridges and Structures, ACMBS-V, Winnipeg, Manitoba, Canada, Edited by P. Lobossière and K. Neale.

Sabrah, T.B., Marzouk, H., and Hussein, A. (2009), "Development of a New Test Facility to Examine Reinforced Concrete Panels under Uniaxial and Biaxial Direct Tension," Journal of Testing and Evaluation, Vol. 37, No. 6 (in print), ASTM International, West Conshohocken, PA, www.astm.org.

Scanlon, A. and Murray, D.W. (1974), "Time Dependent Reinforced Concrete Slab Deflections," Journal of Structural Division, ASCE, Vol. 100, No. 9, pp. 1911-1924.

Sooriyaarachchi, H., Pilakoutas, K. and Byars, E. (2005), "Tension Stiffening Behaviour of GFRP-Reinforced Concrete," Intern. Symposium on FRP Reinforcement for Concrete Structures, ACI SP-230, pp. 975-989.

Sooriyaarachchi, H., Pilakoutas, K. and Byars, E. (2007), "Models for Tension Stiffening for Deflections of GFRP-RC," Proceedings of the 8th International Symposium on Fibre Reinforced Polymers for Concrete Structures, Patras, Greece.

Stevens, N.J., Uzumeri, S.M., Collins, M.P., and Will, G.T. (1991), "Constitutive Model for Reinforced Concrete Finite Element Analysis," ACI Structural Journal, Vol. 88, No. 1, pp. 49-59.

Somayaji, S. and Shah, S.P. (1981), "Bond Stress versus Slip Relationship and Cracking Response of Tension Memebers," ACI Journal, Proceedings Vol. 78, No. 3, pp. 217-225.

Tastani, S.P. and Pantazopoulou, S.J. (2007), "Design Values of Bond-Slip Law for FRP Bars," Proceedings of the 8th International Symposium on Fibre Reinforced Polymers for Concrete Structures, Patras, Greece.

Theriault, M. and Benmokrane, B. (1998), "Effects of FRP Reinforcement Ratio and Concrete Strength on Flexural Behaviour of Concrete Beams," Journal of Composites in Construction, ASCE, Vol. 2, No. 1, pp. 7-16.

Thorenfledt, E., Tomaszewicz, A. and Jensen, J.J. (1987), "Mechanical Properties of High-Strength Concrete and Application in Design," Proceedings of the Symposium 'Utilization of High Strength Concrete,' Stavenger, Norway, Tapir, Trondheim, pp. 149-159.

Tighiouart, B.; Benmokrane, B. and Gao, D. (1998), "Investigation of Bond in Concrete Member with Fibre Reinforced Polymer (FRP) Bars," Construction and Building Materials Journal, Vol. 12, pp. 453-462.

Toutanji, H.A. and Saafi, M. (2000), "Flexural Behaviour of Concrete Beams Reinforced with Glass-Reinforced Polymer (GFRP) Bars," ACI Structural Journal, Vol. 97, No. 5, pp. 712-719.

Uppuluri, V.S., Bakis, C.E., Al-Dulaijan, S.U., Nanni, A., and Boothby, T.E. (1996), "Analysis of the Bond Mechanism FRP Reinforcement Rods: The Effect of Rod Design and Properties," ACMBS-II, 2nd International Conference, Montreal, Canada, Elbadry, ed., pp. 893-900.

Uomoto, T. (2004), "Development of New GFRP with Alkali Resistivity," 4th International Conference on Advanced Composite Materials in Bridges and Structures, Calgary, Alberta, July 20-23.

Vecchio, F.J. and Collins, M.P. (1982), "The Response of Reinforced Concrete to In-Plane Shear and Normal Stress," Publication No. 82-03, Department of Civil Engineering, University of Toronto, Ontario, Canada.

Vecchio, F.J. and Collins, M.P. (1986), "The Modified Compression-Field Theory for Reinforced Concrete Elements Subjected to Shear," ACI Journal, Vol. 83, No.2, pp. 219-231.

Virmani, P. and Clemena, G.G. (1998), "Corrosion Protection-Concrete Structures," Report No. FHWA-RD-98-088, Federal Highway Administration, McLean, Va., 72 p.

Wang, P.T., Shah, S.P., and Naaman, A.E. (1978), "High Strength Concrete in Ultimate Strength Design," Journal of the Structural Division, ACI, Vol. 104, No. ST11, pp. 1761-1773.

Watstein, D. and Mathey, R.G. (1959), "Width of Cracks in Concrete at the Surface of Reinforcing Steel Elevated by Means of Tensile Bond Specimens," ACI Journal, Vol. 56, No. 1, pp. 47-56.

Watstein, D. and Parson, D.E. (1943), "Width and Spacing of Tensile Cracks in Axially Reinforced Concrete Cylinders," Journal of Research, National Bureau of Standards, Vol. 31.

Welch, G.B. and Janjua, M.A. (1971), "Width and Spacing of Tensile Cracks in Reinforced Concrete," Report No. R-76, School of Civil Engineering, University of New South Wales, Kensington, NSW, Australia.

Williams, A. (1986), "Tests on Large Reinforced Concrete Elements Subjected to Direct Tension," Technical Report No. 562, Cement and Concrete Association.

Witt, C. and Jütt, B. (2008), "Corrosion Problems in Bridge Construction-Alternative Solutions using Glass Fibre Reinforcement," In proceedings of Advanced Composite Materials in Bridges and Structures, 5th International Conference, (ACMBS V), Winnipeg, Manitoba, Canada, Edited by P. Lobossière and K. Neale.

Wollrab, E., Kulkarni, S.M., Ouyang, C. and Shah, S.P. (1996), "Response of Reinforced Concrete Panels under Uniaxial Tension," ACI Structural Journal, Vol. 93, No. 6, Nov-Dec, pp. 648-657.

Wu, W-P. (1990), "Thermomechanical Properties of Fibre Reinforced Plastics (FRP) Bars," PhD dissertation, West Virginia University, Morgantown, W.Va., 292 p.

Yankelevsky, D.Z. and Reinhardt, H.W. (1987), "Response of Plain Concrete to Cyclic Tension," ACI Material Journal, Vol. 84, No. 5, 365-373.

Yost, J.R., Gross, S.P., and Dinehart, D.W. (2003), "Effective Moment of Inertia for Glass Fibre-Reinforced Polymer-Reinforced Concrete Beams," ACI Structural Journal, Vol. 100, No. 6, pp. 732-739.